

Maintaining the Intestinal Barrier: The Role
of the Tight Junction Protein Occludin in
Toxoplasma gondii Transmigration of the
Gastrointestinal Tract

Emily Jennifer Jones

Submitted for the degree of Doctor of Philosophy
University of East Anglia
Institute of Food Research

October 2016

This copy of the thesis has been supplied on condition that anyone who consults it is understood to recognise that its copyright rests with the author and that use of any information derived there from must be in accordance with current UK Copyright Law. In addition, any quotation or extract must include full attribution.

Declaration

I certify that the work contained in this thesis submitted by me for the degree of Doctor of Philosophy is my original work except where due reference is made to other authors, and has not been previously submitted by me for a degree at this or any other university.

Part of the work in this thesis has previously appeared in the publication below (Appendix F). E. Jones and C. Weight contributed equally to the manuscript:

Weight CM, et al., Elucidating pathways of *Toxoplasma gondii* invasion in the gastrointestinal tract: Involvement of the tight junction protein occludin, *Microbes and Infection* (2015).

In line with the regulations for the degree of Doctor of Philosophy I have submitted a thesis that has a word count, including footnotes and bibliography, but excluding appendices of 62,278 words.

Abstract

The small intestinal permeability barrier is dependent on tight junction (TJ) complexes that separate the external lumen from the underlying mucosa. Apical TJs consist of integral transmembrane proteins including occludin, claudins and ZO-1 as well as the cytoplasmic plaque of TJ-associated adaptor, scaffolding and signalling proteins. Although the function of occludin at the TJ remains unclear, the dynamic mobility of occludin, claudins and ZO-1 to and from the TJ suggests occludin may play a key role in regulation of TJ structure and function, regulated by occludin phosphorylation status. Defects in TJ barrier function have been implicated in a range of inflammatory diseases such as inflammatory bowel disease (IBD) and pathogens such as *Toxoplasma gondii* target this complex as a route of infection. As oral infection is the primary cause of toxoplasmosis, the first point of contact between *T. gondii* and the host is the small intestinal epithelium and studies by Weight, 2012 show occludin may be involved in *T. gondii* paracellular transmigration of the small intestinal epithelium.

The aim of this research was to investigate *T. gondii* paracellular transmigration using an *in vitro* model of the small intestinal epithelium and elucidate the role of occludin both in regulation of the TJ barrier and as a receptor for *T. gondii* infection. The results presented in this thesis demonstrate that *T. gondii* infects the small intestinal epithelium via the paracellular pathway and occludin was shown to play a key role both in regulation of the TJ paracellular barrier and as a receptor for *T. gondii* infection by parasite-mediated modulation of the occludin C-terminus phosphorylation status and direct binding to occludin ECL1; suggesting *T. gondii* interactions with occludin are a potential mechanism of paracellular transmigration of the small intestinal epithelium.

Table of Contents

List of Non-Standard Abbreviations	10
1 Introduction.....	15
1.1 Small Intestinal Epithelial Barrier	17
1.2 Epithelial Cellular Junctions.....	19
1.2.1 Tight Junction Structure.....	21
1.2.2 Tight Junction Function.....	32
1.2.3 Tight Junction Regulation.....	35
1.3 Tight Junction Interactions with the Immune System	41
1.4 <i>Toxoplasma gondii</i>	46
1.4.1 <i>Toxoplasma gondii</i> Life Cycle and Unique Morphology	47
1.4.2 Toxoplasmosis.....	51
1.4.3 <i>Toxoplasma gondii</i> Host Infection and Dissemination	53
1.4.4 <i>Toxoplasma gondii</i> Virulence Factors.....	56
1.5 <i>Toxoplasma gondii</i> Interactions with Occludin.....	59
1.6 Rationale.....	60
1.7 Hypothesis.....	61
1.8 Aims	61
2 Materials and Methods	62
2.1 Commercial Suppliers.....	62
2.2 Cell Line Culture	62
2.3 <i>T. gondii</i> Culture	62
2.4 Alkaline Phosphatase Assay	66
2.5 Immunocytochemistry	66
2.6 Fluorescence or Confocal Microscopy	67
2.7 Immunoblotting	67
2.8 Transepithelial Electrical Resistance (TEER) and Permeability ...	69
2.9 Recombinant Occludin Peptides	70
2.9.1 Cloning of Occludin EC1, ECL2, ECL1+ECL2 and C-terminus into the 6xHIS-tagged expression vector pET15b	70
2.9.2 Purification of Occludin ECL1, ECL2, ECL1+ECL2 and C-terminus peptides.....	71
2.9.3 Analysis of Occludin EC1, ECL2, ECL1+ECL2 and C-terminus peptides.....	72
2.9.4 Transmigration and Infection Assay	72
2.10 Live Cell Imaging	73
2.11 SILAC Proteomic Analysis.....	75
2.12 <i>In Vitro</i> Occludin Kinase Assay.....	77
2.12.1 Isoelectric Focussing	77
2.12.2 2D Gel Electrophoresis.....	78
2.12.3 Gel Staining.....	78
2.12.4 Mass Spectrometry	79
2.13 <i>T. gondii</i>-Occludin Binding Assay.....	79
2.14 Bioinformatics.....	80
2.15 Statistical Analysis	81

3 Model for Investigating Epithelial Tight Junction Barrier Function	82
3.1 Introduction	82
3.2 Results	84
3.2.1 IEC-6 Culture on Plastic Substrates.....	85
3.2.2 IEC-6 Culture Using an Extracellular Matrix.....	85
3.2.3 Cellular Differentiation of IEC-6 is Induced on Plastic.....	86
3.2.4 IEC-6 Culture on Cell Culture Inserts	88
3.2.5 IEC-6 Polarisation	90
3.2.6 IEC-6 Tight Junction Protein Expression	92
3.2.7 IEC-6 Occludin Expression	92
3.2.8 The IEC-6 Epithelial Barrier	95
3.2.9 TEER and Permeability.....	97
3.3 Discussion.....	98
3.4 Conclusions.....	102
4 <i>Toxoplasma gondii</i> Invasion of IEC-6 and the Involvement of Tight Junction Proteins.....	103
4.1 Introduction	103
4.2 Results	105
4.2.1 <i>Toxoplasma gondii</i> Transmigration of the IEC-6 Monolayer	105
4.2.2 The Tight Junction Barrier is Maintained During <i>Toxoplasma gondii</i> Infection	106
4.2.3 <i>Toxoplasma gondii</i> Live Cell Imaging	109
4.2.4 <i>Toxoplasma gondii</i> Paracellular Route of Infection.....	109
4.2.5 SILAC Proteomic Analysis	111
4.2.6 Role of the Epithelial Tight Junction During Infection	116
4.3 Discussion.....	119
4.4 Conclusions.....	129
5 Changes in Occludin Phosphorylation in Response to <i>Toxoplasma gondii</i> Infection	130
5.1 Introduction	130
5.2 Results	133
5.2.1 Prediction of Novel Occludin Kinases	133
5.2.2 <i>In Vitro</i> Occludin Kinase Assay	135
5.2.3 Occludin Phosphorylation Analysis by Mass Spectrometry	137
5.2.4 IEC-6 occludin phosphorylation footprint modulation by <i>Toxoplasma gondii</i>	139
<i>Toxoplasma gondii</i> Derived Kinases Targeting Occludin	141
5.2.5	141
5.3 Discussion.....	141
5.4 Conclusions.....	146
6 <i>Toxoplasma gondii</i> Interactions with Occludin.....	147
6.1 Introduction	147
6.2 Results	148
6.2.1 <i>Toxoplasma gondii</i> Interactions with Occludin Alter Parasite Attachment and Infection	149
6.2.2 <i>Toxoplasma gondii</i> Bind to the Extracellular Loops of Occludin ...	150
6.2.3 Potential <i>Toxoplasma gondii</i> Derived Occludin Binding Partners	153
6.3 Discussion.....	156
6.4 Conclusions.....	160

7 Discussion	162
7.1 Infection of IEC-6 Cells by <i>Toxoplasma gondii</i>	162
7.2 Modulation of Tight Junction-Associated Proteins During <i>Toxoplasma gondii</i> Infection.....	163
7.2.1 <i>T. gondii</i> Modulation of the Host Actin Cytoskeleton.....	165
7.2.2 <i>T. gondii</i> Modulation of the Host Cell Cycle.....	169
7.2.3 <i>T. gondii</i> Modulation of Occludin Phosphorylation.....	172
7.2.4 <i>T. gondii</i> Binding to Occludin	175
7.3 Proposed mechanism of <i>Toxoplasma gondii</i> paracellular infection of IEC-6 cells.....	177
7.4 Future directions	185
7.4.1 Validate <i>in vivo</i> <i>T. gondii</i> paracellular transmigration and binding to occludin	185
7.4.2 Identify which <i>T. gondii</i> proteins interact with occludin ECL1 to enable paracellular transmigration	186
7.5 Overall conclusions.....	187
Appendix A.....	189
Recombinant Occludin Peptide Generation	189
Appendix B.....	192
SILAC Dataset.....	192
Appendix C.....	206
Functional Annotation of differentially expressed proteins during <i>T. gondii</i> infection of IEC-6	206
Appendix D	209
Tight Junction Proteome.....	209
Appendix E.....	218
BLAST search results and GO annotation	218
Appendix F	224
Publication.....	224
Bibliography	237

List of Figures

1.1: The epithelial junctional complex	22
1.2: Epithelial tight junction structure	24
1.3: Molecular structure of occludin	27
1.4: Architecture of claudin paracellular pores	31
1.5: Tight junction dynamics assessed by fluorescence recovery after photobleaching.....	42
1.6 <i>T. gondii</i> life cycle.....	49
1.7: <i>T. gondii</i> bradyzoite and tachyzoite ultrastructure.....	50
1.8: <i>T. gondii</i> transcellular invasion mechanism	55
2.1: Occludin peptide generation	74
3.1: Morphology of small intestinal epithelial cells cultured on plastic substrate	87
3.2: ALP activity increases with IEC-6 cell culture	89
3.3: Cell culture insert system	91
3.4: IEC-6 are partially polarised when cultured on PET inserts	93
3.5: Comparison between fixation with 2% paraformaldehyde and acetone.....	94
3.6: Occludin expression and localisation in IEC-6	96
3.7: Barrier function of IEC-6 cultured on PET inserts assessed by TEER and Permeability to FITC-dextran.....	99
4.1: <i>T. gondii</i> infection of IEC-6 cells.....	107
4.2: IEC-6 barrier integrity is not affected by <i>T. gondii</i> infection	108
4.3: Live cell imaging of <i>T. gondii</i> infection	110
4.4: <i>T. gondii</i> utilise the paracellular pathway during transmigration and egress	112
4.5: <i>T. gondii</i> paracellular infection mechanism.....	113
4.6: Schematic representation of a SILAC workflow.....	115
4.7: Functional categorisation of the SILAC IEC-6 proteins that decreased in abundance during <i>T. gondii</i> infection.....	117
4.8: Functional categorisation of the SILAC IEC-6 proteins that increased in abundance during <i>T. gondii</i> infection.....	118
5.1: Occludin kinase bioinformatics.....	134
5.2: <i>In vitro</i> occludin kinase assay	136
5.3: <i>T. gondii</i> modulation of IEC-6 in vitro occludin kinase assay.....	140

6.1: <i>T. gondii</i> inhibition of attachment and invasion in response to recombinant murine occludin peptides	151
6.2: <i>T. gondii</i> invasion and transmigration of m-ICc12 in response to recombinant fragments of murine occludin.....	152
6.3: Detection of recombinant occludin peptide immobilisation on Schott Nexterion Slide H	154
6.4: <i>T. gondii</i> binding to recombinant fragments of murine occludin.....	155
6.5: Functional categorisation of the <i>T. gondii</i>-derived proteins predicted to interact with occludin domains.....	158
7.1: Modulation of the host TJ proteome during <i>T. gondii</i> infection	166
7.2: Tight Junction dynamics.....	170
7.3: Impact of CKII-mediated occludin S408 phosphorylation on TJ structure.....	174
7.4: <i>T. gondii</i> invasion of SI epithelial cells	179-184

List of Tables

2.1: List of reagents	63-64
2.2: List of antibodies and cell strains	65
4.1: Tight junction proteins modulated during <i>T. gondii</i> infection of IEC-6.....	121
5.1: Summary of known occludin C-terminus phosphorylation sites and their effect on TJ function.....	132
5.2: CKII occludin C-terminus phosphorylation footprint.....	138

List of Accompanying Material

Video 1: Live imaging of <i>T. gondii</i> paracellular infection.....	CD
--	-----------

List of Non-Standard Abbreviations

2D-GE	Two-Dimensional Gel-Electrophoresis
α -SNAP	Alpha-Soluble NSF-Attachment Protein
AIDS	Acquired Immune Deficiency Syndrome
AJ	Adherens Junction
bTJ	Bilateral Tight Junction
CAM	Calmodulin Kinase
CAR	Coxsackie and Adenovirus Receptor
CDPK	Calmodulin-like Domain Protein Kinase
CK	Casein Kinase
CLMP	Coxsackie and Adenovirus Receptor-like Membrane Protein
CPE	<i>Clostridium perfringens</i> Enterotoxin
c-SRC	Proto-Oncogene Tyrosine-Protein Kinase
DC	Dendritic Cell
DMEM	Dulbecco's Modified Eagle's Medium
ECL	Extracellular Loop
ECM	Extracellular Matrix
EGFR	Epidermal Growth Factor Receptor
ELL	RNA-polymerase II Elongation Factor
EPEC	Enteropathogenic <i>E. coli</i>
ERK	Extracellular-Signal-Regulated Kinases
ESAM	Endothelial Cell-Selective Adhesion Molecule
EVOM	Epithelial Volt-ohm Meter
FAK	Focal Adhesion Kinase
FITC	Fluorescein Isothiocyanate
FLIP	Fluorescence Loss in Photobleaching
FRAP	Fluorescence Recovery After Photobleaching
FRET	Fluorescence Resonance Energy Transfer
GEF	Guanine Nucleotide Exchange Factor
GO	Gene Ontology
GOPC	Golgi-Associated PDZ and Coiled-Coil Motif-Containing Protein

GPI	Glycophosphatidylinositol
GRA	Dense Granule
GSK	Glycogen Synthase Kinase
H&E	Haematoxylin and eosin
HA/P	Cytotoxin Haemagglutinin/Protease
HCV	Hepatitis C Virus
HDM	House Dust Mite
HIS	Histidine
HIV	Human Immunodeficiency Virus
HSP	Heat Shock Protein
ICAM-1	Intercellular Adhesion Molecule-1
ICL	Intracellular Loop
IEF	Isoelectric Focusing
IFN	Interferon
Ig	Immunoglobulin
iIELs	Intestinal Intraepithelial Lymphocytes
IL	Interleukin
IMAC	Immobilised Metal Affinity Chromatography
INSR	Insulin receptor
IP	Immunoprecipitation
JAM	Junctional Adhesion Molecule
JEAP	Junction Enriched and Associated Protein
LB	Luria-Bertani Media
L-PK	L-type Pyruvate Kinase
LPS	Lipopolysaccharide
LSM	Laser Scanning Microscopy
LSR	Lipolysis-Stimulated Lipoprotein Receptor
M cells	Microfold Cells
MAGI	Membrane Associated Guanylate Kinase, WW and PDZ Domain-Containing Protein
MAGUK	Membrane Associated Guanylate Kinase
MAL	Myelin and Lymphocyte
MALT	Mucosa-Associated Lymphoid Tissue

MARVEL	MAL and Related Proteins for Vesicle Trafficking and Membrane Link
MHC	Major Histocompatibility Complex
MIC	Microneme
MJ	Moving Junction
MLC	Myosin II Regulatory Light Chain
MLCK	Myosin II Regulatory Light Chain Kinase
MRM	Multiple Reaction Monitoring
NACo	Nucleus and Adhesion Complex Proteins
Ni-NTA	Nickel-Nitrilotriacetic Acid
N-WASP	Neuronal Wiskott–Aldrich Syndrome Protein
OCEL	Occludin/ELL (RNA polymerase II elongation factor) Domain Containing Protein
OD ₆₀₀	Optical Density at 600nm
PANTHER	Protein Annotation Through Evolutionary Relationship
PDZ	Post-synaptic Density 95/Drosophila discs large/ZO-1
PET	Polyethylene Terephthalate
PI3K	Phosphatidylinositol-3-Kinase
PP	Protein phosphatase
PTEN	Phosphatase and Tensin Homolog Protein
PV	Parasitophorous Vacuole
ROCK	Rho-associated Protein Kinase
RON	Rhoptry Neck Protein
ROP	Rhoptry
SAG	Surface Antigen
scRNA	Scrambled Ribonucleic Acid
SDS-PAGE	Sodium Dodecyl Sulfate Polyacrylamide Gel Electrophoresis
SEM	Scanning Electron Microscopy
SEN-6	Senescence-6
SH3	SRC Homology 3 Domain
SIM	Structured illumination microscopy
siRNA	Small Interfering RNA
SLiM	Short Linear Motif

SPR	Surface Plasmon Resonance
SRM	Selective reaction monitoring
SRS	SAG1-Related Sequences
SV40	Simian Virus 40
TAMP	Tight Junction Associated MARVEL Protein
TCR	T-cell Receptor
TEER	Transepithelial Electrical Resistance
TGF	Transforming Growth Factor
TJ	Tight Junction
TLR	Toll-like Receptor
TM	Transmembrane
TNF	Tumour Necrosis Factor
tTJ	Tricellular Tight Junction
VAMP	Vesicle Associated Membrane Protein
VAP-33	VAMP Associated Protein of 33kDa
VASP	Vasodilator-Stimulated Phosphoprotein
VEGF	Vascular Endothelial Growth Factor
ZO	Zonula-Ocludens
ZONAB	ZO-1-Associated Nucleic Acid Binding Protein (Ybx3)
ZOT	Zonula Occludens Toxin

Acknowledgements

I would like to thank my supervisors Professor Simon Carding for his continued guidance, support and feedback throughout my PhD and Professor Alastair Watson for his help and advice. Special thanks also go to Professor Judith Smith and Dr Kevin Tyler for reading and examining this thesis. At the Institute of Food Research many individuals were instrumental in the success of this project and without them this thesis would not be complete; Dr Caroline Weight for performing the experiments that led to this project, Nikki Horn for all her time and effort in making the production of occludin recombinant fragments both possible and enjoyable, Dr Duncan Gaskin for assistance with production of ECL1 and ever helpful career advice, Dr Francis Mulholland for his expertise in SILAC, 2D-GE and mass spectrometry, Dr Nikolaus Wellner for his knowledge of two-photon imaging, Dr Tamas Korcsmáros for help with SILAC data and network analysis, Dr Alex Jones for her assistance at the beginning of this project and Dr Elizabeth Bassity for her time spent proof reading this thesis. I am forever grateful to all members of the Carding laboratory past and present, particularly Dr Isabelle Hautefort, Dr Elizabeth Bassity, Dr Jo Brooks and Sarah Clements who have not only provided sound scientific advice but have become great friends. You have all helped me along the journey that is a PhD, be that providing encouragement, motivation and much appreciated advice or simply being brilliant wedding planners, costume designers, running buddies or fellow lycra enthusiasts. I would especially like to thank my parents for their encouragement of my early scientific career as well as their continued support and also my husband David for his reassurance throughout the successes and failures that are a necessary part of any scientific endeavour and for his memorable analogies between occludin, *T. gondii* and football. Finally, I would like to thank Ironman® for giving me the endurance required to complete this thesis and for teaching me that 'Anything is Possible™'.

1 Introduction

The human gastrointestinal tract (GIT) comprising of the oesophagus, stomach, small intestine, large intestine, rectum and anus, fundamentally forms a route through which food enters the body, is digested and then waste is excreted. The GIT lumen is also home to a diverse microbiota that varies in density and composition along the GIT [Hooper et al, 2012; O'Hara and Shanahan, 2006]. It is estimated that the human microbiota contains 10^{14} bacteria with 70% residing in the colon (10^{11} – 10^{12} bacteria per gram of colonic content) [O'Hara and Shanahan, 2006; Sekirov et al, 2010]. With the exception of the oesophagus, the GIT has a conserved architecture throughout, consisting of an internal lumen, epithelial lining and underlying stratified layers of the mucosa and submucosa. The epithelium is specialised along the length of the GIT, reflecting a diverse range of functions from resisting highly acidic digestive enzymes in the stomach to water absorption in the colon whilst providing an effective barrier between microbes and host. This thesis focuses on the small and large intestine.

The intestinal epithelium is the largest of the body's mucosal surfaces, covering 400m^2 . It creates a highly effective barrier between the GIT lumen and the body even though it is formed from only a single continuous layer of columnar epithelial cells [Peterson and Artis, 2014]. These cells within the mucosa rest on the basement membrane and connective tissue of the lamina propria, supported by a thin layer of smooth muscle termed the muscularis mucosa. The underlying submucosa is composed of connective tissue, nerves, blood vessels and lymphatics and is lined by a thicker muscle layer, surrounded by the serosa, which separates the intestine from the peritoneal cavity (Figure 3.1B) [Mowat and Agace, 2014; Turner and Turner, 2010].

The small intestine (SI) measures 6-7m in length and approximately 2.5cm in diameter and is divided into three anatomically distinct sections; the duodenum, the jejunum and the ileum, with specific absorptive capabilities whereas the large intestine (LI), comprising the

ascending and transverse sections (proximal colon) and descending and sigmoid sections (distal colon), is shorter in length at ~1.5m and much wider in diameter [Mowat and Agace, 2014]. The SI is the primary site for nutrient and water absorption [Montrose, 2003] and is specialised to maximise absorption by increasing the available surface area to approximately 200m² by ordered folding of the submucosa and further folding of the epithelium into finger-like villi and invaginated crypts of Lieberkühn [Barker et al, 2007; Hooper et al, 2012; Kim and Ho, 2010; Neiss and Reinecker, 2006]. The epithelial brush border of ~1μm microvilli further increases the surface for enhanced nutrient absorption and the gradient of solute exchange across the basement membrane also encourages water absorption via the network of closely residing capillaries. In contrast, villi are absent from the colon, it has limited digestive capability and functions to extract water and solutes from solid waste [Mowat and Agace, 2014].

Along the SI crypt-villus axis and colonic crypt, there is a dynamic system of constant renewal; under normal conditions, the progeny of stem cells in the base of the crypt proliferate, differentiate and migrate upwards, where they are eventually shed into the lumen at an approximate rate of 1400 cells from the villus tip per day [Potten and Loeffler, 1990]. Importantly, the SI epithelial barrier is preserved even during the high turnover cell shedding from the villus tip, a potential site of barrier loss [Duckworth and Watson, 2011]. In inflammatory GI diseases such as inflammatory bowel disease (IBD), cell turnover is accelerated and the potential for barrier loss is increased [Marchiando et al, 2011; Meddings, 2008]. Despite the evidence of gaps in the epithelium possibly created during shedding, the barrier is consistently maintained [Kiesslich et al, 2007; Watson et al, 2005 and 2009].

The predominant cell type along the SI villus are absorptive enterocytes (over 80%), adapted for metabolic and digestive functions, which alongside specialised intestinal epithelial cells (IECs) such as hormone-secreting enteroendocrine cells, mucus-secreting goblet cells, Paneth cells and M (microfold) cells, form a dynamic SI epithelial barrier

[Karam, 1999; Sancho et al, 2003; van der Flier and Clevers, 2009]. Paneth cells are only found in the SI where they migrate to the crypt base and secrete antimicrobial peptides such as lysozyme, defensins and other factors [Bevins and Salzman, 2011; Elphick and Mahida, 2005]. In the colon, the number of goblet cells is increased, comprising 25% of all epithelial cells in the distal colon compared to 10% in the SI [Mowat and Agace, 2014]. This difference in goblet cell number correlates with mucus production; a thin layer is present in the SI whereas a thick double layer consisting of a dense, sterile inner layer and loose outer layer where bacteria reside is present in the LI [Johansson et al, 2013; Pelaseyed et al, 2014].

The continuous layer of IECs forms the body's largest interface with the external environment and creates an effective barrier to luminal bacteria, pathogens, toxins and antigens from entering the lamina propria [Marchiando et al, 2010; Suzuki, 2013]. This thesis focuses on the SI epithelial barrier and its role in *T. gondii* infection.

1.1 Small Intestinal Epithelial Barrier

As well as creating an effective barrier to luminal microorganisms, the SI epithelium permits the absorption of nutrients by selective permeability through the transcellular (through cells) and paracellular (between cells) pathways. The transcellular absorption of sugars, amino acids, peptides, fatty acids, minerals and vitamins is mediated by transporters and channels in the apical and basolateral cell membranes [Broer, 2008; Ferraris and Diamond, 1997; Kiela and Ghishan, 2009]. The paracellular pathway, regulated by apical cellular junctions, forms a barrier to harmful luminal contents whilst allowing the selective transport of ions, solutes and water across the epithelium [Shen, 2012]. Crucially, without this paracellular barrier, absorbed solutes would simply diffuse back across the concentration gradient of the epithelium [Turner, 2009].

Breakdown of the epithelial barrier has been implicated in the pathogenesis of various intestinal and systemic diseases including ischemic retinopathy, pulmonary edema, IBD, oeliac disease, rheumatoid arthritis, psoriasis, cancer, diabetes, allergic disorders and HIV [Harhaj and Antonetti, 2004; Shen et al, 2009; Suzuki 2013]. The common factor of all these diseases is altered epithelial permeability but this connection is only beginning to be understood.

At steady state, cellular junctions regulate the permeability of the epithelial barrier in response to stimuli including nutrients, cytokines and bacteria [Ivanov, 2008; Turner, 2009; Nusrat et al, 2000]. However, under inflammation conditions the epithelial barrier is disrupted [Ivanov et al, 2010; Turner, 2009] and an increase in permeability leads to the symptoms experienced with IBD of reduced solute transport [Simon et al, 1999], leak-flux diarrhoea [Sandle, 2005] and a ‘leaky gut’ that allows the translocation of large luminal antigens that are normally prevented from entry, which may initiate the immune response and cause or maintain intestinal inflammation [Al-Sadi et al, 2011; Buschmann et al, 2013; Odenwald and Turner, 2013]. Clinical data has confirmed a positive correlation between the decline of intestinal barrier function and the degree of mucosal inflammation in patients with CD and UC and increased epithelial permeability often precedes relapse of CD in patients [Arnott et al, 2000; D’Incà et al, 1999; Wyatt et al, 1993]. In addition to the widespread barrier loss caused by severe intestinal inflammation in IBD, targeted barrier loss occurs during pathogen infection [Balda and Matter, 2000; Capaldo and Nusrat, 2009], as discussed later in this chapter.

The economic costs associated with GI diseases is continuing to expand, the latest reported annual costs of IBD to the UK NHS are estimated at £470 million or £631-762 per patient [Buchanan et al, 2011; Cummings et al, 2008; Luces and Bodger, 2006; Molodecky et al, 2012]. These figures reflect lifelong healthcare costs such as medication, anti-TNF α therapy, hospitalisation and surgery as well as productivity losses associated with sick leave and work disability which amount to almost

50% of the total costs [Bassi et al, 2004; Mowat et al, 2011; van der Valk et al, 2014]. Clearly it is important to elucidate the mechanism of epithelial barrier loss to potentially treat these diseases.

1.2 Epithelial Cellular Junctions

In order to investigate SI epithelial barrier function during *T. gondii* infection, it is essential to understand the molecular architecture of cellular junctions. Epithelial cell sheets such as the SI lining are formed by tightly connected adjacent cell membranes held together by a series of intercellular junctions termed the epithelial junctional complex. This was first visualised at the ultrastructural level over 50 years ago by Farquhar and Palade using transmission electron microscopy (TEM). The authors used thin sections of epithelial cells and identified points of cell-cell contact and regions between epithelial cells where the paracellular space was completely eliminated [Farquhar and Palade, 1963].

They identified three distinct morphological structures of the epithelial junctional complex: the apical tight junction (TJ), followed by lateral adherens junctions (AJ) and basolateral desmosomes (Figure 1.1A) and their TEM images revealed the junctional complex as a continuous ring, completely encircling the cell and interconnecting neighbouring cells [Farquhar and Palade, 1963]. Early studies confirmed the epithelial TJ as the point of complete membrane occlusion through the use of tracer molecule diffusion across the paracellular space [Goodenough and Revel, 1970]. The TJ is also responsible for intercellular sealing whereas lateral AJ and desmosomes provide the adhesive force to maintain cell-cell contacts [Gumbiner, 1993; Schneeberger and Lynch 1992].

In some tissues intercellular pore-forming gap junctions are also associated with the junctional complex and allow small molecules to pass between the cytoplasm of neighbouring cells [Goodenough and Paul, 2003].

The AJ is formed by cadherins, a family of glycoproteins that form homotypic adhesive contacts between adjacent cells [Gumbiner, 2005; Perez-Moreno, 2006]. E-cadherin, for example, binds to the catenins p120, β and α , which connect the cadherin complex to the actin cytoskeleton and signalling pathways [Niessen, 2007]. Loss of the AJ results in loss of cell-cell adhesion, ineffective polarisation, differentiation and subsequent apoptosis [Hermiston and Gordon, 1995]. Dysregulation of E-cadherin expression and cellular localisation has also been linked to carcinogenesis and IBD [Hartsock and Nelson, 2008; Mehta et al, 2014]. Formation of the AJ appears to precede the localisation and assembly of the TJ protein complex [Ikenouchi et al, 2007; Rajasekaran et al, 1996; Siliciano and Goodenough, 1988] although the exact order of assembly and disassembly of the TJ molecules remains unknown.

TJs are found in a variety of tissues besides the intestinal epithelium, including the vascular endothelium of the blood-brain, blood-retinal and blood-placental barriers. The SI epithelial TJ located at the boundary between the apical and basolateral plasma membranes forms a selectively permeable barrier that drives passive paracellular absorption and secretion [Turner, 2009]. Early freeze-fracture electron microscopy (EM) offered a lateral view of the intercellular space by fracturing along hydrophobic planes. The TJ was observed by TEM just below the apical microvilli as a series of continuous anastomosing strands that form small punctae or ‘kissing points’ between the outer leaflets of neighbouring cell membranes, essentially forming paired TJ strands that occlude the paracellular space between adjacent cells (Figure 1.1B) [Cereijido 1989; Farquhar and Palade, 1963; Shen et al, 2011; Tsukita et al, 2001]. When visualised by immunofluorescence, TJ proteins create a chicken-wire pattern in sections parallel to the monolayer, mirroring cellular borders (Figure 1.1C) and display a distinct apical punctate pattern when viewed laterally, perpendicular to the monolayer [Matter and Balda, 2003; Tsukita et al, 1996].

The number of TJ strands loosely correlates to barrier function and varies both between tissues and within epithelia, for example ‘leaky’

epithelia such as the gallbladder often have only a single strand whereas ‘tight’ epithelia such as the urinary bladder have at least five strands [Claude and Goodenough, 1973; Marcial et al, 1984; Naftalin and Tripathi, 1985]. The SI has a relatively leaky epithelium for unidirectional nutrient and solute absorption [Anderson and Van Itallie, 2009]. Along the SI crypt-villus axis a permeability gradient forms between the ‘tight’ villus epithelium, which allows a flux of molecules \sim 6-10 \AA , and the relatively ‘leaky’ crypt epithelium, which is permeable to larger molecules of \sim 60 \AA . [Fihn, 2000].

Now, 50 years since its discovery the TJ is known to be more dynamic than the original perception as a static, rigid structure that simply sealed the paracellular space and much progress has been made in the field of TJ structure, function and regulation.

1.2.1 Tight Junction Structure

The first TJ-associated proteins were identified in the 1980’s as zonula occludens-1 (ZO-1) [Stevenson et al, 1986], followed by Cingulin [Citi et al, 1988] and other related peripheral membrane proteins [Jesaitis and Goodenough, 2004; Ohnishi et al, 2004]. With the discovery of the pore-forming function of the TJ, subsequent studies sought to identify integral membrane proteins.

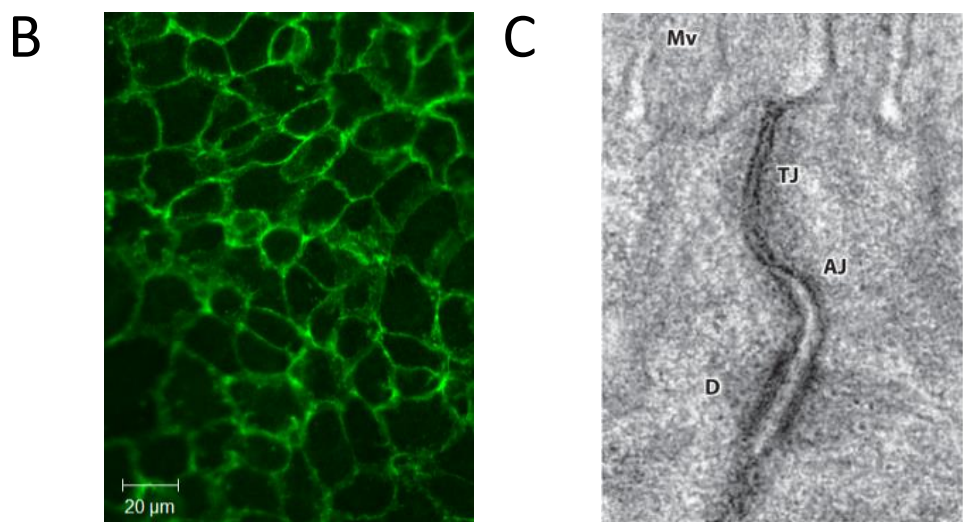
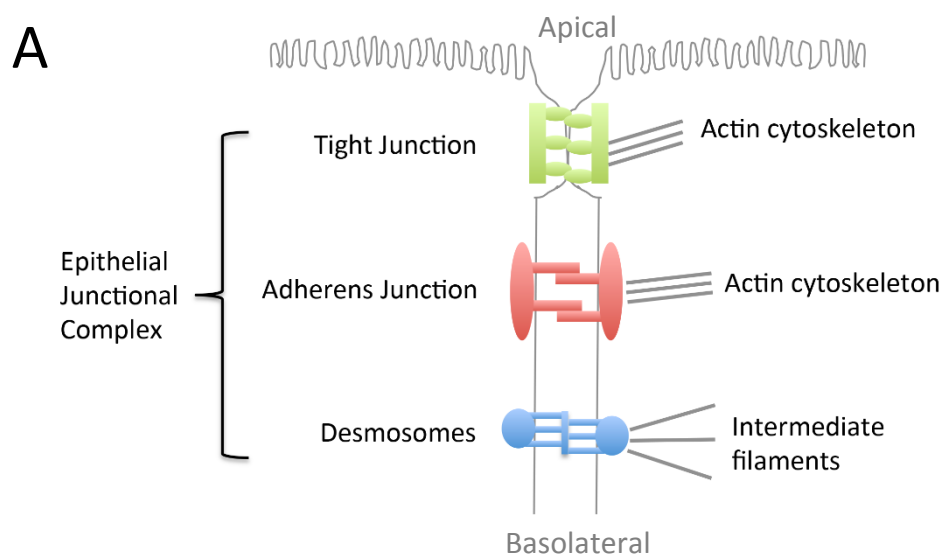


Figure 1.1: The epithelial junctional complex. A) Schematic representation of the apical tight junction, lateral adherens junction and basolateral desmosomes. B) Transmission electron microscopy image from Shen et al, 2011 showing junctional complexes between two villous enterocytes. The tight junction (TJ) is just below the microvilli (Mv), followed by the adherens junction (AJ). The desmosomes (D) are located basolaterally [Shen et al, 2011]. C) Classic 'chicken-wire' junctional staining pattern of β -catenin in IEC-6 cell line. Scale bar 20 μm .

Two main classes of transmembrane proteins have now been discovered: firstly, tetraspanning proteins including occludin, tricellulin, marvelD3, the claudins, and tetraspanin [Fujimoto, 1995; Furuse, 1993; Furuse and Tsukita, 2006; Ikenouchi et al, 2005, Van Itallie and Anderson, 2006] and secondly, members of the single membrane spanning junctional adhesion molecule (JAM) family [Ebnet et al, 2004].

The list of known TJ components (Figure 1.2) is likely to be incomplete as the molecular architecture of the TJ and functional interactions of the TJ proteins are still to be defined.

TAMP Family

Occludin, tricellulin and MarvelD3 are part of the TJ Associated MARVEL Protein (TAMP) family that contain a conserved four transmembrane MARVEL domain [Sanchez-Pulido et al, 2002].

Occludin and MarvelD3 are preferentially located at bicellular TJs (bTJs) and tricellulin exclusively at tricellular TJs (tTJ) where it forms a barrier to macromolecules [Ikenouchi et al, 2005; Raleigh et al, 2010; Steed et al, 2009]. Occludin and tricellulin have long carboxyl terminus (C-terminus) tails that share a similar RNA-polymerase II elongation factor (ELL) domain whereas MarvelD3 has a short C-terminus tail [Raleigh et al, 2010].

The TAMPs have distinct but overlapping functions at the TJ and share no sequence homology with the claudins [Krause et al, 2008]. Tricellulin can partially compensate for occludin loss as upon occludin KD it is redistributed to bicellular junctions [Ikenouchi et al, 2005 and 2008]. However, its contribution to TJ barrier function is still undefined [Raleigh et al, 2010; Van Itallie et al 2010].

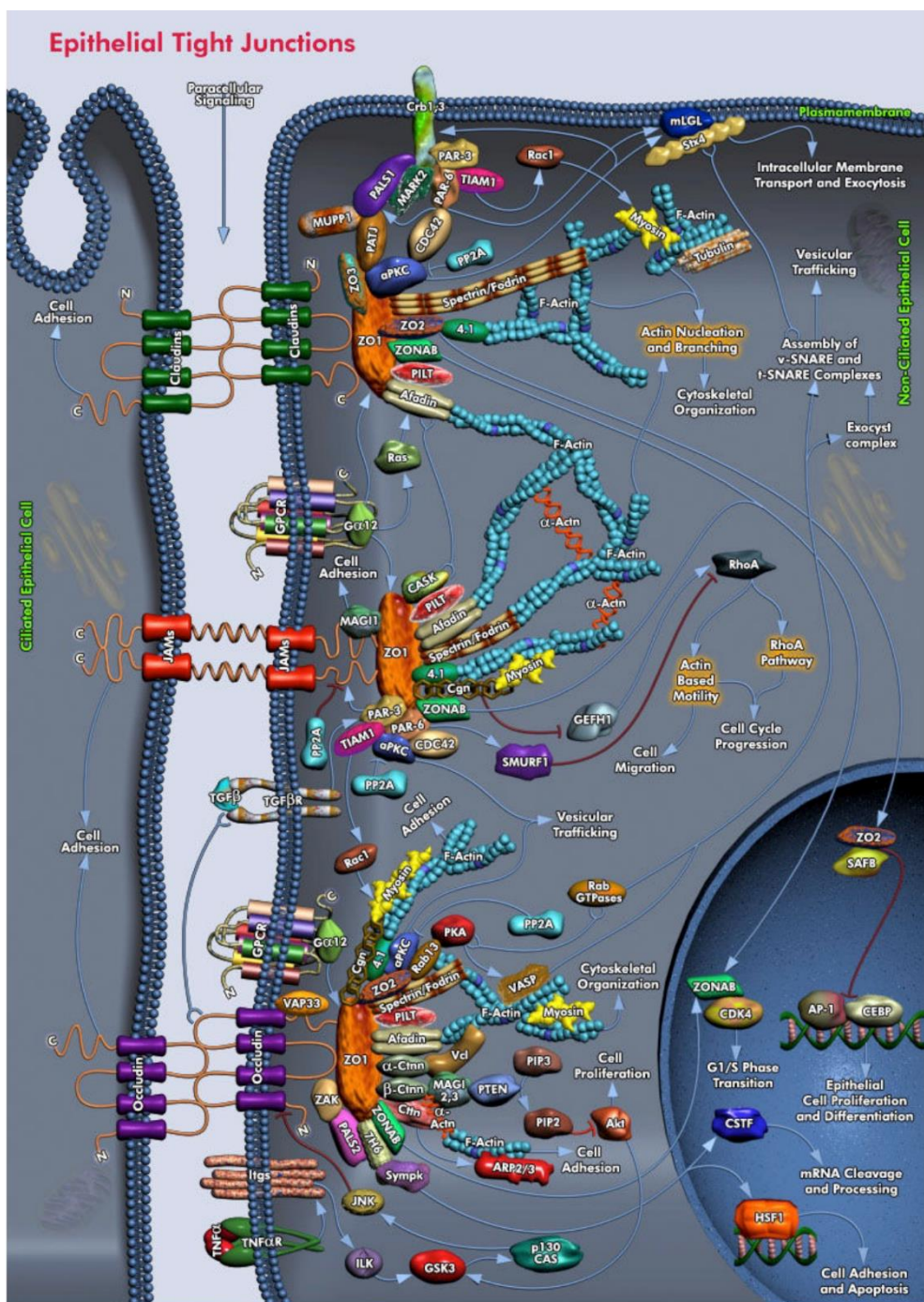


Figure 1.2: Epithelial tight junction structure. Schematic representation of the apical tight junction. Transmembrane occludin, JAMs and claudins seal the paracellular space between adjacent epithelial cells and the cytoplasmic plaque of peripheral scaffolding, adaptor and signalling proteins connect the transmembrane proteins with the structural cytoskeleton and regulate cell polarity, proliferation and differentiation, although the molecular architecture of the TJ is still to be defined. This image is a modification of QIAGEN's original, copyrighted image by Jones, 2015. The original image may be found at www.QIAGEN.com. © 2009 QIAGEN, all rights reserved.

Krug et al, discovered that when tricellulin was only expressed at tTJs, permeability to macromolecules was reduced and when tricellulin was overexpressed and localised to both tTJs and bTJs, permeability to both macromolecules and ions was reduced [Krug et al, 2009]. This suggests tricellulin has an important role in macromolecule permeability associated with the leak pathway. With the knowledge that occludin knockdown (KD) induces the relocalisation of tricellulin to bTJs and remedial occludin expression removes bTJ tricellulin [Ikenouchi et al, 2008], it is likely that tricellulin normally only regulates the leak pathway at tTJs but upon relocalisation to bTJs, partially compensates for occludin regulation of the pore and leak pathways [Furuse, 2010; Krug et al, 2009; Liang and Weber, 2014; Raleigh et al, 2011]. Recently it was shown that the cytoplasmic domain of lipolysis-stimulated lipoprotein receptor (LSR) recruits tricellulin to tTJs [Masuda et al, 2011].

The recently discovered MarvelD3 protein partly co-localises with occludin at bTJs [Steed et al, 2009] and it also immunoprecipitates with both occludin and tricellulin so it seems likely that their functions are also overlapping [Raleigh et al, 2010]. Clearly, all the TAMPs are important for barrier maintenance and further functional analyses are required. This thesis will focus exclusively on occludin.

Occludin

Occludin was discovered by Furuse et al in chicken liver as a 60-65kDa four transmembrane protein and its structure has since been elucidated [Furuse et al, 1993].

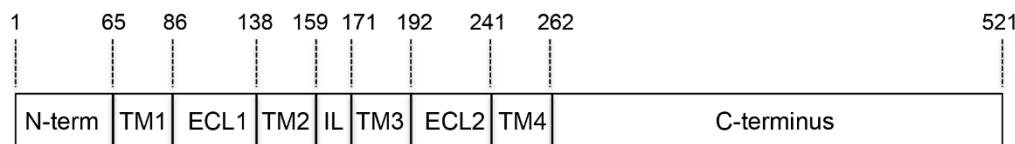
Figure 1.3 illustrates that occludin is a 521 amino acid (aa) polypeptide in mouse or 522 aa polypeptide in humans, consisting of two extracellular loops (ECL), a short intracellular loop (IL), four hydrophobic transmembrane domains (TM), a short cytoplasmic N-terminal domain and a long cytoplasmic C-terminal domain [Furuse et al, 1994].

Both ECL are enriched in tyrosine residues and in ECL1 ~60% of the residues are tyrosine and glycine but the functional significance of this is unclear [Furuse et al, 1993]. *In vitro* studies have demonstrated that post-translational modifications, especially phosphorylation and dephosphorylation of the occludin C-terminus regulate occludin localisation to the TJ as well as paracellular permeability [Balda and Matter, 2008; Rao, 2009].

Many mammalian homologs of the chicken occludin discovered by Furuse et al have since been identified and they all conserve the tetraspan structure along with other distinct structural domains [Ando-akatsuka, 1996; Feldman et al, 2005]. Although the occludin protein structure is well described, the role of differential occludin isoforms is not understood. The Saitou group originally discovered multiple occludin isoforms due to post-translational alternative mRNA splicing [Saitou et al, 1997]. Subsequently, at least four occludin splice variants have been described, which differ in their subcellular distribution and molecular mass [Ghassemifar et al, 2002; Gu et al, 2008; Mankertz et al, 2002; Muresan et al, 2000]. It is thought they may regulate the adhesive properties of the TJ but further investigations are needed to explain their functions.

Since its discovery over 20 years ago, many aspects of occludin structure and function have been studied although its functional role still remains elusive. Occludin has been shown to be a functional component of TJs using *in vitro* epithelial cell lines and *in vivo* models. TJ disruption occurs as a consequence of occludin siRNA KD [Al-Sadi et al, 2011; Raleigh et al, 2010], occludin C-terminus deletion [Balda et al, 1996; Furuse et al, 1994] or occludin overexpression [Balda et al, 1996; Furuse et al, 1993; McCarthy et al, 1996; Wong and Gumbiner, 1997].

A



B

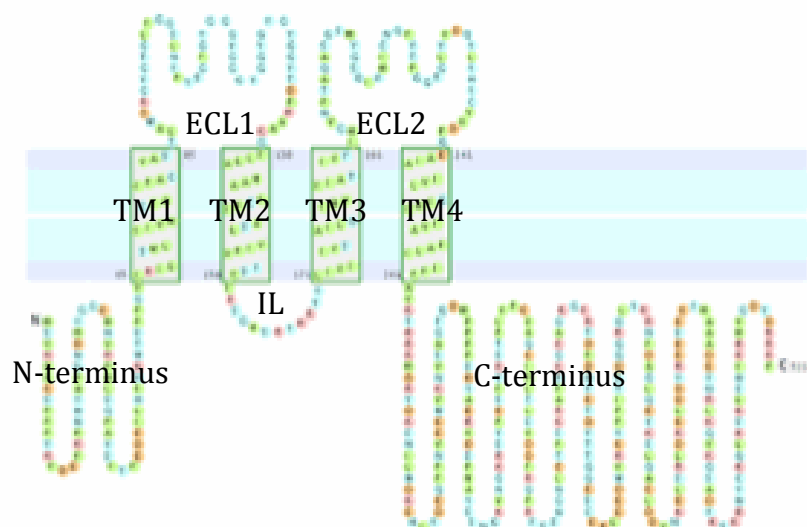


Figure 1.3: Molecular structure of occludin. A) Murine occludin is a 521 aa polypeptide. B) Predicted occludin topology consisting of two extracellular loops (ECL), a short intracellular loop (IL), four hydrophobic transmembrane domains (TM), a short cytoplasmic N-terminal domain and a long cytoplasmic C-terminal domain. Occludin topology predicted by <http://bioinfo.si.hirosaki-u.ac.jp/~ConPred2/>. Image adapted from www.zonapse.net.

With the knowledge that occludin alone cannot form TJ strands the question of whether occludin is required for TJ assembly and function was raised [Saitou et al, 1998]. *In vivo* studies by Saitou et al demonstrated occludin knockout (KO) mice express TJ strands, which are morphologically similar to wild-type mice with no measurable barrier dysfunction in the intestinal epithelium. However, they do present with complex phenotypes such as growth retardation, testicular atrophy, brain calcification and chronic inflammation and hyperplasia of the GI epithelium [Saitou et al, 2000].

These studies suggest occludin is not essential for TJ strand formation but is likely required for paracellular TJ barrier regulation, which explains the disruption of Ca^{2+} absorption in the GI epithelium and gastritis in the occludin KO mice [Saitou et al, 2000; Schulzke et al, 2005]. Similarly, occludin may not be crucial for TJ structure and function, since in its absence, other TJ proteins such as tricellulin or MarvelD3 can partially compensate [Raleigh, 2010; Schulzke et al, 2012].

Claudins

The presence of TJ strands in occludin-deficient cells led to the discovery of claudins, the principle family of integral membrane proteins and the main determinants of the barrier property of the TJ. Claudins-1 and -2 were the first to be identified by Furuse et al and since then 27 claudin family members have been identified in mammals and categorised depending on their function; either pore forming (increase permeability) or barrier sealing (decrease permeability) [Furuse et al, 1998; Krug et al, 2014; Mineta et al, 2011; Schulzke et al, 2012; Tamura and Tsukita, 2014]. In the mouse, claudins -1, -3, -4, -5, -11, -14, -18 and -19 are described as barrier-forming whereas -2, -7, -10, -15, -16 and -17 as pore-forming [Tamura and Tsukita, 2014]. Claudins are expressed in both a homotypic and heterotypic manner in single TJs [Tsukita et al, 2001] and TJ permeability appears to be dependent on this pattern of

claudin expression along the length of the GIT. In the small intestine and colon claudins -3, -7 and -15 are the most highly expressed although claudins -2, and -15 appear to control the paracellular pore pathway in the intestine [Tamura and Tsukita, 2014; Wada et al, 2013] as confirmed by claudin -2 and -15 double KO mice, which die in infancy as a result of fatal defects in intestinal Na^+ -nutrient transport and ultimately malnutrition [Wada et al, 2013]. Interestingly, SI expression of claudins -2 and -15 alters with age. In infant mice, claudin -2 levels are higher than claudin -15 whereas in adult mice this is reversed [Tamura et al, 2011].

Even along the crypt-villus axis claudins are spatially separated; in adult mice claudin -2 is restricted to the crypt whereas claudin -4 is expressed exclusively at the villus [Fujita et al, 2006; Rahner et al, 2001; Tamura et al, 2011; Van Itallie et al, 2001]. These differences in claudin expression and localisation seem to reflect the different barrier properties of intestinal tract. At the villus tip, claudin-4 forms relatively tight paracellular ion barriers and its removal from the TJ by *Clostridium perfringens* enterotoxin for example, causes a loss of barrier function [Saitoh et al, 2015; Sodona et al, 1999; Van Itallie et al, 2001 and 2008; Winkler et al, 2009; Zeissig et al, 2007]. While at the more 'leaky' crypt, claudins-2 or -15 increase TJ ion permeability but maintain a barrier to macromolecules [Amasheh et al, 2002; Wada et al, 2013]. Increased claudin -2 expression has also been implicated in bacterial transmigration of the SI epithelium [Zhang et al, 2013]. Similarly, significantly increased TJ expression of claudin -2 alongside downregulation or redistribution of claudin -4 away from the TJ is observed in both CD and UC patients. This leads to an increased number of pores that allow paracellular flux of Na^+ , which contribute to decreased paracellular permeability and may explain the symptoms of leak-flux diarrhoea [Prasad et al, 2005]. Increased claudin-1 expression has been linked to IBD as well as tumour growth and metastasis in experimental models, suggesting changes in claudin expression may have undesired consequences [Turner, 2009]. In addition to expression changes, some groups suggest TJ permeability could be regulated simply by

displacement of pore-forming claudins by barrier-forming claudins, as demonstrated by the displacement of claudin-2 from the TJ by claudin-8 and subsequent increase in barrier function [Angelow et al, 2007; Shen et al, 2011]. However, it remains poorly understood how different claudins interact with other TJ proteins such as occludin in the intestinal epithelium.

Recently, pioneering work by Suzuki et al solved the crystal structure of claudin-15, which gave an insight into the architecture of the TJ [Suzuki et al, 2014]. Linear claudin polymers were proposed to assemble into the membrane in double rows and associate with claudin polymers on an adjacent cell membrane, forming strands of charge-selective ion pores parallel with the membrane plane and punctuating the paracellular space (Figure 1.4) [Suzuki et al, 2015]. A disulphide bond between conserved extracellular cysteines appeared to be important for this pore formation but it is still not clear how the extracellular domains of different claudin molecules coordinate to assemble pores [Li et al, 2013; Suzuki et al, 2014 and 2015].

Junctional Adhesion Proteins

The JAM family of proteins has at least four members including JAM-A, -B, and -C and the more distantly related JAM-4, JAM-L and coxsackie and adenovirus receptor (CAR) [Coyne and Bergelson, 2005; Liu et al, 2000; Mandell and Parkos, 2005].

They are all part of the immunoglobulin family of adhesion proteins with a long extracellular domain consisting of two immunoglobulin (Ig) loops formed by disulphide bonds and a short intracellular C-terminal domain containing a PDZ (The post-synaptic density 95/Drosophila discs large/ZO-1) binding motif [Martin-Padura et al, 1998]. It seems these proteins are not directly responsible for TJ permeability but may contribute to TJ assembly and modulation [Monteiro and Parkos, 2012; Van Itallie and Anderson, 2014].

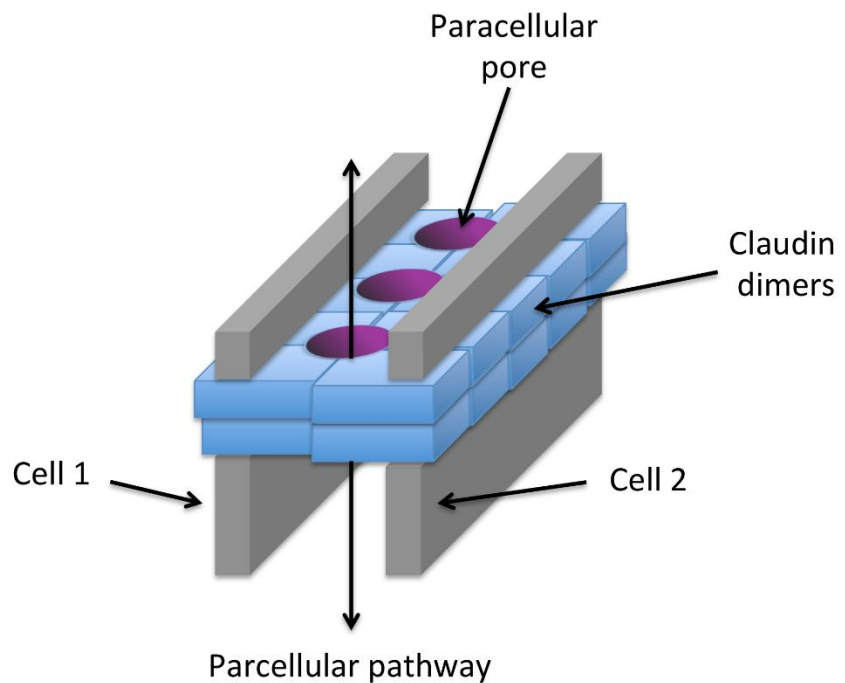


Figure 1.4: Architecture of claudin paracellular pores. Schematic model of the proposed paracellular TJ structure. Claudins dimers in trans on neighbouring cell membranes and in cis on the same cell membrane form polymers within TJ strands and create paracellular pores that regulate the paracellular ion flow. Claudin polymers (blue). Cell membranes (grey). Putative charged β -barrel pores (purple). Arrows indicate the proposed paracellular ion flow. Image adapted from Suzuki et al, 2015.

For example siRNA KD of JAM-A increased permeability of epithelial cells and inhibited TJ reassembly [Liu et al, 2000; Mandell et al, 2004]. JAM-A KO mice presented increased GI permeability and developed intestinal inflammation [Laukoetter et al, 2007; Vetrano et al, 2008] whereas JAM-4 overexpression in mice decreased paracellular permeability to dextran [Hirabayashi et al, 2003].

Similarly, CAR overexpression leads to an increase in TJ barrier function [Cohen et al, 2001], although it should be noted that these findings are yet to be confirmed *in vivo*.

1.2.2 Tight Junction Function

The two established functions of the epithelial TJ are widely described as resembling a ‘gate’ and ‘fence’. Firstly, the ‘gate’ function refers to the TJ barrier that regulates the selective transport of ions and solutes (e.g. nutrients) and water through the paracellular pathway and prevents the transmigration of microorganisms (commensal and pathogenic) and antigens (bacterial or food) [Cereijido et al, 2008; Diamond, 1977; Gumbiner, 1987; Schneeberger and Lynch, 1992]. As TJs are incapable of active transport, as achieved by transcellular transporters, the TJ forms a gradient to drive passive paracellular transport in the appropriate direction across the lumen [Turner et al, 2014]. Secondly, the ‘fence’ function maintains polarity of the plasma membrane by restricting the diffusion of lipids and proteins between the apical and basal membrane domains. [Tsukita et al, 2001].

A direct measurement of the TJ barrier or ‘gate’ function *in vitro* is the measurement of transepithelial electrical resistance (TEER) or ion flux across the epithelium of cells grown on porous supports. To obtain these measurements a continuous current is applied via two electrodes either side of the monolayer, passing through both the transcellular and paracellular pathways [Powell 1981]. The transcellular resistance pathway is predominantly controlled by apical and basolateral

membrane transporters whereas the paracellular resistance results from cell-substrate or cell-cell contacts, primarily the TJ [Shen et al, 2011]. Although TEER reflects both transcellular and paracellular resistance, the paracellular pathway exhibits a significantly lower electrical resistance than the transcellular route and accounts for the majority of the measured resistance, between 74-95% of total passive ion flux across the SI epithelium [Fanning et al, 1998; Matter and Balda, 2003; Reuss, 1991].

It should be noted that our ability to study the specific barrier function of the TJ at the ultrastructural level is limited as it is currently not possible to isolate single TJs; therefore TEER reflects averaged resistance measurements across the cultured epithelial monolayer [Liang and Weber, 2014]. Additionally, as TEER is only a measure of ion flux and does not assess size selectivity, the paracellular diffusion of molecular tracers of various sizes is used to evaluate average TJ pore size. For example, the flux of 5kDa FITC-dextran across epithelial monolayers grown on transwell inserts is commonly used as a measure of TJ barrier function. To ensure measured changes in the TJ barrier are not due to loss of TJ function such as collapse of the paracellular pathway, high resolution morphological analysis should be assessed alongside TEER and tracer flux.

Despite their limitations, both TEER and tracer flux measurements are widely used and have resulted in important discoveries, notably that the TJ barrier is not absolute; it is selectively permeable to certain ions and molecules [Anderson et al, 2004; Goodenough and Revel, 1970; Machen et al, 1972]. Significantly, upon discovery that the number of TJ strands was not proportional to TEER, Claude proposed a model in which the TJ strands are punctuated by pores that are either open or closed to regulate paracellular ion flux [Claude, 1978]. More recent high-resolution studies have described at least two pathways of TJ molecule flux: a ‘pore’ pathway that allows the passage of small uncharged solutes and ions of ~4Å and the ‘leak’ pathway that regulates the passage of larger uncharged macromolecules across the epithelium [Van Itallie et al, 2008; Watson et al, 2005]. These pathways are also distinct in their capacity;

the ion-selective ‘pore’ pathway transports large quantities of small solutes and ions whereas the size-selective leak pathway only transports small volumes of larger molecules across the epithelium [Anderson and Van Itallie, 2009; Van Itallie et al, 2009; Weber et al, 2010]. Studies have indicated these two distinct TJ pathways are differentially regulated and there is no correlation between permeability to small ions such as Na^+ and Cl^- or larger macromolecules such as glucose [Heller et al, 2005; Prasad et al, 2005; Turner et al, 1997; Wang, et al, 2005; Weber et al, 2010]. Interestingly, Al-Sadi et al recently suggested occludin expression *in vitro* and *in vivo* is important for specific maintenance of the leak pathway as occludin depletion increased flux of macromolecules, including bacterial antigens, which lead to an inflammatory response [Al-Sadi et al, 2011]. This possible mechanism of TJ opening requires further investigation.

Although a wealth of information about the pore and leak pathways has been obtained over the last 25 years, it has not been possible to confirm the pore opening and closing events due to the resolution required to isolate single TJs. Once these mechanisms have been elucidated, TJ opening and closing events may present novel targets for oral drug delivery to control conditions such as IBD, which are associated with compromised TJ barriers.

In addition to the barrier or ‘gate’ function, TJs also function as a molecular ‘fence’ dividing the epithelial cell plasma membrane into apical and basolateral domains and limiting the lateral diffusion of lipids and integral proteins between these domains [Tsukita et al, 2001]. The polarised localisation of lipids was originally confirmed by insertion of fluorescently labelled lipids into the apical membrane of cultured Madin-Darby canine kidney (MDCK) cells, where they remained [Dragsten et al, 1981; van Meer and Simon, 1986].

Interestingly, occludin has a possible involvement in the lipid diffusion barrier. Fluorescently labelled apical phospholipid sphingomyelin was added to the apical membrane of MDCK cells expressing C-terminally truncated occludin and rather than remaining at

the apical membrane, it was redistributed to the basolateral membrane [Balda et al, 1996]. Highlighting the potential for occludin to be involved in TJ structural integrity.

1.2.3 Tight Junction Regulation

As well as the transmembrane integral proteins described above, peripheral cytoplasmic structural or signalling proteins arrange into multiprotein complexes termed the ‘TJ plaque’, of which at least 40 components have currently been described. This signal transduction to and from the TJ is important for TJ regulation and cross-talk between the TJ and nucleus coordinates gene expression, proliferation and differentiation [Farkas et al, 2012; Matter and Balda 2003]. Figure 1.2 schematically outlines these known adaptor and scaffold proteins that link the integral TJ proteins to the actin cytoskeleton and depicts the types of signalling molecules recruited to the complex [Aijaz et al, 2006; Matter and Balda, 2003; Schneeberger and Lynch, 2004; Tsukita et al, 2001].

The cytoplasmic plaque proteins are divided into two groups, those with and without PDZ domains. The PDZ proteins include ZO-1, -2 and -3 [Beatch et al, 1996; Fanning and Anderson, 2009; Guillemot et al, 2008; Haskins, 1998; Van Itallie et al, 2009; Willott et al, 1993], Par3 and Par6 [Joberty et al, 2000], Pals1 [Straight et al, 2004], PATJ [Shin et al, 2005], GOPC [Lu et al, 2015], Dlg, Scrib and Lgl [Humbert et al, 2003], MUPP-1 [Hamazaki et al, 2002] and the MAGI proteins [Dobrosotskaya et al, 1997]. Structural protein-protein interactions occur between multiple PDZ domains to form a complex molecular scaffold between the integral membrane proteins, cytoskeletal components and signalling molecules at the TJ [Kim et al, 1995]. Non-PDZ proteins include cingulin [Citi et al, 1989], heteromeric G proteins [Balda et al, 1991; Denker et al, 1996], Rab-13 and PTEN [Matter et al, 2005], kinases [Dorfel and Huber, 2012],

phosphatases, Rho GTPases [Matter and Balda, 2003] and NACos [Matter and Balda, 2009].

Some TJ adaptor proteins form connections with AJ proteins, connecting components of the epithelial junctional complex. For instance, TJ-associated ZO-1 interacts with AJ-associated β -catenin and afadin [Aijaz et al, 2006; Itoh et al, 1997; Rajasekaran et al, 1996; Yokoyama et al, 2001]. Other more peripheral membrane proteins such as cingulin bind directly to adaptor proteins such as ZO-1 or JAM-A and perform both structural and signalling roles at the TJ [Bazzoni et al, 2000; Ebnet et al, 2000; Yano et al, 2013].

Numerous other interactions occur at the TJ between the transmembrane proteins, adaptor proteins and cytoplasmic plaque and these have been reviewed in detail by both Gonzalez-Mariscal et al, and Matter and Balda [Gonzalez-Mariscal, 2003; Matter and Balda, 2003]. These complex multimeric protein interactions are thought to be necessary for correct assembly and organisation of the integral TJ proteins and correct TJ barrier function but their physiology and mechanisms of regulation are still to be elucidated [Fanning and Anderson, 2009; Köhler and Zahraoui, 2005; Matter and Balda, 2003; Steed et al, 2010; Vogelmann and Nelson, 2005].

The cytoskeleton forms a complex structure of protein filaments that extends into the cytoplasm to maintain cell structure. As viewed by EM, an apical belt-like ring of actin, α -actinin and non-muscle myosin II filaments is located immediately beneath the TJ in epithelial cells to allow contraction of the epithelial sheet and these proteins clearly play a critical role in TJ architecture and paracellular permeability [Drenckhahn and Dermietzel, 1988; Glotfelty et al, 2014; Madara, 1987; Mooseker, 1985; Turner and Madara, 1995]. For instance in cultured epithelial cells paracellular permeability is linked to phosphorylation of myosin light chain (MLC) by myosin II light chain kinase (MLCK) or rho-associated protein kinase (ROCK), which activates myosin contractility [Anderson and Van Itallie, 1995; Turner et al, 1997]. Several bacterial toxins also

specifically target the actin cytoskeleton to disrupt the TJ barrier, the best studied being cholera toxin ZOT [Fasano et al, 1995].

TJ connections with the perijunctional cytoskeleton are also essential for assembly of the TJ and maintenance of the TJ barrier and accordingly there are a large number of cytoskeletal proteins associated with the TJ [Van Itallie and Anderson, 2014]. These include a number of actin polymerising proteins including Arp2/3, N-WASP, cortactin and VASP [Ivanov et al, 2005; Katsume et al, 1998; Lawrence et al, 2002; Zhou et al, 2013]. Many cytoplasmic plaque proteins are involved in linking the transmembrane TJ proteins to the actin cytoskeleton, often via binding to ZO proteins [Aijaz et al, 2005; Wittchen et al, 1999]. Examples are the actin-crosslinking protein α -actinin-4, vinculin, α -catenin, anillin and shroom2 [Chen et al, 2006; Etournay et al, 2007; Hildebrand, 2005; Itoh et al, 1997; Reyes et al, 2014; Zemljic-Harpf et al, 2014].

The protein structure of the TJ is known to regulate the TJ permeability barrier by the formation of ion-selective pores and size-selective leak pathways and an insight into this relationship between TJ structure and function was originally provided by studies using latrunculin A to induce barrier loss. As a result of treatment, TJ proteins were redistributed away from the TJ and rapid occludin endocytosis was associated with barrier loss whereas claudin-1 and ZO-1 redistribution occurred much later [Shen and Turner, 2005]. This constant assembly and disassembly of TJ components demonstrates the pronounced plasticity of the TJ. Recently studies using MDCK cells further evaluated occludin trafficking [Fletcher et al, 2014]. The authors discovered a continuous and rapid cycle of occludin endocytosis, recycling and degradation and following internalisation, intracellular occludin was lost from the cytoplasm. Their analysis demonstrated that this loss was due to lysosomal degradation and although ~20% of occludin was recycled back to the plasma membrane via recycling endosomes, the remainder was replaced by newly synthesised occludin [Fletcher et al, 2014; Fletcher and Zappoport, 2014]. Occludin internalisation pathways include clathrin-mediated endocytosis, caveolar endocytosis and macro-

pinocytosis. *In vitro* occludin at the MDCK cell membrane has only a brief half-life of ~15 minutes with very rapid endocytosis and recycling rates of <1 minute although degradation is much slower at ~53 minutes [Fletcher et al, 2014].

A breakthrough in visualising this rapid turnover came with the use of fluorescence recovery after photobleaching (FRAP) and fluorescence loss in photobleaching (FLIP) techniques used to monitor the trafficking of TJ-associated proteins at steady state. In MDCK cells, TJ proteins were N-terminally tagged with enhanced green fluorescent protein (EGFP) and their mobility assessed [Capaldo and Macara, 2007; Shen et al, 2008]. The study by Shen et al was key in understanding the correlation between TJ barrier function and mobility of the TJ proteins. Figure 1.5 is a schematic depicting the technique used to monitor the exchange of proteins between three cellular compartments, the TJ, the lateral membrane and the cytoplasm. During microscopy, a laser transiently photobleaches the tight junction region of the cell and fluorescence recovery or loss patterns are monitored [Shen et al, 2008].

The mobility of ZO-1, occludin and claudin-1 is distinct and recovery of each occurs from a different pool of unbleached fluorescent proteins. FRAP demonstrated occludin is highly mobile at the TJ and using FLIP, occludin diffused within the TJ and lateral membrane rather than between a cytoplasmic pool [Shen et al, 2008]. When the TJ was photobleached continuously, occludin was progressively lost from around the bleached area and subsequent occludin recovery at the photobleached area was fast and began at the edges of the region and progressed towards the centre (Figure 1.5B) [Shen et al, 2008]. Continuous photobleaching of the cytoplasm further confirmed occludin diffusion occurs only within the membrane, as fluorescence was not lost at the TJ [Shen et al, 2008]. The authors also discovered claudin-1 recovery at the TJ was slow and exchange occurred exclusively within the TJ. In contrast, ZO-1 recovery was simultaneous at the centre and edges of the photobleached region and continuous bleaching of the cytoplasmic region caused progressive loss of ZO-1 fluorescence at the TJ, suggesting

ZO-1 exchange occurs between the TJ and a cytoplasmic pool [Shen et al, 2008]. This constant ZO-1 exchange suggests the TJ proteins do not always form a stable protein complex with ZO-1 [Shen, 2012].

Raleigh et al discussed whether ZO-1 could be an intermediate between occludin and claudins -1 and -2 [Raleigh, 2011]. The C-terminus of occludin interacts with the SH3-hinge-GuK unit of ZO-1 [Bal et al, 2012] and subsequently the ZO-1 PDZ domains bind to the C-terminus of claudins [Itoh et al, 1999]. However, Cording et al dismissed this interaction as in their study the C-terminus of the claudins was inaccessible to ZO-1 due to a fluorescent tag yet there were still claudin co-polymerisation with occludin. In fact, the authors presented quantitative fluorescence resonance energy transfer (FRET) evidence for direct molecular interactions between all the TAMPs and claudins [Cording et al, 2013]. The TAMPs themselves were able to form homophilic and heterophilic complexes as well as heterophilic complexes with members of the claudin family and a particularly strong interaction was observed between claudin-1 and all TAMPs which drastically reduced their membrane mobility [Cording et al, 2013]. Co-immunoprecipitation between recombinant occludin and claudin-1 confirmed the occludin C-terminus coiled-coil domain mediates these cis-interactions but the interaction sites were not identified [Cording et al, 2013]. Clearly, the mechanisms that anchor claudin-1 to the TJ remain to be determined.

The exact correlation between dynamic exchange of proteins at the TJ and barrier regulation at steady state is still being investigated and *in silico* computer modelling will be a useful tool for mechanistic analysis of TJ structure and assembly as it has so far been difficult to study at a molecular level [Rossa et al, 2015; Zhang et al, 2013]. It is probable that stimuli which alter the TJ barrier within minutes such as inflammatory cytokines or pathogen infection may also influence the exchange of TJ proteins in order to open the TJ barrier without changing levels of protein expression and this will be investigated as part of this thesis.

A common pathway of TJ regulation in response to these stimuli is MLCK activation of the perijunctional actomyosin ring [Turner, 2009]. Similar to Na^+ -nutrient co-transport, cytokine induced MLCK activation appears to rapidly and reversibly increase paracellular flux through the leak pathway [Clayburgh et al, 2004; Turner et al, 1997] but not the pore pathway regulated by claudins, consistent with the fact that claudins do not directly interact with actin [Turner, 2009]. Of interest here, increased MLCK activation has been associated with IBD [Blair et al, 2006] as well as pathogenic infection by *E. coli*, *H. pylori* and Giardia [Scott et al, 2002; Wroblewski et al, 2009].

However, the mechanism of TJ regulation by MLCK is not defined; MLCK phosphorylation of MLC within the perijunctional actomyosin ring activates myosin ATPase and causes changes to circumferential cytoskeletal tension and contraction but how this opens the paracellular pathway is unclear [Turner, 2009]. Interactions between perijunctional actin and ZO-1, occludin, claudins and other TJ proteins are likely to play an important role alongside mediators such as myosin ATPase, Rho kinases and AMP-activated kinases [Scharl et al, 2009; Shen et al, 2006; Van Itallie et al, 2009].

Although in progress, much work is still to be done to fully understand the connection between TJ architecture, barrier function and paracellular permeability of the pore and leak pathways. This is an area of great interest at present and considerable research is currently being undertaken to piece together a high-resolution three-dimensional model of the TJ molecular structure. Molecular characterisation of TJ barrier regulation will also be essential for the development of novel therapies for intestinal infectious and inflammatory diseases.

1.3 Tight Junction Interactions with the Immune System

The SI TJ forms a dynamic barrier between the external contents of the lumen and the internal tissues. However, the large surface area and selectively permeable barrier of the SI, required for nutrient and water absorption, means the SI epithelium is exposed to a vast array of luminal food antigens and pathogens [Turner, 2009]. Although bacterial colonisation of the SI is low in comparison to the colon, diverse interactions also occur with commensal microbiota [Salzman et al, 2007; Yurist-Doutsch et al, 2014]. Consequently, the SI epithelium is the primary site of contact between luminal antigens and the underlying mucosa-associated lymphoid tissue (MALT) [Turner, 2009].

The dynamic cross-talk between IECs and the underlying immune system protects the host from potentially harmful pathogens whilst maintaining ‘tolerance’ to food antigens or commensal microbiota [Turner, 2009]. This is essential as an inappropriate immune response can lead to allergy or chronic inflammatory disease when directed towards dietary antigens or the microbiota [Mayer, 2003; Mowat, 2003].

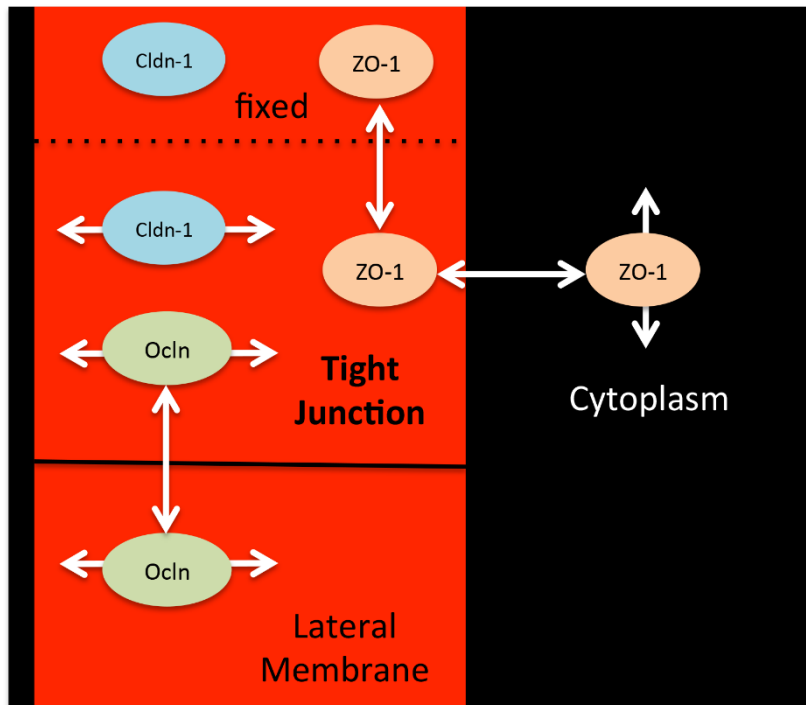
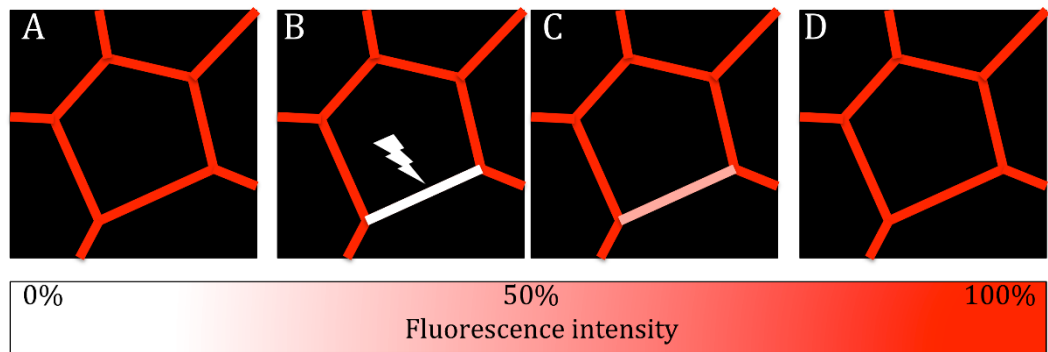


Figure 1.5: Tight junction dynamics assessed by fluorescence recovery after photobleaching. A) Before laser pulse. B) A laser is used to transiently photobleach a region of labelled TJ proteins. C-D) Time-course of fluorescence recovery after photobleaching. E) Recovery occurs from within three cellular compartments: TJ, lateral membrane and cytoplasm. Claudin-1 is largely fixed at the TJ, occludin exchanges with a small lateral pool (20% of total) and ZO-1 is immobile at the TJ and exchanges with an intracellular pool. Image adapted from Weber, 2012.

The first line of SI defence against infection is the physical barrier of the TJ as well as mucus from goblet cells, which traps bacteria, viruses and pathogens, which are subsequently expelled from the SI by peristalsis [Juge, 2012; Lamont, 1992; Pelaseyed et al, 2014].

Mucus also contains antimicrobial peptides (AMPs) such as defensins, cathelicidins and C-type lectins secreted from Paneth cells, which directly kill luminal bacteria, as well as proteolytic enzymes that facilitate digestion of polypeptides and IgA that limits bacterial association with IECs [Hooper and Macpherson, 2010; Mayer, 2003; Salzman et al, 2007].

The second line of defence is created by leukocytes such as macrophages, dendritic cells (DCs), B cells, T cells and intra-epithelial lymphocytes (iIELs), which are distributed throughout the SI epithelium, within the lamina propria and as organised aggregate follicles such as Peyer's patches [Brandtzaeg et al, 2008; McGhee and Fujihashi, 2012; Mowat et al, 2003].

As part of the rapid innate immune response, intestinal macrophages and immature DCs act as phagocytes to clear transmigrating commensal and pathogenic bacteria [Banchereau et al, 2000; Neiss et al, 2005; Schultz et al, 2009; Stagg et al, 2003]. Rescigno et al, also described immature DCs as expressing TJ proteins such as occludin, claudin-1 and ZO-1, which establish TJ-like structures with neighbouring epithelial cells [Rescigno et al, 2001]. By forming these TJ-like structures *in vivo*, the authors suggest DCs open TJs, extend dendrites through the paracellular space to directly sample bacteria from the lumen then shuttle them across the epithelium, whilst maintaining the epithelial barrier [Niess et al, 2005; Rescigno et al, 2001; Rimoldi et al, 2004]. Of interest here, the presence of occludin in these dendrites appears to be sufficient to loosen the TJ contacts, allowing DCs to compete with TJ occludin and open up the TJ like a zip [Rescigno et al, 2001], a mechanism used by *Entamoeba histolica* to alter epithelial barrier function [Goplen et al, 2013] that could potentially be utilised by *T. gondii*. Subsequent DC acquisition of bacterial antigens from the lumen also causes occludin

disappearance from DCs, detachment from TJs and migration to draining lymph nodes [Rescigno et al, 2001], a mechanism that is exploited by pathogens such as *T. gondii* to disseminate through the body. It should be noted that the existence and purpose of these trans-epithelial dendrites remains controversial [Knoop et al, 2013; Nicoletti et al, 2009].

The SI epithelium also contains intestinal intraepithelial lymphocytes (iIELs) located at the basolateral membrane between IECs, which form another line of defence against pathogens and maintain intestinal homeostasis through immune surveillance and regulation of the mucosal immune system [Allison and Havran, 1991; Guy-Grand et al 1991; Inagaki-Ohara et al, 2005; Kaufmann, 1996]. iIELs include conventional T cells as well as subsets of cells expressing a restricted repertoire of T cell receptors including $\gamma\delta$ T cells and $\alpha\beta$ T cells [Cheroutre et al, 2011; Ismail et al, 2011] but their function is poorly understood [Edelblum et al, 2012].

$\gamma\delta$ iIELs constitutively express occludin, JAM-A and ZO-1 as well as AJ β -catenin and E-cadherin which may play a role in preservation of the TJ during pathogen infection, although unlike DCs, they do not cross the epithelial TJ [Alexander et al, 1998; Cepek et al, 1996; Edelblum et al, 2012; Inagaki-Ohara et al, 2005]. The lateral location of $\gamma\delta$ iIELs between epithelial cells suggests they are an important constituent of the TJ barrier and their absence or depletion is associated with increased susceptibility to infection by enteric pathogens [Andrew and Carding, 2005; Mixter et al, 1994]. Understanding the mechanism of $\gamma\delta$ iIEL interactions with the intestinal epithelium and mucosal immune system for the detection and eradication of pathogens, whilst maintaining tolerance to the commensal microbiota, will be important for development of therapeutics against intestinal pathogen infection. Other immune cells in the SI include eosinophils and mast cells, which are involved in allergic reactions and responses to parasitic worms and natural killer cells (NK cells) that recognise and eradicate abnormal cells such as tumour cells and virus infected cells [Mowat and Agace, 2014].

As described earlier in this chapter, the TJ is affected by stimuli such as cytokines [Turner, 2009; Van Itallie et al, 2008; Watson et al, 2005]. An increase in TNF, IL-1 β and IL-16 leads to TJ disruption [Turner, 2009]. TNF-induced MLCK activation in IBD and CD causes increased paracellular flux through the leak pathway as well as immune cell activation, including increased lamina propria T cells and DC migration to the lamina propria as well as enhanced mucosal IFN γ , TNF and IL-10 [Baert et al, 1999; Blair et al, 2006; Clayburgh et al, 2006; Su et al, 2009; Turner et al, 1997; Wang et al, 2005]. However, the link between TJ barrier loss and intestinal inflammation remains controversial. Data from both patients and mouse models confirm that defects in the TJ barrier alone are not sufficient to cause intestinal inflammation [Turner, 2009]. Watson recently raised the question of whether a breech in the TJ barrier causes inflammation or if barrier loss is actually a consequence of inflammation [Watson, 2015]. This is of clinical relevance because intestinal permeability is increased in CD and celiac disease patients as well as their apparently healthy or presymptomatic relatives [Hollander et al, 1986; Katz et al, 1989; Ukbam et al, 1983]. It appears that an increase in TJ barrier permeability, possibly due to an abnormal immune response to food and microbiota-associated antigens, and immune cell activation are both required to promote the onset of IBD. This is further illustrated by both antibiotic use in controlling CD and the absence of the microbiota preventing intestinal disease in animal models of IBD [Balish and Warner, 2002; Ewaschuk et al, 2006].

The diverse interactions between epithelial TJs and the immune system in response to stimuli such as cytokines, luminal antigens and pathogens highlights the importance of understanding the mechanisms of TJ regulation. This indicates a key requirement for further investigation of the barrier function of the epithelial TJ to both aid our understanding of IBD pathogenesis and to elucidate the role during *T.gondii* infection. Therefore, the in vitro model of the SI utilised in this study provides an important insight into this mechanism as it eliminates the immune cells in order to strictly observe *T.gondii* interactions with the TJ.

1.4 *Toxoplasma gondii*

In 1908 Splendore, Nicolle and Manceaux simultaneously isolated a new parasite from rabbits and the African rodent *Ctenodactylus gundi* that was subsequently named *Toxoplasma gondii* in recognition of its bow-like shape [Kim and Weiss, 2008]. It is a ubiquitous protozoan obligate intracellular parasite of the phylum Apicomplexa that infects all warm-blooded animals from mammals to birds and causes toxoplasmosis in humans [Su et al, 2003].

T.gondii is recognised as a significant worldwide zoonotic being one of the most significant sources of food-borne disease worldwide [Kortbeek et al, 2009] and the most common food-bourne parasitic infection requiring hospitalisation [Vaillant et al, 2005].

T.gondii infection is also associated with considerable economic consequences including production losses due to abortion and stillbirth in livestock, equating to the loss of 1.5-2 million animals per year in Europe in 2007 [Buxton et al, 1998; da Silva and Langoni, 2009; Innes et al, 2009; Wang and Yin, 2014]. In France, a national programme for detection and treatment of toxoplasmosis in pregnant women has reduced the rate and severity of congenital infections but the assays have been proven to be poorly reliable and not cost effective [Hill and Dubey, 2002; Villard et al, 2013]. Other significant human pathogen species in the phylum Apicomplexa include *Plasmodium*, *cryptosporidium* and *Neospora* [Carruthers, 2002].

The success of *T.gondii* in global pathogenesis is linked with its broad host range and ability to rapidly cross the restrictive biological barriers of the intestine, blood-brain, blood-retina and placenta [Barragan and Sibley 2002; Smith, 1995].

1.4.1 *Toxoplasma gondii* Life Cycle and Unique Morphology

T.gondii undergoes both a sexual life cycle that occurs only in the feline (definitive host) and an asexual cycle that occurs in all infected hosts (intermediate hosts). A brief overview is presented below and outlined in Figure 1.6. The primary cat host is infected by any of the three infective forms of *T.gondii*, tachyzoites, bradyzoites or sporozoites and ultimately parasites are released as oocytes into the environment [Dubey et al, 1998]. One cat can shed 100 million parasites into the environment per day during acute infection, effectively increasing the likelihood for infection of the next host [Mittal and Ichhpujani, 2011]. Once ingested by intermediate hosts such livestock, mice or humans, the oocysts resist degradation in the stomach and eventually rupture and release bradyzoites into the intestinal lumen [Dubey et al, 1998]. After invasion of SI epithelial cells, the parasites convert into proliferative, motile tachyzoites. These tachyzoites then undergo an asexual lytic cycle [Hoff and Carruthers, 2002] of intracellular growth and multiplication within epithelial cells by endodyogeny before cell rupture and egress of tachyzoites into both the lamina propria and lumen followed by invasion of surrounding SI epithelial cells and dissemination to secondary sites of infection, activating an immune response (acute phase). This immune response causes conversion from tachyzoites to bradyzoite cysts in muscles and the brain (chronic phase) [Blader and Saeij, 2009; Courret et al, 2006]. These slow-replicating dormant cysts persist for the life-time of the host without causing disease but in rare cases, such as if the individual becomes immunocompromised, the cysts rupture causing conversion back to tachyzoites that cause systemic disease and possibly death of the host [Lyons et al, 2002].

Tachyzoites, bradyzoites and sporozoites are morphologically similar although they present specific surface antigens and their polar composition of organelles and inclusion bodies are distinctive. *T.gondii* tachyzoites and bradyzoites express a number of glycophosphatidylinositol (GPI)-anchored surface proteins [Nagel and

Boothroyd 1989; Tomavo et al, 1989], the most abundant of which are members of the surface antigen-1 (SAG1) or SAG2 families [Boothroyd et al, 1998; Burg, 1988; Kasper et al, 1983; Lekutis et al, 2000; Manger et al, 1998] which are differentially expressed during the different *T.gondii* life stages [Lekutis et al, 2001]. *In vitro* bradyzoites primarily express SAG2 whereas tachyzoites primarily express SAG1 and SAG3 [Lekutis et al, 2000 and 2001]. Interestingly, SAG1 has been demonstrated as a critical ligand for promoting tachyzoite attachment and invasion of host cells [Grimwood and Smith, 1992; Mineo et al, 1993; Mineo and Kasper, 1994]. It has also been suggested that SAG2 and SAG3 facilitate rapid parasite invasion [Burg et al, 1988; Cesbron-Delauw et al, 1994; Dzierszinski et al, 2000; Prince et al, 1990; Tomavo, 1996].

T.gondii ultrastructure [Dubey et al, 1998] reveals many specialised polar organelles and inclusion bodies as illustrated in Figure 1.7. These include the outer pellicle membranes, apical microtubule-containing conoid, secretory rhoptries and micronemes, dense granules and the plastid-like apicoplast [Dubey et al, 1998]. All parasite life forms possess similar numbers of rhoptries (ROPs) whereas tachyzoites have few micronemes compared to bradyzoites and more dense granules [Dubey et al, 1998].

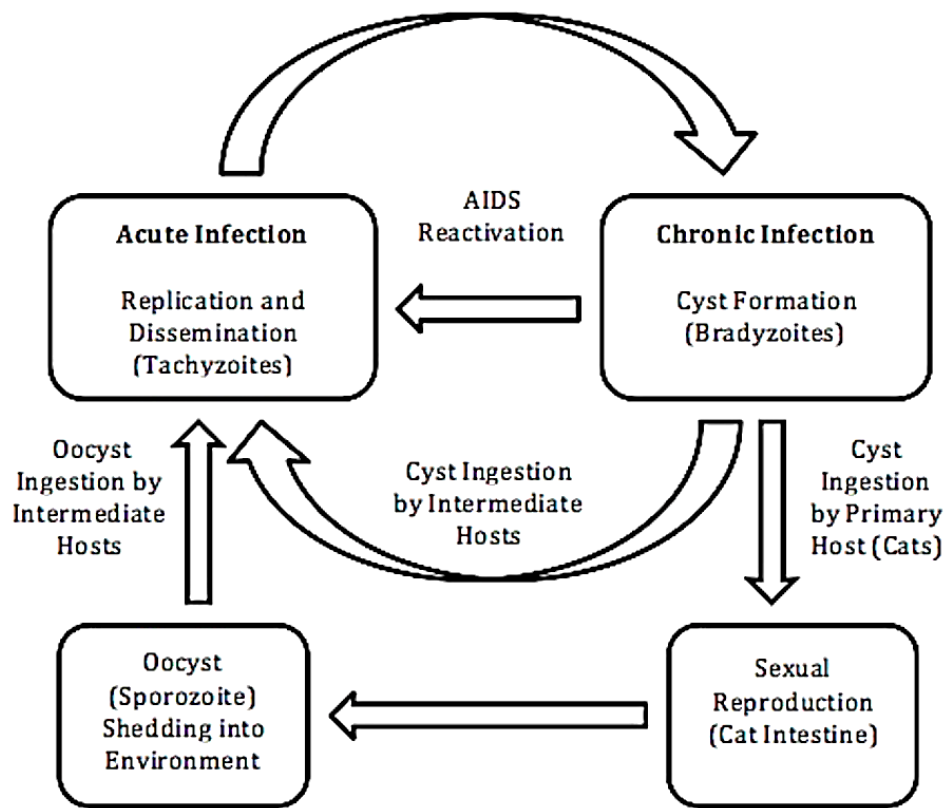


Figure 1.6 *Toxoplasma gondii* life Cycle. Oocysts containing sporozoites shed from the feline gut are ingested by intermediate hosts such as livestock, mice or humans. Proliferative, motile tachyzoites undergo replication and dissemination, activating an immune response and causing the initial acute stage of infection. Immune activation induces conversion to the bradyzoites and cyst formation during the chronic stage of infection. Re-activation of the acute stage of infection can occur following immune suppression such as experiences by individuals with AIDS. If the cysts are re-ingested by the primary feline host, sexual reproduction can occur within the feline intestine.

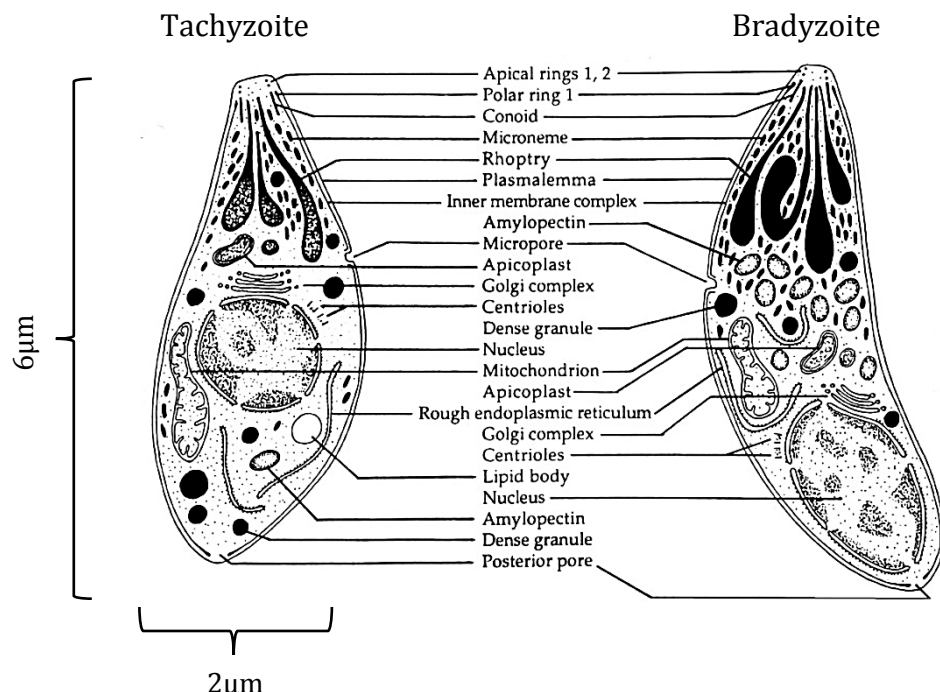


Figure 1.7: *T. gondii* bradyzoite and tachyzoite ultrastructure. Schematic drawings of *T. gondii* tachyzoites (left) and bradyzoites (right). Bradyzoites are slender with a pointed apical conoid and rounded posterior end. Various organelles and inclusion bodies including rhoptries, micronemes and dense granules are present and the nucleus is situated towards the posterior end. The nucleus is situated towards the centre of the cell and the rhoptries are electron dense. Tachyzoites are structurally similar with a crescent shape, more a centrally located nucleus and fewer, less dense rhoptries. Tachyzoites measure approximately 6μm by 2μm. Image adapted from Dubey et al, 1998.

1.4.2 Toxoplasmosis

Toxoplasmosis is widespread throughout the world and in the United States and the United Kingdom it is estimated that 16–40% of the population are infected, whereas in Central and South America and continental Europe, estimates of infection range from 50-80% [Cook et al, 2000; Dubey and Beattie, 1988; Jones et al, 2001].

T.gondii infection arises by various routes in both humans and veterinary hosts. The highly virulent tachyzoite stage undergoes vertical transmission across the placenta barrier during pregnancy and is thus frequently associated with abortion, especially in sheep [Lindsay and Dubey, 2011]. Rarely, humans are infected by blood transfusion or organ transplantation from an infected donor [Derouin et al, 2008]. Most commonly, infection is acquired by oral ingestion of bradyzoite tissue cysts in raw or undercooked meat, particularly pork or lamb [Tenter et al, 2000], similarly by oral ingestion of sporulated oocysts from cat faeces infected soil, food or water that is dependent on water quality and hygiene [Bahia-Oliveira et al, 2003; Bouzid et al, 2008; Isaac-Renton et al, 1998; Jones and Dubey, 2012]. The occurrence of waterborne infection led to the classification of *T.gondii* as a National Institute of Allergy and Infectious Diseases (NIAID) category B priority agent [Kim and Weiss, 2009].

Increased awareness of the hazard to pregnant women caused by contaminated cat faeces as well as the risk of undercooked meat has seen a decrease in worldwide toxoplasmosis [Kim and Weiss 2008]. Improved animal husbandry has also played an important role [Tenter et al, 2000]; keeping cats away from pig houses for example drastically reduced *T.gondii* infection of pork in the USA [Dubey, 2009].

Immunocompetent individuals usually present no signs of infection other than mild flu-like symptoms due to host immune system evasion by the parasite and 80-90% of *T.gondii* infections go unrecognised [Mittal and Ichhpujani, 2011]. In the immunocompromised, particularly those with HIV/AIDS, infection is associated with severe

pathology including ulceration, encephalitis and systemic infection caused by breakdown of the epithelial barrier and bacterial translocation from the lumen to the lamina propria [Dupont et al, 2012; Heimesaat et al, 2006; Kim and Weiss, 2008; Montoya and Lissenfeld, 2004].

If treated quickly with drugs such as pyrimethamine and sulfadiazine before tissue destruction occurs, clinical symptoms can be reduced but no drugs currently available eradicate all parasites [Weiss and Dubey, 2009]. Despite its clinical importance, relatively few drugs against *T.gondii* are currently available and only one vaccine Toxovax is available for use in sheep and goats, although it requires cold storage and has a short shelf life [Garcia, 2009; Innes et al, 2011].

The most common clinical pathologies presented in association with acquired immunodeficiency include ocular toxoplasmosis and infection of the central nervous system (CNS) [Montoya and Remington, 1996; Porter and Sande, 1992]. Interestingly, recent studies have also detected possible rodent behavioural changes associated with chronic *T.gondii* infection. Infection influences the behaviour of mice and rats in order to heighten their contact with cats, thereby increasing the likelihood of parasite transmission to the primary cat host by carnivorousness [Vyas et al, 2007]. The effect on human behaviour has been a subject of great interest. A number of reports have linked *T.gondii* infection with neurological disorders such as schizophrenia [Derouin et al, 2002; Hinze-Selch et al, 2007; Yolken et al, 2001] or increased risk of being in a car accident [Flegr et al, 2002], although verifying this connection may prove a challenge.

Clearly the propagation of parasites across the intestinal TJ barrier to secondary tissues is a critical factor in *T.gondii* pathogenesis and elucidating these mechanisms will be critical for development of targeted therapeutics preventing parasite spread.

1.4.3 *Toxoplasma gondii* Host Infection and Dissemination

As the most common route of human infection is through oral ingestion, the first point of contact between parasites and host is the GIT. Therefore, although *T.gondii* infects most cell types, the SI epithelium is the primary target for parasite invasion before tachyzoites ultimately enter the host circulation and disseminate to secondary tissues [Dubey et al, 1997; Jones and Dubey, 2012; Speer et al, 1998]. *T.gondii* use a variety of strategies to quickly disseminate through the SI, often taking only 15-40 seconds [Carruthers and Boothroyd, 2007; Egarter et al, 2014; Werk, 1985]. Using mouse models tachyzoites rapidly disseminate to all organs of the body and are detected in the Peyer's patches and lymph nodes within two days post infection (p.i), in the ilium within five days p.i, and in the brain and heart by ten days p.i [Courret et al, 2006; Dubey et al, 1997]. Importantly, *T.gondii* tachyzoites transmigrate across epithelial cells in vitro within minutes, providing a valuable laboratory model of SI epithelial infection [Barragan and Sibley, 2003; Lei et al, 2005; Weight and Carding, 2012].

The crucial step for *T.gondii* establishment of infection and subsequent parasite survival and proliferation is parasite attachment to, and invasion of host cells, thus evading host defences [Lei et al, 2005]. For over 20 years it has been known that host cell laminin, lectins and SAG1 act as receptors for tachyzoite attachment and invasion [Furtado et al, 1992; Kasper and Mineo, 1994; Robert et al, 1991]. Since then various mechanisms of host cell infection have been described and it is likely *T.gondii* disseminate using a combination of strategies. For example, some sporozoites and bradyzoites pass completely through host cells prior to invasion of neighbouring cells [Dzierszinski et al, 2004; Speer et al, 1997].

The transcellular or active penetration invasion mechanism has been well described for *T.gondii* tachyzoites, bradyzoites and sporozoites [Morisaki et al, 1995] and as *T.gondii* lacks cilia or flagella, host cell entry

involves an unusual form of gliding motility [Dobrowolski et al, 1997; Plattner et al, 2008].

Transcellular invasion occurs in a series of stages, as depicted in Figure 1.8, including host cell attachment, conoid extension, parasite reorientation, secretion of organelle contents and moving junction (MJ) formation [Carruthers and Boothroyd, 2007]. The parasite then actively enters the cell through the MJ into the non-fusogenic parasitophorous vacuole (PV) using its actomyosin motor complex before separating from the host plasma membrane [Carruthers and Boothroyd, 2007].

Ten years ago Barragan et al first described a significant proportion of tachyzoites clustering within 5µm of an intercellular junction during early infection as well as observing parasites between host cells, adjacent to TJs, which suggested parasites utilise the paracellular route to actively cross the epithelial barrier, avoiding damage to the epithelium and subsequent initiation of an inflammatory response as well as bypassing intracellular replication. Further evidence was provided by the fact that transmigration of the parasites did not alter monolayer barrier integrity. These observations led to the authors to investigate parasite- and host-derived molecules involved in *T. gondii* attachment and invasion. Host recombinant ICAM-1 (intercellular adhesion protein-1) was first found to be upregulated on cellular barriers during transmigration but not cellular invasion, confirmed by human ICAM-1 antibodies inhibiting parasite transmigration [Barragan et al, 2005]. Subsequent ICAM-1 immunoprecipitation identified *T. gondii* MIC2, a microneme adhesion protein secreted from the apical microneme organelle onto the parasite surface, to be involved in parasite transmigration of the host epithelium in order to disseminate to deeper tissues [Carruthers and Tomley, 2008].

Although parasite-host interactions clearly play a role in parasite transmigration, as demonstrated by ICAM-1 interaction with MIC2, it has not been confirmed how parasite binding to host molecules facilitates paracellular transmigration.

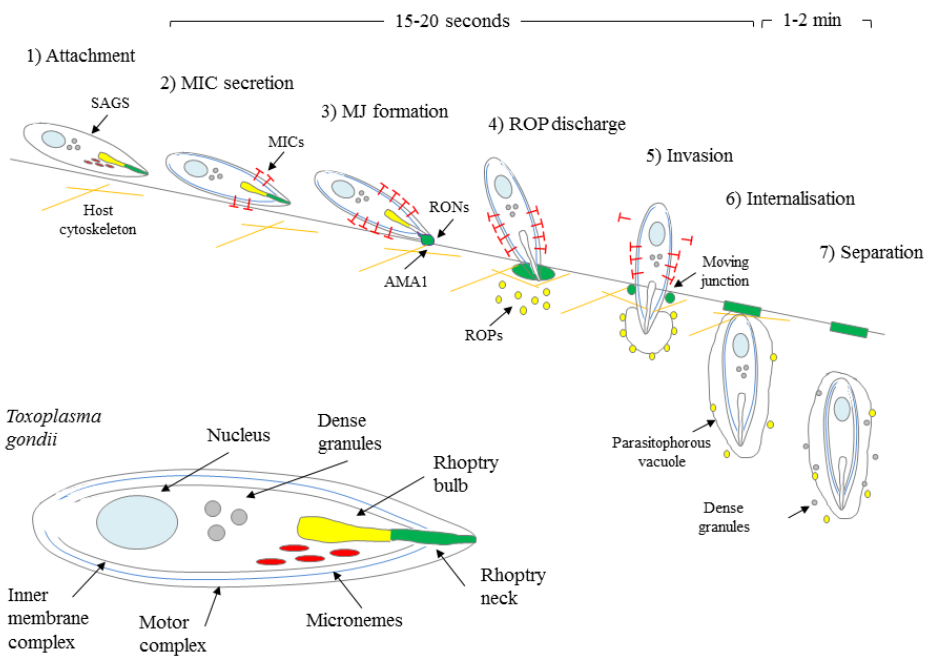


Figure 1.8: *T. gondii* transcellular invasion mechanism. 1) Initial attachment to the host cell surface via SAGs precedes 2) conoid extension, release of MICs and apical attachment. 3) Invasion is initiated by secretion of RONs and association with microneme-derived AMA1, which forms the ring-like MJ. 4) The parasite re-orients and ROPs are discharged from rhoptries into the host cytoplasm where they associate with the developing PV or remain soluble. 5) The parasite actively invades through the MJ, creating the invaginated PV. 6) Once internalised, the PV is closed and 7) the parasite separates from the host plasma membrane and dense granules are released and associate with the PVM. Steps 2-5 take only 15-20 seconds whereas the final steps 6-7 take 1-2 minutes. Magnified view of tachyzoite (inset). Figure adapted from Carruthers and Boothroyd, 2007.

As the molecular mechanism behind this route of *T. gondii* transmigration of the SI is still not understood, it will be investigated as part of this thesis.

1.4.4 *Toxoplasma gondii* Virulence Factors

Potential disease outcome of *T. gondii* infection is highly dependent on parasite virulence. Surprisingly, *T. gondii* population biology has identified only a few dominant strains; serology samples from humans and domestic or farm animals from North America and Europe were grouped into clonal lineages termed types I, II and III [Howe and Sibley 1995; Sibley and Ajioka, 2008] and the recently discovered haplotype 12 [Khan et al, 2011]. The clonal types are closely related [Saeij et al, 2005] and possess different virulence within and between host species; type I is most virulent in mice, type II in humans, type III in livestock and type 12 in wild animals [Boothroyd and Grigg, 2002; Howe and Sibley, 1995; Khan et al 2011]. These differences are also reflected in human disease; ocular toxoplasmosis in humans is associated with Type I but not type II or III strains [Grigg et al, 2001].

The Institute for Genomic Research (TIGR) has generated near complete genomes of the GT1, ME49 and VEG strains of *T. gondii* (Types I, II and III respectively) and the Wellcome Trust Sanger Centre complemented this with the sequencing of chromosomes 1A and 1B from strain RH (Type I) [Khan et al, 2006]. This data including genome sequences is freely available at the genome database ToxoDB available at www.toxoDB.org [Gajria et al, 2008]. This wealth of *T. gondii* genetic information has led to many functional genomics studies.

Although it is unclear how the *T.gondii* population structure evolved, expansion of the lineages dates back ~10,000 years, correlating with the domestication of animals by humans [Su et al, 2003]. The population profile of *T. gondii* also has a clear divide between Europe/North America and South America, as the majority of human cases of toxoplasmosis in Europe/North America are associated with

Type II strains whilst in South America higher incidence of Type I is reported. [Ferreira et al, 2008; Howe et al, 1997; Su et al, 2012]. Expressed sequence tag (EST) alignment of the three lineages to the partial ME49 or whole *T. gondii* genome gave an insight into parasite ancestry. Different Types I and III appear to be derived from type II with a very limited number of genetic crosses [Bontell et al, 2009; Boyle et al, 2006]. Forward-genetics and quantitative trait loci (QTL) mapping identified some of the genes responsible for the phenotypic and virulence differences between types I, II and III in mice and they appear to be closely associated with the host immune response [Sibley et al, 2009]. In mice type I are virulent as they cause lethal acute stage infections whereas types II and III are associated with formation of chronic infections [Appleford and Smith, 2000; Howe et al, 1996; Suzuki et al, 1989].

As described above, an important step during *T. gondii* infection is organelle content secretion into the host cell. Consequently, ROP18 has been identified as a major contributor to differences in virulence [Saeij et al, 2006; Taylor et al, 2006]. ROP18 is a secreted serine-threonine kinase that is found on the PV membrane (PVM) surface and expression is high in virulent types I and II but low in type III [Khan et al, 2009]. Subsequent genetic crosses between types likely led to kinases such as ROP16 and ROP5 that differentially regulate host gene transcription [Behnke et al, 2011; Fentress et al, 2012; Reese et al, 2011; Saeij et al, 2007]. It appears that in mice, highly virulent type I strains highly express ROP18 and ROP5, which cooperatively phosphorylate host immunity-related GTPases (IRGs) to inhibit parasite clearance in IFN- γ activated cells [Hunter and Sibley, 2012]. Additionally, *T. gondii* dense granule protein GRA15 is associated with reduced macrophage IL-12 production via transcription factor NFkB in virulent type I strains [Robben et al, 2004]. In contrast, in type II strains ROP5 is avirulent, leading to reduced IRG phosphorylation and less inhibition of parasite clearance. Also, type II GRA15 increases macrophage production of IL-12, resulting in more effective parasite clearance. Type III strains do not express ROP18 so

parasites are effectively cleared [Hunter and Sibley, 2012], which could explain why types II and III are less virulent in mice. Consequently, each strain appears to be adapted for interactions with specific host cellular responses, such as the immune system, in order to propagate infection of the primary feline host [Khan et al, 2009].

In silico approaches are increasingly being used to identify new genes of interest or genetic pathways. For example Chen et al identified 60 candidate *T. gondii* secretory proteins and using protein-protein interaction data, identified potential interactions with the host cell [Chen et al, 2008]. Recently, Lorenzi et al used a comparative genomics approach with 62 strains of *T. gondii* and found both large regions of conserved genes and specific regions enriched in copy number variation (CNV) and tandem duplication. The authors found these regions were associated with secretory pathogenicity determinants (SPDs); genes encoding secretory proteins in MICs, GRA, ROPs and the SRS superfamily that are associated with host transmission and infection. Highly diverse regions were particularly linked to GRA, ROP and SAG genes such as ROP17, ROP5, GRA3 and SAG3 and SAG2A which have been previously implicated in murine virulence differences between strains. In contrast, MICs associated with host attachment were found to be highly conserved, suggesting *T. gondii* strains may utilise a similar repertoire of these host MIC receptors [Lorenzi et al, 2016].

Manipulation of the *T. gondii* genome has also facilitated the creation of KO mutant strains [Saeij et al, 2008] to assess the genetic basis of migration, virulence and growth [Saeij et al, 2005]. For example KO of SAG3 [Dzierszinski et al, 2000], GRA2 [Mercier et al, 1998], MIC1 and MIC3 [Cerede et al, 2005] all decrease *T.gondii* virulence in mice. Of note, incorporation of fluorescent markers such as GFP, YFP or mCherry into the *T.gondii* genome has permitted parasite detection and imaging of processes such as stage conversion or phagocytosis both *in vitro* and *in vivo* [Dupont et al, 2014; Gubbels et al, 2003; Hitziger et al, 2005; Unno et al, 2009; Zhang et al, 2013]; a property utilised in this thesis.

The work in this thesis aims to further our understanding of parasite host interactions by investigating host cell modulation during infection using the IEC-6 cell line.

1.5 *Toxoplasma gondii* Interactions with Occludin

Since Barragan et al, 2005 first described the exploitation of the paracellular pathway as a mechanism of infection by *T. gondii*, the role of TJ proteins, particularly the transmembrane proteins, during infection has begun to be investigated [Barragan et al, 2005].

In 2006, Dalton et al identified an increased susceptibility to infection and an *in vivo* change in occludin distribution in response to *T. gondii* or *Salmonella typhimurium* infection of mice lacking $\gamma\delta^+$ iELs. Within one hour of infection of wild type mice there was a striking redistribution of occludin and ZO-1 to the apical TJ, whereas in KO mice no redistribution occurred. The difference in occludin redistribution observed in $\gamma\delta^+$ iEL KO mice was linked to an absence of occludin serine phosphorylation and lack of claudin-3 and ZO-1 at the TJ [Dalton et al, 2006]. The authors concluded that $\gamma\delta^+$ iELs played a critical role in maintaining TJ integrity and barrier function in response to *T. gondii* infection in mice [Dalton et al, 2006].

Following on from this Weight, 2011 confirmed a role for occludin in *T.gondii* infection [Weight, 2011; Weight and Carding, 2012]. The authors assessed the previous findings using m-IC_{c12}, a murine SI epithelial cell line [Bens et al, 1996]. In accordance with Barragan et al, 2005, the authors found tachyzoites cluster to cellular junctions and transmigrate through the SI epithelial barrier without altering barrier function [Weight, 2011]. After establishing that occludin was the only TJ protein affected by parasite infection, they found the parasite co-localises and interacts with occludin and a route of invasion was speculated: parasites cluster to cellular junctions and move between cells, associating with the extracellular loops of occludin which aids migration through the

paracellular pathway. It was also found that during *T. gondii* infection, occludin was displaced from the TJ to an intracellular compartment, suggesting a change in phosphorylation status [Weight, 2011].

The work presented in this thesis will further investigate *T.gondii* infection mechanisms *in vitro*, with a focus on the role of occludin, using a SI epithelial cell line.

1.6 Rationale

The small intestinal permeability barrier is dependent on TJ complexes that separate the external lumen from the underlying mucosa. Apical TJs consisting of integral transmembrane proteins including occludin, form a dynamic multimolecular complex that selectively regulates the paracellular transport and flux of ions and molecules through the small intestinal epithelium. Being the first point of contact between host and luminal pathogens and toxins, the small intestinal epithelial TJ complex also constitutes a highly resistant barrier, preventing chronic infection of the underlying tissues. Occludin forms part of a complex that seals the paracellular space between neighboring cells and this pathway can be targeted by the pathogenic protozoan parasite *T. gondii* to transmigrate the epithelium, although the mechanism of paracellular invasion is unclear. The redistribution of occludin to and from the tight junction during *T. gondii* invasion of the small intestine is associated with occludin phosphorylation status. Further investigation is required to determine the role of occludin in *T. gondii* transmigration of the small intestine and is presented in this thesis. The findings will extend the current understanding of pathogen infection of the small intestine and potentially present novel targets for future therapeutics.

1.7 Hypothesis

T. gondii infects the SI epithelium via the paracellular pathway and occludin plays a key role both in regulation of the TJ paracellular barrier by acting as a receptor for *T. gondii* infection by direct binding and by parasite-mediated modulation of the occludin C-terminus phosphorylation status.

1.8 Aims

The role of the SI epithelial TJ barrier during *T. gondii* infection will be investigated to increase our current understanding of the molecular mechanisms of *T. gondii* paracellular transmigration of the epithelium. Following on from the study by Weight, the importance and role of occludin during *T. gondii* infection will be examined.

- Visualise *T. gondii* paracellular transmigration of SI epithelial cells using an *in vitro* model
- Ascertain the involvement of TJ-associated proteins in *T. gondii* infection
- Identify changes in occludin phosphorylation in response to *T. gondii* infection
- Determine if *T. gondii* directly interacts with occludin and if so what the molecular basis of the interaction with occludin is

2 Materials and Methods

2.1 Commercial Suppliers

All general reagents and materials were purchased from Sigma-Aldrich unless otherwise stated. A full list of reagents, antibodies, cell stains and suppliers are provided in Tables 2.1 and 2.2.

2.2 Cell Line Culture

Rat SI epithelial cell line (IEC-6) [Quaroni et al, 1979] were obtained from the European Collection of Cell Cultures (ECACC) and maintained by serial passage in DMEM (Lonza, Basel), supplemented with 2mM/L L-glutamine, 0.1 IU/ml Insulin and 5% FBS (Biosera) at 37°C in 5% CO₂/95% air atmosphere.

Murine small intestinal epithelial cell line (m-IC_{c12}) provided by Alain Vandewalle (Inserm U246, Paris, France, [Bens et al, 1996]), were maintained by serial passage in 1:1 DMEM:HAMS12 (Lonza) supplemented with 2mM/L L-glutamine, 0.1 IU/ml Insulin and 5% FBS (Biosera) at 37°C in 5% CO₂/95% air atmosphere.

2.3 *T. gondii* Culture

The type 1 RH strain of *T. gondii* tachyzoites stably expressing YFP [Gubbels and Striepen, 2003] were maintained by continuous passage in confluent monolayers of Hs27 HFF (European Collection of Cell Cultures) in DMEM supplemented with 2 mmol/L l-Glutamine and 10% FBS at 37C in 5% CO₂. Pelleted parasites were collected after 90% HFF lysis by centrifugation at 1000 g for 15 min.

Product	Supplier	Catalogue No.
35 mm µ-dishes	IBIDI	81156
13mm glass coverslips	BDH	631-0149
660nm Protein Assay kit	Pierce	22660
660nm protein assay kit	Pierce	22660
Amicon Ultra 0.5ml 1kDa Centrifugal Filter	Merck Millipore	UFC5003BK
ATP	NEB	P07565
CellTracker™ Red CMPTX	Molecular Probes	C34552
CKII enzyme	NEB	P60105
CKII peptide substrate	Promega	V5661
Collagen I	Sigma	C7661
Criterion XT MES	BioRad	1610789
Criterion XT precast Bis-tris gel 10% IPG+1 well comb 11cm	BioRad	3450115
DePeX	BDH	101410-638
DMEM	Lonza	BE12-604F
<i>E. coli</i> Rosetta2 (DE3) pLysS	Novagen	71403
E.Z.N.A Plasmid DNA Mini Kit	Omega Bio-tek	D6942
FBS	Biosera	FBS1000HI
Fibronectin	Sigma	F1141
FITC-dextran 3-5kDa	Sigma	FD4-100MG
Float-a-lyzer	Spectrum Labs	G235027, G235065
GelCode Blue	Thermo Scientific	24590
Glutanyl Endopeptidase	Roche Diagnostics	11814021
Halt protease and phosphatase inhibitor cocktail	Thermo Scientific	78441
HAMSF12	Lonza	BE12-719F
Hs27 HFF	ECACC	94041901
IEC-6	ECACC	88071401
Immobiline DryStrip 11cm pH3-11NL	GE Healthcare	17-6003-74
Immobiline DryStrip cover fluid	GE Healthcare	17-1335-01
Immobiline IPG buffer pH3-11NL	GE Healthcare	17-6004-40
Kinase buffer	NEB	9802
L-Arg-HCl	Invitrogen	32460
L-Lys-HCL	Invitrogen	32461
Matrigel	Corning	356237

Table 2.1 List of reagents. Continued p64.

Product	Supplier	Catalogue No.
mem-PER plus membrane protein extraction kit	Thermo Scientific	89842
m-PER mammalian protein extraction kit	Thermo Scientific	89842
Nexterion Slide H	Schott	1070936
Ni-NTA agarose	Qiagen	30230
Ni-NTA Superflow Columns	Qiagen	30622
NuPAGE antioxidant	Invitrogen	NP0005
NuPAGE Bis-Tris gels	Invitrogen	NP0302
NuPAGE Bis-Tris gels	Invitrogen	NP0342
NuPAGE Bis-Tris gels	Invitrogen	NP0322
NuPAGE LDS sample buffer	Invitrogen	NP0007
NuPAGE MES	Invitrogen	NP0002
NuPAGE MOPS	Invitrogen	NP0001
NuPAGE reducing agent (10x)	Invitrogen	NP0004
NuPAGE transfer buffer	Invitrogen	NP0006
PBS	Lonza	17-517Q
pET15b	Novagen	69661
p-NPP	NEB	P0757S
ProLong Gold antifade mountant with DAPI	Invitrogen	P36935
ProQ Diamond	Invitrogen	P33300
PVDF membranes	Invitrogen	LC2002
<i>Pvu</i> 1 restriction enzyme	NEB	R0150
Quant-IT protein assay kit	Molecular Probes	Q33210
SILAC Media Kit	Invitrogen	MS10030
SpectraGel Absorbant	Spectrum Labs	292600
SuperSignal West Pico Chemiluminescent substrate	Pierce	34080AB
SYPRO Ruby	Invitrogen	S12000
Transwell 24 well hanging PET Inserts, 8 µm pore size	BD Biosciences	CLS3422-48EA
Trypsin Gold	Promega	V5280
Vectashield anti-fade mounting medium with DAPI	Vector Labs	H-1500

Table 2.1 List of reagents.

Product	Supplier	Catalogue No.
Biotin-XX goat anti-rabbit IgG	Invitrogen	B2770
CellTracker Red CMPTX dye	Molecular Probes	C34552
Cy5 conjugated goat anti-mouse IgG	Jackson Immunoresearch	115-175-166
Donkey anti-goat IgG FITC-conjugate	Santa Cruz Biotechnology	sc2024
Donkey anti-goat IgG HRP-conjugate	Santa Cruz Biotechnology	sc2020
Donkey anti-goat IgG Texas Red-conjugate	Santa Cruz Biotechnology	sc2783
Donkey anti-mouse IgG HRP-conjugate	Santa Cruz Biotechnology	sc2314
Donkey anti-rabbit IgG HRP-conjugate	Santa Cruz Biotechnology	sc2313
GAPDH anti-rabbit IgG	Santa Cruz Biotechnology	sc25778
Goat anti-occludin C-terminus	Santa Cruz Biotechnology	sc8144 (C19)
Goat anti-occludin ECL	Santa Cruz Biotechnology	sc27151 (Y12)
Goat anti-rat IgG HRP-conjugate	Santa Cruz Biotechnology	sc2006
Goat anti-rat IgG-texas red conjugate	Santa Cruz Biotechnology	sc2782
Hoechst 33342	Invitrogen	H1399
IgG controls	Vector Labs	BA-4000
IgG controls	Vector Labs	I-5000
IgG controls	Vector Labs	I-2000
IgG controls	Vector Labs	I-4000
Mouse anti-β catenin	BD Biosciences	610154
Rabbit anti-occludin	Invitrogen	71-1500
Rat anti-ZO-1	Santa Cruz Biotechnology	sc33725
Rhodamine labelled peanut agglutinin	Vector Labs	RL-1072

Table 2.2: List of antibodies and cell stains.

2.4 Alkaline Phosphatase Assay

IEC-6 cells cultured in plastic 25cm² flasks were rinsed twice with 1ml 1xPBS, removed from the flask using a cell scraper and transferred to a 15ml Falcon tube and centrifuged at 600×g for 5 minutes and the supernatant discarded. The pellet was re-suspended in 100μl *p*-Nitrophenyl Phosphate (p-NPP) solution (1mg/ml n-NPP (NEB) in 10mM diethanolamine, 0.5mM MgCl₂, pH 10.5) for 20 minutes at RT. Adding 50μl 1N NaOH stopped the reaction and the *p*-nitrophenol product absorbance was read at 405nm and compared to a standard curve of ALP activity (U).

2.5 Immunocytochemistry

IEC-6 cells plated onto the apical compartment of polyethylene terephthalate (PET) cell culture transwell inserts (8μm pore size, BD Biosciences) within a 24 well plate were washed in 1xPBS, fixed in either 2% formaldehyde for 20 minutes or acetone for 5 minutes followed by 5 minutes in rehydration buffer (1% BSA in 1xPBS). Cells were then permeabilised with 0.2% Triton X-100 for 10 minutes and incubated with blocking buffer (0.2% Triton X-100, 3% BSA, 3% goat serum, 3% fish skin gelatin in PBS) for 1 hour. All reagents were added to both the apical and basal compartments of PET inserts. The PET membranes were extracted from the insert and incubated with primary antibodies including occludin (Invitrogen), ZO-1 (Santa Cruz) and β-catenin (BD Biosciences), diluted in blocking buffer for 20 hours at 4°C. Controls consisted of either no primary antibody or isotype matched antibodies. Membranes were washed 3 times in 1xPBS prior to secondary or tertiary antibody incubation for 2 hours at RT in a humidified chamber in the dark. A 1:1 mixture of Rhodamine-peanut and -wheat germ agglutinin (Vector Labs) was used to visualise surface cell carbohydrates. The membrane was mounted by placing cell side up on a glass microscope slide with DePeX

(BDH), Vectashield with DAPI (Vector Labs) or ProLong Gold with DAPI (Invitrogen) and covering with a glass coverslip and storing at 4°C in the dark. To visualise intracellular parasites, IEC-6 cells grown on PET inserts were infected with *T. gondii* for 2 hours before removing and washing with 1xPBS to remove unattached parasites prior to PET membrane extraction, fixation with 2% formaldehyde, permeabilisation, incubation and mounting as above.

2.6 Fluorescence or Confocal Microscopy

After mounting slides, fluorescence microscopy images were viewed using an inverted Zeiss AxioVert 200M microscope with the 40x objective unless otherwise stated. Images were analyzed on LSM software or AxioVision image viewer. Confocal microscopy images were viewed using an upright or inverted LSM510 META on a Zeiss AxioVert 200M microscope. Z stacks were composed of 1µm interval sections with the 40× objective unless stated otherwise. To visualize occludin by Z stack, cells were marked for the apical and basal membrane using rhodamine labelled surface carbohydrates and the surface of the PET membrane. Rhodamine and Texas Red fluorochromes were excited by the 543nm laser, YFP-RH *T. gondii* and Alexa Fluor 488 by the 488nm laser, DAPI, Hoechst or Pacific Blue by the 405nm laser and Cy5 by the 633nm laser. All laser intensities were consistent within and between experiments.

2.7 Immunoblotting

IEC-6 cells cultured in plastic 25cm² flasks were rinsed with 1ml ice-cold 1xPBS, removed from the flask using a cell scraper and transferred to a chilled Eppendorf. Cells were lysed using either m-PER or mem-PER protein extraction kits (Thermo Scientific) supplemented with Halt protease and phosphatase inhibitor cocktail (Pierce) and 50 mmol/L

phenylmethysulfonyl fluoride (PMSF) according to the manufacturer's instructions. Protein quantification was determined using the 660nm protein assay kit (Pierce). Samples were separated using NuPAGE Bis-Tris pre-cast gels (10%, 12% or 4-12%, Invitrogen). 10-20 μ l samples were prepared for SDS-PAGE by adding NuPAGE LDS sample buffer (4x), NuPAGE reducing agent (10x) and deionized water and heating at 70°C for 10 minutes. 1x SDS running buffer was prepared by adding 50ml of 20x NuPAGE MES or MOPS SDS running buffer (Invitrogen) to 950ml of deionized water. The upper chamber of an XCell SureLock mini-cell gel running tank (Invitrogen) was filled with 200ml 1xSDS running buffer and 500 μ l NuPAGE antioxidant. The gels were placed in the gel tank and the tank filled with 1x running buffer prior to gel loading alongside a pre-stained molecular marker (10-170kDa, Fermentas). When using MES running buffer gels were run for 35 minutes at 200V constant and when using MOPS running buffer gels were run for 50 minutes at 200 V constant.

Immunoblotting was carried out using the using the XCell II Blot Module (Invitrogen) according to manufacturer's instructions. Briefly, after electrophoresis, proteins were transferred onto pre-cut PVDF membranes (Invitrogen) using transfer buffer consisting of 50ml NuPAGE transfer buffer (20x), 1ml NuPAGE antioxidant, 100ml methanol and 849ml deionized water at 30V constant for one hour. Membranes were subsequently washed, blocked in 5% BSA in Natt buffer (150 mM NaCl, 20 mM Tris Base, 0.1% Tween-20, pH 7.4) for one hour at RT, shaking. Proteins were detected by incubating in 1% BSA in Natt buffer with primary antibodies for 12 h at 4 °C. Membranes were washed 6x for one hour in Natt buffer before addition of secondary HRP conjugates (Santa Cruz) in 1% BSA in Natt buffer for one hour at RT. Membranes were washed as previous before the addition of 1:1 volume of enhanced SuperSignal West Pico Chemiluminescent substrate (Pierce) for 5 minutes and visualisation with a FluorChem E system (ProteinSimple) and Digital Darkroom software (ProteinSimple). Membranes were washed as previous, stripped by incubating in 1:20 dilution acetic

acid:1xPBS for one hour and washed in Natt buffer for one hour prior to probing for a second protein.

2.8 Transepithelial Electrical Resistance (TEER) and Permeability

IEC-6 cells were plated onto the apical compartment of PET cell culture transwell inserts (8 μ m pore size, BD Biosciences) within a 24 well plate. TEER measurements were performed using an Epithelial Tissue Volt Ohmmeter 2 and Endohm chamber (EVOM, World precision instruments) voltmeter to assess paracellular ion flux across the epithelium. TEER values of the cell monolayer were obtained by subtracting the contribution of a blank insert and culture medium. 700 μ l of pre-warmed cell media was placed in the basal Endohm compartment and 200 μ l in the apical insert compartment before being allowed to equilibrate to 15 minutes. Ohm's law was then used to calculate resistance using the equation:

$$Resistance = (R_c - R_i)\pi r^2$$

Where R_c is the resistance of the cells on the insert, R_i is the resistance of the insert and r is the radius of the insert.

The insert was then placed back in the 24 well plate and barrier permeability assessed by measuring the diffusion of 1000 μ g/ml FITC-conjugated dextran (3 - 5kDa, 1mg/ml; Sigma-Aldrich) from the apical to basal compartment. Apical and basal media were collected in 1ml Eppendorf's and centrifuged at 1000 $\times g$ for 10 minutes. The supernatant was transferred to a new Eppendorf and 100 μ l transferred to a black 96 well microplate. The concentration of FITC-dextran was determined from a standard curve (excitation 490nm, emission 520nm).

2.9 Recombinant Occludin Peptides

2.9.1 Cloning of Occludin EC1, ECL2, ECL1+ECL2 and C-terminus into the 6xHIS-tagged expression vector pET15b

DNA regions coding for extracellular loop (ECL) 1 (residues 85 to 138) (184bp) ECL2 (residues 191 to 241) (167bp), ECL1+ECL2 (residues 85 to 241) (485bp) and C-terminus (residues 261 to 521) (800bp) murine occludin fragments were PCR amplified from pBABE-FLAG + Occ plasmid DNA (Britta Engelhardt, Theodor Kocher Institute, University of Bern, Switzerland) [Bamforth et al, 1999] (Appendix A) using the following primer pairs: ECL1-F, ATGCCATATGACACTTGCTTGGACAG-3' and ECL1-R, 5'- AGCAGCCGGATCCTAGCCTTGGCTGCTCTGGGT-3' (full length ECL1); ECL2-F, 5'-ATGCCATATGATAATGGGAGTGAACCC-3' and ECL2-R, 5'-ATGGATCCTACTGGGGATCAACCACAC-3' (full length ECL2); ECL1-F, 5'-ATGCCATATGACACTTGCTTGGACAG-3' and ECL2-R, 5'-ATGGATCCTACTGGGGATCAACCACAC-3' (full length ECL1+ECL2); and C'-F, 5'- ATGCCATATGGCTGTGAAAACCGAAG-3' and C'-R, 5'-ATGGATCCTAAGGTTCCGTCTG-3' (full length C-terminus). PCR products were cloned into the *Nde*I and *Bam*HI sites of the expression vector pET15b (Novagen) (Appendix A) and sequence-verified prior to transforming *Escherichia coli* Rosetta2 (DE3) pLysS (Novagen). Occludin C-terminus, ECL1+ECL2 and ECL2 were previously cloned by Nikki Horn (Institute of Food Research) [Weight, 2011] and ECL1 cloned by E. Jones and Dr Duncan Gaskin (Institute of Food Research) as part of this thesis. The ECL1 sequence was verified by Eurofins (UK) using primers: ECL1-F 5'-TCACCCTGGATGCTGTAGGCA-3' and ECL1-R 5'-CGATCTTCCCCATCGGTGAT-3'.

2.9.2 Purification of Occludin ECL1, ECL2, ECL1+ECL2 and C-terminus peptides

E. coli expressing His-tagged-protein products were purified using Ni-NTA agarose and Ni-NTA Superflow Columns (Qiagen) under denaturing conditions according to the manufacturer's instructions. 10ml Luria-Bertani (LB) media supplemented with 200 µg/ml ampicillin and 35 µg/ml chloramphenicol were inoculated with *E.coli* containing the recombinant plasmids for 20 hours at 37°C shaking at 250rpm. 2.5ml culture was subcultured into 250ml pre-warmed LB media supplemented with antibiotics in a 2L conical flask and grown at 37°C, 250rpm shaking until the optical density at 600nm (OD₆₀₀) reached 0.6. Expression of occludin was induced by adding 2mM of isopropyl-beta-D-thiogalactopyranoside (IPTG) and incubating at 37°C, 250rpm shaking for until the OD₆₀₀ reached 1.0. The cultures were transferred to ice-cold 50ml falcon tubes and centrifuged at 4000×g for 20 minutes at 4°C. The supernatant was removed and the pellet frozen at -20°C.

Bacterial pellets were thawed and resuspended in 10ml Buffer B (8M urea, 10mM NaH₂PO₄, 10mM Tris-Cl, pH 8.0) and incubated with agitation for 60 minutes at RT before centrifuging at 14,000×g for 30 minutes at RT and retaining the supernatant (cleared lysate: CL). 1ml Ni-NTA agarose was added to Ni-NTA Superflow columns (Quiagen) and washed with Buffer B prior to adding lysate supernatant and collecting the flow through (FT). The Ni-NTA column was then washed with 4ml Buffer C (8M urea, 100mM NaH₂PO₄, 10mM Tris-Cl, pH 6.3) three times and the fractions collected (W1-W3). The occludin peptides were eluted five times with 1ml Buffer E (8M urea, 100mM NaH₂PO₄, 10mM Tris-Cl, pH 4.5) (E1-E5).

Protein quantification was determined using the 660nm protein assay kit (Pierce) and samples were concentrated using 1ml 0.5-1kDa float-a-lyzer dialysis device and SpectraGel Absorbant (Spectrum Labs). Concentrated samples were renatured by removal of the urea in 6

sequential dialysis steps with 50 mM Tris (pH 8) buffer containing 8, 6, 4, 2, 1, 0.5M urea and no urea. All dialysis was performed in the presence of 100 mM NaCl, 10% glycerol and 1 mM PMSF.

2.9.3 Analysis of Occludin EC1, ECL2, ECL1+ECL2 and C-terminus peptides

The purity of the recombinant occludin peptides was determined by SDS-PAGE and GelCode Blue staining (Thermo Scientific) or immunoblotting using antibodies specific for occludin C-terminus and ECL (Cell Signalling) (Figure 2.1). Protein quantification was determined using the 660nm protein assay kit (Pierce) or the Quant-IT protein assay kit (Molecular Probes).

2.9.4 Transmigration and Infection Assay

IEC-6 or m-IC_{cl2} cells were cultured in the apical compartment of PET cell culture transwell inserts (8 µm pore size, BD Biosciences) within a 24 well plate and barrier function assessed every 24 hours by TEER as described in section 2.8. At 7-13 days post-seeding TEER was measured prior to removal of the apical media and re-suspension of 5x10⁶ pelleted RH-YFP *T. gondii* tachyzoites and addition to the apical PET compartment for 2 hours.

3-5kDa FITC-conjugated dextran was added to the apical compartment of some PET inserts to measure barrier function during infection. TEER was then recorded and apical and basal media removed for analysis of permeability as described in section 2.8 and flow cytometry as described below. PET membranes were excised and analysed by immunocytochemistry and confocal microscopy as described in section 2.5.

To visualise attached and intracellular parasites, IEC-6 or m-IC_{cl2} were cultured on 13mm glass coverslips (BDH) for four days prior to addition of 5x10⁶ RH-YFP *T. gondii* tachyzoites for 2 hours before washing and removal of unattached parasites. Cells were fixed in 2% PFA for 20 minutes and permeabilised in 0.2% Triton-X-100 for 10 minutes before H&E counterstaining, mounting as described in section 2.5 and viewing using an inverted Zeiss AxioVert 200M microscope. Images were analyzed using AxioVision image viewer.

Transmigrating parasites were identified from the basal compartment by centrifugation and analysis by flow cytometry using a Cytomics FC500 MPL (Beckman Coulter). Data was analysed post-collection using FlowJo version 10 (TreeStar).

2.10 Live Cell Imaging

IEC-6 were plated onto 35 mm µ-dishes (Ibidi) coated with Matrigel® (Corning) and cultured for four days. Cells were labeled by staining with CellTracker™ Red CMPTX (Invitrogen) prior to apical addition of RH-YFP *T. gondii* tachyzoites immediately before imaging. Images were acquired using a LaVision BioTec TriM Scope II 2-photon microscope (Bielefeld) based on a Nikon Eclipse Ti optical inverted microscope with a Nikon 40x water immersion (Apo LWD λS NA 1.15) objective (Nikon UK Ltd) and a temperature control system (Life Imaging Services). Multi photon excitation was provided by a Coherent Chameleon Sapphire laser (Coherent Inc.) at 1060 nm to simultaneously excite CellTracker™ Red and RH-YFP *T. gondii*. Typical image volumes were 100 × 100 × 27 µm and Z-stacks were separated by 1 µm. Time resolved data were acquired by continuous measuring of Z-stacks for up to 30 min. The frame rate was 51.2 s with these parameters. Images were analysed with the Fiji/ImageJ package.

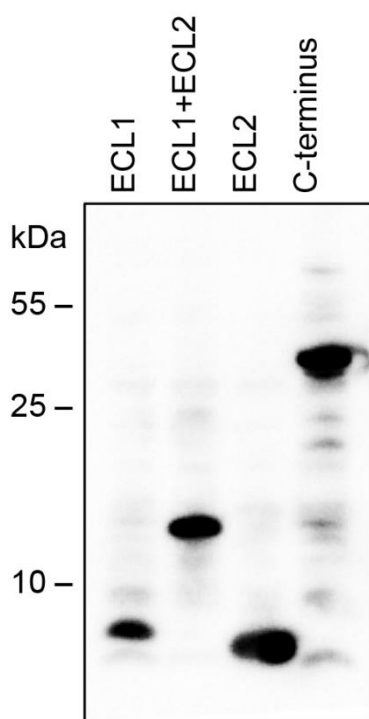


Figure 2.1 Occludin peptide generation. Occludin peptides corresponding to amino acids 85-138 (full length ECL1), 191-241 (full length ECL2), 85-241 (full length ECL1-ECL2) and 261-521 (full length C-terminus) were generated as described in the Materials and Methods section. Peptide purity was assessed by SDS-PAGE and immunoblotting using commercial anti-occludin antibodies (Invitrogen).

2.11 SILAC Proteomic Analysis

The SILAC Protein ID and Quantitation Media kit (Invitrogen) was used according to manufacturer's instructions. IEC-6 cells were cultured on plastic 25cm² flasks for six passages using SILAC DMEM containing either heavy [$\text{U}-^{13}\text{C}_6$]-L-lysine (MW = 152.1259) and [$\text{U}-^{13}\text{C}_6, ^{15}\text{N}_4$]-L-Arginine (MW = 184.1241) or light [$^{12}\text{C}_6$]-L-lysine (MW = 146.1055) and [$^{12}\text{C}_6, ^{14}\text{N}_4$]-L-Arginine (MW = 174.1117) prior to infection of light-labelled 'sample' cells with 2.55×10^7 *T. gondii* (1:10 parasites:cells) and mock infection of heavy labelled 'control' cells with the same volume of media. To dissect the temporal response to infection, a time course of either two hours or twenty-four hours *T. gondii* infection was performed.

Cells from each sample (heavy and light) were trypsinised then lysed using the m-PER kit (Thermo Scientific) to assess incorporation or mixed in a 1:1 ratio and lysed using the Mem-PER kit (Thermo Scientific) to fractionate the samples, as described below. Briefly, cells were washed in 1ml ice cold PBS then scraped into a 2ml Eppendorf prior to centrifugation at 300×g for 5 minutes at 4°C. Pellets were resuspended in 0.5ml ice cold PBS and centrifuged at 300×g for 5 minutes at 4°C. Pellets were next washed in 1.5ml cell Wash Solution (Thermo Scientific) supplemented with Halt protease and phosphatase inhibitor cocktail (Pierce) prior to centrifugation at 300×g for 5 minutes at 4°C. The pellet was then resuspended in 0.75ml Cell Permeabilisation Solution (Thermo Scientific) supplemented with Halt protease and phosphatase inhibitor cocktail (Pierce) prior to centrifugation at 16,000×g for 15 minutes at 4°C and transfer of the supernatant to an Eppendorf (Cytoplasmic Fraction). The remaining pellet was resuspended in 0.5ml Solubilisation Solution (Thermo Scientific) supplemented with Halt protease and phosphatase inhibitor cocktail (Pierce) prior to centrifugation at 16,000×g for 15 minutes at 4°C and transfer of the supernatant to an Eppendorf (Membrane Fraction).

Proteins were separated using NuPAGE Bis-Tris gels (Invitrogen) as described in section 2.7 and proteins stained using GelCode Blue

(Thermo Scientific). Gels were cut into 15 slices prior to being prepared for mass spectrometry. Briefly, gel slices were cut into 1mm cubes, transferred to 1.5ml Eppendorf tubes and washed for 15 minutes in 200mM ammonium bicarbonate (ABC) in 50% (v/v) acetonitrile (1ml) to equilibrate the gel to pH8 and remove the stain, followed by 10 minute incubations in acetonitrile (Fisher) (1ml) to remove excess aqueous solution. Gel cubes were then incubated with 10mM dithiothreitol (DTT) in 50mM ABC (1ml) for 30 minutes at 60°C to reduce any cysteine thiol side chains before being alkylated with 100mM iodoacetamide in 50mM ABC in the dark for 30 minutes. Gel cubes were then washed with two 15 minute incubations in 200mM ABC in 50% (v/v) acetonitrile (1ml) followed by 10 minutes incubation in acetonitrile (1ml) to dehydrate and shrink the gel cubes prior to air drying. The proteins were digested with 200-600ng Trypsin Gold (Promega) in 20-60µl of 10mM ABC. Further known volumes of ABC were added to ensure gel cubes were not dry before incubating at 37°C for 3 hours. Following digest the samples were acidified by incubating with 1% formic acid (same volume as trypsin+ABC) for 10 minutes. The extract peptides were removed and the remaining gel cubes washed with 50% acetonitrile (double the volume of trypsin+ABC+formic acid) to extract further peptides from the gel and combined with the digest samples. The pooled digest samples were then dried on the Medium Drying setting on a Speed Vac SC110 (Savant) fitted with a refrigerated Condensation Trap and a Vac V-500 (Buchi). The samples were then frozen at -80°C prior to analysis. Samples were dissolved in 0.5% formic acid and analysed using an Orbitrap Fusion Tribrid Mass Spectrometer (Thermo Scientific).

The raw MS files were processed by Dr Francis Mulholland (Institute of Food Research) using MaxQuant [Cox and Mann, 2008] and proteins identified by searching against the *Rattus norvegicus* (Rat) UniProt database (downloaded 5.6.14). Search parameters: UniProt rat protein database species, rat; enzyme; trypsin; fixed modifications, carbamidomethylation and oxidation (M). Protein quantitation was performed using MaxQuant to generate heavy and light peptide ratios

(fold-change) and Perseus statistical analysis tool to generate significance-B (p-value <0.05) scores. The raw data was filtered according to >2-fold change (compared to non-infected control) and a Significance-B p-value of <0.05.

2.12 *In Vitro* Occludin Kinase Assay

1ug recombinant occludin C-terminus peptide was incubated with either 200U purified CKII (New England Biolabs), 5µl IEC-6 lysates or 5µl IEC-6 lysates infected with *T. gondii* for 2 hours, prepared as described in section 2.7 in the presence of 1mM ATP (New England Biosciences) in kinase buffer (New England Biosciences) for 30 minutes at RT.

2.12.1 Isoelectric Focussing

Samples were de-salted by adding 480µl Rehydration Buffer (7M urea, 2M thiourea, 2% CHAPS) and concentrated using an Amicon Ultra 0.5ml 3kDa Centrifugal Filter device (Merck Millipore) to 60µl prior to incubation in 140µl Rehydration Buffer supplemented with 0.5M DTT and 1% v/v pH 3-11NL IPG buffer (GE Healthcare) and addition to a re-swelling tray. pH3-11NL IPG strips (GE Healthcare) were placed in the re-swelling tray and covered with 2ml mineral oil and allowed to rehydrate overnight. Isoelectric focussing (IEF) of the occludin C-terminus was performed by transferring the IPG strips to ceramic strip holders, covering in mineral oil and placing on the Ettan IPGphor isoelectric focussing machine (GE Healthcare) with the following parameters: Step and Hold 500VHr, Gradient 500V-1000V (1 hour), Gradient 1000V-6000V (2 hours) and Step and Hold 6000V (40 minutes) (GE Healthcare).

2.12.2 2D Gel Electrophoresis

After IEF the IPG strips were washed in deionized water to remove excess mineral oil and incubated in 5ml Strip Equilibration buffer for 15 minutes (0.122M Tris-acetate, 0.5% w/v SDS, 6M urea, 3% w/v glycerol, 0.01% bromophenol blue) supplemented with 52mM DTT to reduce any cysteine thiol side chains. The IPG strips were then alkylated by incubation in 5ml Strip Equilibration buffer supplemented with 0.135M iodoacetamide in the dark for 15 minutes. The IPG strips were transferred to the top of 11cm pre-cast Criterion XT gels (BioRad) in a Criterion Cell (BioRad) and run using 1xMES buffer (BioRad) and run at 200V constant for 35 minutes.

2.12.3 Gel Staining

Gels were first fixed overnight in 200ml Fixing Solution (50% methanol, 10% acetic acid) and subsequently stained with ProQ Diamond phosphoprotein stain (Molecular Probes). Gels were washed in 200ml deionized water for 10 minutes three times prior to staining with 120ml ProQ Diamond per gel for 90 minutes. Gels were then destained (20% acetonitrile, 50mM sodium acetate pH4) using 160ml solution for 30 minutes three times and washed with 200ml deionized water for 5 minutes twice. Gels were imaged at 50dpi using a Pharos FX+ Imaging System (BioRad) using excitation of 532nm and emission filter at 555nm. Gels were subsequently washed in deionized water for 5 minutes twice before staining for total protein using 120ml SYPRO Ruby (Molecular Probes) overnight prior to destaining (10% methanol, 6% acetic acid) with 200ml solution for 30 minutes and washing in 200ml deionized water twice. Gels were imaged at 50dpi using excitation 532nm and emission filter 555nm. Images were analysed using Quantity One analysis software (BioRad) and protein spots matched using ProteomWeaver 2D Gel Analysis Software (Definiens).

2.12.4 Mass Spectrometry

Samples were prepared for mass spectrometry analysis by Fran Mulholland (Institute of Food Research). Briefly, protein spots of interest were excised from the gel using an Investigator ProPick (Genomic Solutions), put into a 96-well microplate and subjected to in-gel digestion as described above substituting Glutamyl Endopeptidase (Roche Diagnostics) for Trypsin Gold. Samples were analysed using an Orbitrap Fusion Tribrid Mass Spectrometer (Thermo Scientific) and the raw MS files processed by Dr Francis Mulholland (Institute of Food Research). Files were converted to MASCOT Generic Format (mgf) format using MS Convert (<http://proteowizard.sourceforge.net>) and then searched using MASCOT (Matrix Science). Search parameters: MS1 5ppm; MS2 0.5Da; UniProt mouse protein database (downloaded 5.6.14); species, mouse; enzyme; glutamyl endopeptidase; fixed modifications, carbamidomethylation and oxidation (M).

2.13 *T. gondii*-Occludin Binding Assay

IEC-6 cells were plated onto 13 mm diameter glass coverslips (BDH) and cultured for 4 days prior to apical addition of either RH-YFP *T. gondii* tachyzoites (control) or RH-YFP *T. gondii* tachyzoites pre-incubated with 2 µM recombinant occludin peptides for 15 min, for 2 h. To visualize intracellular parasites, IEC-6 cells were permeabilised and H&E counterstained before mounting and imaging of parasitophorous vacuoles using an inverted Zeiss AxioVert 200M microscope. Images were analyzed on AxioVision image viewer with 6–12 fields of view recorded for each slide.

For peptide-parasite binding assays His-tagged occludin peptides or a His-tagged mCherry protein (20 µM in 6 M urea in buffer I (PBS with 1 mM CaCl and 0.05% Tween-20)) were immobilised onto Schott Nexterion H slides (Jena) of a 16-well superstructure in a humidified

chamber for 2 h at 20 °C. Wells were washed in decreasing concentrations of urea (4–0 M) in buffer I then blocking solution for 1 h (25 mM ethanolamine in 100 mM sodium borate buffer). The wells were then washed in buffer I and incubated with YFP *T. gondii* tachyzoites (10⁷ per well) for 2 h at 20 °C. Slides were fixed with 3.7% formaldehyde (FA) prior to mounting and bound parasites were visualized by UV microscopy (Zeiss AxioVert 200M microscope and AxioVision image viewer). Parasites were counted using fluorescent pixel counts at 63× magnification (Adobe Photoshop CS6) with 6–12 fields of view recorded for each well.

2.14 Bioinformatics

To identify novel IEC-6 occludin kinases the bioinformatics ExPASy kinase-specific prediction software NetPhos (version 2.0) and NetPhosK (version 1.0) were used to predict occludin C-terminus phosphorylation sites by searching for homologous kinase target motifs within the occludin C-terminus aa sequence. NetPhos searches were performed using the default settings for parameter limitations. NetPhosK searches were performed using the default settings for parameter limitations set at a threshold of 0.5 and were without filtering.

The murine occludin ECL1, ECL1+2, C-terminus and whole protein aa sequences were BLAST searched against the ME49, VEG and RH *T. gondii* genomes to search for potential binding proteins within the *T. gondii* genome databases at www.toxodb.org using an expectation value of 10, maximum descriptions 500 and low complexity filter.

2.15 Statistical Analysis

All data was assessed for normal distribution using the Kolmogorov-Smirnov test and for homogeneity of variance by the Bartlett's test. For parametric data, an independent *t* test, or a one-way ANOVA was carried out. For non-parametric data the Mann-Whitney U test and the Kruskal-Wallis test was used. Post-Hoc analyzes were carried out with Tukey's Multiple Comparison Test or Dunn's and Dunnett's Multiple Comparison tests. Data was analyzed using Prism GraphPad software (Versions 5 and 6). P values of less than 0.05 were considered significant. *P < 0.05, **P < 0.01, ***P < 0.001, ****P < 0.0001. Any data points that were two or more standard deviations away from the mean were considered outliers and disregarded from analysis. Error bars represent (\pm SEM) unless stated otherwise.

3 Model for Investigating Epithelial Tight Junction Barrier Function

3.1 Introduction

The SI represents the first point of contact between *T. gondii* and its host [Suzuki, 2013]. This chapter characterises IEC-6 as an *in vitro* model of SI epithelial cells suitable for studying *T. gondii* infection of the SI epithelium. The m-IC_{c12} cell line also utilised in this thesis has previously been fully characterised by Weight for *T. gondii* infection studies [Weight, 2011]. Briefly, murine m-IC_{c12} SI cells, described by Bens et al were originally derived from the lower part of the intestinal microvilli from 20-day-old L-type pyruvate kinase (L-PK)/Tag1 transgenic mice harbouring the SV40 virus [Bens et al, 1996] which halts replicative senescence to achieve immortalization via inactivation of senescence-6 (SEN-6), pRB and p53 genes [Lehman et al, 1993]. Within 13 days m-IC_{c12} develop a confluent monolayer of partially polarised cuboid cells, with an apical brush border and well-formed TJ. They retain a differentiated crypt-like phenotype and form a confluent domed monolayer [Bens et al, 1996]. To obtain this phenotype, m-IC_{c12} cell culture media requires supplementation with a variety of hormones, cofactors and growth factors [Weight, 2011].

Although used successfully by Weight as an *in vitro* model of the SI to study *T. gondii* infection, immortalised cell lines such as m-IC_{c12} originate from cancer cells so although widely used, these cancer-derived cell lines have limitations. The well-established human colon-derived Caco-2 cell line for example, has been used as a model of the SI for over thirty years, but can display altered proteomic profiles compared to the *in vivo* SI, leading to altered permeability, TEER and TJ protein expression [Hidalgo, 2001; Lenaerts et al, 2007]. Of note, considerable variation in Caco-2 barrier function also occurs between laboratories [Hayashi et al, 2008; Volpe et al, 2008]. Additionally, other common SI cell line models are often not of SI origin, for example the colonic carcinoma HT29 or T84

and canine kidney-derived MDCK. Ideally, *in vitro* models would be derived from the SI epithelium.

Although primary and secondary cell lines provide the most functionally similar model to the SI due to being derived directly from native tissue, they are not easily sustainable for long-term culture. Non-immortalised cell lines are therefore a preferable alternative to cancer-derived or virus-immortalised cells. These cell lines offer functional models as they are derived from primary cells, originally taken from healthy tissue. Importantly, for this thesis the *in vitro* cell model needs to reflect the complex physiology of the SI, mimicking the physical and biological barrier of the epithelial monolayer.

The non-immortalised IEC-6 cell line used in this thesis was originally derived from adult germ-free rat SI ileum [Quaroni et al, 1979]. Morphological and immunochemical studies by Quaroni et al confirmed IEC-6 derived from SI epithelial crypt cells and all four epithelial cell types could be identified [Quaroni et al, 1979]. They described a pre-confluent homogenous population of epithelial-like cells growing as tight colonies of closely opposed cells and ultrastructural features were characteristic of intestinal crypt-villus cells, including large oval nuclei, a well-developed Golgi and ER network, numerous mitochondria, apical microvilli and well-defined junctional complexes with associated microfilaments at points of cell-cell contact [Quaroni et al, 1979]. Being non-transformed, IEC-6 offer advantages over immortalised cell lines for studying cellular differentiation and remain non-differentiated when cultured in the absence of mesenchymal factors [Wood et al, 2003].

IEC-6 has been used over the last thirty years to study SI epithelial cells *in vitro*, including mucosal repair, barrier function, metabolism, proliferation, polarization and differentiation, as well as pathogen infection. For example, Guo et al used IEC-6 to examine the involvement of polyamines in epithelial AJ and TJ barrier function. The authors examined the effects of polyamine depletion on E-cadherin, β -catenin, α -catenin, ZO-1, ZO-2 and JAM-A and found only AJ E-cadherin expression was altered [Guo et al, 2003]. Later, Cario et al investigated TLR2

signalling in TJ barrier regulation and found TLR2 stimulation preserved the TJ barrier in response to stress-induced damage via MyD88 [Cario et al, 2007]. Kimura et al used IEC-6 to examine the effect of bacterial endotoxin LPS on TJ barrier function and found apical or basolateral administration altered the effect on the TJ barrier; barrier function was not altered by apical LPS but was disrupted by basolateral LPS [Kimura et al, 1997]. These studies suggest IEC-6 is a suitable model for investigating the barrier function of the TJ. IEC-6 has also been utilised to investigate pathogen infection with Maciel et al examining epithelial barrier function following *C. difficile* toxin A challenge [Maciel et al, 2007].

To date, few reports have used IEC-6 to investigate TJ protein expression and function or *T. gondii* infection. At the time of writing (September 2015), only eight publications have utilised IEC-6 to investigate occludin expression. Recently, Chen et al explored the regulation of occludin by α SNAP in acute pancreatitis and discovered downregulation of α SNAP leads to reduced occludin, enhanced apoptosis and ultimately increased TJ permeability [Chen et al, 2014]. Presently, IEC-6 has also only been described in three publications investigating *T. gondii* infection. Dimier and Bout found *T. gondii* tachyzoites actively invaded and replicated within IEC-6 but replication was inhibited by IFN- γ [Dimier and Bout, 1993]. More recently IEC-6 was compared to a cat kidney cell line (CRFK) for bradyzoite infection susceptibility and cystogenesis [Muno et al, 2015]. These studies indicate IEC-6 is a suitable model for examining *T. gondii* infection.

With the exception of these publications, limited information is available regarding IEC-6 growth characteristics on different substrates, which was addressed in this chapter.

3.2 Results

Characterisation of IEC-6 was undertaken to determine optimal culture conditions for development of an *in vitro* model of the SI for investigating TJ dynamics and *T. gondii* infection. A variety of substrates

including glass, plastic and permeable membranes were tested with or without an extracellular matrix (ECM) for development of polarised cell monolayers expressing TJ and AJ proteins.

3.2.1 IEC-6 Culture on Plastic Substrates

IEC-6 cultured on plastic substrates at a density of 5×10^4 formed a homogenous, confluent monolayer within four days. Within seven days post-confluence, cells organised into complex multicellular secondary structures, which increased in complexity by day fourteen and cells survived for at least twenty days.

IEC-6 initially form linear aggregates or ‘ridges’ then accumulate into large multicellular aggregates and ultimately organise into complex multicellular structures (Figure 3.1A-E) confirming studies by Wood [Wood et al, 2003]. For comparison, m-IC_{c12} cells grown here on plastic gradually formed a complex of secondary dome-like structures as seen in Figure 3.1K-O and described by Bens et al, 2006 [Bens et al, 2006].

A non-coated plastic substrate was used for proteomic analysis by western blotting and mass spectrometry (Chapters 4 and 5). Typically 2×10^6 cells were recovered from a 25cm² plastic flask after seven days of culture.

3.2.2 IEC-6 Culture Using an Extracellular Matrix

An ECM was used here to mimic the stratum of the SI *in vivo* to provide structural support and promote cellular proliferation and differentiation in otherwise non-responsive cell lines [Adams and Watt, 1993]. Naturally occurring components of the *in vivo* SI ECM such as collagen, laminin or fibronectin are used to create a thin ECM on culture-ware [Rothen-Rutishauser et al, 2000] or a thicker artificial matrix such

as Matrigel® can be used as a physiological basement matrix [Kleinman and Martin, 2005; Wolpert et al, 1996].

Carroll et al demonstrated a shift from a crypt-like phenotype to an enterocyte-like phenotype when IEC-6 were cultured on Matrigel® [Carroll et al, 1988]. The authors concluded that Matrigel® was required for IEC-6 to form a differentiated phenotype as the ECM enhanced proliferation and induced a multicellular structure within twelve hours as compared to growth of IEC-6 for four days on non-coated plastic [Carroll et al, 1988]. However, as depicted in Figure 3.1A-E, IEC-6 grown for at least seven days post confluence developed a complex morphology, suggesting a differentiated phenotype can be achieved without an ECM. Culturing IEC-6 on plastic coated with a thin collagen I and fibronectin ECM at $<10\mu\text{g}/\text{cm}^2$ appeared to have no effect on cellular proliferation or differentiation. After seven days, IEC-6 cells cultured on an ECM demonstrated the same phenotype as those cultured on uncoated plastic (Figure 3.1F-J) and similarly survived for at least twenty days.

These findings suggest IEC-6 retain the potential for differentiation *in vitro* and components of the IEC-6 cell culture media are capable of inducing cellular attachment, proliferation and differentiation. Therefore, an ECM was only used when a basal mucosa-like substrate was required for two-photon imaging of transmigrating *T. gondii* (Chapter 4).

3.2.3 Cellular Differentiation of IEC-6 is Induced on Plastic

To confirm IEC-6 differentiation on plastic alone, alkaline phosphatase (ALP) activity was assessed. ALP is a hydrolase expressed by brush border membranes of differentiated IECs [Quaroni and Hochman, 1996; Wood et al, 2003] and its enzymatic activity is correlated with the degree of differentiation of IECs [Matsumoto et al, 1990]. Apical media from IEC-6 cells cultured on plastic 25cm² flasks was examined for ALP-mediated *p*-nitrophenol phosphate hydrolysis using a colorimetric assay (Figure 3.2).

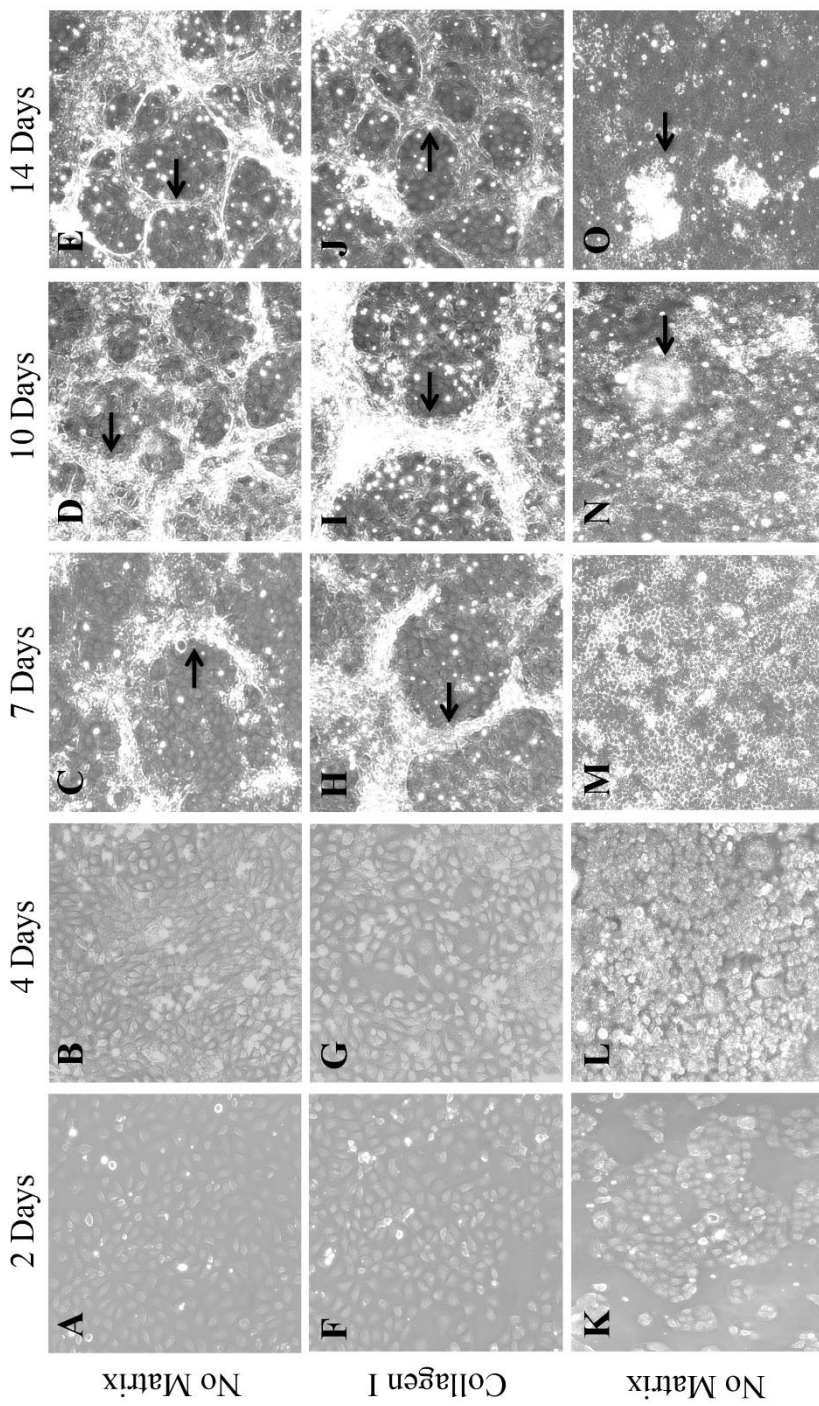


Figure 3.1: Morphology of small intestinal epithelial cells cultured on plastic substrate. IEC-6 cells (A-J) or m-IC_{c12} cells (K-O) were cultured for 14 days on uncoated plastic 6-well tissue culture plates or those coated with a collagen I and fibronectin matrix (F-J). Cells were analysed by light microscopy. Magnification 10x. Black arrows indicate areas of secondary structure formation

Pre-confluence levels of ALP were low at day two, corresponding to high cellular growth and proliferation. As the monolayer became confluent, ALP activity increased reaching a 53-fold change within eight-days of culture and attaining 78-fold change plateau within twelve-days of culture. This parallels the morphology seen in Figure 3.1 and previous studies on IEC-6 differentiation, which show an increase in ALP activity with culture [Ametani et al, 1996; Jeng et al, 1994; Wood et al, 2003]. It should be noted that these results reflect only one timecourse assay.

3.2.4 IEC-6 Culture on Cell Culture Inserts

Permeable cell culture inserts provide a well-characterised *in vitro* model of the SI epithelium as the inserts form apical (luminal) and basal (mucosal) compartments analogous to the *in vivo* SI lumen and mucosa [Cereijido et al, 1978 and Hidalgo et al, 1989] as depicted in Figure 3.3.

TJ barrier function was measured by TEER and tracer flux through the monolayer and the membrane was excised for immunocytochemical analysis of TJ and AJ protein expression.

Corning® Transwell® 24 well hanging polyethylene terephthalate (PET) tissue culture inserts with a pore size of 8µm were used for this study to allow transmigration of *T. gondii*, which are approximately 2µm by 6µm [Dubey et al, 1998]. The insert pores were easily visible by light microscopy (Figure 3.3 inset). IEC-6 cultured at a density of 5×10^5 per insert formed a confluent monolayer within six to twelve hours, suggesting increased proliferation compared to culture on plastic substrates.

This enhanced growth on Transwell inserts has been previously described for other cell lines [Matter and Balda, 2003]. Within 24 hours IEC-6 obtained the complex multicellular morphology described in 3.2.2, further suggesting an increased rate of differentiation than with culture on plastic substrates.

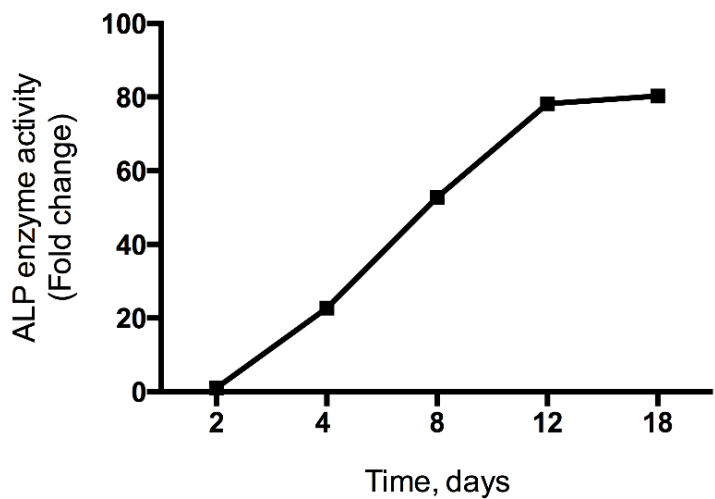


Figure 3.2: ALP activity increases with IEC-6 cell culture. IEC-6 cells were cultured for 18 days in 25cm² plastic flasks. ALP (U) was measured using a colorimetric assay on cell lysates at different times post-seeding. One unit (U) is defined as the amount of enzyme that hydrolyses 1μmol of p-NPP in a total reaction volume of 1ml in 1 minute at 37°C. Fold change in ALP activity is shown in relation to values obtained at the start of assessment (Day 2). Data representative of one timecourse assay.

A few cells were found on the underside of the inserts having migrated through the pores, however these only formed small clusters. Cells survived for up to twenty-one days before detaching from the membrane. The data presented here confirms IEC-6 cultured on PET inserts acquire a differentiated phenotype.

3.2.5 IEC-6 Polarisation

The apparent IEC-6 differentiated phenotype on PET inserts was assessed by immunohistochemistry and confocal microscopy to visualise TJ and AJ protein localisation. IEC-6 were cultured at a density of 5×10^5 per insert for seven days and as shown in Figure 3.4B (XY plane) and 3.4B' (YZ-plane), expression of N-acetylglicosamine and galactosyl (β -1,3) N-acetylgalactosamine (surface carbohydrates) was restricted to the apical cell surface and 3.4C and 3.4C' suggests a basal nucleus. Primary antibody and post-mounting staining specificity was confirmed (Methods section 2.5) using either species specific IgG or no primary antibody or stain. All controls were negative for non-specific secondary antibody or stain fluorescence (Figure 3.4F-H).

IEC-6 monolayers cultured on PET inserts reached approximately 16 μ m depth at seven days post-seeding days, 23 μ m within fourteen days and 30 μ m at twenty-one days post-seeding. Depth was greatest at points of multicellular formations and a confluent monolayer was present beneath the secondary cell layers. Compared to other intestinal cell lines such as T84, IEC-6 monolayers display a thin monolayer with flattened non-columnar cell morphology, suggesting only partial polarisation was achieved on PET inserts. Despite this, IEC-6 still provides an optimal model of the SI epithelium for investigation of *T. gondii* infection.

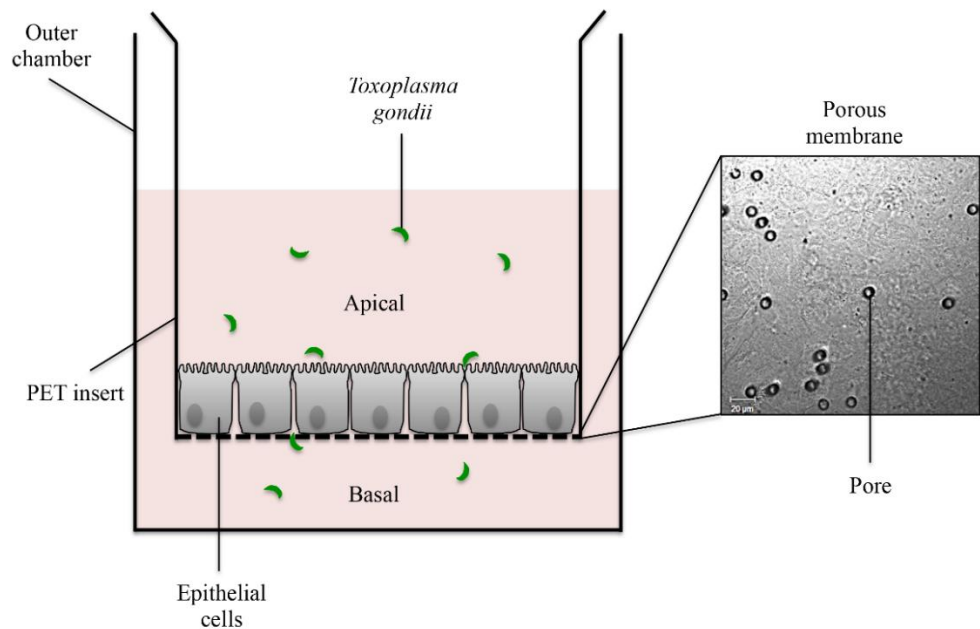


Figure 3.3: Cell culture insert system. Corning® Transwell® 24 well hanging PET tissue culture insert system schematic. PET insert positioned in an outer chamber in a 24 well plate with the cell monolayer cultured on the permeable membrane support, forming an apical and basal side of the monolayer. Inset: 8μm PET insert pores are visible as distinct dark circles. *T. gondii* transmigration of the monolayer will be investigated using this model. Magnification 40×, scale bar = 20μm.

3.2.6 IEC-6 Tight Junction Protein Expression

IEC-6 expression and localisation of TJ and AJ proteins was assessed by immunocytochemistry. Defined lateral membrane β -catenin, surface carbohydrates and basal nucleus and were observed (Figure 3.4A-C and A'-C') suggesting a partially polarised monolayer with defined apical and basal protein partitioning was acquired. ZO-1 expression demonstrated both membrane and cytoplasmic localisation, analogous with its dynamic mobility between the apical TJ, lateral membrane and cytoplasm [Shen, 2008] (Figure 3.4D).

3.2.7 IEC-6 Occludin Expression

Occludin imaging proved challenging in IEC-6 as defined membrane expression patterns were difficult to capture, similar to m-IC_{c12} [Weight, 2011].

The process of fixation appeared to affect occludin staining patterns; 2% paraformaldehyde (PFA) fixation gave higher levels of occludin staining in the nucleus whereas acetone fixation emphasised membrane occludin (Figure 3.5). Of note, only PFA retained *T. gondii* fluorescence so this method of fixation was used for infection studies. Confocal XZ-stack images in Figure 3.6 A'-C' show cell depth increased between fourteen to twenty-one days and the multicellular layers are most visible at day twenty-one as irregular areas of staining (Figure 3.6C). Occludin clearly localises to the apical membrane, visible as bright punctate fluorescence throughout the timecourse but most visible at day twenty-one (Figure 3.6C'). The basal nucleus and apical surface carbohydrates are also visible in figure 3.6C', suggesting polarisation is achieved when IEC-6 are cultured longer than the seven-days described in Figure 3.4. This data confirmed IEC-6 expressed apical membrane-associated occludin alongside other TJ and AJ proteins.

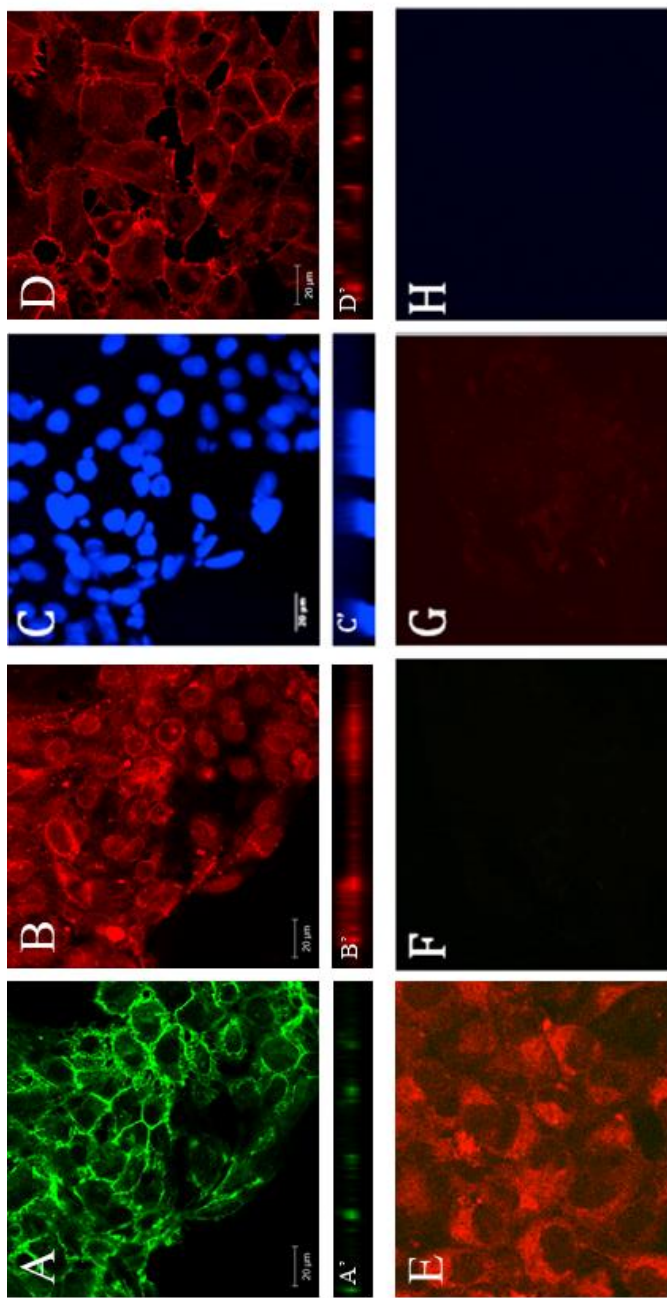


Figure 3.4: IEC-6 are partially polarised when cultured on PET inserts. IEC-6 cells were cultured for 7 days on PET inserts. Cells were fixed with 2% PFA and stained for antibodies specific for A) β -catenin, B) surface carbohydrates, C) Hoechst nuclear stain, D) ZO-1 and E) CellTracker Red. Negative controls for F) β -catenin (anti-rat IgG), G) ZO-1 (anti-mouse IgG), and H) Hoechst nuclear stain (no stain). Images A-H represent the XY plane of view and A'-D' represent the XZ plane of view taken with a Zeiss LSM confocal microscope and analysed using Fiji [Schindelin et al, 2012]. Magnification 40x. Scale bar 20 μ m.

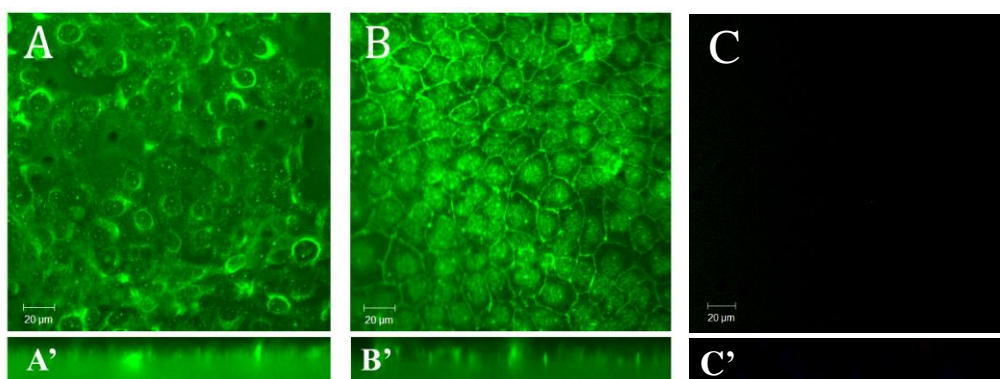


Figure 3.5: Comparison between fixation with 2% paraformaldehyde and acetone. Cells were cultured on PET inserts for 7 days and fixed with 2% PFA (A and A') or acetone (B and B') and stained for antibodies specific for occludin (green) and analysed by confocal microscopy. 2% PFA fixation displays higher background staining, which is also present in the nucleus, whereas acetone emphasises membrane-associated occludin. C) Negative control for occludin (rabbit IgG primary antibody). A-C) XY plane of view and A'-C') XZ plane of view showing the apical punctate pattern of occludin expression. Magnification 40x. Scale bar 20μm.

Due to low antibody-specificity IEC-6 did not provide the anticipated advantage over m-IC_{c12} for occludin localisation studies. Therefore, a cell-free slide-based approach for studying *T. gondii* interactions with occludin is presented in chapter 6.

Dalton et al and Weight both described a redistribution of occludin in response to *T. gondii* infection of the murine SI [Dalton et al, 2006; Weight, 2011]. Immunoblotting of occludin in both the insoluble and soluble fractions (Method section 2.7) from IEC-6 cultured on plastic 25cm² flasks revealed two occludin species, as described by Farshori and Kachar, 1999, the lower molecular weight species (~60kDa) located at lateral membrane or cytoplasmic vesicular locations and the higher molecular weight bands (~65kDa) located primarily at the TJ [Farshori and Kachar, 1999; Wong et al, 1997].

Although IEC-6 occludin immunoblotting proved challenging, over the time-course of thirteen days, the higher molecular weight occludin species was associated with the membrane fraction and the lower molecular weight occludin species with the cytoplasmic fraction (Figure 3.6E).

3.2.8 The IEC-6 Epithelial Barrier

As described earlier, the TJ forms a highly selective barrier between luminal contents and the underlying tissue of the intestine. Therefore, it was important to confirm a functional IEC-6 TJ barrier prior to *T. gondii* invasion studies. The barrier function of IEC-6 pore and leak pathways when cultured on PET inserts was assessed using TEER and permeability to FITC-dextran.

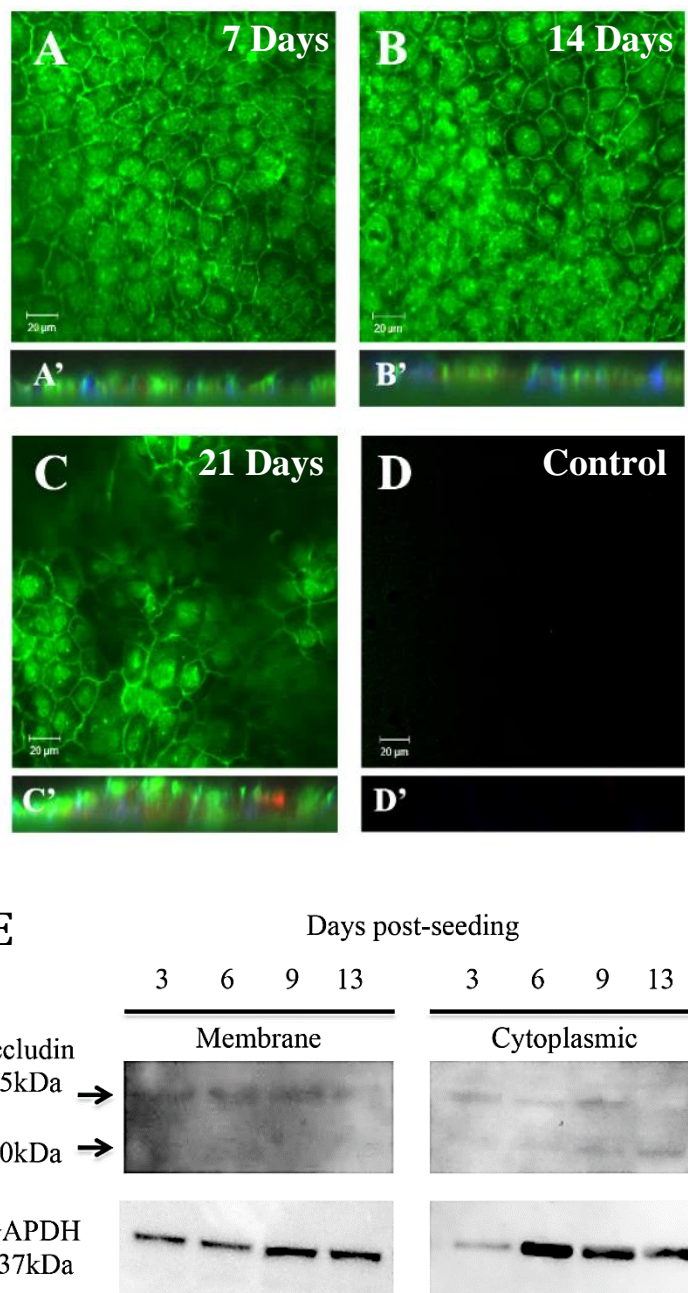


Figure 3.6: Occludin expression and localisation in IEC-6. A-C) IEC-6 were cultured on PET inserts for 7, 14 or 21 days, fixed with 2% PFA and stained for antibodies specific for occludin (green), surface carbohydrates (red) or Hoechst nuclear stain (blue) and analysed by confocal microscopy. D) Negative control for occludin (green, rabbit IgG). A-D represents XY images and A'-D' represents XZ images. Magnification 40x. Scale bar 20μm. E) IEC-6 were cultured on plastic 25cm² flasks for thirteen days and analysed by immunoblotting for occludin. Protein expression was analysed in both membrane and cytoplasmic fractions (Method section 2.7).

3.2.9 TEER and Permeability

IEC-6 cells seeded at a density of 5×10^5 per PET insert were cultured for up to twenty-days and TEER recorded (Figure 3.7A). TEER quickly increased from $24\Omega.\text{cm}^2$ to $130\Omega.\text{cm}^2$ within twelve hours post seeding and then steadily increased to reach a peak of $270 \Omega.\text{cm}^2$ at four to six days post-seeding. After six days TEER fluctuated and declined until day twenty when cells detached from the membrane. The minimal variation of TEER measurements between replicates suggested a stable pattern of IEC-6 TJ barrier formation so IEC-6 monolayers at four to six days post seeding presented optimal TJ barrier function.

IEC-6 monolayer permeability was measured by the flux of fluorescent 3-5kDa FITC-Dextran from the apical to basal PET insert compartment. IEC-6 were cultured on PET inserts for seven days and $1000\mu\text{g/ml}$ 3-5kDa FITC-Dextran added to the apical compartment as depicted in Figure 3.3. After two hours the level of FITC-dextran in the basal compartment was assessed. A blank insert was used as a control to measure the maximum level of diffusion through the membrane. In the control, a maximum of 19.7% tracer diffused to the basal compartment whereas with an intact IEC-6 monolayer, only 0.9% of the tracer diffused to the basal compartment (Figure 3.7B). It should be noted that this experiment was only performed once.

These results confirm PET inserts are suitable for monitoring barrier function in response to *T. gondii* infection. Partially polarised IEC-6 monolayers cultured for between four and seven days present optimal barrier function according to TEER and permeability so will be used to study *T. gondii* infection and proteomics (Chapter 4 and 5).

3.3 Discussion

The results presented here characterise IEC-6 culture on a range of substrates for investigating *T. gondii* infection. Early studies by Quaroni et al and Carroll et al suggested IEC-6 do not express antigens specific for a differentiated brush border without an ECM whereas more recent studies by Wood et al along with data presented here, suggest IEC-6 do possess a differentiated phenotype in culture [Carroll et al, 1988; Quaroni et al, 1979; Wood et al, 2003]. Monolayer culture on permeable inserts are known to promote more extensive polarisation and differentiation [Matter and Balda, 2003] so although IEC-6 monolayers grown on PET inserts were relatively thin, the expression of surface carbohydrates and a basal nucleus also indicated partial polarisation within seven days of culture. Thus confirming IEC-6 grown on PET inserts are both differentiated and partially polarised, important for investigating the apical TJ barrier function in response to *T. gondii* infection.

As described in chapter 1.6, regulation of the TJ barrier by formation of ion-selective pores and size-selective leak pathways requires a direct relationship between TJ structure and function. IEC-6 culture on PET inserts allows functional TEER and FITC-dextran flux measurements as well as TJ structure assessment by the localisation of TJ proteins. However, TEER and permeability measurements should be analysed with caution as both are influenced by factors other than those specifically attributed to TJ function [Fanning et al, 1999; Yap et al, 1998].

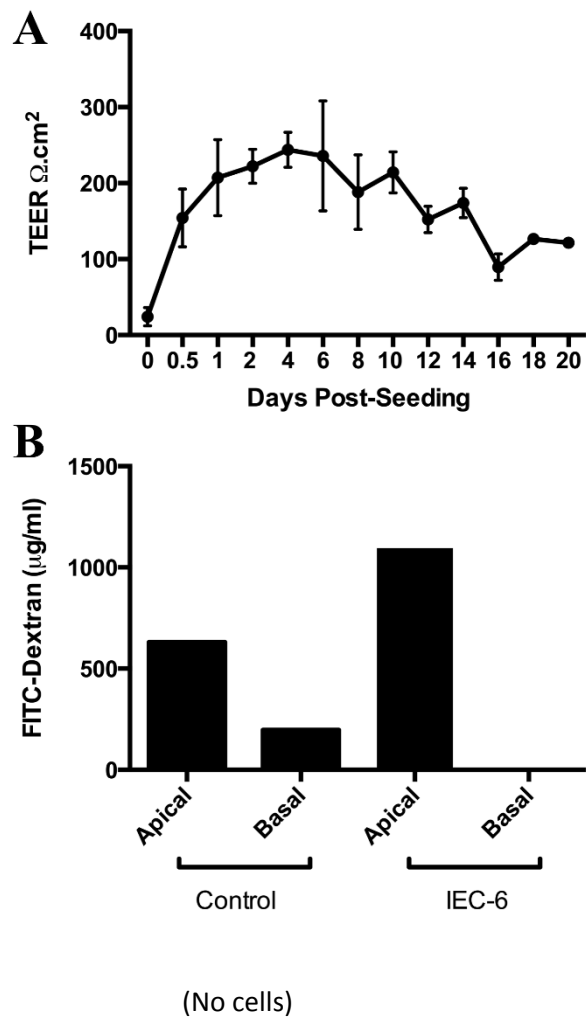


Figure 3.7: Barrier function of IEC-6 cultured on PET inserts assessed by TEER and Permeability to FITC-dextran. A) Cells were cultured on PET inserts and TEER measurements taken for up to 20 days. Each time-point represents three experiments with three biological replicates. B) Cells were cultured on PET inserts for 7 days. 1000 $\mu\text{g/ml}$ FITC-dextran was added to the apical compartment and migration into the basal compartment was measured after 2 hours. Control represents the maximum FITC-dextran migration through a blank PET insert. Results represent one experiment.

TEER measurements for instance account for both transcellular and paracellular resistance but as membrane resistance is generally much higher than intracellular resistance, changes in TEER represent a change in paracellular resistance [Reuss, 1991]. It should be noted that TEER is also extremely sensitive to factors such as culture media change or areas of low resistance such dead cells within the monolayer so cell monolayers should be allowed to equilibrate and morphological analysis of cultures should accompany these measurements [Fanning et al, 1999]. Although permeability to tracer molecules is less sensitive to defects in the cell monolayer, the contribution of transcellular migration should not be overlooked [Matter and Balda, 2003].

In vivo epithelia display a wide range of electrical resistances, for example typical TEER in the rabbit distal colon is $385 \Omega\text{cm}^2$, compared to $300,000 \Omega\text{cm}^2$ in the rabbit urinary bladder. *In vitro* cell lines display a similar range of barrier resistances, Caco-2 TEER is $125-250 \Omega\text{cm}^2$ compared to MDCK $60-4000 \Omega\text{cm}^2$ [Itallie and Anderson, 2009]. These differences are attributed to 'tight' or 'leaky' epithelia [Shen et al, 2011].

In this study, the average TEER increase from $24.2\Omega\text{.cm}^2$ to $243.8\Omega\text{.cm}^2$ confirms IEC-6 produce measurable barrier changes, important for investigating *T. gondii* effects on the TJ barrier. Published studies using IEC-6 produce a variety of TEER values; either low values of approximately $20\Omega\text{.cm}^2$ [Bastian et al, 1999], mid-range of $91 \Omega\text{.cm}^2$ [Xinwai et al, 2014] or higher values of $>400 \Omega\text{.cm}^2$ [Xia et al, 2002], likely due to different culture conditions and insert systems [Matter and Balda, 2003]. The second cell line used in this thesis, m-IC_{c12} reaches a maximum TEER of $120\Omega\text{.cm}^2$ [Bens et al, 1996]. These IEC-6 and m-IC_{c12} TEER values, although widely accepted, are low compared to other intestinal cell lines such as T84, which consistently reach over $1000 \Omega\text{.cm}^2$ [Tang and Goodenough, 2003], likely due to differences in their claudin expression [Furuse et al, 2001; Shen et al, 2011]. Within seven days of culture, IEC-6 monolayers were also impermeable to 3-5kDa FITC-Dextran, suggesting a functional paracellular leak pathway.

Although no single protein serves as an indicator of TJ structural

assembly [Anderson and Itallie, 1995; Stevenson et al, 1986], the localisation of specific TJ-associated components such as cytoplasmic plaque proteins or integral transmembrane proteins indicate a fully formed TJ [Balda and Matter, 2008; Le Shen et al, 2008]. Comparable with studies such as those by Le Shen et al, immunofluorescence localisation of the transmembrane protein occludin and cytoplasmic plaque protein ZO-1 to a TJ membrane location with a typical apical punctate pattern were used here as markers of TJ complex formation, suggesting the TJ was fully formed within 7-days post-seeding used in this thesis [Le Shen et al, 2008]. It is however well known that staining TJ proteins can be problematic, particularly with densely cultured transwell monolayers [Matter and Balda, 2003]. Unlike other cell lines such as MDCK where occludin forms a defined chicken wire-like pattern, IEC-6 occludin staining was less distinct and non-specific. It is known that the method of fixation can alter TJ protein staining but other fixation protocols trialled here such as ice-cold methanol fixation did not improve occludin staining [Matter and Balda, 2003]. The non-specific occludin staining pattern obtained with 2% PFA fixation may be due to cross-linking of proteins to the cytoskeleton. This cross-linking retains cellular stasis but reduces protein antigenicity, which results in increased background staining [Matter and Balda, 2003]. The presence of non-specific cytoplasmic and nuclear occludin staining prevents conclusive measurements of the redistribution of occludin in response to *T. gondii* infection. Therefore a novel proteomic strategy is used to assess the impact of *T. gondii* infection of TJ protein localisation (Chapter 4).

The plasticity of the TJ has previously been assessed using FRAP and FLIP [Shen et al, 2008; Liang and Weber, 2014; Turner et al, 2014; Weber, 2012]. Consistent with these studies, expression of ZO-1 seen here localised within both an apical membrane and cytoplasmic pool [Turner et al, 2014] whereas AJ β -catenin expression is restricted to a defined lateral membrane location [Yamada et al, 2005]. Occludin immunofluorescence could not confirm the distinct lateral membrane and TJ localisation previously described, possibly due to low specificity of the

antibody used in this study and insufficient optimisation of the method [Shen et al, 2008; Liang and Weber, 2014; Turner et al, 2014; Weber, 2012]. Additional occludin antibodies have become available since these experiments were performed and these may yield enhanced occludin immunocytochemistry in future. Immunoblotting confirmed the presence of both high and low molecular weight occludin species in IEC-6, required for investigating occludin phosphorylation changes in response to *T. gondii* infection (chapter 5).

3.4 Conclusions

Using a PET insert system, an *in vitro* model of the small intestinal epithelium was established for *T. gondii* infection assays.

4 *Toxoplasma gondii* Invasion of IEC-6 and the Involvement of Tight Junction Proteins

4.1 Introduction

In this chapter *T. gondii* paracellular transmigration of the SI epithelium was examined and *in vitro* changes in the host cell proteome in response to infection were investigated, with a focus on TJ-associated proteins.

To identify novel host cellular responses, it is first necessary to consider the mechanisms of host infection and dissemination by *T. gondii*. Prior to invasion, *T. gondii* organelle contents are secreted into the host cell, many of which could directly modulate the host cell proteome. For example, as described in chapter 1, ROP18, ROP5 and GRA15 have been identified as major contributors to parasite virulence [Hunter and Sibley, 2012; Robben et al, 2004]. The next stage of infection involves transmigration of the SI epithelial barrier; the TJ paracellular pathway presents a potential route for rapid parasite dissemination to the hosts underlying tissues. However, the *T. gondii* paracellular route of infection has not yet been visualised. Following transmigration of the SI epithelial barrier, *T. gondii* exploit the motility of immune cells such as DCs in an intracellular Trojan Horse-like mechanism to spread throughout the body to secondary sites of infection, such as the brain, where bradyzoite cyst formation ultimately protects parasites from the immune system. An example of this was shown by recent studies using two-photon microscopy of mouse SI explants which indicated neutrophils and monocytes accumulated at foci of *T. gondii* infection [Coombes et al, 2013; Gregg et al, 2013]. These neutrophils contained viable parasites and were capable of transluminal migration across the intestinal epithelium, further facilitating parasite dissemination [Coombes et al, 2013]. During the course of infection, free tachyzoites were also identified in the gut lumen, likely from localised sites of replication in the SI epithelium,

suggesting a potential mechanism for re-entry and spread within the lumen [Gregg et al, 2013].

This evidence suggests *T. gondii* utilise a variety of strategies to disseminate throughout the host and may subvert a variety of host intracellular mechanisms. To investigate the involvement of host proteins during *T. gondii* infection, a number of experimental approaches have been used. For example, Barragan et al used co-immunoprecipitation to identify an interaction between host ICAM-1 and parasite MIC2, a microneme adhesion protein [Barragan et al, 2005]. Many groups have since utilised DNA microarrays to successfully investigate host cell transcriptome changes in response to infection with various *T. gondii* strains. For example, analysis of mouse brain infected with *T. gondii* found that genes involved in immune responses and cell activation were upregulated and those involved in neurological function were downregulated [Jia et al, 2013; Tanaka et al, 2013]. It is however the cellular protein complement that represents the biological function of genes and as a result, mass spectrometry (MS) based proteomics studies have increasingly been used to identify cellular proteins as well as their modification, quantification and localisation [Mann, 2006; Wastling et al, 2009].

Since the application of proteomics to *T. gondii*, a number of groups have investigated the *T. gondii* proteome. This has been applied to the whole parasite proteome [Cohen et al, 2002; Krishna et al, 2015; Possenti et al, 2013; Xia et al, 2008; Zhou et al, 2013] as well as defined sub-sets such as excreted proteins [Zhou et al, 2005] or the rhoptry organelle proteome [Bradley et al, 2005]. These studies led to an improved understanding of the host-parasite relationship and revealed possible host-pathogen interactions such as novel parasite kinases, phosphatases and proteases that are likely to be involved in host cell invasion [Bradley et al, 2005].

Currently limited information is available regarding the specific role of the TJ proteome during *T. gondii* infection and the paracellular route of infection has not previously been visualised. Therefore, high-

resolution multi-photon live imaging is used here to observe the paracellular route of parasite infection alongside a proteomics method to investigate host proteome changes in response to *T. gondii* infection of the SI epithelium, with a novel focus on the involvement of TJ proteins.

4.2 Results

Recombinant RH-strains of *T.gondii* tachyzoites expressing the YFP protein were used as they are highly fluorescent, necessary for visualisation of intracellular or transmigrating parasites [Gubbels et al, 2003]. As *T. gondii* infection of IEC-6 has not been previously described, parasite infection kinetics were initially optimised.

4.2.1 *Toxoplasma gondii* Transmigration of the IEC-6 Monolayer

To investigate the effects of parasite infection on IEC-6, the monolayer was assessed during *in vitro* transmigration using the PET insert system (Methods section 2.5 and 2.9.4). Immunofluorescence imaging of confluent IEC-6 cell monolayers cultured on PET inserts for four days and infected at a ratio of 5:1 parasites to cells for up to four hours confirmed *T. gondii* attached to the monolayer and clustered to cellular junctions, often with more than one parasite per cell (Figure 4.1A). This attachment occurred in a non-homogenous manner with a few cells ($26.5 \pm 10.3\%$) being infected with two to six parasites whereas the majority of cells were non-infected, comparable with previously reported figures of 17-35% [Dimier and Bout, 1993; Kowalik et al, 2004].

Parasites were seen to migrate from the apical to basal plane during infection, consistent with parasites using the paracellular route of invasion (Figure 4.1B-C) [Barragan et al, 2005]. IEC-6 were also cultured

on glass coverslips for four days and infected with *T. gondii* for two hours prior to fixation with 2% PFA and H&E staining in order to visualise formation of the parasitophorous vacuole, which was clearly visible as a white halo (figure 4.1D), indicating the onset of parasite replication after two hours infection.

Using confocal imaging (Methods section 2.6) of confluent IEC-6 cell monolayers cultured on PET inserts for four days and infected at a ratio of 5:1 parasites to cells for four hours, Z stack images composed of approximately 18 sections at 1 μ m intervals were taken at two, three and four hour time-points. To visualise parasite location within the plane of view by Z stack, cells monolayers were marked for the apical and basal membrane using rhodamine labelled surface carbohydrates and the surface of the PET membrane. Parasites were seen in the mid-basal plane of view (>9 μ m cell depth) within two hours and proportionally more parasites were mid-basally located after four hours, calculated by counting the number of parasites visible at >9 μ m cell depth for each time point (Figure 4.1E-G). Here, two hours infection was found to be optimal for capturing paracellular transmigration events as more parasites were associated with the apical plane close to the cellular junction, calculated by counting the number of parasites at <5 μ m cell depth, analogous with previous *in vitro* studies [Dalton et al, 2006; Weight, 2011].

4.2.2 The Tight Junction Barrier is Maintained During *Toxoplasma gondii* Infection

The integrity of the IEC-6 monolayer during *in vitro* parasite infection was assessed to determine if the epithelial barrier remained intact during parasite transmigration using TEER measurements and 3-5kDa FITC-dextran flux from the apical to basal PET insert compartment (Methods section 2.8). IEC-6 barrier function and membrane integrity were not affected by *T. gondii* as both TEER and paracellular permeability remained stable during the two-hour course of infection (Figure 4.2A-B).

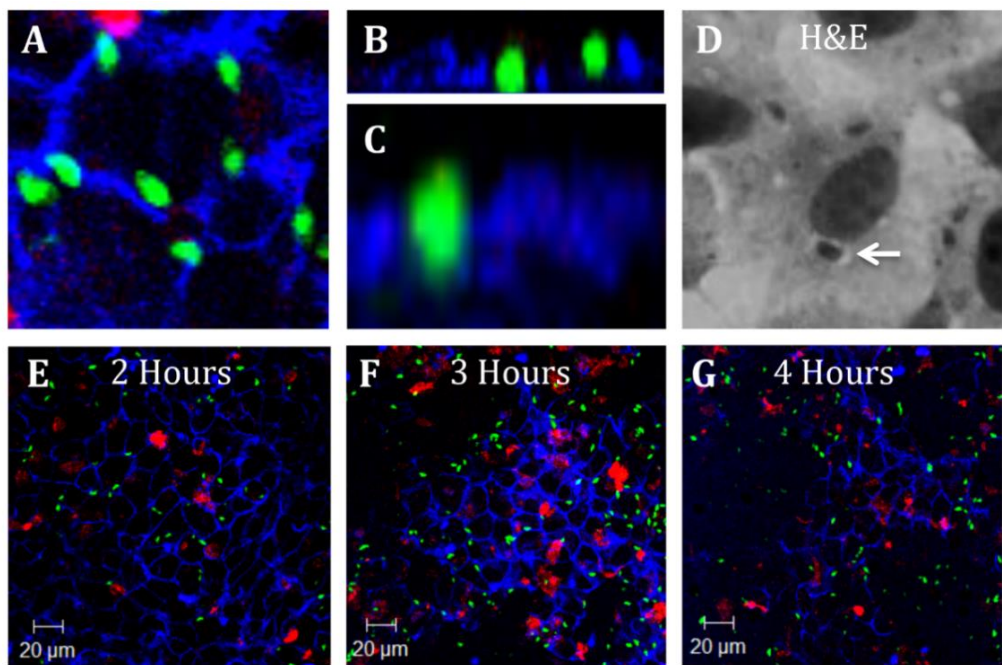


Figure 4.1: *Toxoplasma gondii* infection of IEC-6 cells. A-F) Cells were cultured on PET inserts for four days, infected with *T. gondii* (green) for up to four hours, fixed with PFA and stained for lateral membrane β -catenin (blue) and cell surface carbohydrates (red). A) Magnified image illustrating parasite clustering to cellular junctions. B-C) Magnified images showing parasites within the paracellular space between cells. D) Cells were cultured on glass coverslips for four days, infected with *T. gondii* for two hours prior to fixation with 2% PFA and H&E staining. The parasitophorous vacuole is clearly visible as a white halo (white arrow). E) Cells were cultured on PET inserts for four days, infected with *T. gondii* (green) for up to four hours and fixed with PFA. Mid plane ($9 \mu m$ cell depth) merged XY image of *T. gondii* (green), β -catenin (blue) and cell surface carbohydrates (red), at two hours p.i, F) three hours p.i and G) four hour's p.i. Magnification 40 \times .

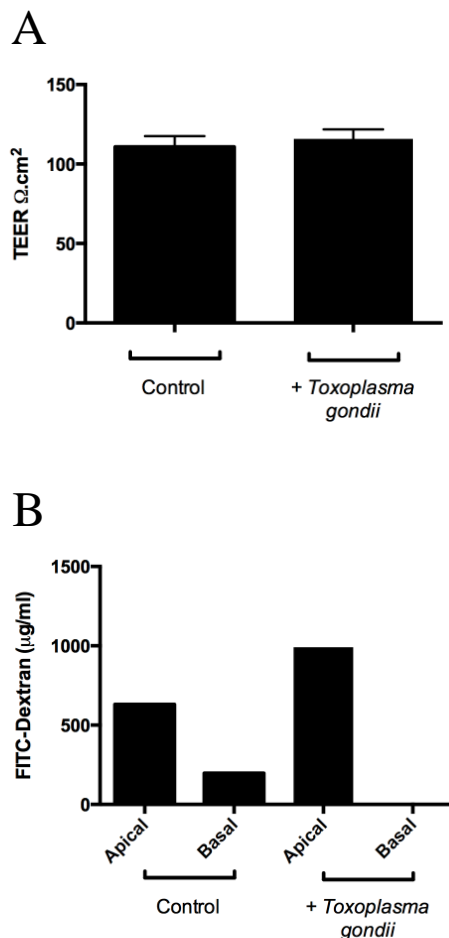


Figure 4.2: IEC-6 barrier integrity is not affected by *Toxoplasma gondii* infection. IEC-6 were cultured on PET inserts for seven days prior to infection with *T. gondii* for two hours. A) No change in TEER due to parasite infection. TEER measurements from uninfected IEC-6 (control) were compared to infected IEC-6 (+*Toxoplasma gondii*) after two hours. Data represents two independent experiments with eighteen biological replicates. B) 1000 $\mu\text{g}/\text{ml}$ 3-5kDa FITC-Dextran was added to the apical compartment of the PET insert and after two hours the level of FITC-dextran in the basal PET compartment was assessed. A blank insert (control) with no cells was used as a control to measure the maximum level of tracer diffusion through the membrane compared to no tracer diffusion when a confluent IEC-6 monolayer was infected (+*Toxoplasma gondii*). Data represents two independent experiments with four biological replicates.

4.2.3 *Toxoplasma gondii* Live Cell Imaging

Parasite clustering to cellular junctions and localisation within the paracellular space suggest *T. gondii* transmigrate the IEC-6 monolayer via the paracellular pathway [Barragan et al, 2005]. As paracellular infection has not yet been visualised using live imaging, high-resolution multi-photon imaging was used here to investigate the route of infection (Methods section 2.10).

Confluent IEC-6 cell monolayers were cultured on Matrigel® matrix coated 35mm µ-dishes for four days, stained with CellTracker™ red and apically exposed to YFP-*T. gondii*. Matrigel® was used as a basal mucosa-like substrate to allow parasite dissemination away from the IEC-6 monolayer. Live two-photon imaging confirmed extracellular parasites were actively motile, demonstrating circular gliding motility [Håkansson et al, 1999] and clustering to cellular junctions within five minutes of infection. The XY and equivalent XZ images in figure 4.3 represent the three layers of the epithelium presented in the accompanying video (Video 1) and corresponding figures: above the monolayer, the apical cell surface and the basal cell monolayer.

4.2.4 *Toxoplasma gondii* Paracellular Route of Infection

Live two-photon imaging confirmed *T. gondii* utilise the paracellular route of transmigration in IEC-6. Video 1 and the corresponding video stills (Figures 4.4 and 4.5) show a parasite initially located in close contact with the apical cellular junction, which is shown as a clear non-stained region between CellTracker red labelled host cells (Figure 4.4A and A'). The parasite re-orientates after 52 seconds (Figure 4.4B and B') and rapidly transmigrates through the paracellular space between host cells (Figure 4.4C and C'). The whole process taking less than 1 minute 42 seconds.

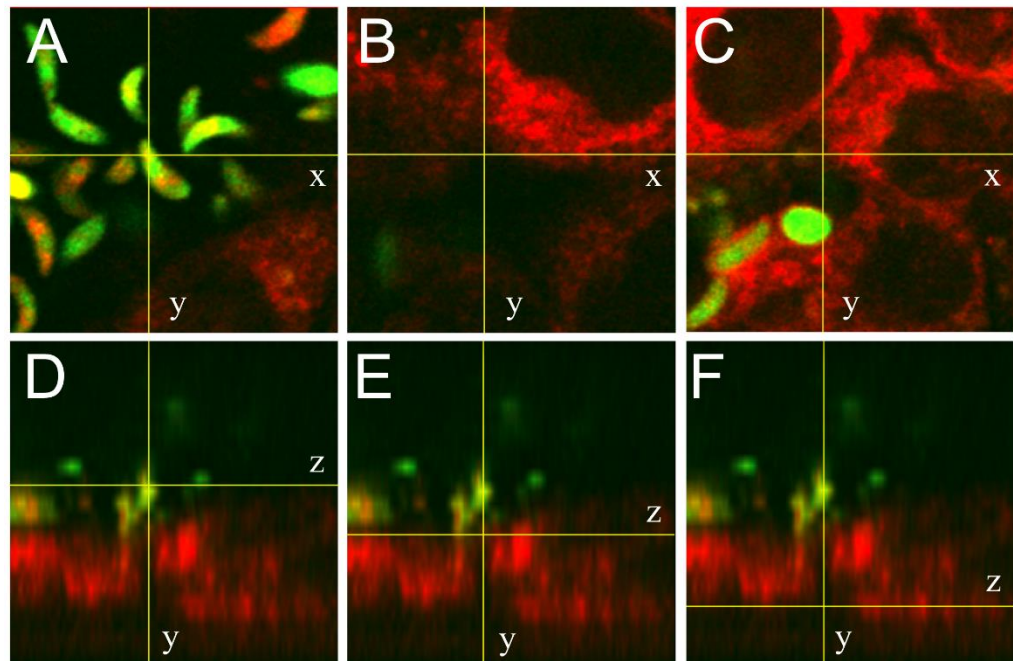


Figure 4.3: Live cell imaging of *Toxoplasma gondii* infection. A) IEC-6 monolayers cultured on Matrigel® matrix coated 35mm µ-dishes for four days were stained with CellTracker™ red (red) and apically infected with *T. gondii* (green) immediately prior to two-photon live imaging. Three layers of the epithelial monolayer are clearly visible in both the XY (A-C) and YZ (D-F) plane of view. A and D) Parasites above the monolayer. B and E) The apical surface of the epithelium. Cellular junctions are visible as unstained regions between cells (red). C and F) Intracellular parasites within a PV in the basal region of the monolayer. Images are representative of those obtained from two experiments with replicates. Images were acquired using a LaVision BioTec TriM Scope II two-photon microscope (Bielefeld) based on a Nikon Eclipse Ti optical inverted microscope. Z-stacks were separated by 1 µm and the video frame rate was 51.2 s. Images were analysed with the Fiji/ImageJ package. Magnification 40x.

Equivalent basal images (Figure 4.4D-F) show paracellular parasite egress through the IEC-6 monolayer, although the cellular junction is less visible. The process of egress was slower at 3 minutes 24 seconds. Due to limitations with the microscope field of view it was not possible to capture both transmigration and egress of the same parasite. The proposed route of paracellular transmigration is schematically represented in figure 4.5D-F.

4.2.5 SILAC Proteomic Analysis

The SILAC method metabolically incorporates a heavy (isotope-labelled) or light (normal) form of an amino acid into all cellular proteins followed by MS analysis for identification and quantitation of proteins such as occludin [Amanchy et al, 2005; Chen et al, 2000, Ong et al, 2002].

The schematic in Figure 4.6 represents a flow chart of the Invitrogen™ SILAC protein identification method as described in 2.11. Briefly, two IEC-6 populations were grown on plastic 25cm² flasks for six passages using SILAC DMEM containing either heavy [$\text{U}-\text{C}_6^{13}$]-L-lysine (MW = 152.1259) and [$\text{U}-\text{C}_6^{13}, \text{N}_4^{15}$]-L-Arginine (MW = 184.1241) or light [C_6^{12}]-L-lysine (MW = 146.1055) and [$\text{C}_6^{12}, \text{N}_4^{14}$]-L-Arginine (MW = 174.1117) prior to infection of light-labelled cells at a ratio of 1:10 cells:*T. gondii*. To dissect the temporal response to infection, a time course of either two hours or twenty-four hours *T. gondii* infection was performed. Cells from each sample (heavy and light) were mixed in a 1:1 ratio based on cell number prior to processing to reduce quantification errors due to unequal labelling [Harsha et al, 2008].

The samples were subsequently lysed and separated into membrane and cytoplasmic protein fractions. Two independent replications of the SILAC assay were undertaken with the second replicate modified to enhance protein identification and sensitivity.

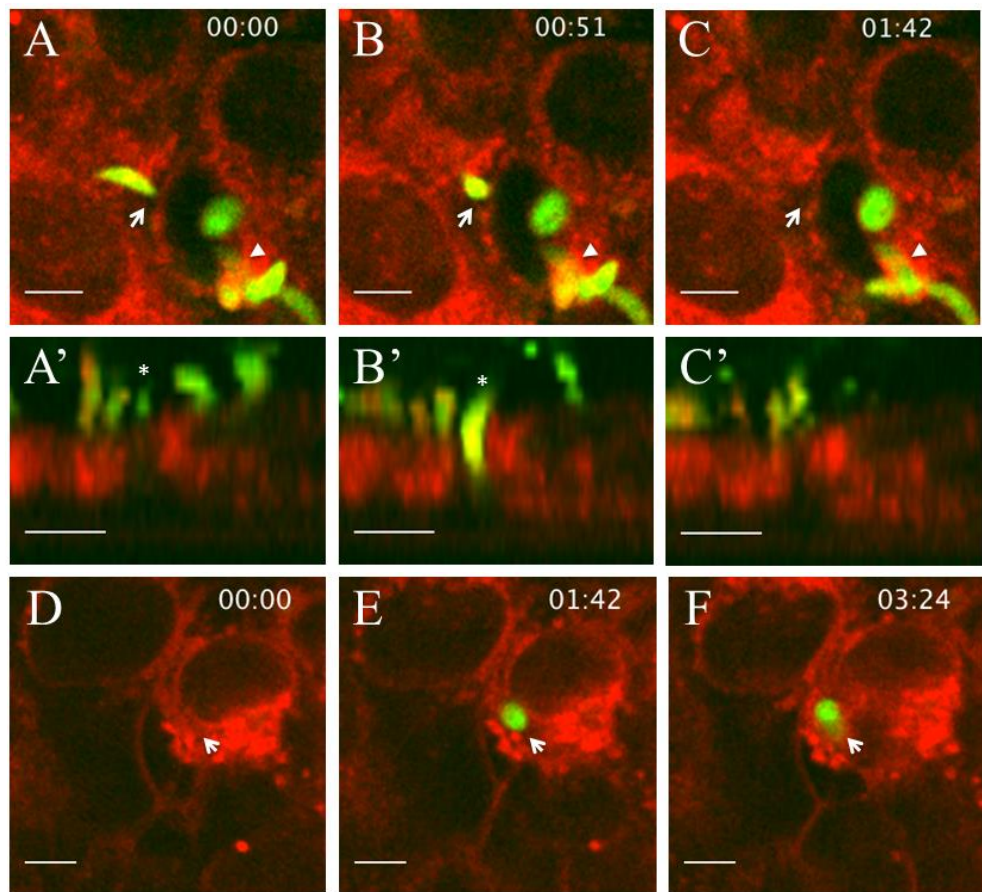


Figure 4.4: *Toxoplasma gondii* utilise the paracellular pathway during transmigration and egress. IEC-6 monolayers cultured on Matrigel® matrix coated 35mm µ-dishes for four days were stained with CellTracker™ red (red) and apically infected with *T. gondii* (green) immediately prior to two-photon microscope live imaging. Sequential XY frames from Video 4.2 show a transmigrating parasite targeting the epithelial cellular junction (white arrows). Following initial localisation to the cellular junction A), the parasite re-orientates B) and enters the paracellular junction C). A static intracellular parasite is clearly visible (White arrowheads). Corresponding YZ images show the parasite (marked *) localizes above the epithelial cellular junction A'), re-orientates and moves between cells in the paracellular junction B') and transmigrates through the epithelium C'). The paracellular junction region is visible as a non-stained space between cells (red). D-F) Basal images show parasite egress through the paracellular space (white arrow) between cells (red). The proposed route of paracellular transmigration involves G) Parasite localisation to the apical cellular junction, H) transmigration through the paracellular space and I) basal egress out of the paracellular space. Images representative of those obtained from two experiments with replicates. Images were acquired using a LaVision BioTec TriM Scope II two-photon microscope (Bielefeld) based on a Nikon Eclipse Ti optical inverted microscope. Z-stacks were separated by 1 µm and the video frame rate was 51.2 s. Images were analysed with the Fiji/ImageJ package. Magnification 40x. Scale bar = 5 µm.

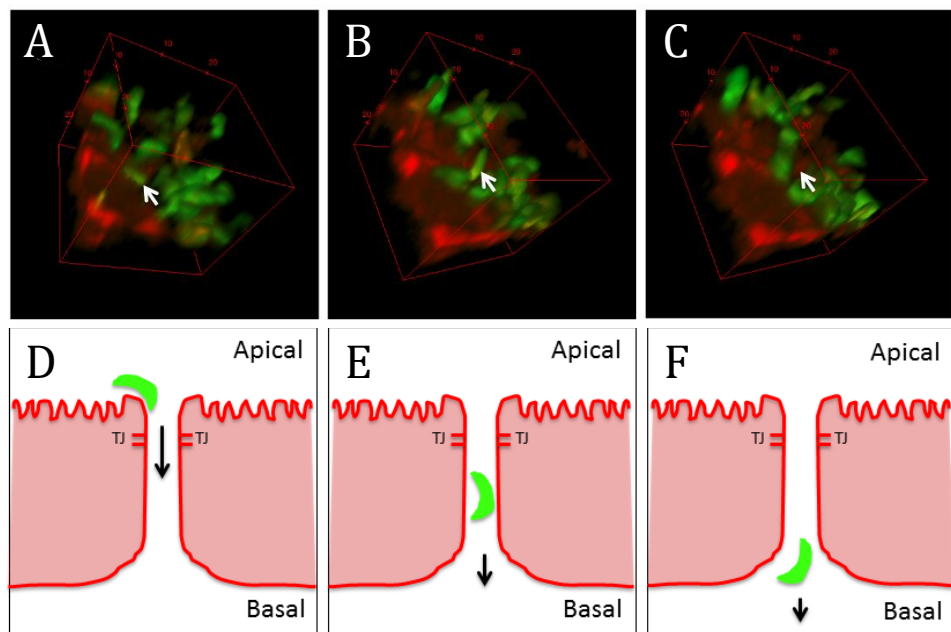


Figure 4.5: *Toxoplasma gondii* paracellular infection mechanism. IEC-6 monolayers cultured on Matrigel® matrix coated 35mm µ-dishes for four days were stained with CellTracker™ red (red) and apically infected with *T. gondii* (green) immediately prior to two-photon microscope live imaging. A-C) 3D representation of frames from Video 4.2 show a transmigrating parasite (white arrow) targeting the epithelial cellular junction. Following initial localisation to the cellular junction A), the parasite re-orientates B) and enters the paracellular junction C). D-F) Schematic representation of the proposed paracellular route of infection. A) A parasite targets the epithelial cellular junction and adheres to the cell. B) The parasite enters the paracellular space. C) The parasite transmigrates the epithelium and disseminates away from the SI. Images are representative of those obtained from two experiments with replicates. Images were acquired using a LaVision BioTec TriM Scope II two-photon microscope (Bielefeld) based on a Nikon Eclipse Ti optical inverted microscope. Z-stacks were separated by 1 µm. Images were analysed with the Fiji/ImageJ package.

Therefore the two assays were not directly comparable and only the data from the second, more sensitive replicate are presented here as ~2000 more proteins were identified per sample.

As the heavy or light peptides are isotopically distinct, incorporation leads to a known mass shift [Mann, 2006]. The relative intensity of the light and heavy peptides is easily distinguished by MS and allows the differential quantification of proteins in the samples. Heavy and light L-lysine peak pairs are separated by 6.0204 Da and heavy light L-Arginine peak pairs by 10.0124 Da. As Arginine containing peptides ionize more readily than Lysine containing peptides, double labelling results in increased sensitivity and sequence coverage [Ong et al, 2003].

The raw MS files were processed using MaxQuant [Cox and Mann, 2008] and proteins identified by searching against the Rattus norvegicus (Rat) UniProt database (downloaded 5.6.14). Protein quantitation was performed using MaxQuant to generate heavy and light peptide ratios (fold-change) and Perseus statistical analysis to generate significance-B (p-value) scores. Raw data files are included in Appendix B. The raw data was filtered according to >2-fold change (compared to non-infected control) and a p-value of <0.05. Due to the large number of host proteins modulated during the time course, only data related to proteins with functional information are discussed.

In total, we identified 3489 host membrane proteins and 3396 cytoplasmic proteins at two hours p.i and 3464 membrane proteins and 3172 cytoplasmic proteins at twenty-four hours p.i. At two hours p.i a total of 50 membrane proteins exhibited a significant 2-fold or greater increase in their abundance and 14 exhibited a decrease.

Similarly, 57 cytoplasmic proteins exhibited a significant 2-fold or greater increase in their abundance and 11 exhibited a decrease. After twenty-four hours of infection, a total of 78 membrane proteins exhibited a significant 2-fold or greater increase in their abundance and 67 exhibited a decrease. Similarly, 121 cytoplasmic proteins exhibited a significant 2-fold or greater increase in their abundance and 35 exhibited a decrease.

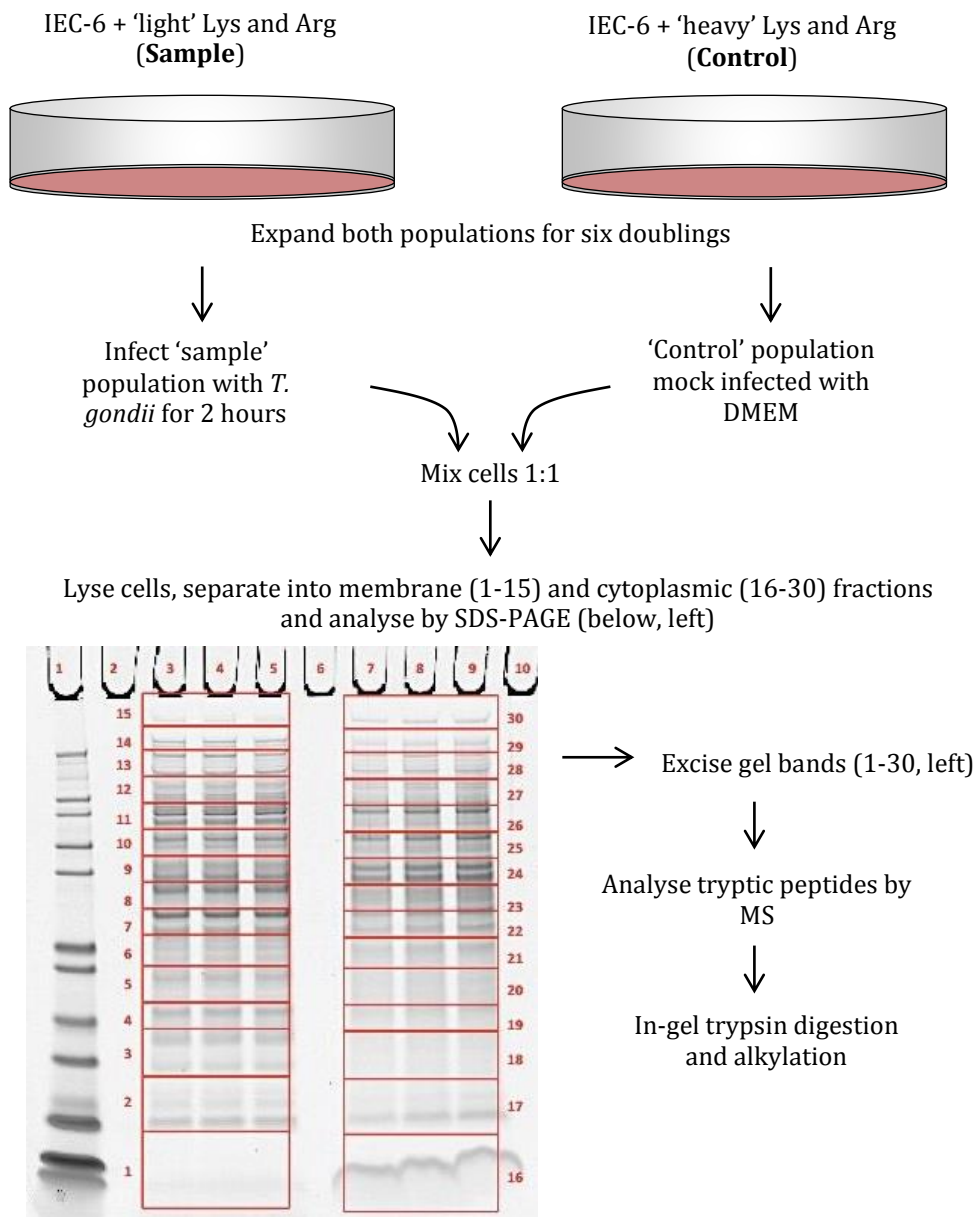


Figure 4.6: Schematic representation of SILAC workflow. Two IEC-6 samples were cultured for six passages in SILAC DMEM containing either 0.1mg/ml heavy L-lysine and L-Arginine or light L-lysine and L-arginine. After 100% incorporation, light labelled cells were infected with *T. gondii* for two hours. Cells were mixed in a 1:1 ratio and lysed with Thermo Scientific™ Mem-PER mammalian protein extraction reagent. Triplicate samples were separated by SDS-PAGE and stained with coomassie before gel bands were excised. After in-gel digestion and alkylation peptides were analysed using a Thermo Scientific™ Orbitrap Fusion™ Tribrid™ mass spectrometer.

Functional annotation of the identified proteins was carried out using the protein annotation through evolutionary relationship (PANTHER) Gene Ontology (GO) classification system (<http://www.pantherdb.org> Version 10) [Mi et al, 2013]. After two hours of infection the majority of proteins demonstrating a decrease in abundance were structural molecules (14.3%), or involved in protein-protein binding (26.5%) or catalytic activity (36.7%) (Figure 4.7A). Similarly, after twenty-four hours of infection the majority were involved in catalytic activity (35.7%), protein-protein binding (28.6%) or were structural molecules (10.7%) (Figure 4.7B). After two hours of infection the majority of proteins demonstrating an increase in abundance were involved in catalytic activity (36.3%), protein-protein binding (22.0%) or were structural molecules (19.8%). (Figure 4.8A) and after twenty-four hours of infection the majority of proteins demonstrating an increase in abundance were involved in catalytic activity (48.6.3%) or protein-protein binding (25.7%) (Figure 4.8B). In addition, analysis of the differentially expressed proteins using the PANTHER overrepresentation test (version 10 release 2015-04-30) revealed a significant ($p<0.05$) enrichment of proteins involved in biological processes such as regulation of apoptotic signalling pathway at two hours p.i and numerous processes such as metabolic pathways, negative regulation of apoptotic signalling, response to nutrient levels, response to hormones and the stress response at twenty-four hours p.i. (Appendix C), processes which are discussed in relation to *T. gondii* paracellular transmigration in chapter 7.

4.2.6 Role of the Epithelial Tight Junction During Infection

The TJ complex is composed of adaptor or scaffold proteins as well as regulatory proteins such as kinases and phosphatases which all form protein-protein interactions with their substrates.

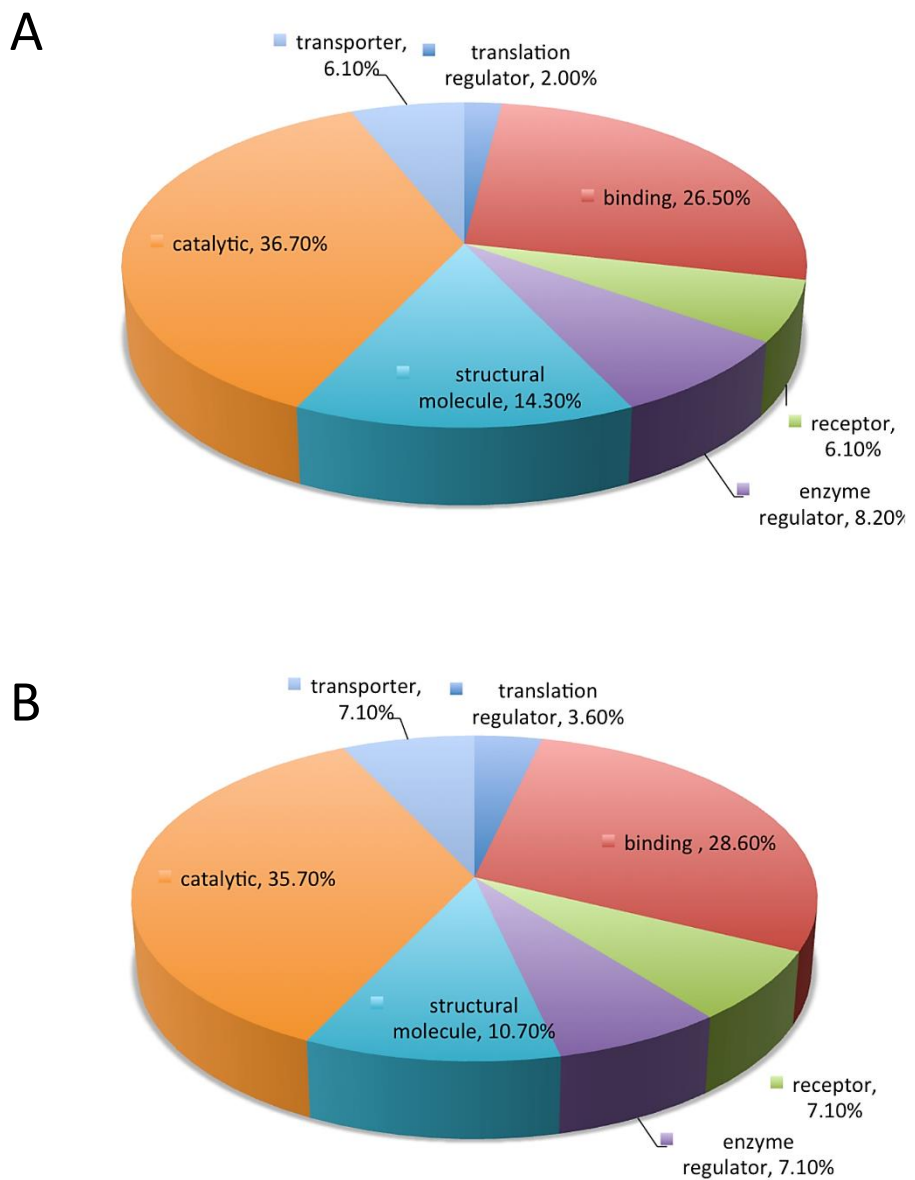


Figure 4.7: Functional categorisation of the SILAC IEC-6 proteins decreasing in abundance during *T. gondii* infection. Numbers correspond to the percentage of identified proteins in each category compared to the total number of proteins. GO annotation was provided by <http://www.pantherdb.org> (version 10). A) Quantification of the predicted function of IEC-6 proteins that decreased in abundance after two hours *T. gondii* infection. B) Quantification of the predicted function of IEC-6 proteins that decreased in abundance after twenty-four hours *T. gondii* infection. A list of all identified proteins is provided in Appendix B.

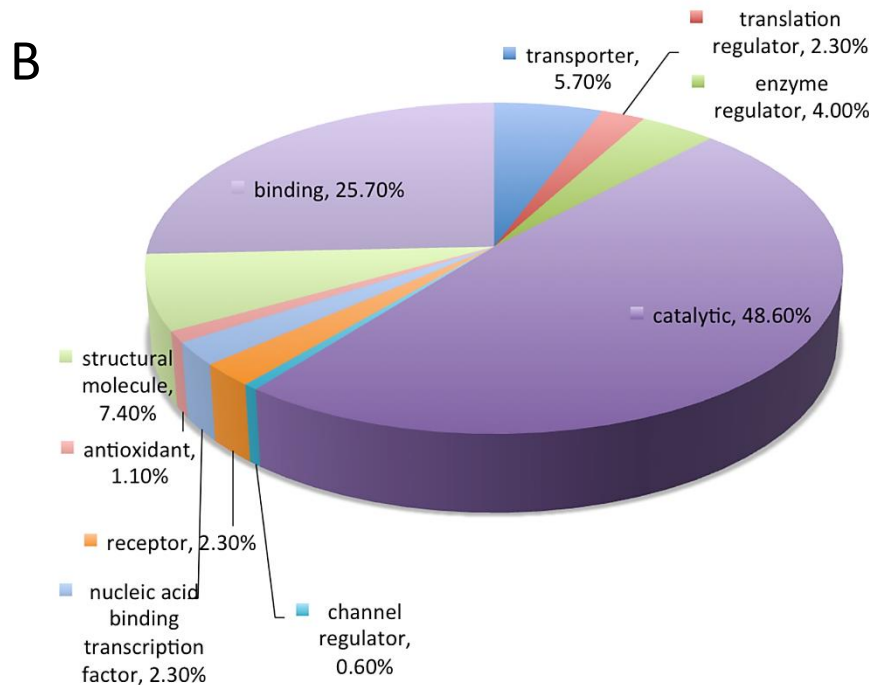
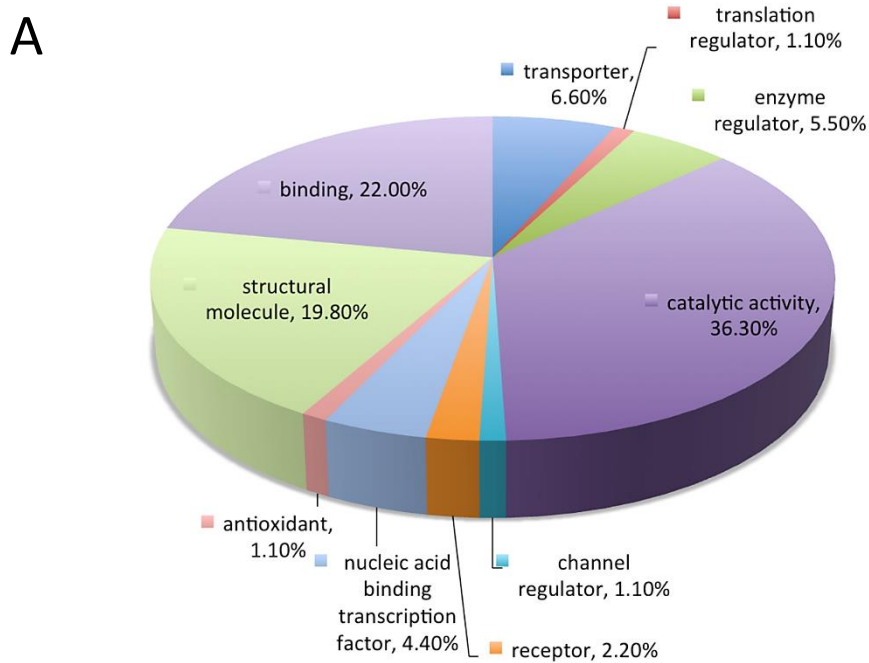


Figure 4.8: Functional categorisation of the SILAC IEC-6 proteins increasing in abundance during *T. gondii* infection. Numbers correspond to the percentage of identified proteins in each category compared to the total number of proteins. GO annotation was provided by <http://www.pantherdb.org> (version 10). A) Quantification of the predicted function of IEC-6 proteins that increased in abundance after two hours *T. gondii* infection. B) Quantification of the predicted function of IEC-6 proteins that increased in abundance after twenty-four hours *T. gondii* infection. A list of all identified proteins is provided in Appendix B.

A comprehensive list of known TJ proteins was constructed by integrating current functional annotations, protein-protein interactions and known signalling pathways [Aijaz et al, 2006; Anderson and Van Itallie, 2009; Balda and Matter 2008 and 2009; Chiba et al, 2008; Dorfel and Huber, 2012; Furuse and Tsukita, 2006; Gonzalez-Mariscal et al, 2008; Kohler and Zahraoui, 2005; Liu et al, 2003; Matter et al, 2005; Matter and Balda, 2003 and 2014; McNeil et al, 2006; Morimoto et al, 2005; Müller et al, 2005; Salama et al, 2006; Schneeberger and Lynch, 2004; Suzuki et al, 2006; Tang, 2006; Turksen and Troy, 2004; Ye et al, 2006; Zahraoui, 2005] (Appendix D).

Comparison between the SILAC dataset and known TJ protein list by Dr Tamás Korcsmáros (Institute of Food Research) using scripts written in Python identified nine IEC-6 TJ-associated proteins significantly modulated by *T. gondii*. The rat Uniprot IDs were inferred human orthologs with the InParanoid webservice, summarised in Table 4.1; at two hours p.i Bcar1, Ybox3 and Mras increased in abundance (red box) and at twenty-four hours p.i Cstf and Ybx3 TJ-associated proteins increased in abundance (red box) and Akt1, Arhgef11, Cldn15 and Prkcl decreased in abundance (green box). These proteins will be discussed in detail in chapter 7.

4.3 Discussion

In this chapter *T. gondii* IEC-6 infection kinetics were established and parasites were confirmed to utilise the paracellular route of infection as well as extensively modulating the host cell proteome upon infection.

During *T. gondii* infection the IEC-6 barrier function was maintained, suggesting tachyzoites do not disrupt the integrity or function of the TJ barrier.

The non-homogenous tachyzoite binding to the IEC-6 monolayer described here has been frequently observed in previous studies [Dvorak and Crane, 1981; Mineo and Kasper, 1994] and confluent monolayers are typically less infected than non-confluent monolayers as parasites preferentially attach to cells in mid-S phase of the host cell-cycle [Grimwood et al, 1996]. This may explain the low percentage of infected cells in this study as the majority of cells in a confluent culture are in G₀ or resting phase rather than mid-S phase [Black and Boothroyd, 2000].

After oral infection, *T. gondii* attachment and transmigration of the SI epithelium are crucial for dissemination within the host to reach secondary sites of infection such as the brain, eyes or developing foetus. Barragan and Sibley suggest establishment of this early wave of rapidly migrating parasites may be particularly important to assure dissemination prior to the onset of an immune response [Barragan and Sibley, 2002].

As seen by two-photon live cell imaging (Figure 4.3-4.4 and Video 4.1), *T. gondii* paracellular transmigration is a complex multi-stage process involving gliding motility and targeting to cellular junctions prior to initial attachment. Video 4.1 highlights the rapid re-orientation of the parasite and entry into the paracellular space. The parasite then appears to transmigrate through the monolayer, leaving the paracellular space empty (figure 4.4A-C). This process is rapid, with the transmigration stage taking less than the speed of one video frame (<52 seconds), comparable with 15-40 seconds in previous studies [Carruthers and Boothroyd, 2007; Egarter et al, 2014; Werk, 1985]. The equivalent basal images (Figure 4.4D) show parasite egress from the monolayer, although the cellular junction is less visible.

Time p.i	Fraction	Fold change	Count	Protein IDs	Protein names	Protein function	Gene names	Fold change
2 hours	cytoplasm	4.308673	3	Q63767	Breast cancer anti-estrogen resistance protein 1	Scaffolding/Adaptor Proteins Transcriptional and Postranscriptional Regulators	Bcar1	4.31
2 hours	cytoplasm	3.352105	7	Q62764	Y-box-binding protein 3 (ZONAB)	Signalling Proteins	Ybx3	3.35
2 hours	membrane	2.648375	6	Q5RKJ7	Ras-related protein M-Ras	Transcriptional and Postranscriptional Regulators	Mras	2.65
24 hours	cytoplasm	26.30956	2	M0RAG5	Cleavage stimulation factor subunit 2	Transcriptional and Postranscriptional Regulators	Cstf2	26.31
24 hours	cytoplasm	4.738214	15	Q62764	Y-box-binding protein 3 (ZONAB)	Transcriptional and Postranscriptional Regulators	Ybx3	4.74
24 hours	cytoplasm	2.0884	13	P47196	RAC-alpha serine/threonine-protein kinase	Kinases and Phosphatases	Akt1	2.09
24 hours	membrane	2.4222	2	F1LQS9	Rho guanine nucleotide exchange factor 11	Signalling Proteins	Arhgef11	2.42
24 hours	membrane	3.386	4	D3ZQJ0	Claudin 15	Tight junction Transmembrane Proteins	Cldn15	3.39
24 hours	membrane	5.059193	5	Q62764	Y-box-binding protein 3 (ZONAB)	Transcriptional and Postranscriptional Regulators	Ybx3	5.06
24 hours	membrane	2.2822	11	Q62074	Protein kinase C iota	Kinases and Phosphatases	Prkci	2.28

Table 4.1: Tight junction proteins modulated during *Toxoplasma gondii* infection of IEC-6. The raw SILAC MS files were processed using MaxQuant [Cox and Mann, 2008] and proteins identified by searching against the Rattus norvegicus (Rat) UniProt database (downloaded 5.6.14). Protein quantitation was performed using MaxQuant to generate heavy and light peptide ratios (fold-change) and Perseus statistical analysis to generate significance-B (p-value) scores. The raw data was filtered according to >2-fold change (compared to uninfected control) and a p-value of <0.05. Using these criteria proteins were considered to be significantly increased (red) or decreased (green) in abundance at either two or twenty-four hours p.i.

Although the observations here describe only the paracellular pathway, we cannot rule out the possibility that parasites may also cross the IEC-6 monolayer *in vitro* or SI *in vivo* by the transcellular route [Barragan et al, 2005]. However, this is unlikely as *T. gondii* rarely exit a host cell from the basal side when apically infected [Morisaki et al, 1995; Tardieu and Menard, 2008]. Parasite transmigration of the SI via the paracellular pathway is also preferable to transcellular invasion in the early stages of infection as the replication and cytolytic stage ultimately destroys the host cell, which leads to tissue injury and induction of an inflammatory response which could limit early parasite dissemination from the SI to secondary immunoprivileged sites of infection [Black and Boothroyd, 2000].

The requirement for host cell invasion prior to *T. gondii* replication highlights the intimate relationship that has evolved between the parasite and host cell that leads to modification of host cell functions and changes in host protein abundance. Previous studies have described how *T. gondii* reorganises the host organelles and cytoskeleton, induces an anti-apoptotic state and highjacks immune cell migration [Laliberte and Carruthers, 2008]. Others have focused on identifying global host cell transcriptome or proteome changes in response to *T. gondii* infection of macrophage or HFF cells *in vitro* and brain tissue *in vivo* [Blader et al, 2001; Nelson et al, 2008; Sahu et al, 2014; Saeij et al, 2007; Xia et al, 2008; Zhou et al, 2011 and 2013]. However, as the initial site of *T. gondii* infection *in vivo* is the SI, we developed a quantitative SILAC proteomics method to examine IEC-6 host cell proteome modulation in response to *T. gondii* infection. Functional classification of the IEC-6 proteome of infected and non-infected cells identified changes in the abundance of catalytic, binding and structural proteins as well as statistically significant enrichment of differentially regulated proteins involved in cell metabolism, glycolysis, organelle organisation, cellular transport, cell cycle, transcription, cell structure and the cellular stress response; all analogous with previous studies [Nelson et al, 2008; Zhou et al, 2011]. Host cells have also evolved lines of defence against parasite invasion and

replication; at both two and twenty-four hours of infection we confirmed increased abundance of host cell proteins involved in negative regulation of apoptotic signalling pathways [Nelson et al, 2008].

The finding that host ICAM-1 significantly increased in abundance with a fold change of 4.16 (Appendix B P202) during infection was particularly interesting as this has previously been shown by a number of groups in a variety of biological barriers encountered by *T. gondii* [Barragan et al, 2005; Furtado et al, 2012; Klok et al, 1999; Nagineni et al, 2000; Pfaff et al, 2005; Sumagin and Parkos, 2014; Yang et al, 2005]. Barragan et al first confirmed a mechanism of paracellular transmigration mediated by interactions between host ICAM-1 and parasite adhesin MIC2 [Barragan et al, 2005]. The authors found that only the parasite surface form of MIC2, not the secreted form, bound to host ICAM-1 as the mature secreted form of MIC2 lacks the integrin I/A-domain. Thereby suggesting that the host-parasite interaction is similar to that of $\beta 2$ integrins and that *T. gondii* may utilise a similar mechanism of paracellular transmigration to leuckocyte vascular extravasation or transepithelial migration [Barragan et al, 2005; Sumagin and Parkos, 2015].

Taken with the live imaging evidence for the paracellular route of infection described above, this finding led to our novel hypothesis that *T. gondii* may interact with and modulate apical TJ-associated proteins during paracellular transmigration of the SI epithelium. A mechanism that has been exploited by viruses and bacterial pathogens, although how this contributes to disease development and progression is poorly understood [Zihni et al, 2014].

Accordingly, identifying the components of the TJ protein complex modulated in response to *T. gondii* will be an important step towards understanding the molecular mechanisms of paracellular parasite infection and will aid the development of therapeutic strategies against *T. gondii*. The SILAC proteomics data set was examined for modulation of TJ-associated proteins in response to *T. gondii* infection. Although, it should be noted that we are only just beginning to understand the

function of the TJ in molecular terms, as the architecture of the TJ remains incomplete and further important constituents may remain to be defined.

After two hours of *T. gondii* infection three host proteins associated with the TJ were modulated; Bcar1, Ybox3 and Mras compared to six after twenty-four hours of infection including Cstf2, Ybx3, Akt1, Arhgef11, Cldn15 and Prkcl. These proteins relate to early parasite infection strategies such as attachment, TJ disruption and paracellular transmigration as well as the initiation of intracellular PV formation. As not all cells in the monolayer are infected at this stage, a large proportion of host cells remain unchanged and this may account for the low number of proteins that appear to be modulated at this time point.

Breast cancer antioestrogen resistance 1 (Bcar1 also known as p130CAS), is an adaptor protein that belongs to the CAS family of scaffold proteins that are associated with the formation of multi-protein signalling complexes that play a role in cell motility, cell adhesion, cytoskeleton remodelling, invasion, survival and proliferation [Defilippi et al, 2006; Leal et al, 2015]. As Bcar1 relays signals downstream of integrins via c-SRC, FAK and PI3 kinases, it is tempting to speculate that the upregulation of Bcar1 may be due to parasite attachment to host surface integrins [Furtado et al, 1992]. Although here there was no change observed in its abundance during infection, PI3K is known to associate with occludin and JAM-A to mediate the recruitment of PTEN to the TJ and activate Akt, though changes in kinase activity were not measured in this study [Matter et al, 2005].

Mras is a Ras-related protein whose downstream effector afadin (AF6) binds to ZO-1 at the TJ to maintain cell-cell contacts [Kuriyama et al, 1996; Quilliam et al, 1999]. However, competitive binding of Mras to ZO-1 may disrupt the TJ barrier, a possible consequence of its increased abundance at the host cell membrane [Yamamoto et al, 1997]. As ZO-1 also directly interacts with occludin, it is possible that increased Mras binding to ZO-1 modulates the localisation of occludin at the TJ [Furuse et al, 1994].

The proteins modulated at twenty-four hours p.i correlate with a later stage of infection where PV formation extensively remodels the host cell proteome and alters subcellular protein compartmentalisation. However, as *T. gondii* does not infect all cells to which parasites attach, some cells will be affected by *T. gondii* secreted factors. For example, parasites secrete ROP and MIC proteins into neighbouring cells to prepare them for invasion; the host cell cycle for instance has been shown to be targeted as *T. gondii* preferentially infect cells in the S-phase [Blader and Saeij, 2009; Grimwood et al, 1996; Koshy et al, 2012; Lavine and Arrizabalaga, 2009; Molestina et al, 2008].

The upregulation of Ybox binding protein 3 (Ybox3, also known as ZONAB) at both two and twenty-four hours p.i is therefore interesting as it has been linked to cell cycle progression. As ZO-1 sequesters and inhibits ZONAB in the cytoplasm, the increased ZONAB abundance in the host cell cytoplasm at two hours p.i may lead to ZONAB accumulation in the nucleus and interaction with the G₁/S phase regulator CDK4, which leads to increased expression of genes that promote cell cycle progression to S-phase [Balda et al, 2003; Matter et al, 2005]. The increased ZONAB abundance in the membrane at twenty-four hours p.i suggests junctional localisation of the transcription factor and inactivation of the pathway.

Likewise, the Rho guanine nucleotide exchange factor (GEF) 11 (ARHGEF11, also known as PDZ-RhoGEF) has been linked to cell cycle progression. ARHGEF11 mediates RhoA-activated actomyosin at the TJ and binds to ZO-1 [Itoh et al, 2012]. Downstream RhoA signalling regulates paracellular permeability via GEF-H1 as well as promoting S-phase progression via ZONAB [Zihni et al, 2014].

Decreased abundance of ARHGEF11 has been shown to disrupt TJ assembly and establishment of the TJ barrier with Rho signalling pathways playing a central role. For example, phosphorylation of the Rho target MLC is significantly downregulated in ARHGEF11-depleted cells, although ARHGEF11 depletion does not affect occludin expression [Itoh, 2013; Samarin et al, 2007]. The decrease in abundance of ARHGEF11 at

the host membrane may therefore promote cell cycle progression to the preferential S-phase as well as disrupt the TJ barrier in a Rho dependant mechanism, which is potentially important for parasite paracellular transmigration.

Further evidence for parasite modification of the host cell cycle is provided by the 26-fold increase in abundance of cleavage stimulation factor 2 (Cstf2 also known as Cstf-64), a member of the cstf complex that plays a role in polyadenylation of mRNA [Takagaki et al, 1992]. Cstf2 has been shown to be significantly upregulated during the G₀ to S-phase transition [Martincic et al, 1998]. As Cstf2 binds to the molecular scaffold protein symplekin, which associates with ZO-1 at the TJ and ZONAB in the nucleus [Chang et al, 2012; Xing et al, 2004], the significantly increased abundance of Cstf2 in the host cell cytoplasm may promote association with ZONAB in the nucleus and instigate progression of the host cell cycle to S-phase.

RAC- α serine threonine protein kinase (Akt, also known as protein kinase B, PKB) has been shown to play a role in TJ regulation in the intestine by forming a complex with ZO-2 and JAM-A [Monteiro et al, 2013]. This complex formation at the TJ may explain the decreased abundance of Akt in the host cytoplasm. It has been confirmed that the PI3K/Akt pathway is a major target for *T. gondii*-dependant inhibition of apoptosis via Akt phosphorylation of Bad [Datta et al, 1997; Danial, 2008; Quan et al, 2013], a mechanism required to promote host cell survival [Duronio, 2008; Kim and Denkers, 2006; Scheid and Woodgett, 2001]. The PI3K/Akt pathway has also been implicated in Claudin-2 expression via inhibition of GSK-3 β and nuclear translocation of β -catenin, demonstrating the complexity of this signalling pathway [Amasheh et al, 2010; Wang et al, 2011].

The decrease in abundance of claudin-15 (cldn15) is particularly interesting as it directly relates to TJ barrier function. In the SI epithelium, expression of claudins varies between the crypt and villus and is associated with TJ permeability [Amasheh et al, 2002; Wada et al, 2013]. For example a decrease in claudin-15 at the TJ is known to

increase permeability and can initiate IBD [Darsigny et al, 2009]. Interestingly, *Clostridium perfringens* enterotoxin binding to claudin-3 and -4 leads to their dissociation and subsequent TJ degradation [Sonoda et al, 1999]. It is possible that *T. gondii* similarly disrupts claudin-15 at the TJ during paracellular transmigration either by directly binding to claudin-15 or indirectly via parasite binding to other TJ proteins such as occludin, although the interaction between claudins and occludin is not well understood. Of note, claudins have been shown to interact with cell surface receptors such as integrins [Ding et al, 2012; Stone, 2011; Furtado et al, 1992], reiterating the possible mechanism of *T. gondii* induced TJ disruption via binding to host integrins prior to infection.

The decrease in atypical protein kinase C ι (Prkci) abundance at the host cell membrane is noteworthy as aPKC is directly associated with the phosphorylation status of the transmembrane TJ proteins occludin and claudins [Andreeva et al, 2001; Aono et al, 2008; Raleigh et al, 2011; Rao, 2009; Sjo and Magnusson, 2010; Suzuki et al, 2009]. Hyperphosphorylated occludin is located at the TJ and plays a role in TJ assembly [Sakakibara et al, 1997] and similarly, claudin phosphorylation has been linked to TJ assembly and function. For example, PKC θ phosphorylation of claudin-1 and -4 is required for TJ insertion [Banan, 2005]. In contrast, PP2A phosphatase dephosphorylation decreases claudin-1 and ZO-1 localisation at the TJ and reduces barrier function [Nunbhakdi-Craig et al, 2002]. As *T. gondii* secrete PP2 phosphatase as well as a number of ROP-derived kinases into the host cell prior to infection [Bradley et al, 2005; Dubremetz, 2007; Gilbert et al, 2007; Jan et al, 2009; Laliberte and Carruthers, 2008], claudin dephosphorylation could contribute to TJ disruption during parasite infection. It is tempting to speculate that either *T. gondii* infection modulates host kinase interactions with occludin or parasite-derived kinases and phosphatases directly target occludin in order to disrupt the TJ and enhance *T. gondii* transmigration of the paracellular pathway.

As the signalling pathways associated with these modulated host proteins demonstrate complex cross talk, network analysis is currently in

progress to fully understand the interactions between the modulated host proteins and the effect of their abundance changes on downstream signalling pathways. It should be noted that modelling of the TJ signalling complex is challenging as a wealth of information must be integrated into the mathematical model; TJ-associated protein-protein interactions may be weak or transient and TJ assembly and disassembly is highly dynamic and occurs over a short time. Clearly there is still much to be learnt in order to understand the complex interplay between TJ-associated proteins and downstream signalling pathways and how these are modulated during *T. gondii* infection. Elucidating how the dysregulation of junctional signalling mechanisms contributes to disease development will be key for diseases associated with a loss of TJ barrier function such as IBD.

One drawback of the SILAC method is that only quantifies changes in protein abundance and not changes in protein function, for example enzyme activity levels. Therefore future validation should include functional studies, such as analysis of changes in PI3K activity, potentially utilising an *in vitro* kinase assay as described in chapter five. In addition, SILAC does not discriminate between host-cell proteins modulated by direct parasite infection or parasite secreted factors. In future therefore, filtered conditioned media from parasite cultures or infected cells could be used as additional controls to identify host proteins modulated by secreted factors. As infected and non-infected cells were analysed simultaneously by SILAC, a technique that could be used to isolate infected cells and distinguish between host proteome modulation by intracellular parasites or transmigrating parasites would be single-cell laser dissection [Fink et al, 2006; Xu and Caprioli, 2002]. This would increase resolution and permit targeted proteomic analysis of SI epithelial cells *in vitro* or *in vivo* at specific stages of infection.

In order to validate the differentially expressed TJ proteins, immunohistochemistry could be used to ensure protein expression corresponds with the SILAC results presented here. Another attractive future experiment would be to confirm our *in vitro* findings *in vivo*, using

the SILAC rodent model [Krüger et al, 2008; McClatchy et al, 2007; Wu et al, 2004]. To verify the physiological relevance of the identified TJ proteins modulated during *T.gondii* infection, site directed mutagenesis of cell lines or gene KO mice [Furuse, 2009] could be utilised in combination with confocal or two-photon live microscopy to assess changes in parasite paracellular transmigration. Encouraging preliminary experiments also suggest co-immunoprecipitation of host cell lysates with *T. gondii* and MS analysis could also be used in future to identify *T. gondii* proteins interacting with the host TJ [Weight, unpublished].

4.4 Conclusions

This chapter has provided evidence for *T. gondii* tachyzoite transmigration of the SI epithelium via the paracellular route at an early stage of infection, an effective mechanism for rapid traversal of the epithelium. To our knowledge, this novel finding is the first live-imaging observation of *T. gondii* utilising the paracellular route of transmigration. We also examined modulation of the IEC-6 proteome in response to infection and highlighted the important role of the TJ-associated proteins. Although it was not possible to identify occludin in differentially infected SILAC labelled IEC-6 cell cultures, many of the modulated proteins show cross talk with occludin downstream signalling pathways and further analysis of these interactions is in progress. We predict that secretion of parasite-derived kinases into the host cell during infection alters the occludin phosphorylation status, disrupting the TJ barrier and increasing parasite paracellular transmigration. These changes in phosphorylation status during infection will be investigated using an *in vitro* kinase assay in Chapter five.

5 Changes in Occludin Phosphorylation in Response to *Toxoplasma gondii* Infection

5.1 Introduction

The previous chapter confirmed parasites utilise the paracellular route of infection and described changes in the host TJ proteome in response to *T. gondii* infection. As a number of parasite derived kinases and phosphatases are secreted into the host cytoplasm during infection, it could be predicted that the cytoplasmic occludin C-terminus phosphorylation status is modulated during infection and will be investigated in this chapter.

Pathogens such as enteropathogenic *E. coli* (EPEC) [Simonovic et al, 2000; Zhang et al, 2010], *C. difficile* [Nusrat et al, 2001], *C. perfringens* [Fujita et al, 2000; Sonoda et al, 1999] and *S. typhimurium* [Jepson et al, 1995] as well as the Der p 1 allergen [Wan et al, 2000] and reovirus [Barton et al, 2001] have been shown to disrupt the TJ protein complex and dissociate occludin from intestinal epithelial TJs in order to transmigrate the epithelium. This has been linked to a shift from hyperphosphorylated TJ-associated occludin to non-phosphorylated intracellular compartment-associated occludin [Rao, 2009; Simonovic et al, 2000; Weight, 2011]. Transient occludin phosphorylation or dephosphorylation by *T. gondii* could therefore present a mechanism for occludin localisation to and from the TJ, enabling parasite paracellular infection of the SI epithelium.

Occludin phosphorylation was first described in 1997 due to the range of occludin bands resolved by SDS-PAGE [Furuse et al, 1993; Saitou et al, 1997]. The molecular weight of these bands in MDCK I cells is between 62kDa-82kDa depending on the phosphorylation status of serine (S), threonine (T) and tyrosine (Y) residues in the occludin C-terminus [Sakakibara et al, 1997]. Occludin phosphorylation also appears to play a central role in TJ regulation; Sakakibara et al demonstrated that

occludin phosphorylation is directly involved in TJ assembly and that highly phosphorylated occludin is predominantly located at the TJ [Sakakibara et al, 1997]. Similarly, Wong, Farshori and Kachar also confirmed phosphorylation regulates occludin localisation to and from the TJ at steady state [Farshori and Kachar, 1999; Wong, 1997]. Consequently, non-phosphorylated occludin species are located intracellularly in the vesicular compartment, serine-threonine phosphorylated species at the lateral membrane and the functionally active multiple-serine hyper-phosphorylated species exclusively at the TJ [Andreeva et al, 2001; Sakakibara et al, 1997; Tsukamoto and Nigam 1999; Wong, 1997]. This occludin trafficking pattern to and from the TJ mirrors the FRAP studies, described in chapter 1, in which occludin is first delivered to the lateral cell membrane then traffics within the membrane to the TJ [Shen et al, 2008].

Dorfel and Huber have extensively reviewed occludin phosphorylation in epithelial cells and the authors conclude several known kinases such as c-Src, ROCK, cPKC, PKC η PKC ζ , CKII and VEGF dynamically and reversibly phosphorylate occludin to modulate TJ structure and permeability. Table 5.1 summarises the current known effects on TJ function associated with phosphorylation of occludin C-terminus aa residues. Human aa residues are stated with corresponding murine residues in brackets and the experimental models relate to hypo-(red) or hyper- (green) phosphorylated cellular occludin [Dorfel and Huber, 2012]. Phosphatases such as PP1, PP2A, and DEP-1, which have been associated with TJ integrity, also reverse the action of kinases to play an important role in coordinating occludin phosphorylation but they have been much less studied [McCole, 2013; Seth et al, 2007].

Kinase	Residue	Cell lines	Occludin expression	Functional outcome
cSrc	Y398/Y402	Caco-2 MDCK Rat-1	Overexpression	TEER ↓ inulin permeability ↑ junctional occludin ↓
			Y398D/Y402D mutation	TJ-assembly ↓ inulin permeability ↑ interaction of occludin with ZO-1, -2 and -3 ↓
			Inhibition/KD	TEER ↑ inulin permeability ↓ TJ-assembly ↑
cSrc	Y473 (mouse)	MDCK	Y398D/Y402D mutation	junctional occludin ↑
			Y473D-mutation	interaction of occludin with PI3K ↑
			Y473D-mutation	interaction of occludin with PI3K ↓
ROCK	(T382)/S507 (mouse)	COS-7	overexpression	TEER ↑
			Inhibition/KD	TEER ↑
			overexpression	insoluble occludin ↑ junctional occludin ↑
cPKC	S338 (mouse)	MDCK	overexpression	TEER ↑ inulin permeability ↓ junctional occludin ↑
			T403D/T404D mutation	TEER ↑ inulin permeability ↓ junctional occludin ↑
			Inhibition/KD	TEER ↑ inulin permeability ↓ junctional occludin ↑
nPKC η	T403/T404 (438)	MDCK Caco-2	T403D/T404D mutation	TEER ↓ junctional ZO-1 ↓ junctional occludin ↓
			Inhibition/KD	TEER ↓ inulin permeability ↑ junctional occludin ↓ TJ-assembly ↓
			T424A/T438A mutation	junctional occludin ↓ TJ-assembly ↓
aPKC ζ	T424/T438 (T403/T404)	Rat-1 MDCKII Caco-2		

Table 5.1: Summary of known occludin C-terminus phosphorylation sites and their effect on TJ function. The cellular kinases affected by occluding mutation and resulting overexpression (green) or reduction (red) in each experimental model refer to human aa residues with corresponding murine residues in brackets. The functional effect of occludin residue mutation on the TJ is represented as an increase (up arrow) or decrease (down arrow). Image adapted from Dorfel and Huber, 2012.

Deregulated TJ protein phosphorylation has also been associated with inflammatory intestinal diseases such as IBD or cancer so it is therefore an important regulatory mechanism of TJ barrier function [Dorfel and Huber, 2009].

At the time of writing it is not clear whether the phosphorylation of occludin by various kinases is mutually exclusive or if they could act in combination and it is also probable that other kinases target the occludin C-terminus aa residues and this will be investigated as part of this chapter.

5.2 Results

5.2.1 Prediction of Novel Occludin Kinases

To identify novel IEC-6 occludin kinases the bioinformatics ExPASy kinase-specific prediction software NetPhos and NetPhosK were used to predict occludin C-terminus phosphorylation sites by searching for homologous kinase target motifs within the occludin C-terminus aa sequence [Blom et al, 2004]. 50 potential occludin C-terminus serine, threonine and tyrosine phosphorylation sites were identified, 26 of which conformed to consensus kinase sequence motifs (Figure 5.1). The search threshold was set to 0.05 to reduce the number of false-positives. Comparison with the SILAC dataset presented in chapter four (Appendix B), confirmed the IEC-6 cell line expressed 15 kinases that could potentially phosphorylate the occludin C-terminus in an *in vitro* kinase assay: CKI, CKII, ROCK, EGFR, Src, Yes, Lyn, INSR, Cdk5, GSK, FAK, PKC δ , PKC ι and MAPK as well as phosphatase PP1. Searching for novel occludin C-terminus phosphorylation sites targeted by these IEC-6 kinases identified three CKII, two PKC, one EGFR/INSR and one RSK C-terminus phosphorylation site. The locations of these novel phosphorylation sites are depicted in Figure 5.

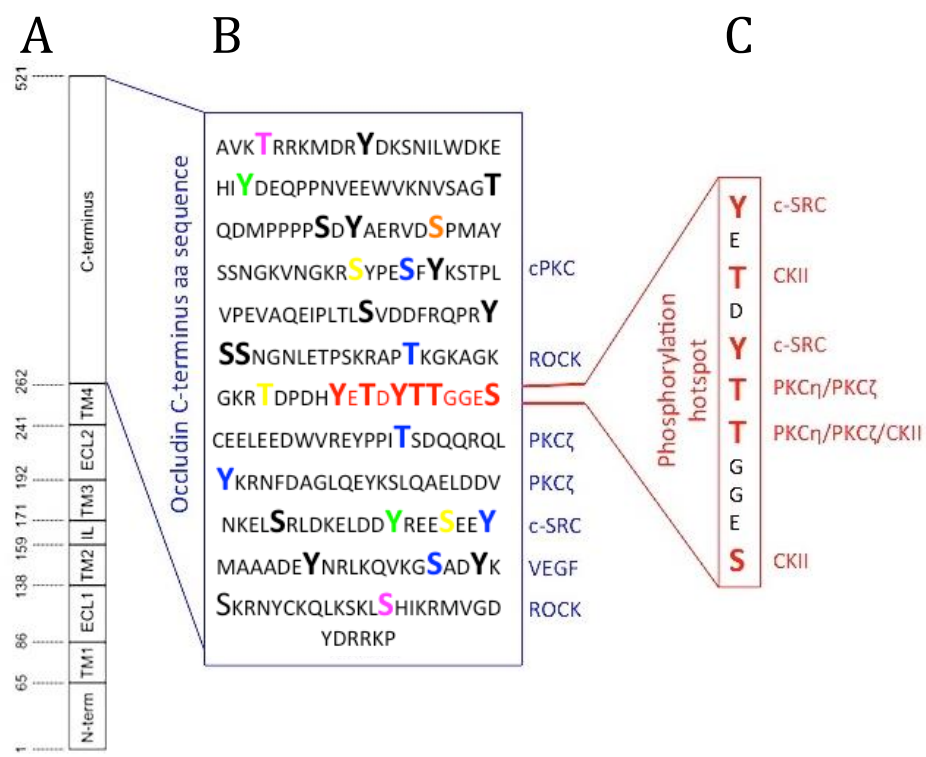


Figure 5.1: Occludin kinase bioinformatics. A) Full-length murine occludin sequence. B) Murine occludin C-terminus aa phosphorylation sites and kinases predicted using ExPASy kinase prediction software NetPhos and NetPhosK by searching the occludin C-terminus sequence for known kinase target motifs [Blom et al, 1999 and 2004] at a threshold of 0.05. Predicted occludin C-terminus aa phosphorylation sites are highlighted in BOLD: tyrosine (Y), threonine (T) and serine (S). Novel CKII phosphorylation sites are indicated in yellow, PKC in pink, EGF in green and RSK in orange and Occludin aa c-terminus residues that have been experimentally confirmed are highlighted in blue and the kinase is indicated. C) The occludin phosphorylation hotspot aa residues [Dorfel and Huber, 2012] are highlighted in red and the experimentally confirmed kinase is indicated [Andreeva et al, 2006; Basuroy et al, 2003; Cordenonsi et al, 1999; Du et al, 2010; Elias et al, 2009; Jain et al, 2011; Kale et al, 2003; Murakami et al, 2009; Raleigh et al, 2011; Smales et al, 2003; Sundstrom et al, 2009; Suzuki et al, 2009; Yamamoto et al, 2008].

5.2.2 *In Vitro* Occludin Kinase Assay

Since O'Farrell and Klose demonstrated that proteins could be separated based on their isoelectric point and molecular weight, two-dimensional gel electrophoresis (2D-GE) has been used as a method of separating complex protein samples [O'Farrell, 1975; Klose, 1975]. Furthermore, labelling using fluorescent dyes such as ProQ Diamond [Steinberg et al, 2003] and Phos-tag [Kinoshita et al, 2004] has been used to quantitate protein phosphorylation. Using these properties a novel *in vitro* kinase assay was developed here to assess changes in occludin phosphorylation status.

The *in vitro* kinase assay reflects a simplified cellular system where recombinant occludin C-terminus peptides were incubated in the presence of active purified kinase and the phosphorylation status assessed by 2D-GE and MS. As 2D-GE separates post-translationally modified proteins, the spots on a 2D gel reflect differences in the extent of occludin phosphorylation.

To confirm the *in vitro* kinase assay could detect changes in occludin phosphorylation, the ubiquitously expressed serine/threonine kinase CKII was initially used as the source of kinase [Dorfel et al, 2009 and 2013]. Recombinant occludin C-terminus peptides incubated with purified CKII in the presence of ATP were compared with no kinase controls. The peptides were separated horizontally by their net charge using pH4-11 1D isoelectric focusing (IEF) strips prior to vertical separation based on their molecular weight in conjunction with SDS-PAGE.

In the presence of CKII, a series of phosphorylated occludin species were detected using the ProQ Diamond phosphoprotein stain [Schulenberg et al, 2003] (Figure 5.2D) compared to the control (Figure 5.2B). SYPRO Ruby total protein staining confirmed high abundance of non-phosphorylated occludin and low abundance of highly phosphorylated occludin (Figure 5.2A and C) [Steinberg et al, 2003].

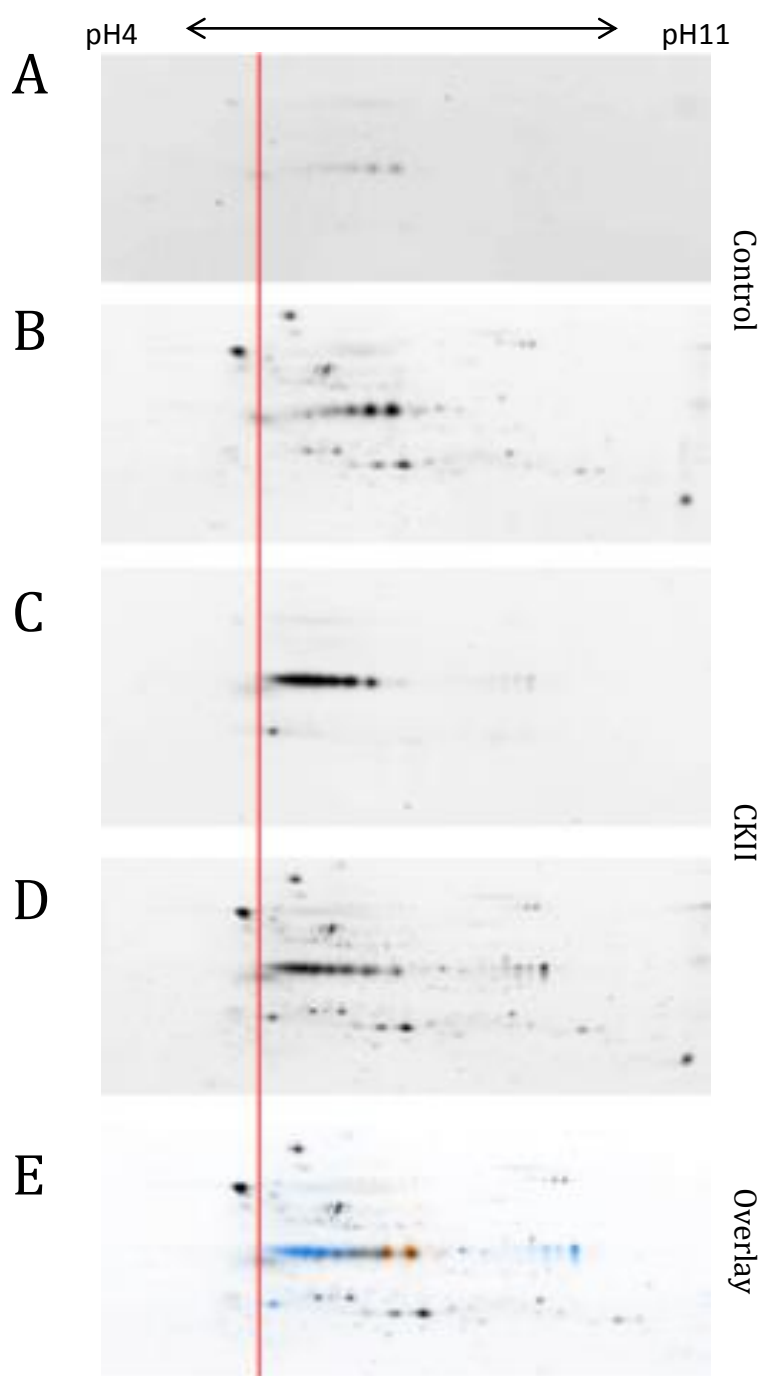


Figure 5.2: *In vitro* occludin kinase assay. Recombinant occludin C-terminus peptides were incubated with purified CKII in the presence of ATP and compared with no kinase controls. A) Control samples stained using SYPRO Ruby for total protein, image intensity 52%. B) Control sample stained using ProQ Diamond for phosphoproteins, image intensity 69%. C) CKII sample stained using SYPRO Ruby for total protein, image intensity 52%. D) CKII sample stained using ProQ Diamond for phosphoproteins, image intensity 69%. E) Overlay image of ProQ Diamond control in orange and CKII in blue. A-E) 2D-GE images were aligned using conserved protein spots, depicted as a vertical red line.

For comparison, both sets of images were taken at an intensity of 52% and 69% respectively. The blue spot mobility shift towards the left of the gel in the overlay image (Figure 5.2E) confirmed an increase in phosphorylation in the presence of CKII, whereas the orange spot mobility shift towards the right of the gel confirmed the presence of non-phosphorylated total protein in the control.

5.2.3 Occludin Phosphorylation Analysis by Mass Spectrometry

The ExPASy Peptide Cutter software [Gasteiger et al, 2005] was used to predict potential occludin C-terminus protease cleavage sites. Peptide cleavage of the occludin C-terminus phosphorylation hotspot region, and protein sequence coverage for trypsin, asp-N endopeptidase and glutamyl endopeptidase were compared by MS. Glutamyl endopeptidase gave the greatest occludin sequence coverage at 53% and optimal 12aa peptide length within the hotspot region.

To verify the predicted novel CKII occludin C-terminus phosphorylation sites: S334 T392 and S470, the seven phosphorylated peptide spots in Figure 5.1B were picked from gels and analysed by MS (Method section 2.12). Although each spot identified several of the phosphorylated residues, seven unique occludin C-terminus aa residues phosphorylated by CKII (Table 5.2) were identified; confirming the presence of the previously experimentally validated T399 phosphorylation site and although the predicted CKII sites were not detected, six novel occludin C-terminus aa residues were found to be phosphorylated by CKII. Further experimental validation will be required to confirm the biological significance of these findings.

Residue	Peptide score	Peptide Hits	Experimentally confirmed
S311	67	5	No
S319	30	1	No
S324	57	8	No
S325	58	7	No
S368	35	11	No
S369	63	7	No
T399	12	1	Yes

Table 5.2: CKII occludin C-terminus phosphorylation footprint. The seven phosphorylated peptide spots were picked from gels and analysed using an Orbitrap Fusion Tribrid Mass Spectrometer (Thermo Scientific). The raw MS files were converted to MASCOT Generic Format (mgf) format using MS Convert (<http://proteowizard.sourceforge.net>) and searched using MASCOT (Matrix Science). Phosphorylation sites were considered significant with a peptide score of ≤ 30 and at least two detected peptide hits. The detected phosphorylation sites were subjected to a literature search to confirm if they had been previously experimentally confirmed.

5.2.4 IEC-6 occludin phosphorylation footprint modulation by *Toxoplasma gondii*

To investigate the IEC-6 occludin phosphorylation footprint, the *in vitro* kinase assay was modified to include IEC-6 lysates as the source of native cellular kinases. IEC-6 monolayers cultured in 25cm² plastic flasks for seven days were either non-infected or infected with *T. gondii* for two hours, lysed and incubated with recombinant fragments of occludin C-terminus and compared with no kinase controls as above.

Subsequent 2D-GE identified a series of phosphorylated occludin species in the presence of infected (Figure 5.3F) and uninfected IEC-6 lysates (Figure 5.3D) compared to no kinase controls (Figure 5.3B) using the ProQ Diamond phosphoprotein stain [Schulenberg et al, 2003]. SYPRO Ruby total protein staining [Steinberg et al, 2003] confirmed a high abundance of non-phosphorylated occludin in the control (Figure 5.3A) and low abundance of highly phosphorylated occludin due to incubation with non-infected IEC-6 and infected IEC-6 (Figure 5.3C and E). The occludin C-terminus protein spot mobility shift towards the left of the ProQ Diamond stained gels (Figure 5.3D and F) demonstrated high abundance of phosphorylated occludin C-terminus species in the presence of non-infected and infected IEC-6 lysates, whereas the spot mobility towards the right of the gel (Figure 5.3B) confirmed the presence of non-phosphorylated occludin species in the control.

It should be noted that the apparent abundance of phosphorylated occludin C-terminus in the control is due to the high intensity of the image (80%) and does not reflect the actual low abundance of phosphorylated occludin C-terminus. Due to these inconsistencies it was not possible to quantify any differences between the non-infected and infected samples and it was only possible to perform this experiment once in the time available.

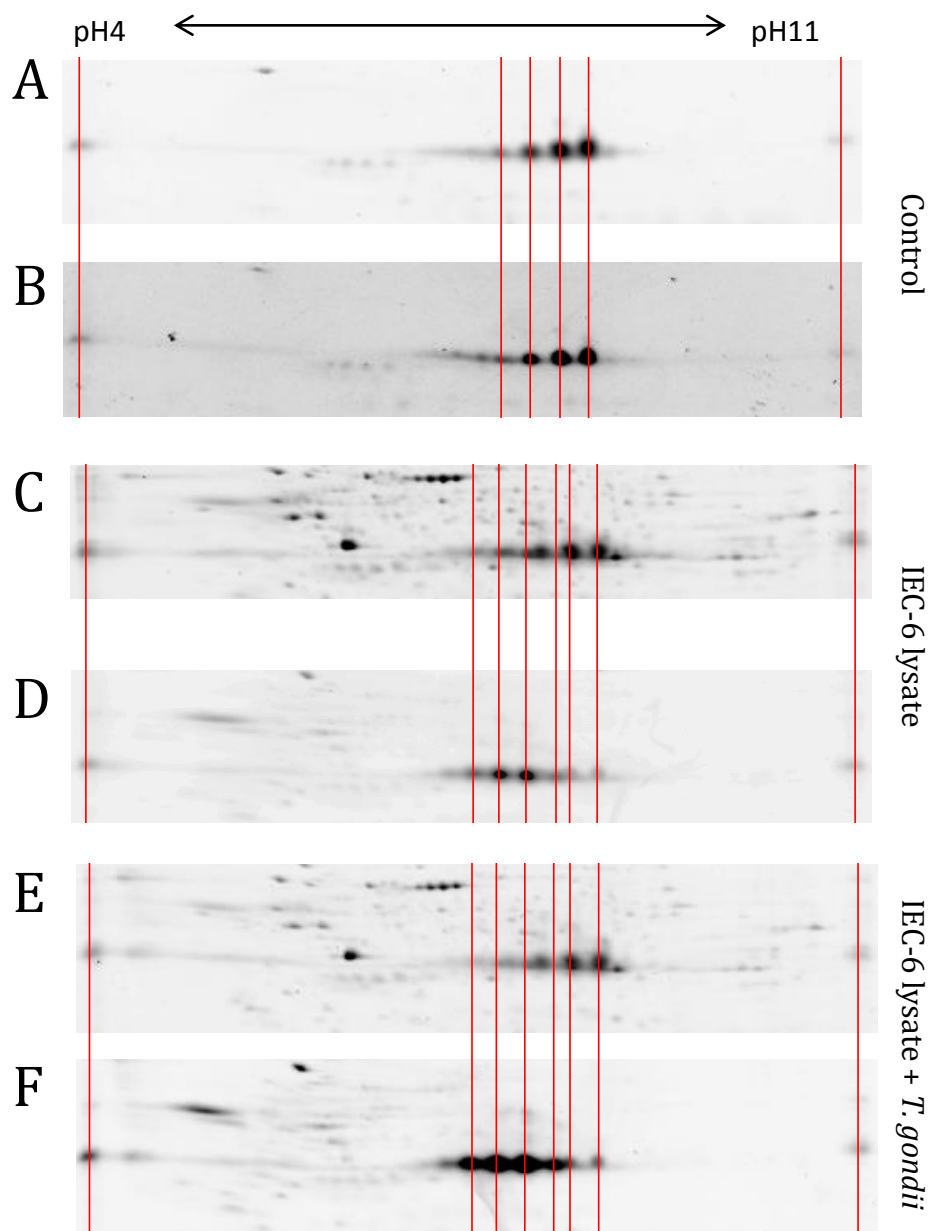


Figure 5.3: *Toxoplasma gondii* modulation of IEC-6 *in vitro* occludin kinase assay. IEC-6 monolayers cultured in 25cm² plastic flasks for seven days were uninfected or infected with *T. gondii* for two hours. IEC-6 were subsequently lysed and incubated with recombinant fragments of occludin C-terminus peptides in the presence of ATP and compared with no lysate controls. A) Control samples stained using SYPRO Ruby for total protein, image intensity 52%. B) Control sample stained using ProQ Diamond for phosphoproteins, image intensity 80%. C) Non-infected IEC-6 lysate sample stained using SYPRO Ruby for total protein, image intensity 55%. D) Non-infected IEC-6 lysate sample stained using ProQ Diamond for phosphoproteins, image intensity 55%. E) Infected IEC-6 lysate sample stained using SYPRO Ruby for total protein, image intensity 55%. F) Infected IEC-6 lysate sample stained using ProQ Diamond for phosphoproteins, image intensity 58%. A-E) 2D-GE images were aligned using conserved protein spots at the far left and right of the images (red lines). Protein spots analysed by MS are crossed by a vertical red line.

5.2.5 *Toxoplasma gondii* Derived Kinases Targeting Occludin

Potential *T. gondii* proteins targeting the occludin C-terminus were identified using a bioinformatics approach; the rat occludin C-terminus sequence was searched against the *T. gondii* genome using NCBI-BLAST provided at www.toxodb.org (release number 24 14th April 2015) [Gajria et al, 2008]. The database was used to search for occludin homology with the *T. gondii* ME49, GT1 and VEG strain genomes as the RH strain genome was incomplete at the time of writing. 53 parasite-derived proteins were identified as potentially interacting with the occludin C-terminus (Appendix E) and functional classification of C-terminus interacting parasite proteins using GO annotation revealed involvement in phosphorylation and dephosphorylation (5.6%) but the majority of proteins were unclassified (83%). Two parasite-derived kinases were predicted to interact with the occludin C-terminus: wee kinase and calmodulin kinase (CAM) TgCDPK1, a calmodulin-like domain protein kinase (CDPK) family member, as well as one tyrosine/serine/threonine phosphatase (Appendix E).

5.3 Discussion

The occludin *in vitro* kinase assay identified six novel CKII occludin C-terminus phosphorylation sites and preliminary results confirm the *in vitro* kinase assay is able to detect occludin C-terminus phosphorylation by infected and non-infected IEC-6 lysates, although differences between the occludin phosphorylation footprint remain to be identified.

The balance between host kinases and phosphatases is known to regulate occludin phosphorylation at a range of C-terminus sites, directly affecting its function at the TJ [Cummins, 2011; Dorfel and Huber, 2011 and 2012].

Many of these known occludin phosphorylation sites are located within a highly conserved 11aa sequence representing a Serine-Threonine kinase hotspot within the proximal occludin C-terminus, close to the hydrophobic coiled-coil occludin ELL (OCEL) domain [Buschmann et al, 2013; Dorfel and Huber, 2012]. The six hotspot aa residues are targeted by six different kinases including c-Src, nPKC η and CKII and the location of this hotspot near a cysteine residue previously associated with occludin self-association suggests targeted phosphorylation in this region could play a role in occludin dimer formation between neighbouring cells [Nusrat el al, 2000], essential for TJ barrier regulation as well as ZO-1 recruitment and association with claudins [Bellmann et al, 2013; Blasig et al, 2006; Li et al, 2005; McCaffrey et al, 2008; Nusrat et al, 2000; Schulzke and Gunzel, 2012; Walter et al, 2009]. It is currently unknown if the occludin C-terminus aa residues are phosphorylated sequentially or randomly and whether the phosphorylation of some aa residues is functionally more important than others [Sakakibara et al, 1997].

Several groups have examined the effect of occludin phosphorylation on TJ molecular structure and barrier function by various kinases, many of which are expressed in IEC-6. CKII for example has been widely studied and is confirmed to phosphorylate at least three occludin C-terminus aa residues in mouse, *Xenopus laevis* and human [Cordenonsi et al, 1999; Dorfel et al, 2009; Smales et al, 2003]. Furthermore, studies by Raleigh et al provided some functional insight; CKII mediated phosphorylation of occludin S408 modulates interactions between ZO-1, Claudins-1 and -2 and implicates S408 phosphorylation and dephosphorylation as a molecular switch that regulates paracellular TJ structure and function [Raleigh et al, 2011]. Using phosphomimetic mutations, Dorfel and Huber found triple CKII phosphorylation increased TEER, enhanced TJ disassembly and association with ZO-1 but not ZO-2. In contrast mono-phosphorylated S408 displayed reduced binding to ZO-1 [Dorfel and Huber, 2013]. With the recent mapping of the ZO-1 binding site to occludin C-terminus aa residues 468-475 [Tash et al, 2012], the authors proposed that CKII phosphorylation modulates the ZO-1 and -2

binding site as a mechanism of TJ assembly and function [Dorfel et al, 2013]. Interestingly, *in vitro* binding assays suggested S408 dephosphorylation also promotes occludin trafficking to the TJ and increased association with ZO-1, claudin-1 and -2 [Raleigh et al, 2011]. With the knowledge that the ZO proteins also act as NACos, differential binding of ZO-1 or -2 to occludin in response to CKII phosphorylation could also modulate TJ gene expression [Dorfel and Huber, 2013]. Other occludin kinases have been less studied; tyrosine kinases have been associated with TJ destabilisation and disruption, possibly by preventing interactions with ZO-1 [Kale et al, 2003]. Furthermore, CKI has been shown to phosphorylate occludin but the aa residues targeted and physiological effects are currently unknown [Dorfel and Huber, 2012].

Cellular kinases and phosphatases may not require direct interaction with occludin to elicit an effect on TJ barrier function. For instance, phosphorylation of occludin Y397 by Src-associated kinases activates another tyrosine kinase, focal adhesion kinase (FAK) to induce TJ barrier disruption via the actin cytoskeleton, and it is not currently known if FAK can directly phosphorylate occludin or if a secondary mechanism is involved [Siu et al, 2009]. Likewise, PP1 has been suggested to interact and phosphorylate occludin serine residues but its primary dephosphorylation target may be an additional TJ protein [Seth et al, 2007].

Clearly, the dynamic phosphorylation and dephosphorylation of occludin plays a vital role in TJ structure and function, although the aa residues targeted by cellular kinases and phosphatases as well as their specific effect on occludin function are still unknown. Many more kinases and phosphatases targeting occludin are likely still to be discovered. Consequently, an *in vitro* kinase assay was developed to further investigate occludin phosphorylation. CKII was confirmed to phosphorylate the occludin C-terminus and ten novel targeted aa residues were identified. Additional validation will be required using phospho-specific antibodies, mutation of phosphorylated residues, kinase inhibitors or siRNA knockdown as well as functional evaluation *in vitro* or

in vivo, to uncover the physiological significance of this finding. An attractive future study would be to identify whether occludin function at the TJ is differentially regulated by different kinases and phosphatases and the effect on occludin mobility within the TJ. It should however not be overlooked that these kinases and phosphatases may also target other components of the TJ such as ZO-1, -2 and -3, claudins and JAM in order to regulate the TJ barrier function.

Recent analysis of the *T. gondii* genome identified 108 predicted active kinases [Peixoto et al, 2010], 38 of which are located in the parasite rhoptry and potentially secreted directly into the host cell cytoplasm during infection, although few of their host substrates have been identified [Bradley et al, 2005; Dubremetz, 2007; Yamamoto et al, 2009]. Other secreted parasite proteins include MIC-associated adhesins involved in host attachment. ROP-associated proteases, phosphatases, actin binding Toxofilin and the small GTPase Rab11 involved in invasion and formation of the PV, as well as RON-associated proteins involved in MJ formation [Bradley and Sibley, 2007; Kim, 2004; Poupel et al, 2000].

Here, two parasite-derived kinases are predicted to interact directly with the occludin C-terminus, wee kinase and CDPK1 as well as one dual specificity phosphatase. Clearly, the parasite phosphatase could play a role in occludin dephosphorylation and dissociation from the TJ seen during infection [Weight and Jones et al, 2015]. Interestingly, CDPKs have been linked to parasite host cell attachment and egress, although the mechanism is not fully understood [Kieschnick et al, 2001; Lim et al, 2012]. Calmodulin-dependant kinases have previously been shown to interact with TJ JAM [Martinez-Estrada et al, 2001]. As JAM also associates with occludin, cingulin and ZO-1 [Martín-Padura et al, 1998], and CDPK binding to JAM is attenuated by TJ dissociation [Martinez-Estrada et al, 2001], this suggests a possible role for *T. gondii* CDPK1 (TgCDPK1) in host TJ structure reorganisation. Further evidence is provided by TgCDPK1 sensitivity to KT5926, an inhibitor of MLCK [Kieschnick et al, 2001]. MLCK plays a key role in host TJ permeability by regulating actin reorganisation and localisation of ZO-1 and occludin to

the TJ [Cunningham and Turner, 2012; Shen et al, 2006]. TgCDPK1 phosphorylation of host occludin may therefore promote occludin recruitment to the TJ via interactions with JAM, ZO-1 and the actin cytoskeleton and facilitate parasite paracellular infection via parasite binding to occludin at the TJ. The SILAC dataset described in chapter four also identified a decrease in host PKC ι during infection, suggesting parasites may additionally modulate host kinase, protease or phosphatase expression to facilitate infection. A decrease in PKC ι has been associated with increased TEER and depletion of pore-forming claudin-2 from the TJ, suggesting a key role for PKC ι in TJ protein recruitment and paracellular permeability [Lu et al, 2015]. As claudin-2 interacts with occludin at the TJ, its loss may reduce occludin mobilisation at the TJ. Both of these mechanisms, secretion of parasite derived kinases and phosphatases or modulation of host kinase and phosphatase expression, potentially play an important role in occludin phosphorylation and dephosphorylation during *T. gondii* infection.

The evidence for occludin redistribution from the apical TJ to an intracellular location during *T. gondii* infection alongside the link between occludin phosphorylation and cellular localisation [Farshori and Kachar, 1999; Weight and Jones et al, 2015; Wong, 1997] led to the hypothesis that the occludin phosphorylation status is modulated during *T. gondii* paracellular infection.

To investigate the effect of *T. gondii* infection on occludin phosphorylation, infected and uninfected IEC-6 lysates were substituted as the source of kinase in the *in vitro* assay. This revealed IEC-6 cellular kinases were active under the experimental conditions and able to phosphorylate the recombinant occludin C-terminus peptide *in vitro*. Although the preliminary results suggest a possible increase in phosphorylated occludin species in response to infection (Figure 5.2D and F), it was not possible within the time frame to quantify the modification of occludin phosphorylation or identify the targeted C-terminus aa residues.

The preliminary *in vitro* kinase assay results provide a starting point for future studies; whole parasites, parasite lysates and conditioned media (secreted kinases) should be included in future *in vitro* kinase assays to determine the direct effect of parasites in comparison to infected cells. In addition, purified host-derived or parasite-derived kinases could be utilised in the occludin *in vitro* kinase assay to determine the significance of phosphorylation of particular C-terminus aa residues. Comparison of occludin phosphorylation at different stages of parasite infection, such as 2 hours or 24 hours p.i may also give an insight into the role of occludin in both early paracellular infection and later intracellular PV formation.

As low occludin sequence coverage and low protein abundance are a major limitation of the current MS-based phosphoproteomics technique, in future affinity based enrichment of phosphopeptides by immobilised metal affinity chromatography (IMAC), titanium dioxide chromatography or phospho-antibody co-immunoprecipitation could be coupled with targeted MS to overcome these proteomics challenges [Delom and Chevet, 2006; Hjerrild and Gammeltoft, 2006; Rigbolt and Blagoev, 2012].

5.4 Conclusions

This chapter confirmed the occludin *in vitro* kinase assay was suitable for quantifying recombinant occludin C-terminus phosphorylation. Using purified CKII six novel CKII occludin C-terminus phosphorylation sites were identified. Preliminary results also confirmed host IEC-6 kinases are active and able to phosphorylate the occludin C-terminus peptide *in vitro*, although it was not possible to quantify modulation of occludin phosphorylation in response to IEC-6 *T. gondii* infection. Although a key role for occludin phosphorylation during *T. gondii* infection was proposed, further studies are required to fully understand the molecular mechanisms and consequence of occludin phosphorylation during paracellular infection.

6 *Toxoplasma gondii* Interactions with Occludin

6.1 Introduction

The previous chapters described *T. gondii* paracellular transmigration and modulation of TJ proteins during *T. gondii* infection, including occludin phosphorylation. It is possible that *T. gondii* interacts directly with the extracellular domains of occludin during parasite paracellular transmigration of the SI epithelium. Therefore, in this chapter this hypothesis is tested to determine whether *T. gondii* interacts with occludin extracellular loop (ECL) domains.

Occludin is not exclusively required for TJ formation but it is a functional component, possibly dependent on the adhesive capabilities of its ECL domains [Furuse et al, 1996; Tsukita et al, 2001; Van Itallie and Anderson, 1997]. Due to their position within the paracellular space, the ECLs of occludin are thought to functionally regulate paracellular permeability by forming homophilic interactions with adjacent cells to create a barrier to macromolecules but not charged ions, potentially regulating the TJ leak pathway [Al-Sadi et al, 2011; Balda et al, 2000; Hartsock and Nelson, 2008]. However, despite many studies, the role of occludin in paracellular permeability and the functional relevance of its ECL domains still remains unclear.

Medina et al and Bellmann in separate studies confirmed occludin ECL2 forms homologous interactions on adjacent cells and is required for occludin localisation at the TJ [Bellmann et al, 2014; Medina et al, 2000]. Occludin ECL2 is also known to interact with claudins and JAM-A and disruption of these interactions inhibits reformation of TJ's [Furuse et al, 1998; Nusrat et al, 2005]. Interestingly, the addition of synthetic ECL1 peptides to epithelial cells results in increased TEER and occludin localisation to the TJ [Lacaz-Vieira 1999; Van Itallie et al, 1997]. Similarly, Tavelin et al established ECL1 significantly increased TJ permeability and

specifically identified ECL1 peptide residues 90-103 as responsible for this barrier disruption [Tavelin et al, 2003]. In contrast, Wong and Gumbiner found ECL2 peptides reversibly disrupted the TJ barrier and reduced occludin localisation at the TJ whilst not affecting other TJ proteins. The authors also reported that ECL1 was inactive [Wong and Gumbiner, 1997].

These marked differences between ECL1 and ECL2 on the TJ may be explained by differences in the cell lines and occludin peptide sequences used, given that ECL1 is only ~53% conserved between chickens and humans [Tavelin et al, 2003]. Differences in peptide concentration and administration, solubility and correct folding of the peptides, experimental time course and maturity of the cell monolayers in the above studies may have also played a role. The variance between studies also raises the possibility that occludin ECL1 and ECL2 may differentially regulate the TJ barrier by either directly mediating paracellular permeability or acting as a regulator of other TJ proteins such as claudins.

The specific interaction between *T. gondii* and occludin has to date only been described by Weight using recombinant occludin peptides [Weight, 2011]. This interaction, particularly between parasites and the ECL of occludin, will be further investigated in this chapter.

6.2 Results

The murine SI epithelial cell line, m-IC_{c12} was used in this chapter to confirm and quantify previous findings by Weight [Weight, 2011].

Functional recombinant occludin C-terminus, ECL1+ECL2, ECL1 and ECL2 peptides were produced (Figure 2.1) and to our knowledge this is the first report of functional recombinant ECL1 being expressed in a prokaryotic system as previous studies with ECL1 have utilized synthetic peptides [Lacaz-Vieira 1999; Tavelin et al, 2003; Van Itallie et al, 1997; Wong and Gumbiner, 1997].

As both ECL1 and ECL2 are highly hydrophobic and form insoluble polymers in solution, soluble stocks of the recombinant occludin peptides were produced immediately prior to each assay to prevent peptide aggregation.

6.2.1 *Toxoplasma gondii* Interactions with Occludin Alter Parasite Attachment and Infection

Confluent m-IC_{c12} monolayers grown on glass coverslips for four days were apically infected for two hours with either *T. gondii* alone (control) or *T. gondii* pre-incubated with 2µM recombinant occludin peptides for 15 minutes prior to co-culture. Of note, yields of ECL1 peptides were poor compared to ECL1+2, ECL2 and the C-terminus, therefore ECL1 could not be included in this cell-based assay.

To distinguish between *T. gondii* attachment and invasion of the m-IC_{c12} monolayer, haematoxylin and eosin (H&E) staining of cells post-infection highlighted the PV (Figure 6.1A inset), indicative of intracellular infection. Although the ‘domed’ morphology of confluent m-IC_{c12} monolayers caused difficulties in parasite visualisation, in control samples the total number of attached parasites was 36.0% ($\pm 13.9\%$) higher than the number of invading parasites, which indicates that although attachment is necessary for successful invasion, not all attached parasites invade host cells (Figure 6.1A).

Significant changes in *T. gondii* attachment and invasion were observed in response to parasite interactions with occludin ECL1+ECL2 in comparison with ECL2 or C-terminus peptides. In agreement with the results presented in chapter three, parasite infection of host cells was non-homogeneous with many parasites being associated with a few cells and the majority of cells having no parasite interactions (Figure 6.1B). Figure 6.1C and D show *T. gondii* pre-incubation with ECL1+ECL2 both significantly increased the number of invading parasites ($p \leq 0.0001$) and significantly decreased the number of attached parasites ($p \leq 0.0001$). In

contrast, pre-incubation with ECL2 had no effect on parasite attachment or invasion ($p \geq 0.05$) but interestingly, a significant decrease in attachment was observed by pre-incubation with occludin C-terminus ($p \leq 0.001$) (Figure 6.1C and D).

Confluent m-IC_{c12} monolayers grown on PET inserts for four days were apically infected for two hours with either *T. gondii* pre-incubated with recombinant occludin ECL2 peptide or *T. gondii* administered simultaneously with the occludin ECL2 peptide and the results compared to addition of *T. gondii* alone (control). In agreement with results shown in chapter four, administration of *T. gondii* alone did not affect the barrier integrity of m-IC_{c12} assessed by TEER. In contrast, addition of ECL2 simultaneously with parasites significantly increased TEER ($p \leq 0.005$), which was attenuated by pre-incubation with parasites (Figure 6.2A). M-IC_{c12} monolayer permeability to FITC-dextran also decreased with the addition of occludin peptides, which was again attenuated by pre-incubation with parasites, although this did not reach statistical significance (Figure 6.2B).

Although these results suggest *T. gondii* interact with the occludin ECL1+ECL2, ECL2 and C-terminus peptides *in vitro*, addition of the recombinant occludin ECL2 peptide appears to significantly alter the barrier function of the m-IC_{c12} monolayer. This raises the question of whether the observed changes to *T. gondii* attachment and invasion were due to alteration of the TJ barrier function via interactions between recombinant occludin peptides and native cellular occludin rather than solely due to parasite interactions with occludin.

6.2.2 *Toxoplasma gondii* Bind to the Extracellular Loops of Occludin

A cell-free chamber-slide assay was developed to assess parasite binding to occludin in a cell-free system.

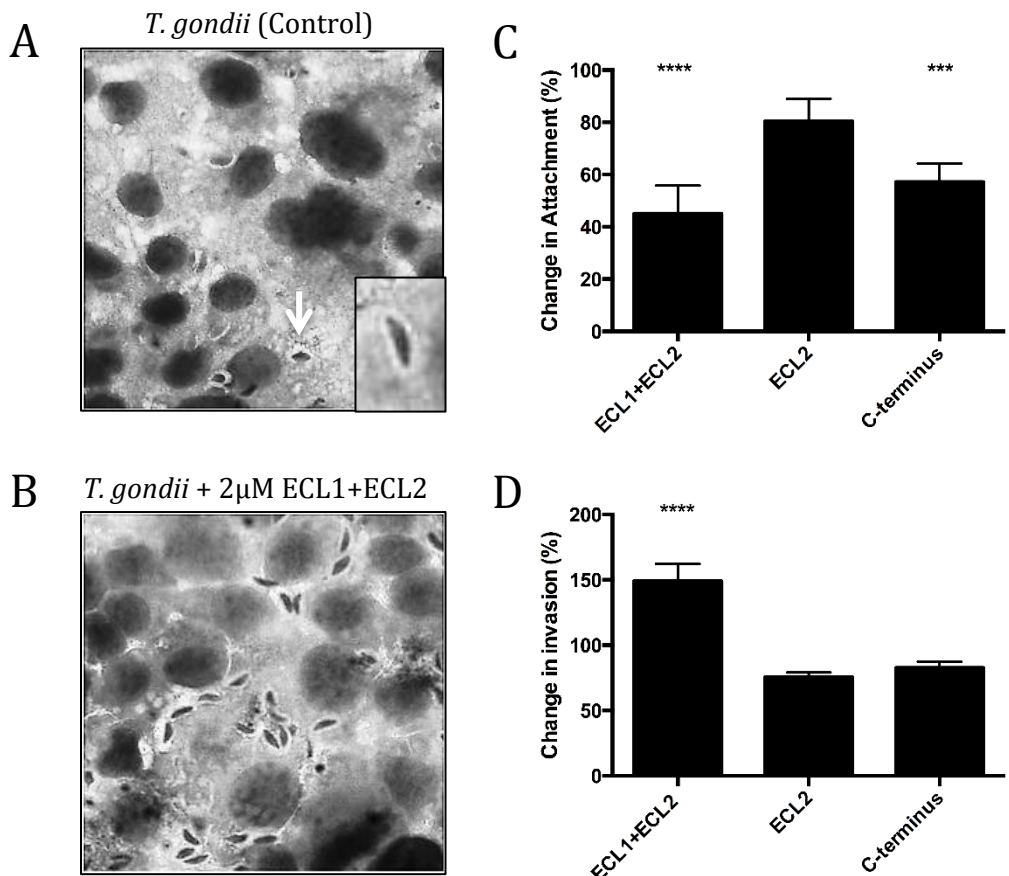


Figure 6.1: *Toxoplasma gondii* inhibition of attachment and invasion in response to recombinant murine occludin peptides. Confluent m-IC_{c12} cell monolayers grown on glass coverslips for four days were apically infected with A) 5 \times 10⁶ *Toxoplasma gondii* for 2 hours (control) or B) 5 \times 10⁶ *Toxoplasma gondii* pre-incubated with 2.0 μ M recombinant ECL1+ECL2 for 15 minutes prior to infection for 2 hours. Intracellular invaded parasites were identified by the white halo of the parasitophorous vacuole (Inset and white arrow). Percentage change in attachment C) and invasion D) when parasites are pre-incubated with recombinant fragments of occludin compared to cells treated with parasites only (control). Data representative of three independent experiments with 3-4 biological replicates. ***P \leq 0.001 ****P \leq 0.0001.

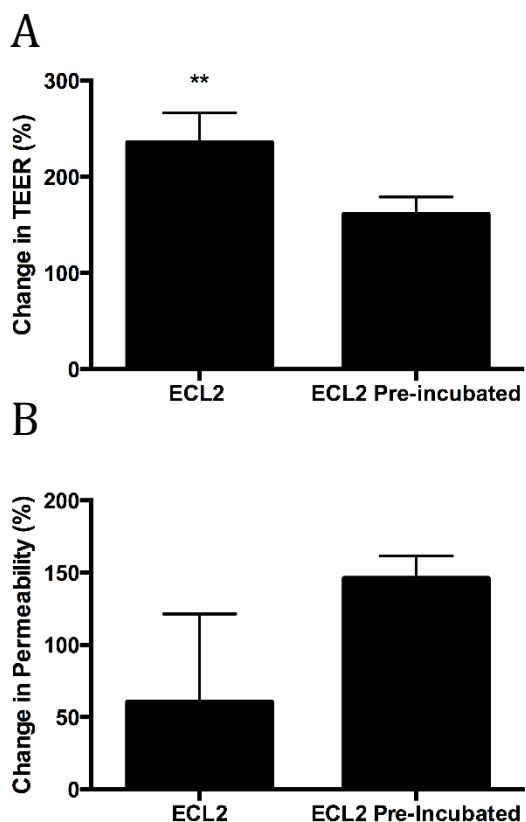


Figure 6.2: *Toxoplasma gondii* invasion and transmigration of m-IC_{c12} in response to recombinant fragments of murine occludin. Confluent m-IC_{c12} cell monolayers grown on PET inserts for thirteen days were apically infected with 5x10⁶ *Toxoplasma gondii* for 2 hours (control) or 5x10⁶ *Toxoplasma gondii* pre-incubated with 2.0µM recombinant ECL1+ECL2 for 15 minutes prior to infection for 2 hours. TEER was measured pre- and post-infection and cellular permeability to 1000µg/ml FITC-dextran measured post-infection. A) Percentage change in TEER and B) permeability when parasites are pre-incubated with recombinant fragments of occludin compared to cells treated with parasites only (control). Data representative of one independent experiment with 3-4 biological replicates. **P≤0.01.

His-tagged occludin peptide immobilisation was assessed by fluorescence microscopy using a Penta.HIS alexa fluor 488 conjugated antibody (Qiagen). The signal intensity in the green channel was at least 500 fluorescence units in the sample wells, compared to zero in the control wells and although peptide immobilisation was sparse at 30 μ M protein concentration per well (Figure 6.3A), limited peptide quantities were available, especially for ECL1. Some variation in peptide immobilisation was observed between the ECL1+2 and ECL1 peptides compared to the ECL2 or C-terminus peptides, likely due to differences in HIS-tag availability to the fluorescent antibody (Figure 6.3A and B). Importantly, these differences did not correspond with levels of *T. gondii* binding.

Significant differences in *T. gondii* binding were reproducibly observed in slide wells containing immobilised occludin ECL1+ECL2 and ECL1 peptides in comparison with ECL2, C-terminus or control peptides (Figure 6.4A and B). Parasites were seen to significantly bind and aggregate in wells containing ECL1+ECL2 or ECL1 ($p \leq 0.01$) compared to low density parasite binding and minor aggregation in wells containing C-terminus ($p \geq 0.05$) or ECL2 ($p \geq 0.05$) and low parasite binding in control wells containing either no peptides or m-Cherry ($p \geq 0.05$).

6.2.3 Potential *Toxoplasma gondii* Derived Occludin Binding Partners

A bioinformatics approach was used to identify putative *T. gondii* occludin binding partners. The rat occludin sequence was BLASTED against the *T. gondii* genome using NCBI-BLAST (www.toxodb.org release number 24 14th April 2015) [Gajria et al, 2008]. The database was used to search for occludin homology with the *T. gondii* ME49, GT1 and VEG strain genomes. The RH strain genome was incomplete at the time of writing (September 2015).

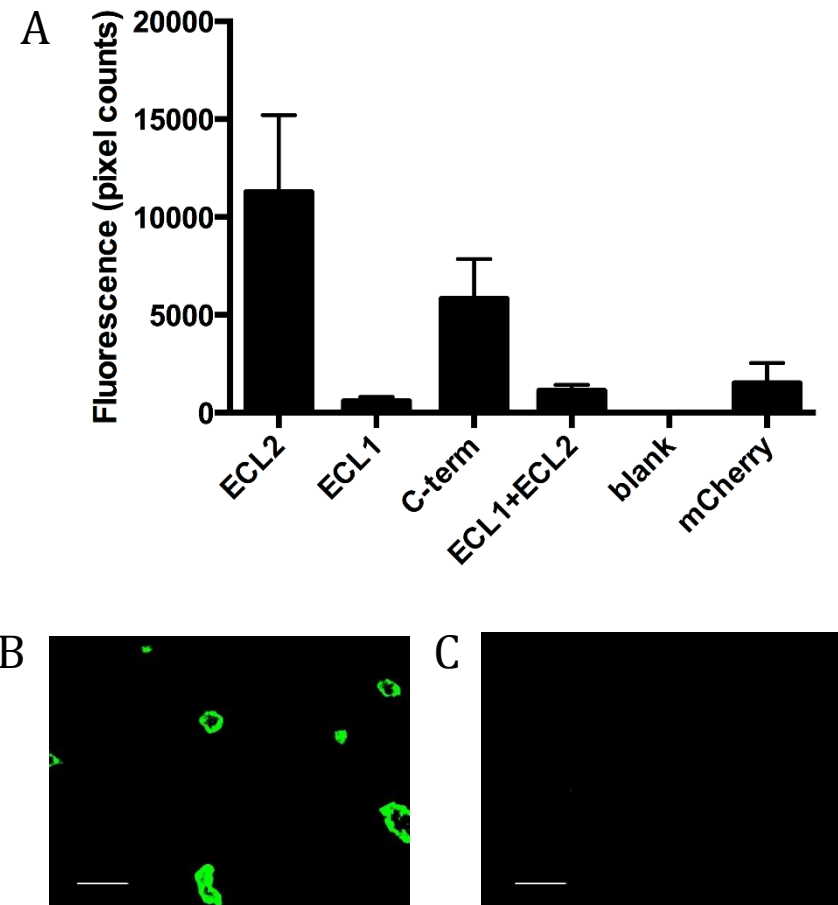


Figure 6.3: Detection of recombinant occludin peptide immobilisation on Schott Nexterion Slide H. A) $30 \mu M$ HIS-tagged occludin peptides ECL1+ECL2, ECL1, ECL2 and C-terminus, as well as HIS-tagged mCherry protein (control) and buffer alone (blank) were immobilised onto individual wells of Scott Nexterion H Slides (Jena, Germany). Peptides were detected using a Penta-HIS alexa fluor 488 conjugated antibody (Qiagen), visualised by fluorescence microscopy and quantified by fluorescent alexa fluor 488 pixel area. B) representative immunofluorescence image of occludin ECL2 peptide immobilisation. C) Representative immunofluorescence image of buffer alone (blank). Data representative of one independent experiment with biological replicates. Scale bar 20 μ m.

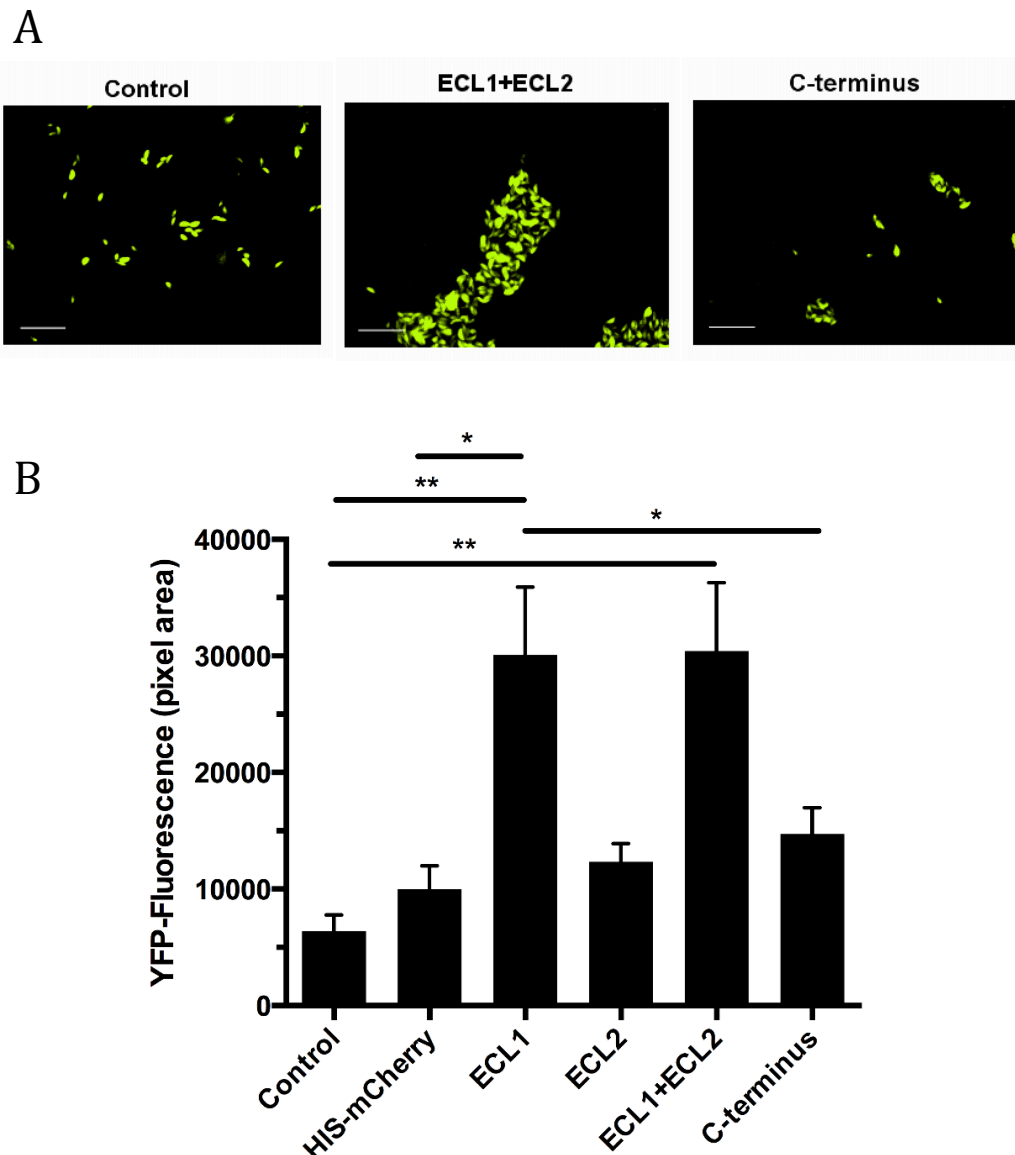


Figure 6.4: *T. gondii* binding to recombinant fragments of murine occludin. His-tagged occludin peptides ECL1, ECL2, ECL1+ECL2 and C-terminus, His-tagged mCherry protein and buffer alone (control) were immobilised onto individual wells of Scott Nexterion H Slides (Jena, Germany). 1×10^7 *Toxoplasma gondii* were added per well for 2 hours. Bound parasites were visualised by fluorescence microscopy A) and quantified by fluorescent YFP pixel area B). Scale bar = 20 μ m. Data representative of six independent experiments with biological replicates. **P=≤0.01

129 parasite-derived proteins were predicted to interact with occludin ECL1 compared to only 16 with occludin ECL2 (Appendix E). Functional classification of these ECL1 proteins using GO annotation revealed involvement in protein folding (2.3%), protein transport (3.9%) as well as phosphorylation and dephosphorylation (3.1%). The majority of proteins were unclassified (79.1%) (Figure 6.5). 48 parasite-derived proteins were identified as interacting with the full-length occludin (Appendix E), suggesting parasite specificity for interactions with occludin domains.

It was not within the scope of this project to undertake further in-depth bioinformatics investigation of these findings, although they do present an interesting area for future research.

6.3 Discussion

In this chapter, evidence suggests *T. gondii* specifically bind to the occludin ECLs. Many pathogens have developed mechanisms for targeting TJ-associated proteins to infect the SI epithelium and specific interactions with occludin ECL domains during infection have been described, although the mechanism is unknown. This interaction is of particular interest as the ECLs of occludin are integral to maintaining the epithelial TJ barrier [Nusrat et al, 2005]. For example *Entamoeba histolytica* expresses an occludin-like protein that can alter epithelial barrier function by displacing host occludin-occludin interactions via its ECL domains [Goplen et al, 2013].

Here evidence is provided for *in vitro* *T. gondii* tachyzoite binding to occludin ECL1. Pre-incubation of *T. gondii* with the ECL1+ECL2 and to a lesser extent the C-terminus peptide, significantly reduced attachment to the epithelial cells in comparison with ECL2, suggesting *T. gondii* tachyzoites physically interact with the ECL1+2 and C-terminus peptide, which blocks cellular parasite attachment. This peptide intercalation into

the TJ or interaction with endogenous occludin would interfere with normal TJ function and potentially affect *T. gondii* transmigration. Additionally, the specific interaction between *T. gondii* and the ECLs means appropriate control peptides are difficult to achieve; here the occludin C-terminus peptide was used alongside an unrelated m-cherry peptide. Furthermore, the purification or detection tags added to the peptide fragments may affect their *in vitro* function due to their molecular size. In this study the small polyhistidine-tag (6xHIS-tag) was utilised to mitigate this effect.

Addition of the ECL2 peptide to m-IC_{c12} significantly disrupted the TJ barrier, as described in previous studies using synthetic peptides corresponding to occludin ECL2. Wong and Gumbiner found ECL2 at <5μM significantly disrupted TJ function of *Xenopus* kidney cell line A6 and decreased the amount of occludin at the TJ without affecting other TJ proteins. Nusrat et al later confirmed ECL2 associated with T84 occludin and impeded functional TJ assembly [Nusrat et al, 2005; Wong and Gumbiner, 1997].

The results of the solid phase *in vitro* chamber slide-based occludin peptide binding assay suggest *T. gondii* interacts directly with ECL1. The lack of charged residues in ECL1 as well as a high proportion of tyrosine and glycine residues led to speculation that this domain was involved in sealing the paracellular space [Ando-Akatsuka et al, 1996].

To predict parasite-derived occludin-binding proteins occludin ECL sequences were BLAST searched against the *T. gondii* genome and the protein functions classified using GO annotation. Following attachment to cellular junctions, parasites secrete a range of effector proteins from specialised organelles. Based on this it was hypothesised that these act upon the TJ proteins during infection. The BLAST search of potential ECL1 binding partners identified ROP25, GRA6, a putative MIC protein and a SAG1-related sequence (SRS) protein.

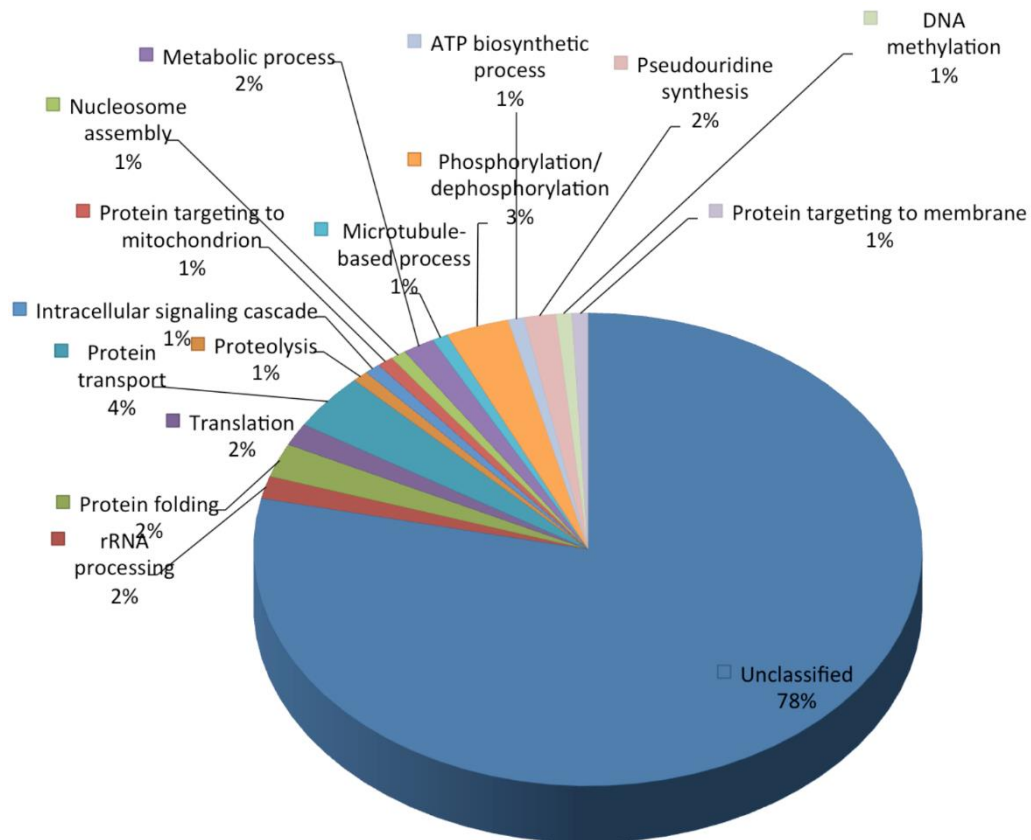


Figure 6.5: Functional categorisation of the *T. gondii*-derived proteins predicted to interact with occludin domains. The numbers correspond to the percentage of identified proteins in each category compared to the total number of proteins. The occludin ECL1 domain was first searched for *T. gondii* homologues using NCBI-BLAST search and GO annotation was provided by www.toxodb.org (version 7.3). Proteins without a GO classification were designated unclassified. A list of all identified proteins is provided in Appendix E.

MIC2 for example, has been shown to bind host ICAM1, a known receptor for *T. gondii* paracellular transmigration [Barragan et al, 2005]. The predicted interaction between a putative *T. gondii* MIC protein and ECL1 suggests binding to ECL1 could contribute to *T. gondii* paracellular transmigration.

During the initial stages of infection, microneme proteins are secreted from the apical microneme organelle onto the parasite surface to facilitate adhesion and invasion [Carruthers and Tomley, 2008]. The next stage of parasite infection involves rhoptry protein secretion into the host cell where they traffic to the host nucleus, remain in the cytoplasm to facilitate PV formation, or relocate to the PV membrane [Hunter and Sibley, 2012]. ROPs including ROP25 identified here, are serine/threonine kinases, proteases or phosphatases that potentially play a role in the regulation of occludin via phosphorylation, a mechanism described in chapter five in which the phosphorylation status of occludin is altered in response to parasite infection.

During the later stages of infection, dense granule proteins are secreted into the PV where they can contribute to controlling the host immune responses [Shastri et al, 2014]. GRA6 for example has been shown to recruit monocytes and neutrophils to sites of infection to promote parasite dissemination [Ma et al, 2014] and an interaction with occludin ECL1 could play a role in this mechanism.

The potential interaction between ECL1 and SRS29C (formerly SRS2) is particularly noteworthy as the SRS protein superfamily of *T. gondii* surface proteins are known to facilitate host cell attachment and invasion as well as evasion and modulation of the host immune response [Templeton, 2007]. The SRS proteins typically contain one or two domains with multiple cysteine residues that create disulphide bonds and a GPI anchor that promotes attachment to the host cell surface [Manger 1998]. SAG1 for example interacts with host cell proteoglycans through the formation of a deep, positively charged docking site [Mineo et al, 1993]. However, the roles of the superfamily members remains poorly understood. Targeted gene deletion studies recently identified SRS29C as

a negative regulator of virulence; high expression was linked to reduced host inflammatory response, a mechanism that presumably promotes parasite proliferation and dissemination before the host immune response can limit tachyzoite infection [Wasmuth et al, 2012]. Taken together this evidence suggests SRS29C could facilitate initial host cell attachment and paracellular transmigration via interactions with occludin ECL1, promoting parasite dissemination at an early stage of infection.

This homology-based analysis is somewhat limited as it does not give an indication of whether the predicted interactions are functionally relevant and does not account for structural interactions. These methods are also known to be prone to high false-positive rates [Lin et al, 2004; Wuchty, 2011]. However, as the *T. gondii* genome currently contains many uncharacterised proteins with unknown structures, highlighted by numerous unclassified proteins in the GO results, our preliminary analysis of potential parasite-occludin interactions was based on sequence similarity alone. Further in-depth bioinformatics analysis and integration with the SILAC data presented in chapter four would help identify biologically relevant candidate host-parasite interactions and potentially the molecular mechanisms by which *T. gondii* interact with the host cell. In addition, co-immunoprecipitation of recombinant occludin peptides with *T. gondii* lysates, combined with sensitive MS, would identify the molecular *T. gondii* proteins that interact with occludin.

6.4 Conclusions

This chapter has provided evidence for *T. gondii* tachyzoite binding to the ECLs of occludin. Taken together with the findings in chapter three for *T. gondii* transmigration through the paracellular pathway, a model of parasite infection is proposed whereby paracellular *T. gondii* binding to ECL1 via parasite surface proteins disrupts occludin

homodimer formation between neighbouring cells, consequently disrupting the TJ barrier and permitting parasite transmigration and dissemination to secondary sites of infection. To our knowledge, this novel finding is the first description of a role for occludin ECL1 during *T. gondii* infection and the above model describes a potential mechanism for parasite paracellular transmigration of the SI epithelium.

7 Discussion

In this thesis infection of the SI epithelium was modelled *in vitro* using the IEC-6 and m-IC_{c12} cell lines (chapter four and six). The results reveal *T. gondii* paracellular infection of the SI epithelium and illustrate the importance of interactions between parasites and the TJ, specifically the TJ protein occludin (chapter six). Modulation of the occludin C-terminus domain phosphorylation status is important for occludin localisation to the TJ and subsequent parasite binding to the occludin ECLs represents a mechanism of paracellular transmigration of the TJ barrier (chapter five and six).

7.1 Infection of IEC-6 Cells by *Toxoplasma gondii*

T. gondii is an obligate intracellular parasite that requires host cell invasion for replication and survival by evading host detection and defence mechanisms as well as to access host metabolites. As oral infection is the primary cause of toxoplasmosis, the first point of contact between *T. gondii* and host is the intestinal epithelium, permitting rapid parasite dissemination away from the GI tract to immunoprivileged sites and establishment of chronic infection. As *T. gondii* infection triggers inflammatory pathology resembling that of chronic IBD [Pizarro et al, 2003], elucidating the mechanisms of pathogenic TJ disruption and the complex interplay between TJ signalling pathways will further understanding of the mechanisms of pathogen infection as well as give an insight into the initiation and progression of diseases such as CD and UC. As such, *T. gondii* utilised in this thesis can be viewed as an experimental model for studying mechanisms of TJ disruption that leads to intestinal inflammatory disease with the aim of identifying new therapeutic targets to treat these diseases [Egan et al, 2012].

7.2 Modulation of Tight Junction-Associated Proteins During *Toxoplasma gondii* Infection

T. gondii have evolved novel mechanisms for promoting infection, including intracellular PV formation to provide an environment in which to avoid clearance by host autophagy or phagocytosis as well as specialised apical secretory organelles termed micronemes and rhoptries that sequentially release proteins into the host cell [Sharma and Chitnis, 2013]. Micronemes firstly discharge MICs to the parasite surface where they form adhesive complexes that bind to host cell receptors [Soldati et al, 2001] and secondly rhoptry contents are secreted directly into the host cell cytoplasm where they manipulate a range of host cell processes such as metabolism, cell cycle and apoptosis as well as reorganising the host cell cytoskeleton and organelles [Laliberte and Carruthers, 2008; Nelson et al, 2008; Zhou et al, 2011].

The *in vitro* two-photon imaging presented in chapter four reveals the complex multi-stage processes involved in parasite paracellular transmigration, to our knowledge visualised for the first time in this thesis. Parasites exhibit gliding motility and target cellular junctions before attachment, reorientation, entry into the paracellular space, transmigration through the epithelium and egress from the paracellular space. During all stages of infection *T. gondii* maintains an intimate relationship with the host cell, therefore identifying the mechanisms involved will be important in further understanding the interactions between parasites and host cells.

The apical TJ that occludes the paracellular space between cells of the SI epithelium functions as both a barrier and fence, separating the inner organs and tissues from the outside environment as well maintaining cell polarity [Anderson and Van Itallie, 2009; Cereijido et al, 2008]. The continuous cycle of TJ assembly and disassembly of the TJ-complex controls the paracellular permeability; regulated by dynamic interactions between the integral transmembrane proteins occludin, JAM-A and claudin(s) with the cytoplasmic plaque of peripheral adaptor,

scaffold and signalling proteins that link the junctional membrane to the actomyosin cytoskeleton [Balda and Matter, 2008; Shen et al, 2011]. Furthermore, bidirectional signalling to and from the cell interior regulates cellular differentiation, proliferation, migration and survival [Balda and Matter, 2009] but the complex interplay between TJ molecular structure and function is only beginning to be understood.

The results presented in chapter four indicate *T. gondii* intimately interacts with the host cellular junction prior to re-orientation, (Video 1); potentially secreting organelle contents into the paracellular space or host cell cytoplasm. With the knowledge that even host cells that are not infected contain physiologically relevant amounts of *T. gondii* effector proteins [Koshy et al, 2012], this finding may reflect parasite modification of the host TJ by secreted effector proteins as a mechanism of preparing the host cell for transmigration.

To ensure their intracellular replication and survival *T. gondii* have evolved strategies to modulate host cell structure and function such as subversion of the host actin cytoskeleton and cell cycle progression. It has to date been difficult to dissect the complex interactions between parasites and the host as both organisms share similar components such as the cytoskeleton. However, recent studies such as the SILAC technology described in this thesis have provided new insights into the potential mechanisms of host cell subversion.

Parasite modulation of host TJ-associated Bcar1, Ybox3 and Mras proteins at two hours p.i and Cstf2, Ybx3, Akt1, Arhgef11, Cldn15 and Prkci proteins at twenty-four hours p.i implies extensive remodelling of the host TJ proteome occurs during infection and a number of downstream signalling pathways were hypothesised to be affected, emphasising the complexity of apical TJ protein-protein interactions and the necessity for understanding the mechanisms of TJ regulation.

Figure 7.1 illustrates the striking connection between these modulated TJ-associated proteins (highlighted in cyan) and ZO-1, ZO-2, JAM-A and β 1-integrin; inferring *T. gondii* disrupts associations between surface receptors and the integral transmembrane TJ proteins occludin

and claudin(s) as well as their interactions with TJ-associated adaptor and scaffolding proteins and ultimately their connections to the actin cytoskeleton and the host cell cycle.

7.2.1 *T. gondii* Modulation of the Host Actin Cytoskeleton

Recent studies have described the importance of host actin in entry of *T. gondii* into host cells [Gonzalez et al, 2009]. The parasite MJ for instance has been shown to be associated with formation of a host ring-shaped F-actin structure, proposed to be necessary for parasite anchoring and propulsion into the host cell, although it is not known how the host cortical actin barrier is breached to enable formation of the PV [Delorme-Walker et al, 2012]. Parasite nutrient acquisition via recruitment of host mitochondria and ER to the PV, which enables parasite access to host metabolites, has also been linked to the host actin cytoskeleton [Gonzalez et al, 2009] in a process involving invagination of the PV membrane and delivery of lysosomes by host microtubules, although the exact mechanism of nutrient entry is unclear [Coppens et al, 2006; Sibley et al, 1995]. Remodelling of the host actin cytoskeleton may also be involved in *T. gondii* division and egress [Chandramohanadas et al, 2009; Hu et al, 2006]. Interestingly, *T. gondii* toxofilin a secreted ROP effector protein, has been shown to sequester host actin monomers and cap actin filament ends [Bradley et al, 2005; Delorme-Walker et al, 2012; Poupel et al, 2000], a potential mechanism of host actin cytoskeleton remodelling [Frenal and Soldati-Favre, 2009].

The mechanism of parasite induced host actin cytoskeleton remodelling is not currently known, therefore the proposed *T. gondii* disruption of the host TJ-complex described in this thesis may initiate host actin cytoskeleton remodelling via disruption of interactions between the integral TJ proteins and TJ-associated adaptor and scaffolding proteins.

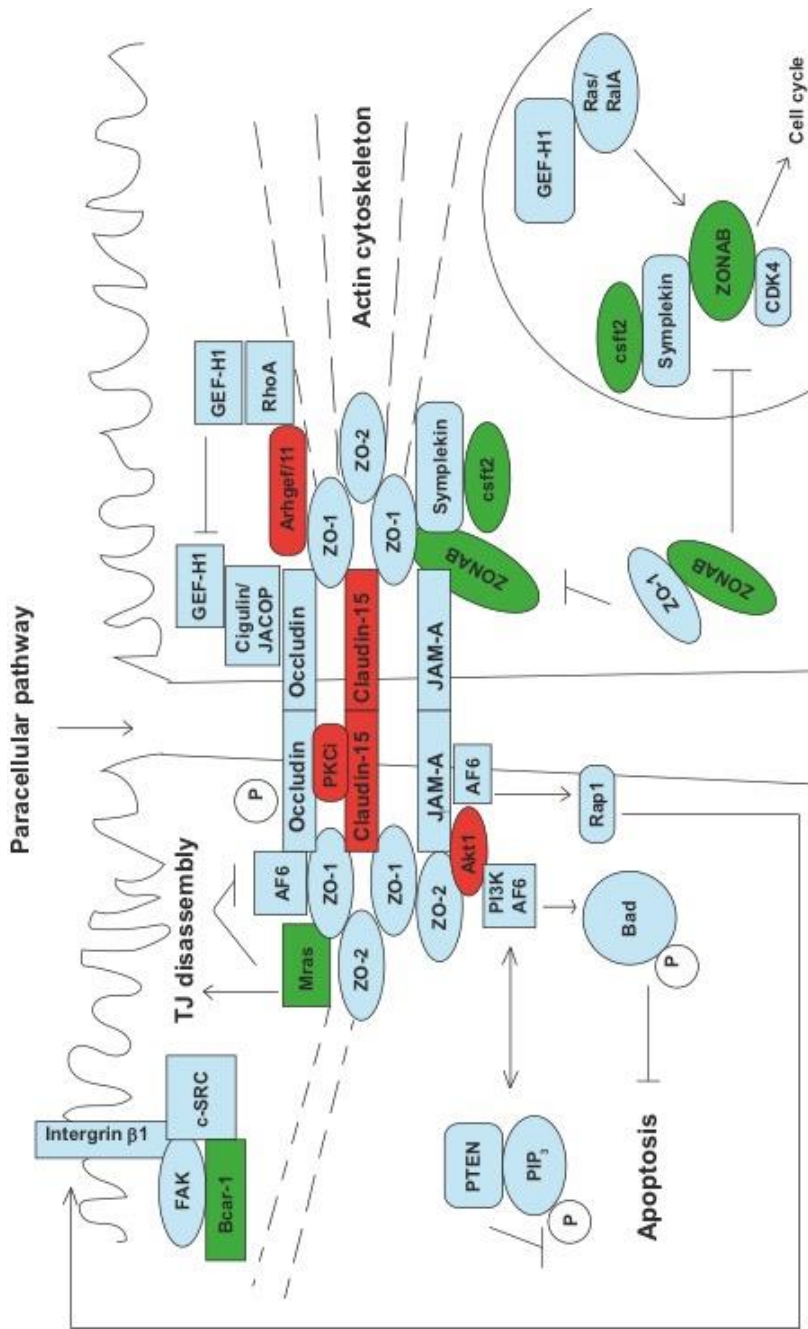


Figure 7.1: Modulation of the host TJ proteome during *T. gondii* infection. Schematic representation of the IEC-6 TJ-associated proteins modulated during infection and predicted downstream signalling pathways. The TJ-associated proteins demonstrating a significant increase in abundance by SILAC are highlighted in red and those demonstrating a significant decrease in green.

Parasite-mediated changes to Arhgef11, Akt, Mras and Csft2 abundance could be predicted to affect the direct or indirect binding to the ZO proteins or JAM-A to physically disrupt interactions with occludin and claudin(s) [Monteiro et al, 2013] that in turn promotes dissociation of downstream signalling components such as PTEN, AF6 and PI3K from the TJ-complex that alter host actin cytoskeleton dynamics [Matter et al, 2005]. AF6 for example is recruited to the forming PV where it activates PI3K and recruits PIP₂ and PIP₃ and knockdown of ARF6 has been shown to reduce parasite internalisation [Da Silva et al, 2009]. It could therefore be hypothesised that *T. gondii* dissociation of Akt from the TJ-complex via disruption of the integral TJ-proteins is a parasite mechanism of inducing AF6 induced PI3K activation and subsequent PIP₂ and PIP₃ recruitment (Figure 7.1).

Combining the modulated TJ-associated proteins and the reduction of pore-forming claudin-15 during infection described in this thesis with the dynamic model of occludin, ZO-1 and claudin mobility within the TJ described by Shen et al, gives a potential insight into the association between the TJ-associated proteins during *T. gondii* paracellular transmigration (Figure 7.2). The mobility of ZO-1, occludin and claudin-1 within the TJ is distinct; occludin is highly mobile between an apical TJ and lateral membrane location whereas claudin(s) either remain static within the TJ or exchange between the apical TJ and lateral membrane. ZO-1 however is highly mobile between the apical TJ, lateral membrane and cytoplasmic pool, allowing rapid signal dissemination between the TJ and cell interior [Van Itallie and Anderson, 2013; Shen, 2008]. Additionally, ZO-1 has been shown to interact with both occludin and claudin(s), anchoring them to the TJ complex [Bal et al, 2012; Itoh et al, 1999], recently confirmed by proximity-based proteomic studies which identified the ZO-1 N-terminus as interacting with the integral transmembrane proteins whereas the C-terminus as interacting with the actin cytoskeleton [Fredriksson et al, 2015; Van-Itallie et al, 2013].

This implies alterations in ZO-1 mobility between the TJ, lateral membrane and cytoplasm may be the mechanism that links the integral

transmembrane proteins to the actin cytoskeleton [Van Itallie et al, 2013]. The predicted association between these TJ proteins and ZO-1 mobility at steady state prior to parasite infection is shown in Figure 7.2A; transmembrane occludin and claudin dimers on neighbouring cells form the semi-permeable paracellular TJ barrier, stabilised by ZO-1 localisation to the complex. The peripheral plaque of scaffolding and adaptor proteins links the integral TJ proteins to the actin cytoskeleton and nuclear signalling pathways, maintaining the paracellular barrier [Matter and Balda, 2009; Turner, 2009]. Figure 7.2B depicts the predicted mechanism of modulation of the TJ barrier during *T. gondii* infection; the association between ZO-1 and the occludin and claudin(s) dimers on neighbouring cells is disrupted either by parasite secreted factors or physical interactions between parasites and the integral TJ proteins such as occludin described in this thesis. This leads to loss of ZO-1 mediated occludin stabilisation at the TJ and transient occludin re-localisation to the lateral membrane and intracellular cytoplasmic location [Weight, 2011].

This proposed mechanism is supported by evidence from a number of pathogens that also disrupt occludin, claudin(s) and ZO-1 at the TJ to overcome the epithelial barrier and infect host cells. EPEC for example has been shown to disrupt TJs by dissociating occludin, ZO-1 and the barrier-forming claudins from the TJ-complex [Muza-Moons et al, 2004; Philpott et al, 1996; Simonovic et al, 2000; Spitz et al, 1995], promoting claudin and occludin re-localisation to the cytoplasm and ZO-1 re-localisation to sites of bacterial pedestal formation [Hanajima-Ozawa et al, 2007; Peralta-Ramirez et al, 2008]. *Vibrio cholera* derived ZOT also dissociates ZO-1 from the TJ complex possibly by PKC alterations of actin filaments [Fasano et al, 1995; Pierro et al, 2001; Schmidt et al, 2007;] and *Helicobacter pylori* CagA induces dissociation of ZO-1 from the TJ [Amieva et al, 2003]. *Salmonella* also causes a decrease in ZO-1 and phosphorylated occludin [Kohler et al, 2007]. Although it is understood that disruption of the TJ complex by extracellular stimuli leads to MLCK regulated contraction of actin filaments and opening of the TJ during

pathogen paracellular infection, the complete mechanism of TJ disruption has to date remained elusive. [Shen et al, 2006].

The TJ permeability barrier is likely maintained during *T. gondii* transmigration by the fixed pool of claudin dimers that can be recruited to the TJ complex independently of TJ-associated scaffolding proteins [Shen, 2008; Van Itallie and Anderson, 2014]. This is supported by the evidence that *Salmonella* infection is associated with an increase in barrier-forming claudin-1 at the TJ [Kohler et al, 2007]. Therefore, the loss of pore-forming claudin-15 [Suzuki et al, 2014] from the TJ complex during infection, identified by SILAC in chapter four, indicates the pore-forming claudins may be displaced by barrier-forming claudins; a potential host cell response to maintain the integrity of the TJ barrier. Furthermore, the decrease in host PKC γ at twenty-four hours correlates with claudin-15 displacement as it has been associated with depletion of pore-forming claudin-2 from the TJ complex [Lu et al, 2015]. *C. perfringens* enterotoxin (CPE) is an example of this mechanism as it displaces claudin-4 and claudin-19 from TJ strands creating permeable ion pores [Saitoh et al, 2015; Sonoda et al, 1999]. As claudin-19 crystal structure is comparable to claudin-15, parasite binding may induce similar conformational changes to disrupt claudin polymers, disassemble TJ strands and increase TJ permeability [Saitoh et al, 2015].

7.2.2 *T. gondii* Modulation of the Host Cell Cycle

The altered abundance of host cell Cstf2, Ybox3 and Arhgef11 also indicates parasite manipulation of the TJ to alter progression of the host cell cycle, which is required for parasite intracellular infection and replication as *T. gondii* preferentially infect cells in the S-phase [Blader and Saeij, 2009; Dvorak and Crane, 1981; Grimwood et al, 1996; Koshy et al, 2012; Lavine and Arrizabalaga, 2009].

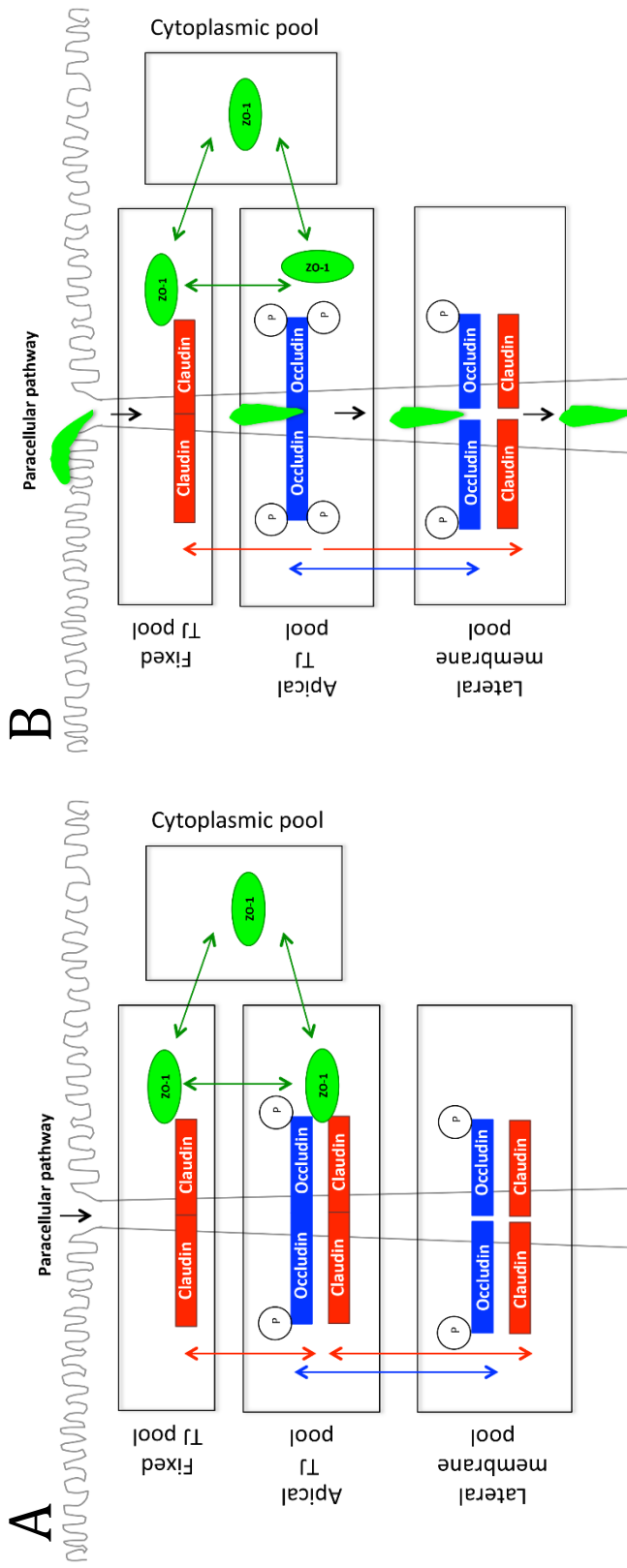


Figure 7.2: Tight Junction dynamics. Tj-associated occludin (green), claudin(s) (red) and ZO-1 (yellow) mobility between the four cellular compartments: The apical and fixed Tj pool, lateral membrane pool and cytoplasmic pool. Movement of proteins between the pools is indicated by their corresponding arrows A) Transmembrane occludin and claudin(s) dimers on neighbouring cells form the semi-permeable paracellular Tj barrier, stabilised by ZO-1 localisation to the complex. Occludin is mobile between the apical Tj and lateral membrane and claudin(s) are mobile between the apical and fixed Tj as well as the lateral membrane whereas ZO-1 is mobile between the apical and fixed Tj pools and cytoplasmic pool. B) Predicted association between ZO-1 and the occludin and claudin(s) dimers on neighbouring cells is disrupted either by parasite secreted factors or physical interactions between parasites and the integral Tj proteins. This leads to loss of ZO-1 mediated occludin stabilisation at the Tj and transient occludin re-localisation to the lateral membrane. Claudin(s) re-localise to the lateral membrane or the fixed Tj pool where they maintain the Tj permeability barrier during transmigration. ZO-1 remains mobile between the apical and fixed Tj pool and the cytoplasmic pool. Adapted from Weber, 2013.

Media from *T. gondii* infected cells has been shown to induce non-infected cells to enter S-phase, suggesting *T. gondii* secreted factors stimulate host cell modulation [Lavine and Arrizabalaga, 2009]. Using HFF cells *T. gondii* infection has been shown to induce host cell cycle progression from the G₀ to S-phase and remain arrested at S-phase until intracellular invasion induces arrest at G₂ phase to enable parasite proliferation [Brunet et al, 2008; Molestina et al, 2008].

RhoA mediated GEF-H1 regulation of cell cycle progression has been linked to occludin localisation to the TJ, illustrated in figure 7.1 (highlighted in brown). GEF-H1 recruitment to the TJ via binding to Cingulin or JACOP, which also bind to occludin at the TJ, results in GEF-H1 inhibition. Whereas if it is not sequestered at the TJ, GEF-H1 promotes RhoA-mediated actin cytoskeleton reorganisation which leads to cell cycle progression from G₁ to S-phase via activation of Ras or RalA and ultimately ZONAB in the nucleus [Balda et al, 2003; Matter et al, 2005; Terry et al, 2010].

Interestingly, occludin expression and TJ strand formation has been directly linked to actin cytoskeleton dynamics and the cell cycle [Kojima et al, 1998; Runkle et al, 2011]. Parasite-mediated dissociation of occludin from the TJ may therefore represent a mechanism of TJ-complex disruption and promotion of the GEF-H1, RhoA, ZONAB signalling pathway that mediates actin cytoskeleton remodelling and cell cycle progression to S-phase.

This novel link between occludin and parasite-mediated cell cycle progression; that occludin expression, localisation to the TJ and the number of TJ strands are directly associated with host cell cycle progression to S-phase, may describe a novel potential mechanism of parasite infection, intracellular replication and survival. Significantly, it may also explain the intracellular cytoplasmic re-localisation of occludin during parasite infection [Weight, 2011]. This hypothesis was formed from the previous finding that TJ strands were disrupted and occludin lost from cell borders during cell cycle progression to S-phase [Kojima et al, 1998]. As occludin is known to localise with centrosomes in MDCK

cells [Runkle et al, 2011], occludin re-distribution from the apical TJ to centrosomes may be the missing link that explains why *T. gondii* promotes TJ disruption during infection. Furthermore, phosphorylation of occludin at S490 near the coiled-coil domain appears to be a switch that promotes occludin endocytosis to an intracellular location prior to association with centrosomes [Runkle et al, 2011]. This finding also provides a potential explanation for the observed loss of TJ occludin in disorders associated with hyperproliferation such as diabetic retinopathy or epithelial cancers [Antonetti et al, 1998; Birkenfeld et al, 2008; Harhaj et al, 2006; Kimura et al, 1997; Lemieux et al, 2009; Osanai et al, 2006; Soler et al, 1999; Tobioka et al, 2002] and also the abnormal postnatal growth retardation and hyperplasia of the gastric epithelium in occludin knockout mice [Schulzke et al, 2005].

7.2.3 *T. gondii* Modulation of Occludin Phosphorylation

The requirement for static claudin paracellular pores in maintaining the TJ permeability barrier, particularly in response to occludin loss, may explain the apparent discrepancies in occludin function described in previous studies and explain why occludin alone cannot form functional TJ strands [Saitou et al, 1998] and how the TJ barrier is maintained during *T. gondii* infection even though occludin is re-distributed to an apparently intracellular vesicular location [Dalton, 2006; Weight, 2011]. Although TJ barrier regulation and remodelling by the continuous cycle of TJ-associated occludin endocytosis, internalisation, recycling and degradation is not a novel finding [Fletcher et al, 2014; Ivanov et al, 2004; Shen et al, 2008; Marchiando et al, 2010; Turner et al, 2014], it demonstrates the plasticity of occludin within the TJ complex, regulated by the phosphorylation status of the occludin C-terminus [Rao, 2009; Simonovic et al, 2000]. The location of the occludin C-terminus phosphorylation hotspot near a cysteine residue associated with occludin dimer formation [Buschmann et al, 2013; Dorfel and Huber,

2012], implies occludin C-terminus phosphorylation may regulate occludin dimer formation and subsequent association with claudin(s) and ZO-1; a process confirmed by triple CKII phosphorylation of occludin C-terminus enhancing binding to ZO-1 and discovery of occludin S408 as a molecular switch controlling paracellular TJ permeability [Dorfel and Huber, 2013; Raleigh et al, 2011].

Linking the preliminary occludin C-terminus phosphorylation status changes described in chapter five with the proposed roles of the TJ proteins occludin, claudin(s) and ZO-1 during *T. gondii* paracellular infection indicates transient occludin phosphorylation and dephosphorylation during *T. gondii* infection disrupts occludin interactions with claudin(s) and ZO-1.

For example CKII mediated phosphorylation of S408 has been shown to enhance occludin dimer formation and reduce occludin association with ZO-1. Claudin-2 is then able to form dimers on neighbouring cells that create paracellular ion pores, promoting paracellular ion flux through the paracellular pathway and enhancing highly mobile occludin within the TJ. Conversely, occludin S408 dephosphorylation enhances occludin association with ZO-1 via the U5-GuK domain. ZO-1 in turn binds claudin-2 via the PDZ domain. Claudin-2 mobility is therefore increased which disrupts the function of the paracellular pore pathway. ZO-1 therefore acts as a scaffold to maintain the complex when occludin S408 is phosphorylated (Figure 7.3) [Raleigh et al, 2011; Turner et al, 2014].

The parasite kinase TgCDPK1, predicted to interact with the occludin C-terminus in chapter five, may be the regulatory kinase that alters the TJ complex structure during infection. As CDPK has been associated with JAM and cingulin as well as localisation of ZO-1 and occludin to the TJ via actin cytoskeleton reorganisation [Martinez-Estrada et al, 2001; Martin-Padura et al, 1998], it is possible that TgCDPK1 phosphorylation of occludin promotes occludin recruitment to the apical TJ complex, stabilised by interactions with JAM, cingulin, ZO-1, RhoA, Arhgef11 and the actin cytoskeleton.

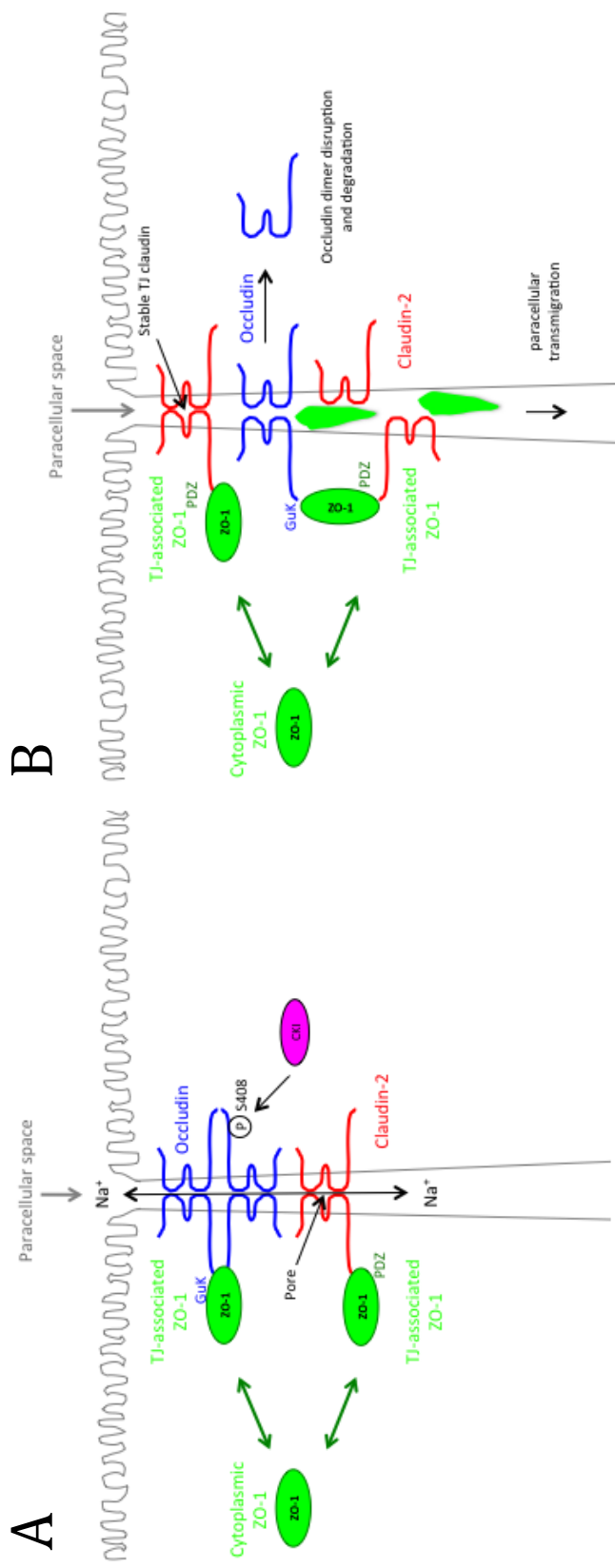


Figure 7.3 Impact of CKII-mediated occludin S408 phosphorylation on TJ structure. A) CKII mediated phosphorylation of S408 enhances occludin dimer formation and reduces occludin association with ZO-1, allowing claudin-2 to form dimers on neighbouring cells to create paracellular ion pores. B) Occludin S408 dephosphorylation enhances occludin association with ZO-1 via the U5-GuK domain, which in turn binds claudin-2 via the PDZ domain, increasing claudin-2 mobility and disrupting the function of the paracellular pore pathway. Image adapted from Raleigh et al, 2011.

7.2.4 *T. gondii* Binding to Occludin

The increased recruitment of occludin to the apical TJ during *T. gondii* infection alludes to a further role for occludin as a receptor during parasite paracellular transmigration [Dalton et al, 2006; Weight, 2011]. As occludin is a major transmembrane protein of the TJ with two extracellular domains, of which ECL1 forms homodimers with neighbouring cells, it is possible that *T. gondii* interacts directly with these domains during parasite paracellular transmigration of SI epithelium. Subsequently in chapter six, occludin ECL1 was identified as a potential host receptor, possibly interacting with a putative parasite secreted MIC effector protein that could be predicted to promote paracellular transmigration as the microneme proteins accumulate on the parasite surface during the initial stages of infection [Carruthers, 2006].

Clostridium perfringens has been shown to bind to the ECL2 of claudins -3 and -4 in order to disrupt the TJ complex [Fujita et al, 2000; Takahashi et al, 2005]. Therefore *T. gondii* binding to occludin ECL1 could be predicted to disrupt occludin dimer interactions on neighbouring cells, transiently opening the epithelial TJ during paracellular transmigration, a proposal substantiated by the observation that occludin ECL1 confers cell-cell adhesion and addition of occludin ECL1 peptides to cell monolayers impairs TJ function [Lacaz-Vieira 1999; Tavelin et al, 2003].

Parasite surface molecules and complementary host cell ligands largely mediate initial contact with the host cell; parasite surface SAG1 and laminin for example have been implicated in attachment to host cells via the $\beta 1$ integrin receptor [Furtado et al 1992; Mineo et al, 1993].

Although SAG1 is important for host cell attachment, it is not absolutely required as SAG1 mutants are still capable of invasion [Grimwood and Smith, 1996]. Differential SAG expression in *T. gondii* type I, II and III has also been linked to parasite virulence. Expression of SAG3 for instance has been linked to acute virulence [Tomavo, 1996] and although SAG1 appears to be expressed in both the virulent RH (Type I) and avirulent ME49 (Type II) strains [Lekutis et al, 2001], SRS2 antigen

abundance is low in type I but highly abundant in type II and III strains [Manger et al, 1998]. Although the functional significance of this correlation is currently unknown, it suggests *T. gondii* expression of surface antigens may account for the multitude of parasite-host interactions, many of which demonstrate crossover functions or redundancy, that facilitate infection of the broad parasite host range.

The fact that *T. gondii* possesses the ability to attach and invade almost any nucleated cell alongside the expression of occludin in a broad range of cell types [Feldman et al, 2005] indicates the novel interaction between *T. gondii* and occludin ECL1 described in this thesis may be a conserved mechanism for parasite paracellular transmigration of host epithelial cell monolayers including the SI epithelium, blood-brain barrier and placenta and could potentially be linked to parasite virulence. Further analysis of *T. gondii* binding to ECL1 will be required to reveal if drugs targeting this interaction could be a therapeutic strategy to block the early stages of infection and prevent toxoplasmosis.

In summary, the data presented in this thesis provides an insight into the fundamental signalling mechanisms between parasite and host and the complex regulation of the TJ permeability barrier both at steady state and in response to *T. gondii* infection. *T. gondii* infection of IEC-6 appears to modulate two main signalling pathways to enable parasite infection, intracellular replication and survival: Firstly, subversion of the host actin cytoskeleton and secondly, modulation of the host cell cycle. The proteins involved in these signalling pathways often exhibit multiple roles and demonstrate extensive cross-talk with the integral transmembrane proteins and the cytoplasmic plaque of scaffolding, adaptor and signalling proteins as well as components of adherens junctions [Gonzalez-Mariscal, 2003; Matter and Balda, 2003]. Therefore, further in depth pathway reconstruction maps and network analysis of the proteins involved in signalling pathways downstream of the integral TJ proteins will be required to fully understand how *T. gondii* modulation of the TJ-complex connects TJ architecture to TJ barrier function and the paracellular permeability of the pore and leak pathways, as well to

elucidate how the interaction between *T.gondii* and occludin promotes host actin cytoskeleton remodelling and host cell cycle progression to S-phase.

As effective treatments against toxoplasmosis have not yet been developed, the involvement of occludin in the host cell cycle offers a novel approach for disease prevention; by identifying the *T. gondii* protein interacting with occludin ECL1, blocking of this complementary parasite receptor could potentially prevent toxoplasmosis. Furthermore, the knowledge that infection by pathogens such as *Helicobacter pylori*, *Salmonella Typhi* and *Citrobacter rodentium* have all been associated with development of GI carcinomas, though the molecular mechanisms responsible are yet to be determined [Lax and Thomas, 2002] led to the hypothesis that promotion of cell hyperproliferation, by *T. gondii* modulation of the host cell cycle, could potentially increase the rate of malignant transformation and contribute to the early stages of carcinogenesis.

7.3 Proposed mechanism of *Toxoplasma gondii* paracellular infection of IEC-6 cells

Based on the results presented in this thesis, the following model of *T. gondii* paracellular infection of the SI epithelium is proposed (Figure 7.4). The SI epithelial cell monolayer is represented by columnar cells with apical microvilli and basal nucleus. Occludin and claudin form dimers on neighbouring cells. Occludin phosphorylation status is represented by the number of phosphorylated C-terminus residues (P). The dynamic behaviour of TJ-associated proteins is represented by mobility between three cellular compartments; cytoplasmic vesicular pool, lateral membrane pool and apical TJ pool. ZO-1 migrates between all three pools whereas claudins and occludin only migrate between the lateral and TJ membrane location. Claudin(s) also maintain a fixed TJ pool (chapter 1) [Shen, 2008].

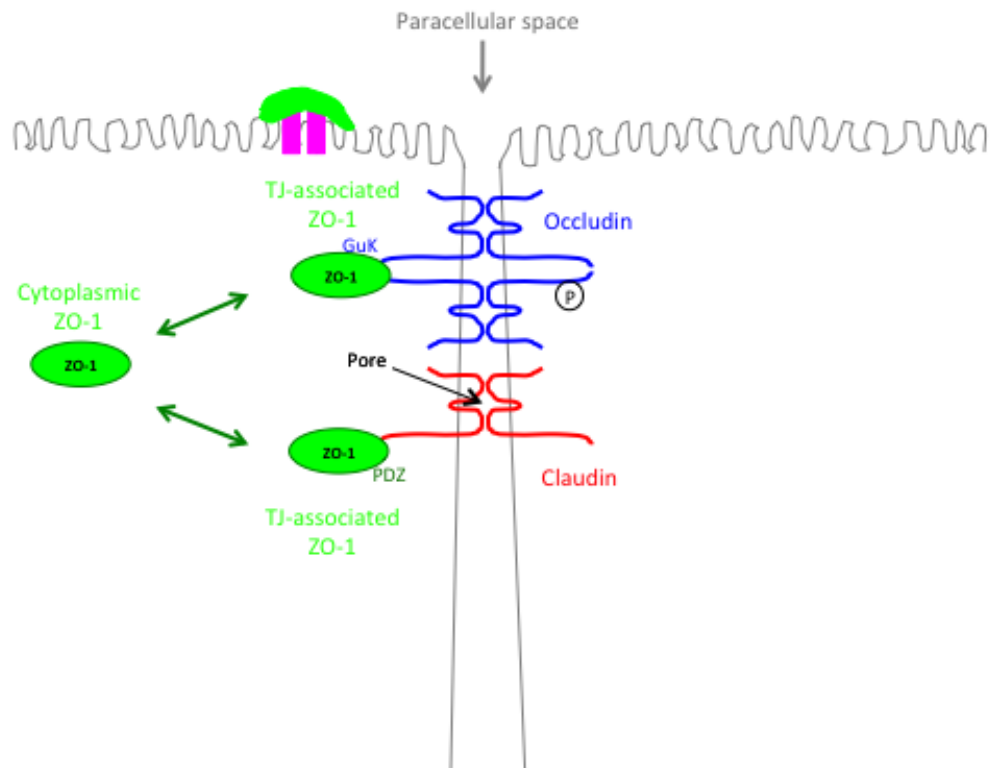


Figure 7.4A: Parasites adhere to the apical host membrane. *T. gondii* gliding motility brings parasites into close proximity with SI epithelial cells followed by cellular contact mediated by interactions between parasite surface antigens, such as SRS or MIC proteins, and apical host membrane proteins such as β -Integrin or ICAM-1 (purple). The TJ complex is stable at steady state: occludin is mobile within the apical TJ, claudin(s) are mobile between the apical TJ and lateral membrane pools and ZO-1 is mobile between all three cellular pools. Claudin(s) form dimers on neighbouring cells to create paracellular ion pores and also retain a fixed, non-mobile TJ pool.

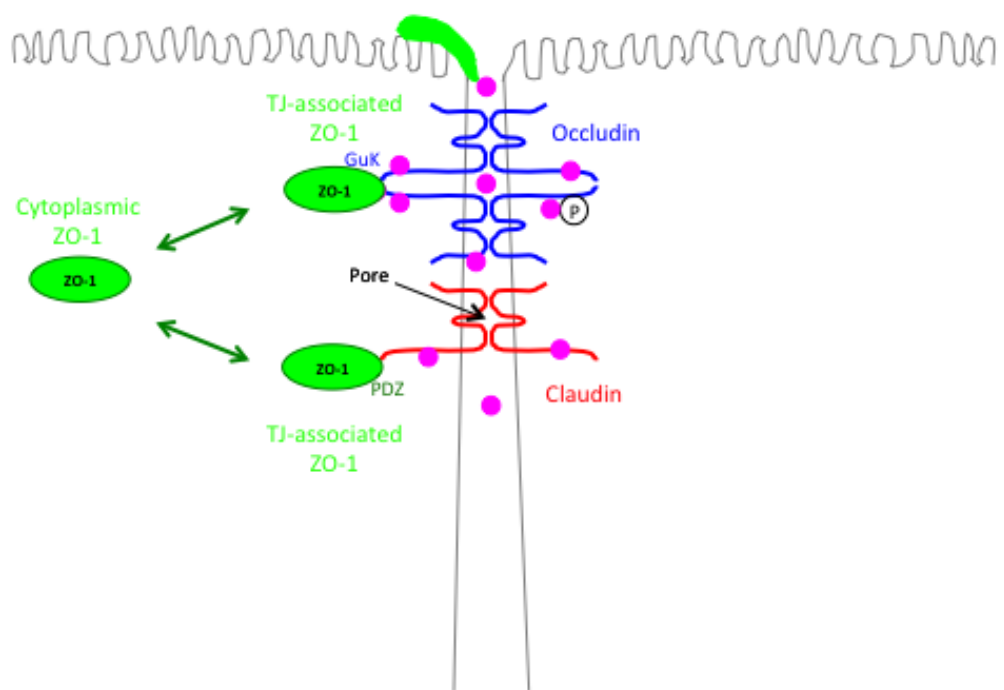


Figure 7.4B: Secretion of parasite effector proteins. Parasite attachment, reorientation and sequential secretion of effector proteins (purple circles) into the host cell subverts a variety of host mechanisms such as actin cytoskeleton rearrangement well as redistributing host cell proteins such as ICAM-1 and PKC from the apical surface to a lateral membrane location.

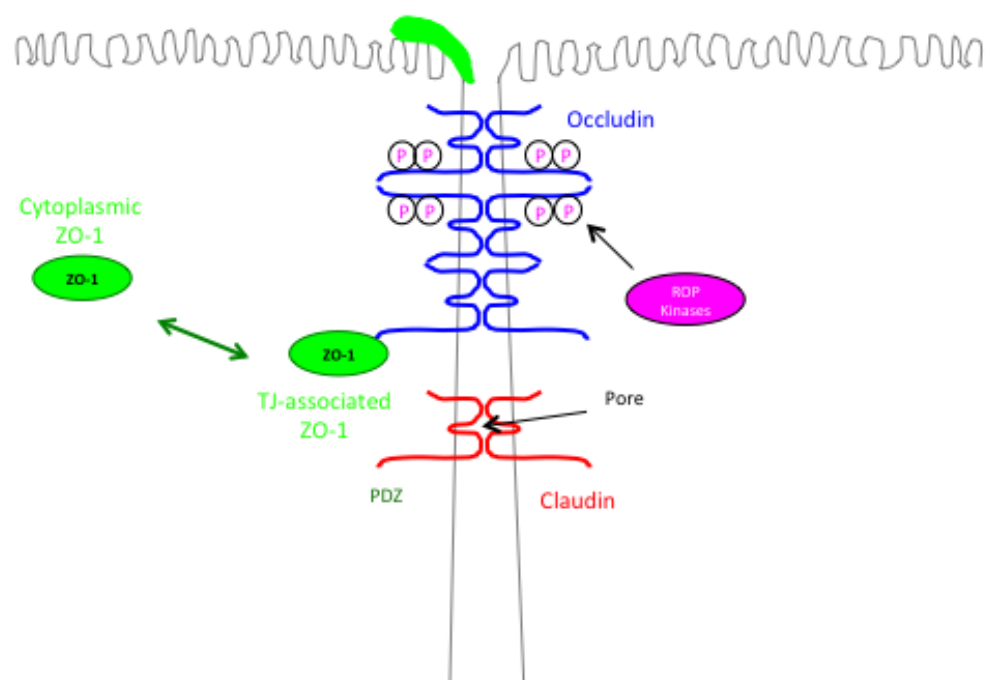


Figure 7.4C: Occludin hyperphosphorylation and TJ complex disruption. Direct secretion of parasite ROP kinases (purple ellipse) into the host cytoplasm causes hyperphosphorylation of the occludin C-terminus, enhancing mobility within the apical TJ, promoting occludin dimer formation and reducing occludin association with ZO-1, which remains mobile between the apical TJ, lateral membrane and cytoplasm. Claudin mobility between the apical TJ and lateral membrane is not altered.

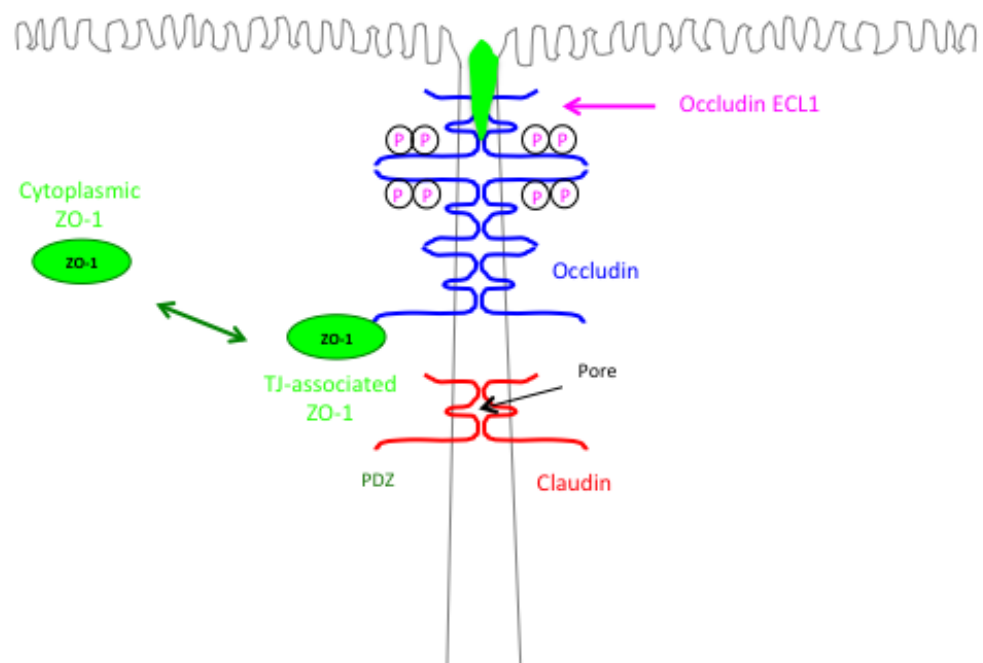


Figure 7.4D: Parasite binding to occludin ECL1. Parasite binding to occludin ECL1, acting as a parasite attachment receptor, via parasite surface molecules with homology to ECL1 leads to paracellular transmigration.

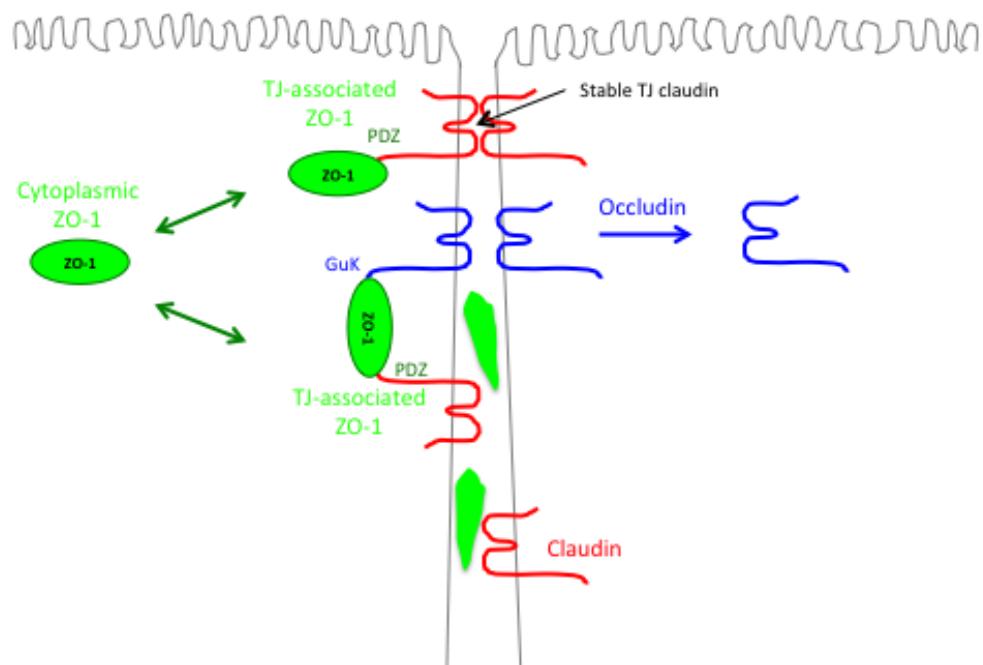


Figure 7.4E: Occludin dimer disruption. Parasite binding to ECL1 disrupts occludin dimers and enhances occludin association with ZO-1 via the GuK domain, which in turn binds claudin(s) via the PDZ domain, increasing claudin(s) mobility between the apical TJ and lateral membrane and disrupting the function of the paracellular pore pathway, whilst retaining a fixed, non-mobile apical TJ pool that maintains the TJ barrier. As parasites transmigrate through the paracellular pathway occludin ECLs are dissociated and accumulate on the parasite surface [Weight, 2011], leading to TJ occludin degradation and recycling to an intracellular cytoplasmic vesicular compartment by endocytosis [Weight, 2011]. Occludin is then redistributed to the host nucleus where it promotes cell cycle progression to S-phase. Interactions between lateral host membrane proteins such as ICAM-1 and *T. gondii* surface molecules such as MIC2 facilitates transmigration through the paracellular space.

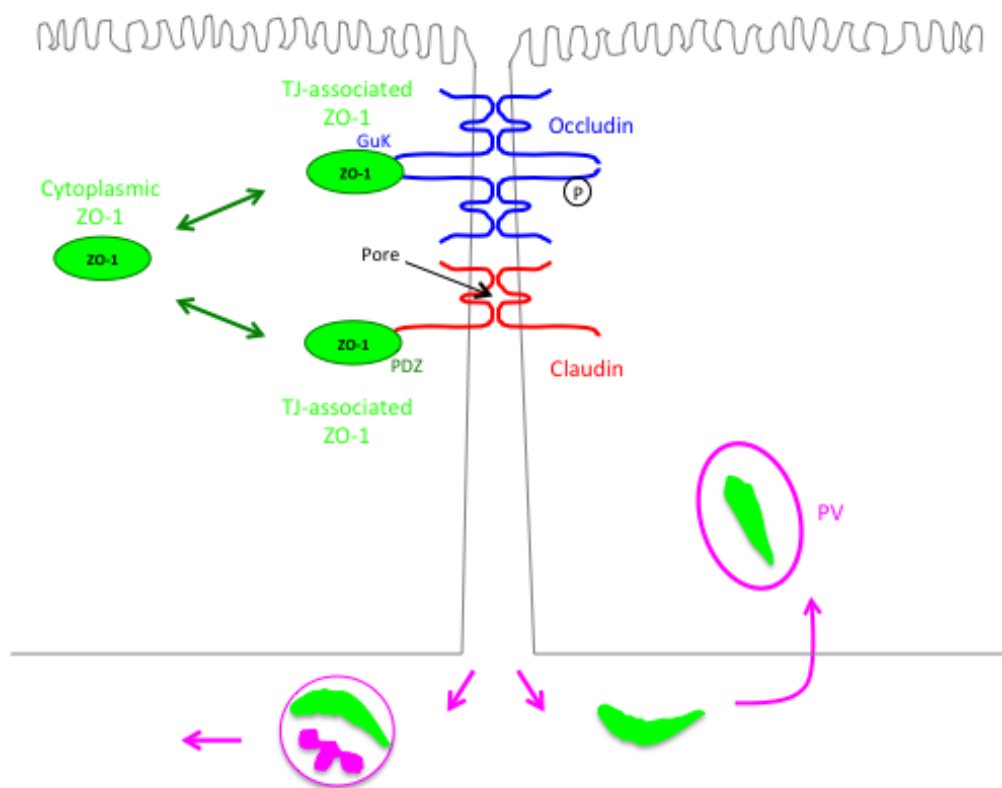


Figure 7.4F: Parasite dissemination or basolateral re-invasion. Transmigration and egress out of the paracellular space leads to parasite invasion of SI epithelial-associated immune cells (purple circle) in a Trojan horse mechanism or basolateral re-invasion of neighbouring cells that requires gliding motility and MJ formation at the host-parasite interface followed by active invasion, intracellular PV formation (purple oval), GRA release and extensive modulation of host cell structure and function such as recruitment of host organelles. Interactions between occludin on the parasite surface and basolateral membrane expressed occludin may assist MJ formation and recruitment of occludin to the PV [Weight, 2011].

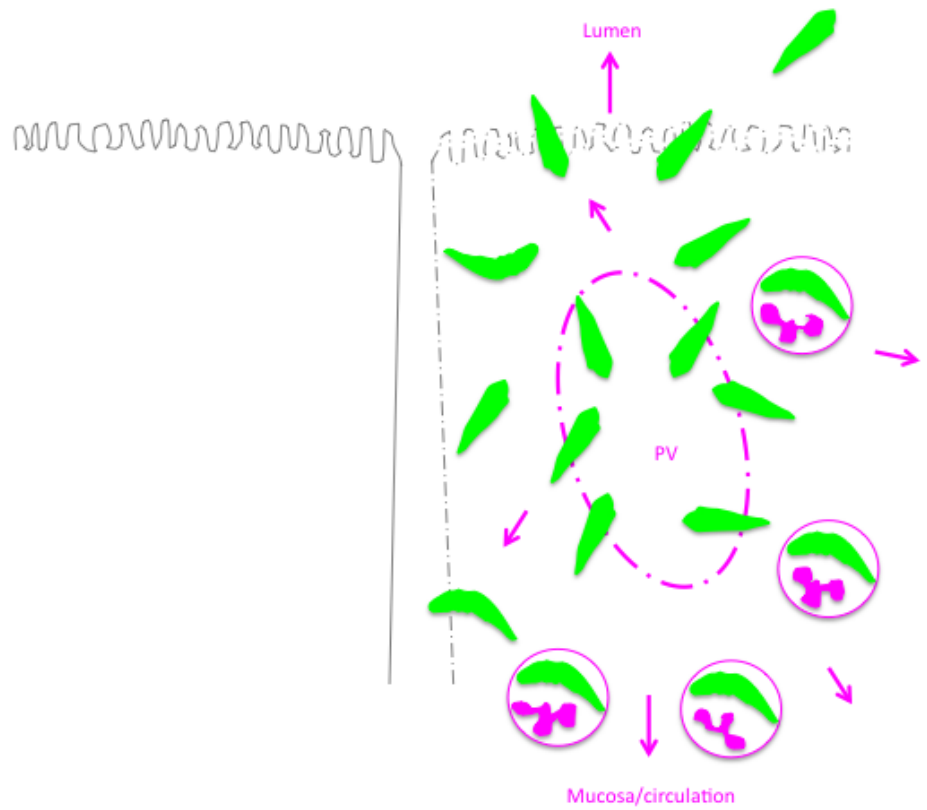


Figure 7.3G: Establishment of the lytic cycle. Intracellular replication within the PV (purple oval) modulates host structure and function to enable parasite nutrient acquisition. Parasite replication ultimately leads to host cell lysis, tissue destruction and parasite dissemination into the lumen and underlying mucosa eliciting a potent host immune response (purple circles) and clearing of the acute tachyzoite stage of infection accompanied by transformation of bradyzoites into tissue cysts and chronic infection.

7.4 Future directions

7.4.1 Validate *in vivo* *T. gondii* paracellular transmigration and binding to occludin

The *T. gondii* infection studies in this thesis were performed *in vitro* using the IEC-6 cell line and although cultured IEC-6 display morphological characteristics of SI epithelial absorptive enterocytes and develop a measurable paracellular barrier, it remains unclear if *in vitro* infection is relevant to infection *in vivo* as certain aspects of the model may not emulate the complexity of the SI epithelial TJ barrier in tissues parasites normally infect.

Therefore, the next stage of this research will be to investigate interactions between *T. gondii* and the TJ-complex *in vivo* and examine *T. gondii* manipulation of the host immune response during parasite paracellular infection and ultimately integrate the findings into the paracellular transmigration mechanism described in this thesis.

Animal models are useful to study the complexity of parasite-host interactions; as mice are natural hosts for *T. gondii*, physiologically relevant murine models such as *ex vivo* SI epithelial explants or the *in vivo* intestinal loop model could be utilised in conjunction with two-photon microscopy to directly visualise real-time interactions between *T. gondii* and the SI epithelium [Caserta et al, 2011; Millet et al, 2014; Sumagin et al, 2014]. For example, two-photon excited SI epithelial autofluorescence or SI epithelial staining with CellTracker™ red, combined with fluorescent YFP-parasites would provide *in vitro* confirmation of the paracellular route of infection presented chapter four of this thesis [Klinger et al, 2011; Orzekowsky-Schroeder et al, 2011]. Similar to studies by Coombes and Gregg, mice expressing fluorescent reporter genes such as CD11c-YFP (DCs), MHCII-GFP (IECs) and LysM-gGFP (neutrophils and monocytes) could also be utilised to simultaneously visualise real-time interactions between fluorescently tagged parasites and specific immune

cell populations, cytokines or cell signalling events [Beuneu et al, 2010; Chtanova et al, 2014; Coombes et al, 2013; Faust et al, 2000; Garrod et al, 2012; Gregg et al, 2013; Lindquist et al, 2004].

Additionally, mice expressing fluorescent occludin or ZO-1 fusion proteins within the SI epithelium could be utilised to confirm parasite binding to occludin *in vivo*, although it should be noted that current models utilise YFP and GFP reporter genes which would be incompatible with YFP-*T.gondii* [Marchiando et al, 2010]. Generation of parasite RH strains expressing fluorescent reporters such as mCherry or Tomato would therefore be beneficial [Gregg et al, 2013]. Accompanying these studies with fluorescently labelled claudin(s) would provide *in vitro* confirmation of predicted interactions between *T. gondii* and differentially located claudins described in this thesis.

7.4.2 Identify which *T. gondii* proteins interact with occludin ECL1 to enable paracellular transmigration

Although the identity of occludin ECL1-*T. gondii* binding partners was not established here, preliminary data from co-immunoprecipitation and MS analysis by Weight identified *T. gondii*-derived proteins including SAG1, SAG2, MIC4 and a number of ROP and GRA proteins as potentially interacting with occludin [Weight, unpublished]. These results are interesting as parasite surface proteins SAG1 and SAG2 could potentially bind directly to ECL1 and MIC4 could transiently associate with ECL1 to promote attachment and paracellular transmigration [Carruthers, 2006]. Combining these preliminary results with the bioinformatics searches presented in chapter six of this thesis suggests MIC proteins and SAG-1 related sequences potentially interact with occludin ECL1, a finding also described recently by Lorenzi et al who found that MIC proteins are highly conserved between *T. gondii* strains and that MICs play a role as host receptors. This provides a starting point for further investigation as the parasite-derived occludin binding proteins have not yet been

identified. As the occludin ECL1 peptide was successfully produced as part of this thesis, it could be employed as bait in yeast two-hybrid screening of *T. gondii* library or used in HIS-tag pull down experiments with *T. gondii* lysates to identify novel binding partners and verify the bioinformatics findings. Searching the results for potential parasite transmembrane proteins or those expressing signalling peptides, may enable discrimination between *T. gondii* surface molecules and secreted effectors interacting with ECL1 [Hakimi and Bougdour, 2015]. Putative parasite-ECL1 interactions should be verified by investigating the effect of mutation or deletion of ECL1 aa residues or parasite-derived proteins on attachment, transmigration and invasion of IEC-6 by utilising both the cell-based infection model and cell-free binding model described in chapter six of this thesis. Combining the site-directed mutations with crystallography could also potentially uncover the structural basis of ECL1-parasite interactions. For example, the *Clostridium perfringens* enterotoxin-host complex has been crystallised and ECL2 residues 194-319 identified as the binding site [Van Itallie et al, 2008]. Similarly identifying *T.gondii*-occludin ECL1 binding sites may therefore provide important structural information for potential therapeutic intervention.

7.5 Overall conclusions

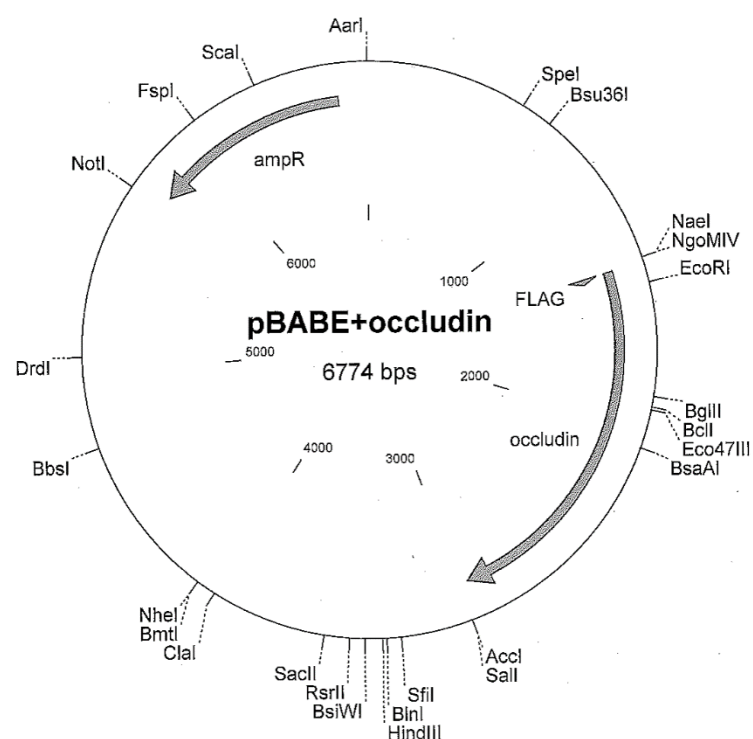
In summary the results presented in this thesis confirm *T. gondii* utilises the paracellular route of infection in an in vitro model of the SI epithelium. Intercellular TJs were shown to be integral to the regulated maintenance of TJ barrier function alongside the dynamic plasticity of the TJ-associated proteins. Consequently occludin was proposed to play a key role in parasite paracellular transmigration, replication and survival through *T. gondii* modulation of the occludin C-terminus domain phosphorylation status, direct parasite binding to the occludin ECLs, occludin dissociation from the TJ and occludin redistribution to the cytoplasm that leads to progression of the host cell cycle to S-phase.

Potential parasite candidate proteins were revealed for each stage of paracellular transmigration, demonstrating the complex interactions between parasites and the SI epithelial TJ as well revealing extensive parasite modulation of downstream signalling pathways. Therefore, occludin has been shown to play an important role both in regulation of the TJ paracellular barrier and as a receptor for *T. gondii* infection, intracellular replication and survival.

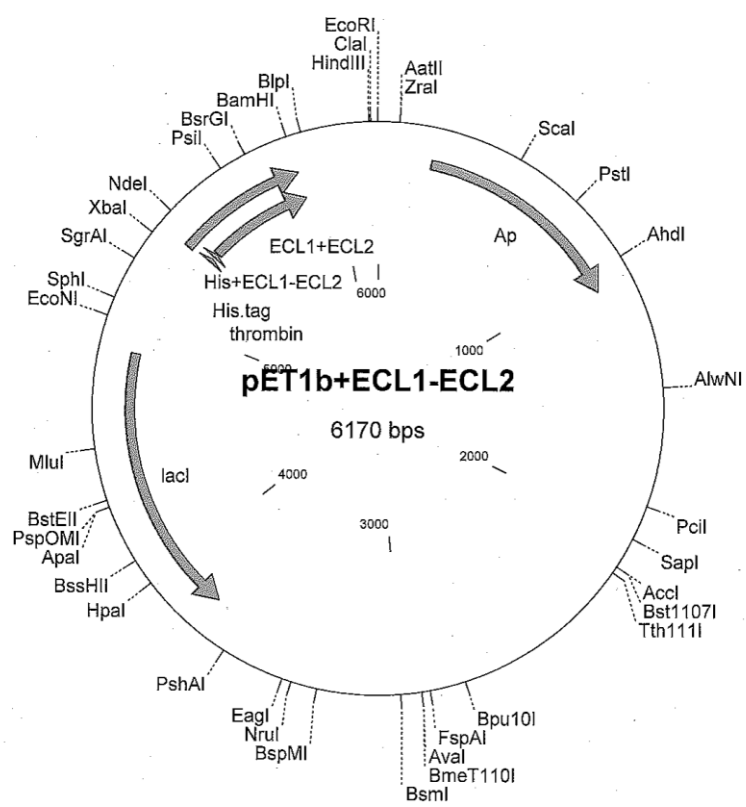
Appendix A

Recombinant Occludin Peptide Generation

DNA regions coding for extracellular loop (ECL) 1 (residues 85 to 138) (184bp) ECL2 (residues 191 to 241) (167bp), ECL1+ECL2 (residues 85 to 241) (485bp) and C-terminus (residues 261 to 521) (800bp) murine occludin fragments were PCR amplified from pBABE-FLAG + Occ plasmid DNA (Britta Engelhardt, University of Bern, Switzerland) [Bamforth et al, 1999] and cloned into the *Nde*I and *Bam*HI sites of the expression vector pET15b (Novagen).



Plasmid map of pBABE-FLAG-tagged occludin (Britta Engelhardt, University of Bern, Switzerland)



Example of plasmid map of pET15b expression vector containing HIS-tagged ECL1+ECL2 (Novagen)

Appendix B

SILAC Dataset

The raw SILAC MS files were processed using MaxQuant [Cox and Mann, 2008] and proteins identified by searching against the *Rattus norvegicus* (Rat) UniProt database (downloaded 5.6.14). Protein quantitation was performed using MaxQuant to generate heavy and light peptide ratios (fold-change) and Perseus statistical analysis to generate significance-B (p-value) scores. The raw data was filtered according to >2-fold change (compared to uninfected control) and a p-value of <0.05.

Time p.i (hours)	Fraction	Fold change	Intensity	PEP	Mol. weight [kDa]	Count	Sequence coverage [%]	Protein IDs	Protein names	Gene names
2	Membrane	59.89458	1.71E+09	0	45.972	6	39.4	Q6IFW1	Keratin 33A, type I	Krt33a
2	Membrane	46.63527	1.12E+10	0	54.698	3	35.4	A7M746	Keratin 83, type II	Krt83
2	Membrane	29.38929	9.55E+09	0	52.732	22	43	A7M776	Keratin Kb23, type II	Kb23
2	Membrane	15.0775	1.60E+09	6.03E-108	57.609	3	17.5	G3V908	Keratin Kb15	Kb15
2	Membrane	12.192	2.56E+07	0	45.835	2	36.1	Q8IFW0	Keratin 33B, type I	Krt33b
2	Membrane	11.17418	2.14E+07	9.08E-11	25.493	2	6	D3ZUG4	similar to keratin associated protein 10-7	LOC690460
2	Membrane	11.12694	3.24E+08	5.40E-58	15.782	5	31.2	Q5BJB3	Coiled-coil-helix-coiled-coil-helix domain containing 2	Chchd2
2	Membrane	10.78272	1.17E+09	0	46.837	6	32.6	F1MAF7	Keratin 31, type I	Krt31
2	Membrane	9.66931	2.81E+08	5.01E-35	11.284	15	40	Q71D11	Dermcidin	Dcd
2	Membrane	7.738141	4.73E+07	2.13E-170	49.906	5	46.7	P85108	Tubulin beta-2A chain	Tubb2a
2	Membrane	7.035317	1.85E+07	8.73E-10	76.357	3	1.7	Q7TQM5	Keratinocyte proline-rich protein	Kprp
2	Membrane	6.892258	1.15E+07	6.66E-11	9.5981	3	20.5	Q5RK28	Normal mucosa of esophagus-specific gene 1 protein	Nmes1
2	Membrane	6.558237	2.87E+08	1.17E-21	18.903	2	6.6	D3ZX50	Keratin-associated protein 11-1	Krtap11-1
2	Membrane	6.558237	4.84E+07	8.86E-09	51.467	7	6	R4HD46	Fatty acid desaturase 3	Fads3
2	Membrane	6.539367	3.44E+07	9.23E-12	9.4109	3	27.3	P59645	FXYD domain-containing ion transport regulator 3	Fxyd3
2	Membrane	6.110975	46.6100	0.00014914	14.352	2	10.4	Q569C0	Transmembrane protein 100	Tmem100
2	Membrane	6.030272	3.71E+07	1.05E-72	24.393	3	57.4	P62494=	Ras-related protein Rab-11A	Rab11a
2	Membrane	5.852402	30.7200	1.31E-06	25.668	2	10.3	Q62876	Syntoglyrin-1	Syng1
2	Membrane	5.783356	2.41E+08	1.62E-165	83.635	7	19.5	D3ZY51	Plakophilin 1 (Predicted)	Pkp1
2	Membrane	5.366822	49.11000	0.00033328	33.427	2	6.8	D3ZFX1	Transmembrane protein 164	Tmem164
2	Membrane	5.232589	5.54E+09	9.08E-224	54.483	8	13.6	G3V939	Keratin 82, type II	Krt82
2	Membrane	5.154108	4.49E+08	1.28E-92	27.747	11	39.5	G3V9A3	stratifin	Sfn
2	Membrane	5.085694	4.36E+07	8.64E-11	45.392	2	6.3	D3Z812	cancer susceptibility candidate 4	Casc4
2	Membrane	4.937053	1.38E+07	5.81E-08	85.756	4	4.9	P07851	Nephrilysin	Mme
2	Membrane	4.319281	3744500	0.00013304	13.965	2	15.4	B0K010	thioredoxin domain containing 17	Txndc17
2	Membrane	4.216385	4.02E+07	3.33E-53	43.704	6	16.6	Q9ESS9	homocysteine-inducible, endoplasmic reticulum stress-inducible, ubiquitin-like domain member 1	Herpud1
2	Membrane	4.2084	8720600	3.11E-10	80.275	3	7.1	A2VD12	Pre-B-cell leukemia transcription factor-interacting protein 1	Pbxip1

Time p.i (hours)	Fraction	Fold change	Intensity	PEP	Mol. weight [kDa]	Count	Sequence coverage [%]	Protein IDs	Protein names	Gene names
2	Membrane	4.1978	8.16E+07	8.24E-171	42.009	10	28.2	D3ZRN3	actin, beta-like 2 Tim17-B-like	Actbl2 LOC10091113
2	Membrane	4.159215	5.57E+07	3.48E-45	18.377	3	21.5	D4ACAS	mitochondrial import inner membrane translocase subunit	0
2	Membrane	4.010749	1.38E+07	1.69E-06	10.119	3	32.6	D4AT5T1	splicing factor 3b, subunit 5	Sf3b5
2	Membrane	3.952413	1.75E+07	1.83E-75	88.039	2	4.8	P52631	Signal transducer and activator of transcription 3	Stat3
2	Membrane	3.833033	7.44E+07	1.58E-40	82.095	8	20.3	Q5XIL4	sorbin and SH3 domain containing 3	Sorbs3
2	Membrane	3.799825	9365200	1.18E-09	29.438	3	14.4	F1M6N0	similar to keratinocytes proline-rich protein	LOC686143
2	Membrane	3.781004	2.82E+08	9.66E-83	47.655	9	24.9	B5DFB2	retinoblastoma binding protein 4	Rbbp4
2	Membrane	3.744196	2.67E+08	1.41E-31	51.658	9	20.8	Q9WTQ2	Podocalyxin	Podxl
2	Membrane	3.737061	4.00E+07	6.91E-12	167.12	6	2.8	Q63041	Alpha-1-macroglobulin	A1m
2	Membrane	3.687996	1.62E+07	2.48E-16	89.386	3	5.1	F1LR77	tetratricopeptide repeat domain 13	Ttc13
2	Membrane	3.674349	6.57E+07	1.03E-18	69.116	11	17.2	Q925R7	Polypeptide N-acetylgalactosaminyltransferase 10	Galnt10
2	Membrane	3.487237	3.66E+07	1.09E-16	65.572	6	13.4	D3ZFB1	Uncharacterized protein	Osg9
2	Membrane	3.358361	6.94E+07	3.53E-118	75.364	9	18	Q5RKH6	Protein OS-9	Ybx1
2	Membrane	3.24707	5.94E+08	1.25E-159	35.802	15	45.7	Q76MJ6	Nuclease-sensitive element-binding protein 1	Snrpa
2	Membrane	3.146435	1.03E+08	2.24E-29	31.176	2	22.4	Q5U214	small nuclear ribonucleoprotein polypeptide A	Comt1l
2	Membrane	3.117556	1.50E+08	1.26E-12	28.987	3	9.2	D3ZM21	Catechol-O-methyltransferase domain containing 1	Slc39a7
2	Membrane	2.772618	2.32E+08	6.93E-43	49.499	7	7.3	Q6MGB4	H2.K region expressed gene 4	Nup35
2	Membrane	2.757328	5.59E+08	2.21E-86	34.801	11	35.1	Q68FV1	Nucleoporin NUP53	Fdrx
2	Membrane	2.69629	6.76E+09	3.25E-241	54.362	77	66.8	P56522	NADPH:adrenodoxin oxidoreductase, mitochondrial	Mras
2	Membrane	2.648375	7.22E+08	6.74E-17	23.901	6	35.1	Q5RKJ7	Ras-related protein M-Ras	Slc6a6
2	Membrane	2.569967	1.60E+09	3.24E-65	69.868	45	17.9	P31643	Sodium- and chloride-dependent taurine transporter	Ccar2
2	Membrane	2.413477	6.85E+08	1.36E-301	102.79	30	35.5	F1LM55	cell cycle and apoptosis regulator 2	Cat
2	Membrane	2.410636	2.08E+09	1.54E-258	59.756	48	55.6	P04762	Catalase	Prss1
2	Cytoplasmic	82.11529	1.62E+09	5.28E-48	25.959	2	8.1	P00762	Anionic trypsin-1	Plb1
2	Cytoplasmic	46.17658	3.16E+08	0.00022865	129.95	6	2.4	F1M7W5	Phospholipase B1, membrane-associated	Krt33a
2	Cytoplasmic	29.26373	2.60E+09	2.72E-136	45.972	11	22	Q6IFW1	Keratin 33A	

Time p.i (hours)	Fraction	Fold change	Intensity	PEP	Mol. weight [kDa]	Count	Sequence coverage [%]	Protein IDs	Protein names	Gene names
2	Cytoplasmic	12.07919	7.48E+08	6.14E-61	11.284	26	34.5	Q71D1	Dermcidin	Dcd
2	Cytoplasmic	10.6953	2.76E+08	4.54E-39	24.674	7	30.2	P07895	Superoxide dismutase [Mn], mitochondrial	Sod2
2	Cytoplasmic	10.50155	1.655E+08	6.98E-14	64.365	3	5.7	Q8TF66	Leucine-rich repeat-containing protein 15	LRRC15
2	Cytoplasmic	6.608949	5.07E+07	5.22E-13	167.12	7	2.5	Q63041	Alpha-1-macroglobulin	A1m
2	Cytoplasmic	6.352029	5.15E+07	0.0014899	19.973	4	8.2	D3ZM70	V-set and transmembrane domain containing 2A	Vstm2a
2	Cytoplasmic	6.133841	1.10E+07	0	61.49	2	46.7	Q5U2U8	Bc2-associated athanogene	Bag3
2	Cytoplasmic	6.102398	3460700	6.39E-06	31.217	2	11.6	D5LG85	Nitric oxide synthase adaptor protein c	NOS1AP
2	Cytoplasmic	6.076811	1.63E+07	2.50E-05	15.957	2	34.7	Q8K3F3	Protein phosphatase 1 regulatory subunit 14B	Ppp1r14b
2	Cytoplasmic	4.979088	2.34E+07	1.45E-10	32.921	3	10.2	Q66H74	Golgi phosphoprotein 3-like	Golph3l
2	Cytoplasmic	4.749691	1.52E+07	0.00010831	90.198	3	3.7	D3ZK36	ubiquitin-like with PHD and ring finger domains 2, E3 ubiquitin protein ligase	Uhrf2
2	Cytoplasmic	4.696559	2.33E+07	7.17E-10	28.404	2	13.3	Q6PT56	Adaptin ear-binding coat-associated protein 2	Ncap2
2	Cytoplasmic	4.596222	1.58E+07	4.14E-13	31.591	2	6.1	P20070	NADH-cytochrome b5 reductase 3	Cyb5r3
2	Cytoplasmic	4.565376	1.41E+08	1.12E-35	105.54	8	9.3	Q6TQE1	Zinc finger CCCH domain-containing protein 18	Zc3h18
2	Cytoplasmic	4.545455	4.77E+07	8.62E-12	24.387	5	19.5	B2GUX7	Cellular repressor of E1A-stimulated genes (Predicted)	Creg1
2	Cytoplasmic	4.532886	1.69E+07	5.79E-10	73.113	4	6.4	Q8VII6	Choline transporter-like protein 1	Slc4a1
2	Cytoplasmic	4.418718	4.99E+07	6.14E-59	41.616	5	23.2	Q3MHS2	Zinc finger protein 830	Znf830
2	Cytoplasmic	4.415791	1.75E+07	6.42E-48	19.119	2	45.6	G3V816	Nucleoside diphosphate kinase	Nme3
2	Cytoplasmic	4.331254	1.89E+07	7.10E-10	29.888	2	12.3	F1LMW7	Myristoylated alanine-rich C-kinase substrate	Marcks
2	Cytoplasmic	4.308673	4.01E+07	9.75E-21	94.475	3	10.1	Q63767	Breast cancer anti-estrogen resistance protein 1	Bear1
2	Cytoplasmic	4.261303	1.86E+07	1.54E-06	15.782	2	22.7	Q5BJB3	Coiled-coil-helix-coiled-coil-helix domain containing 2	Chchd2
2	Cytoplasmic	4.137532	8.07E+08	5.24E-174	41.963	15	41.8	D3ZRN3	Nuclear ubiquitous casein and cyclin-dependent kinase	Actb12
2	Cytoplasmic	4.014291	3.28E+07	1.56E-60	27.14	3	11.9	Q9EPJ0	actin, beta-like 2	Nucks1
2	Cytoplasmic	3.89818	2.73E+07	7.79E-13	69.76	4	6.1	Q5XA6	substrate 1	Smpd1
2	Cytoplasmic	3.835091	6324000	9.02E-277	46.517	2	48	P29457	sphingomyelin phosphodiesterase 1, acid lysosomal	Serpinh1
2	Cytoplasmic	3.772304	2.32E+07	1.23E-16	29.466	2	27.9	M0R6G6	Serpin H1	Nudcd3
									Nudec domain containing 3	

Time p.i (hours)	Fraction	Fold change	Intensity	PEP	Mol. weight [kDa]	Count	Sequence coverage [%]	Protein IDs	Protein names	Gene names
2	Cytoplasmic	3.682156	1.64E+07	1.59E-07	9.9884	2	26	B2RZD1	Sec61 beta subunit	Sec61b
2	Cytoplasmic	3.647771	2.26E+07	2.03E-22	36.988	3	25.8	Q3B8Q0	Microtubule-associated protein RP/EB family member 2	Mapre2
2	Cytoplasmic	3.624764	7.15E+08	2.56E-93	36.612	14	32.6	P42123	L-lactate dehydrogenase B chain	Ldhb
2	Cytoplasmic	3.473428	1.24E+07	1.13E-15	48.7	3	10.5	Q3KR72	Actin-binding LIM protein 1	Ablim1
2	Cytoplasmic	3.461525	1.59E+08	2.37E-59	23.212	5	32.2	M0R7B4	similar to Histone H1.2	LOC84828
2	Cytoplasmic	3.400988	1.44E+07	1.55E-07	10.119	2	32.6	D4AT5T1	splicing factor 3b, subunit 5	Sf3b5
2	Cytoplasmic	3.353117	5.65E+07	1.38E-16	105.44	6	7.5	Q5U2M4	DNA ligase	Lig3
2	Cytoplasmic	3.352105	2.38E+08	0	30.803	7	48.6	Q62764	Y-box-binding protein 3	Ybx3
2	Cytoplasmic	3.260303	1.94E+08	9.52E-87	37.66	4	13.8	P07154	Cathepsin L1	Ctsl1;Catl
2	Cytoplasmic	3.161955	9.33E+07	4.84E-41	101.06	7	9	M0RBL7	family with sequence similarity 115, member C	Fam115c
2	Cytoplasmic	3.147624	2.72E+08	4.19E-61	38.822	8	34.7	Q9JIK1	Reticulon-4	Rtn4
2	Cytoplasmic	3.112744	1.69E+08	1.34E-108	63.867	7	30.3	D4A9I4	5'-3' exoribonuclease 2	Xrn2
2	Cytoplasmic	3.034441	8.28E+07	3.89E-34	23.425	4	26.9	B0BNK1	RAB5C, member RAS oncogene family	Rab5c
2	Cytoplasmic	2.917153	1.05E+08	8.25E-80	59.103	10	18.2	M0R686	immunity-related GTPase family, Q	Irgq
2	Cytoplasmic	2.857633	7.52E+08	2.64E-47	73.562	15	14.1	P41177	Nucleolar and coiled-body phosphoprotein 1	Nolc1
2	Cytoplasmic	2.851684	7.65E+07	6.07E-38	92.216	9	14	O08837	Cell division cycle 5-like protein	Cdc5l
2	Cytoplasmic	2.834387	2.05E+08	7.83E-18	65.868	7	7.3	D4A8Z3	ferric-chelate reductase 1	Frrs1
2	Cytoplasmic	2.778472	4.75E+08	3.32E-170	60.303	14	35.3	D4A7U1	Zyxin	Zyx
2	Cytoplasmic	2.777392	2.12E+08	8.96E-73	74.226	11	22.5	Q99PF5	Far upstream element-binding protein 2	Khsrp
2	Cytoplasmic	2.715473	1.48E+08	8.81E-36	65.695	11	22.3	F1LQW3	splicing factor proline/glutamine-rich	Sfpq
2	Cytoplasmic	2.678595	3.82E+08	0	53.422	15	48.2	Q6PT25	Desmin	Des
2	Cytoplasmic	2.663967	3.55E+08	2.38E-229	50.9	13	31.3	Q9JKB7	Guanine deaminase	Gda
2	Cytoplasmic	2.622057	1.74E+08	9.97E-56	29.585	11	30.5	Q6GT74	Basigin	Bsg
2	Cytoplasmic	2.592957	2.04E+08	6.58E-113	24.549	2	26.4	D4AC36	eukaryotic translation initiation factor 3, subunit F	Eif3f
2	Cytoplasmic	2.569505	2.41E+08	2.72E-78	203.91	31	16.4	F1LN42	tensin 1	Tns1

Time p.i (hours)	Fraction	Fold change	Intensity	PEP	Mol. weight [kDa]	Count	Sequence coverage [%]	Protein IDs	Protein names	Gene names
2	Cytoplasmic	2.515344	2.07E+08	4.34E-23	57.013	13	11.5	Q4KLZ0	vanin 1	Vnn1
2	Cytoplasmic	2.511049	8.90E+08	0	49.937	3	56.8	Q6AYZ1	Tubulin alpha-1C chain	Tuba1c
2	Cytoplasmic	2.314279	1.82E+09	1.01E-209	106.21	38	20.4	Q6P7A9	Lysosomal alpha-glucosidase	Gaa
2	Cytoplasmic	2.08481	2.70E+09	0	82.411	48	26.8	D3ZL13	N-acetylglucosaminidase, alpha	Naglu
2	Cytoplasmic	2.084289	1.73E+09	3.26E-101	61.332	11	9.9	Q9EQV6	Tripeptidyl-peptidase 1	Tpp1
24	Membrane	48.14173	7745900	0.0014712	76.357	3	1.4	Q7TQM5	Keratinocyte proline-rich protein	Kprp
24	Membrane	44.19889	1.68E+09	2.39E-135	45.972	14	24.3	Q6IFW1	Keratin 33A	Krt33a
24	Membrane	24.75248	6.86E+08	2.83E-84	25.203	11	45.3	Q9WU50	GTP:AMP phosphotransferase AK4, mitochondrial	Ak4
24	Membrane	19.69822	2.57E+08	2.38E-44	35.076	8	35.6	P48284	Carbonic anhydrase 4	Ca4
24	Membrane	18.57217	3.17E+07	9.61E-07	21.635	2	6.9	P23593	Apolipoprotein D	Apod
24	Membrane	18.23021	3.27E+07	1.84E-20	11.284	5	22.7	Q71D1	dermcidin	Dcd
24	Membrane	16.00558	1.69E+07	1.60E-22	505.99	6	2	Q9WU10	Protocadherin	Fat1
24	Membrane	10.16829	2.02E+07	1.04E-08	65.724	2	8.1	Q8CH93	Hyaluronan synthase 1	Has1
24	Membrane	9.683354	1.43E+07	8.69E-10	122.89	3	3.8	Q9R1N3	Sodium bicarbonate cotransporter 3	Slc4a7
24	Membrane	9.505703	9.15E+07	4.77E-19	51.467	6	14.7	R4HD46	Fatty acid desaturase 3	Fads3
24	Membrane	8.559328	6.32E+08	7.60E-42	55.903	9	10	Q63016	Large neutral amino acids transporter small subunit 1	Slc7a5
24	Membrane	8.457375	2.95E+08	2.23E-34	41.466	28	17.6	P07308	Acyl-CoA desaturase 1	Scd1
24	Membrane	7.648183	7.41E+07	1.03E-15	26.667	3	15.7	P0C057	Histone H2A.Z	H2afz
24	Membrane	7.467702	1.14E+09	8.37E-38	53.962	17	14.4	P11167	Solute carrier family 2, facilitated glucose transporter member 1	Slc2a1
24	Membrane	7.294478	6.77E+08	3.13E-06	101.07	2	1.8	D3ZD62	N-deacetylase/N-sulfotransferase (heparan glucosaminyl) 2	Ndst2
24	Membrane	7.173087	1.17E+10	0	54.018	49	70.7	Q8R4A1	ERO1-like protein alpha	Ero1l
24	Membrane	6.937218	9.67E+07	1.27E-12	44.024	2	12	Q5M9H3	TGF-beta receptor type-1	Tgfb1
24	Membrane	6.317519	1.07E+08	8.62E-15	34.354	3	16.5	D3ZT1	mesenteric estrogen-dependent adipogenesis	Medag
24	Membrane	6.098677	1.63E+08	4.85E-55	46.263	5	26.5	Q5U2U5	Perilipin	Plin2
24	Membrane	6.083465	9988200	8.56E-05	69.286	2	2.2	F1YH3	mitochondrial tRNA translation optimization 1	Mto1

Time p.i (hours)	Fraction	Fold change	Intensity	PEP	Mol. weight [kDa]	Count	Sequence coverage [%]	Protein IDs	Protein names	Gene names
24	Membrane	5.906326	2.47E+08	1.11E-45	84.071	8	21.3	A2RRU1	Glycogen [starch] synthase, muscle	Gys1
24	Membrane	5.893099	2.99E+07	7.70E-07	36.346	4	8	P38552	Galectin-4	Igals4
24	Membrane	5.714612	4.855E+07	1.05E-05	45.009	4	6.2	P20961	Plasminogen activator inhibitor 1	Serpine1
24	Membrane	5.681172	5.97E+07	4.24E-15	29.888	2	25	F1LMW7	Myristoylated alanine-rich C-kinase substrate	Marcks
24	Membrane	5.552779	1.72E+08	2.93E-147	87.184	8	16	B5DF27	Lysyl oxidase homolog 2	Loxl2
24	Membrane	5.551854	1.66E+07	9.69E-11	13.312	2	12.7	BOK036	Succinate dehydrogenase assembly factor 1, mitochondrial	Sdhaf1
24	Membrane	5.461198	1.20E+08	6.33E-39	78.178	7	13.2	P18163	Long-chain-fatty-acid-CoA ligase 1	Acsl1
24	Membrane	5.403653	2.50E+07	2.37E-18	67.472	3	8.9	Q6MGC3	WD repeat domain 46	Wdr46
24	Membrane	5.369992	1.09E+08	0	61.984	2	59.7	B5DFG	heterogeneous nuclear ribonucleoprotein L	Hnrnl
24	Membrane	5.287089	5.20E+07	2.65E-88	41.772	2	14.9	Q6MG75	negative elongation factor complex member E	Nelfe
24	Membrane	5.158628	2.60E+09	1.30E-250	102.54	50	48.9	P27381	Hexokinase-2	Hk2
24	Membrane	5.143504	2.03E+07	4.18E-13	57.205	3	7.9	D3ZRS2	lysophosphatidylcholine acyltransferase 4	Lpcat4
24	Membrane	5.137426	3.55E+07	6.88E-28	10.301	5	33.3	Q8VH49	HIG1 domain family member 1A, mitochondrial	Higd1a
24	Membrane	5.125576	5.51E+09	7.56E-151	25.109	93	47.3	P62804	Histone H4	Hist1h4b
24	Membrane	5.059704	8.64E+09	0	87.01	70	53.4	D3ZQR7	Procollagen-lysine,2-oxoglutarate 5-dioxygenase 2	Plod2
24	Membrane	5.059193	2.40E+08	5.43E-170	30.803	5	42.1	Q62764	Y-box-binding protein 3	Ybx3
24	Membrane	5.029928	2.62E+09	1.13E-74	13.99	44	55.2	Q00715	Histone H2B type 1	Hist1h2bf
24	Membrane	5.018317	8.82E+08	1.21E-47	17.827	18	34.8	Q4QQV3	Protein FAM162A	Fam162a
24	Membrane	4.970179	2.26E+07	1.01E-202	106.2	4	25.1	M0R544	Glucosidase, alpha, acid, isoform CRA_a	Gaa
24	Membrane	4.855076	2.55E+07	8.34E-13	29.299	3	15.8	Q5M916	Multiple myeloma tumor-associated protein 2 homolog	Mmttag27
24	Membrane	4.770082	1.44E+08	1.63E-46	14.068	5	36.7	Q618Q6	Histone H2A	Hist1h2af
24	Membrane	4.692192	8.99E+08	8.84E-124	17.076	16	57.1	F1M5V2	GLI pathogenesis-related 2	Glipr2
24	Membrane	4.635209	3.01E+07	1.71E-13	15.991	3	30.2	D3ZCM4	DnaJ (Hsp40) homolog, subfamily C, member 15 (Predicted)	Dnajc15
24	Membrane	4.618298	3258800	3.24E-07	131.72	2	4.4	D3ZVN3	zinc finger CCCH-type containing 4	Zc3h4
24	Membrane	4.536793	3.02E+07	9.37E-20	9.4109	2	27.3	P59645	FXYD domain-containing ion transport regulator 3	Fxyd3

Time p.i (hours)	Fraction	Fold change	Intensity	PEP	Mol. weight [kDa]	Count	Sequence coverage [%]	Protein IDs	Protein names	Gene names
24	Membrane	4.524068	4.315E+07	1.33E-25	19.918	5	26	Q9JKW1	Mitochondrial import inner membrane translocase subunit Tim22	Timm22
24	Membrane	4.499235	7.62E+07	6.99E-78	24.393	3	61.1	P62494	Ras-related protein Rab-11A	Rab11a
24	Membrane	4.466878	1.78E+09	3.69E-207	37.716	46	49.6	D4A1V5	methylenetetrahydrofolate dehydrogenase (NADP+-dependent) 2	Mthfd2
24	Membrane	4.428502	6959800	0.00066508	14.756	2	7.1	D4A7K0	transmembrane protein 242	Transm242
24	Membrane	4.410143	8.61E+09	0	39.351	57	74.2	P05065	Fructose-bisphosphate aldolase A; Fructose-bisphosphate aldolase	Aldoa
24	Membrane	4.307189	8.00E+07	2.14E-26	41.679	5	20.4	G3V9A4	2-5-oligoadenylate synthase 1A	Oas1a
24	Membrane	4.298487	2.81E+09	1.00E-277	58.071	43	47.4	Q794F9	4F2 cell-surface antigen heavy chain	Slc3a2
24	Membrane	4.264938	2.98E+08	1.29E-34	71.637	13	16.4	B5D5N9	Low affinity cationic amino acid transporter 2	Slc7a2
24	Membrane	4.244843	4.34E+07	1.90E-25	14.189	6	38.8	D4A9Y2	hypothetical protein	LOC691931
24	Membrane	4.21763	1.11E+09	7.80E-154	73.562	33	31.2	P41177	Nucleolar and coiled-body phosphoprotein 1	Nolc1
24	Membrane	4.186202	4.64E+08	1.00E-100	31.351	14	40.6	Q5RIM0	MKI67 FHA domain-interacting nucleolar phosphoprotein	Mki67ip
24	Membrane	4.161119	2.47E+09	1.40E-252	60.141	20	22.6	Q00238	Intercellular adhesion molecule 1	Icam1
24	Membrane	4.130354	1.01E+08	2.42E-90	52.502	5	15.5	B0BND5	ribosomal RNA processing 9, small subunit	Rrp9
24	Membrane	4.008177	8.22E+07	2.69E-88	16.31	9	41.1	Q6DQ97	Phospholipase A2, membrane associated	Pla2g2a
24	Membrane	3.978041	8.92E+07	3.05E-100	80.02	3	17.7	D3ZY39	ribosomal RNA processing 1B	Rrp1b
24	Membrane	3.879728	9.40E+08	3.77E-85	34.801	23	45.2	Q68FY1	Nucleoporin NUP53	Nup35
24	Membrane	3.733572	2.77E+08	2.95E-82	41.536	14	28.2	A1AP52	Ribosome biogenesis regulatory protein homolog	Rrs1
24	Membrane	3.668513	3.17E+08	1.57E-45	483.19	22	6.2	F1MAP9	E3 ubiquitin-protein ligase	Huwel1
24	Membrane	3.577689	9.59E+08	0	79.139	32	29.2	P97560	Antigen peptide transporter 1	Tap1
24	Membrane	3.570281	1.66E+08	7.13E-39	62.359	12	21	M0RBD8	midasin homolog	Mdn1
24	Membrane	3.507049	1.40E+08	3.07E-157	40.345	5	37	P10824	Guanine nucleotide-binding protein G(i) subunit alpha-1	Gnai1
24	Membrane	3.497849	2.13E+08	2.21E-20	49.499	5	7.3	Q6MGB4	H2-K region expressed gene 4	Slc39a7
24	Membrane	3.385813	4.11E+10	0	55.764	145	81	Q5U3Z7	Serine hydroxymethyltransferase	Shmt2
24	Membrane	3.366333	9.21E+08	1.01E-115	15.782	8	31.2	Q5BJB3	coiled-coil-helix-coiled-coil-helix domain containing 2	Chchd2

Time p.i (hours)	Fraction	Fold change	Intensity	PEP	Mol. weight [kDa]	Count	Sequence coverage [%]	Protein IDs	Protein names	Gene names
24	Membrane	3.218021	2.48E+09	0	50.622	42	81.1	D4A6C5	Rho GTPase activating protein 1	Argap1
24	Membrane	3.196931	4.29E+08	1.43E-14	37.178	17	12.1	Q5XIA8	Growth hormone-inducible transmembrane protein	Ghitm
24	Membrane	3.179246	1.41E+10	0	60.897	106	68.4	P54001	Prolyl 4-hydroxylase subunit alpha-1	P4ha1
24	Membrane	3.159657	3.04E+08	1.20E-28	67.269	11	19.2	Q8VIA9	High affinity cationic amino acid transporter 1	SltZa1
24	Membrane	3.134658	9.31E+08	2.81E-111	42.662	27	62.8	Q63707	Dihydroorotate dehydrogenase (quinone), mitochondrial	Dhodh
24	Membrane	3.030395	1.85E+09	3.27E-193	38.789	15	45.3	Q95571	RT1.A(U) alpha chain	RT1-EC2
24	Membrane	3.007519	3.60E+08	5.50E-83	94.766	20	28.5	Q5RT2	pre-rRNA processing protein FTS13	FtsJ3
24	Membrane	3.004838	3.95E+08	8.21E-81	23.009	11	30.2	Q6AYQ9	Peptidyl-prolyl cis-trans isomerase	Ppic
24	Membrane	2.991952	2.96E+08	1.56E-75	92.33	16	26	G3V6F5	Zinc phosphodiesterase ELAC protein 2	ElaC2
24	Membrane	2.959631	7.79E+09	0	32.56	144	69.5	P13084	Nucleophosmin	Npm1
24	Cytoplasmic	142.2819	1.45E+09	5.37E-82	46.707	2	10	Q9ESY6	Glyceraldehyde-3-phosphate dehydrogenase, testis-specific	Gapdhs
24	Cytoplasmic	34.34066	2.39E+09	6.16E-207	52.732	6	49.1	A7M776	Type II keratin Kb23	Kb23
24	Cytoplasmic	26.30956	2.26E+07	2.81E-07	54.068	2	7.3	M0RAG5	Cleavage stimulation factor subunit 2	Cstf2
24	Cytoplasmic	22.61932	1.93E+07	1.15E-12	74.591	3	11.4	F1M609	Acyl-coenzyme A oxidase	Acox1
24	Cytoplasmic	20.262219	3.20E+07	8.24E-12	49.885	3	8.7	Q5XIV9	Interferon-related developmental regulator 1	Ifrd1
24	Cytoplasmic	19.46548	1.355E+08	1.99E-162	77.023	6	24.6	Q6IE69	Glutamine-fructose-6-phosphate aminotransferase [isomerizing] 2	GfpT2
24	Cytoplasmic	18.53774	7.05E+07	2.59E-17	67.176	4	15.6	Q6AXQ5	2,5-phosphodiesterase 12	Pde12
24	Cytoplasmic	16.75266	1.64E+08	1.03E-98	21.987	3	33.3	P15865	Histone H1.4	Hist1h1e
24	Cytoplasmic	15.49715	6.13E+07	1.06E-08	11.284	4	22.7	Q71D1	Dermcidin	Dcd
24	Cytoplasmic	14.52264	2.69E+07	2.81E-08	67.181	3	7.7	D4ABT4	NADPH-dependent diflavin oxidoreductase 1	Ndor1
24	Cytoplasmic	13.83566	6.59E+07	1.85E-15	10.902	4	45.1	P26772	10 kDa heat shock protein, mitochondrial	Hspe1
24	Cytoplasmic	13.49236	3.71E+09	0	60.955	50	54.8	P63039	60 kDa heat shock protein, mitochondrial	Hspd1
24	Cytoplasmic	13.33422	1.15E+07	3.58E-15	30.997	2	7.2	Q35796	Complement component 1 Q subcomponent-binding protein,	C1qbpb
24	Cytoplasmic	12.94147	2.70E+07	6.62E-15	31.516	3	16.6	P14604	Enoyl-CoA hydratase, mitochondrial	Echs1

Time p.i (hours)	Fraction	Fold change	Intensity	PEP	Mol. weight [kDa]	Count	Sequence coverage [%]	Protein IDs	Protein names	Gene names
24	Cytoplasmic	12.10214	1.01E+09	4.20E-113	24.674	14	41.4	P07395	Superoxide dismutase [Mn], mitochondrial	Sod2
24	Cytoplasmic	11.90646	2.62E+07	1.04E-17	61.514	2	10	Q5BJU7	Wiskott-Aldrich syndrome protein family member 1	Wasf1
24	Cytoplasmic	10.6969	4.44E+07	1.65E-10	108.54	3	5.2	D3ZUF9	Pitrysin metallopeptidase 1 (Predicted)	Pitm1
24	Cytoplasmic	10.63253	3.49E+07	5.57E-31	68.61	2	14.3	B2GV74	Kinesin light chain 2 (Predicted)	Klc2
24	Cytoplasmic	9.143275	8.80E+08	5.88E-46	51.83	10	30.7	G3V936	Citrate synthase;Citrate synthase, mitochondrial	Cs
24	Cytoplasmic	8.979885	7.04E+07	1.20E-23	56.171	5	18.7	Q5PPF5	Zinc finger CCCH-type with G patch domain-containing protein	Zfpat
24	Cytoplasmic	8.95175	2.42E+09	4.35E-288	35.683	22	63.6	P04636	Malate dehydrogenase, mitochondrial;Malate dehydrogenase	Mdh2
24	Cytoplasmic	8.944544	2.16E+07	6.10E-11	71.643	2	6.2	D4A0T2	Influenza virus NS1A binding protein (Predicted)	Ivns1abp
24	Cytoplasmic	8.934954	3.45E+07	7.77E-11	69.798	2	5.3	B2RYL8	DEAD (Asp-Glu-Ala-Asp) box polypeptide 41	Ddx41
24	Cytoplasmic	8.73744	1.46E+09	2.18E-192	60.303	20	43.6	D4A7U1	Zyxin	Zyx
24	Cytoplasmic	8.584428	1.32E+09	4.98E-116	55.764	23	49.8	Q5U3Z7	Serine hydroxymethyltransferase	Shmt2
24	Cytoplasmic	8.49329	1.43E+08	1.57E-26	60.897	9	19.3	P54001	Prolyl 4-hydroxylase subunit alpha-1	P4ha1
24	Cytoplasmic	8.458806	1.36E+08	5.90E-121	54.037	6	13.6	Q6P6R2	Dihydrolipoyl dehydrogenase, mitochondrial	Dld
24	Cytoplasmic	8.388558	1.10E+08	5.67E-27	49.412	5	25.3	D4ADE7	CD3e molecule, epsilon associated protein	Cd3eap
24	Cytoplasmic	8.071025	1.83E+08	2.09E-12	15.782	2	22.7	Q5BIB3	Coiled-coil-helix-coiled-coil-helix domain containing 2	Chchd2
24	Cytoplasmic	8.01282	1.76E+08	5.84E-21	67.603	6	15.7	Q3BN8	Pescadillo homolog	Pes1
24	Cytoplasmic	7.943443	3.66E+09	4.46E-300	73.562	45	28.8	P41777	Nucleolar and coiled-body phosphoprotein 1	Nolc1
24	Cytoplasmic	7.793017	6.21E+08	3.20E-162	71.206	19	34.3	F1LQJ7	Phosphoenolpyruvate carboxylkinase 2 (mitochondrial)	Pck2
24	Cytoplasmic	7.560293	4.05E+08	2.68E-40	14.068	4	35.9	M0RDH42	Histone H2A	Hist1h2af
24	Cytoplasmic	7.4638	4.03E+07	9.56E-05	43.851	2	8.8	D3ZQ63	Methyltransferase like 2 (Predicted)	Mettl2b
24	Cytoplasmic	7.451565	2.76E+08	2.75E-103	80.46	10	19	Q5XHZ0	Heat shock protein 75 kDa, mitochondrial	Trap1
24	Cytoplasmic	7.422803	3.58E+08	3.04E-147	84.597	15	26.6	G3V910;	Procollagen-lysine,2-oxoglutarate 5-dioxygenase 2	Plod2
24	Cytoplasmic	7.251632	5.666E+07	4.57E-19	48.242	3	19.4	P50442	Glycine amidinotransferase, mitochondrial	Gatm
24	Cytoplasmic	7.029877	2.32E+09	1.16E-201	48.332	29	52.6	P04182	Ornithine aminotransferase, mitochondrial	Oat
24	Cytoplasmic	6.971556	2.10E+09	1.02E-225	61.415	30	47	P10860	Glutamate dehydrogenase 1, mitochondrial	Glud1

Time p.i (hours)	Fraction	Fold change	Intensity	PEP	Mol. weight [kDa]	Count	Sequence coverage [%]	Protein IDs	Protein names	Gene names
24	Cytoplasmic	6.935294	9.26E+07	1.64E-43	28.295	5	21	Q9ZDV6	Thioredoxin-dependent peroxide reductase, mitochondrial	Prdx3
24	Cytoplasmic	6.869547	3.05E+07	1.81E-11	27.245	3	15.7	070351	3-hydroxyacyl-CoA dehydrogenase type-2	Hsd17b10
24	Cytoplasmic	6.754931	7.83E+07	4.18E-15	51.859	6	16.2	D4ACM9	microfibrillar-associated protein 1A	Mfap1a
24	Cytoplasmic	6.710058	1.06E+09	3.19E-242	47.314	23	47.2	P00507	Aspartate aminotransferase, mitochondrial	Got2
24	Cytoplasmic	6.676459	2.82E+08	1.56E-26	22.649	4	22.1	D3ZBN0	Histone H1.5	Hst1h1b
24	Cytoplasmic	6.63086	1.30E+07	4.02E-275	10.62	3	21.6	M0R544	Glucosidase, alpha, acid, isoform	Gaa
24	Cytoplasmic	6.581978	1.78E+10	7.55E-273	25.109	130	46.8	G5BV28	Histone H4	Hst1h4b
24	Cytoplasmic	6.56211	7.22E+08	2.91E-186	54.018	14	39.7	Q8R4A1	ERO1-like protein alpha	Ero1l
24	Cytoplasmic	6.559958	1.56E+08	2.10E-281	59.71	4	48.6	Q7TP47	Heterogeneous nuclear ribonucleoprotein Q	Syncrip
24	Cytoplasmic	6.335931	7.26E+07	1.63E-87	44.695	8	26.9	P17764	Acetyl-CoA acetyltransferase, mitochondrial	Acat1
24	Cytoplasmic	6.280223	1.40E+09	1.54E-183	45.972	8	35.4	Q6IFW1	Keratin 33A	Krt33a
24	Cytoplasmic	6.220066	8.94E+07	4.03E-61	70.622	6	29.1	Q63560	Microtubule-associated protein 6	Map6
24	Cytoplasmic	6.205784	1.71E+07	1.39E-09	49.628	3	9.3	Q6IMX8	Acyl-coenzyme A thioesterase 2	Acot2
24	Cytoplasmic	6.112096	3.04E+07	7.40E-12	55.903	3	8.4	Q63016	Large neutral amino acids transporter small subunit 1	Slc7a5
24	Cytoplasmic	6.110602	2.30E+07	1.60E-09	62.669	3	8.6	Q5PPG7	Eukaryotic translation initiation factor 2D	Eif2d
24	Cytoplasmic	6.107989	3.27E+08	4.18E-27	26.667	9	30.1	P0C057	Histone H2A.Z	H2afz
24	Cytoplasmic	6.010338	1.76E+08	4.21E-129	57.609	2	18	G3V908	type II keratin Kb15	Kb15
24	Cytoplasmic	5.967655	7.04E+09	1.26E-82	13.99	52	55.2	Q00715	Histone H2B type 1	Hst1h2bf
24	Cytoplasmic	5.834306	1.31E+09	2.78E-200	56.516	21	41.6	F1LM88	Aldehyde dehydrogenase, mitochondrial	Aldh2
24	Cytoplasmic	5.728361	2.96E+07	1.59E-05	57.632	2	6	Q5PQS6	Protein SMG9	Smg9
24	Cytoplasmic	5.714939	4.76E+07	1.12E-09	29.888	2	28.6	F1LMW7	Myristoylated alanine-rich C-kinase substrate	Marcks
24	Cytoplasmic	5.712654	2.49E+08	4.23E-148	65.351	12	24.7	D3ZJH9	Malic enzyme	Me2
24	Cytoplasmic	5.697681	2.07E+07	9.99E-08	58.02	3	5.4	Q5FVF9	Biotinidase	Btd
24	Cytoplasmic	5.694761	3.04E+07	1.01E-23	53.396	3	11.2	P17955	Nuclear pore glycoprotein p62	Nup62
24	Cytoplasmic	5.674403	1.83E+07	7.03E-06	96.445	3	3.5	D3ZJR1	Epidermal growth factor receptor pathway substrate 15-like 1	Eps15l1

Time p.i (hours)	Fraction	Fold change	Intensity	PEP	Mol. weight [kDa]	Count	Sequence coverage [%]	Protein IDs	Protein names	Gene names
24	Cytoplasmic	5.560189	3.39E+07	9.35E-48	83.635	2	4.9	D3ZY51	Plakophilin 1 (Predicted)	Pkp1
24	Cytoplasmic	5.546004	1.29E+08	2.10E-24	36.148	6	15.6	P13086	Succinyl-CoA ligase [ADP/GDP-forming] subunit alpha,	Sucg1
24	Cytoplasmic	5.524557	2.21E+07	4.93E-08	71.114	3	6.8	B1H282	Glycosyltransferase 25 domain containing 1	Colgt1
24	Cytoplasmic	5.409206	2.17E+07	1.40E-07	54.362	2	8.9	P56522	NADPH:adenodoxin oxidoreductase, mitochondrial	Fdxr
24	Cytoplasmic	5.401026	6321800	0.00021578	61.523	3	3.8	Q5NDL0	EGF domain-specific O-linked N-acetylglucosamine transferase	Eogt
24	Cytoplasmic	5.391998	1.60E+07	6.14E-43	68.575	2	6.2	D3ZX56	DEAD (Asp-Glu-Ala-Asp) box polypeptide 55	Ddx55
24	Cytoplasmic	5.349024	1.63E+07	7.80E-20	81.042	2	4.5	O54924	Exocyst complex component 8	Exoc8
24	Cytoplasmic	5.281783	1.40E+09	0	50.967	25	49.1	P56574	Isocitrate dehydrogenase [NADP], mitochondrial	Idh2
24	Cytoplasmic	5.211862	3.75E+07	9.39E-13	49.522	3	10.6	P85834	Elongation factor Tu, mitochondrial	Tufm
24	Cytoplasmic	5.08285	2.59E+07	2.36E-14	116.29	4	7.1	Q5X178	2-oxoglutarate dehydrogenase, mitochondrial	Ogdh
24	Cytoplasmic	5.073052	1.40E+08	5.76E-32	64.786	3	5.3	Q5U2V1	FK506 binding protein 10	Fkbp10
24	Cytoplasmic	5.023106	6.71E+08	2.11E-212	73.857	15	29.9	P48721	Stress-70 protein, mitochondrial	Hspa9
24	Cytoplasmic	4.984548	3.01E+08	7.14E-76	47.872	13	36.5	P15650	Long-chain specific acyl-CoA dehydrogenase, mitochondrial	Acdl
24	Cytoplasmic	4.913522	1.23E+09	5.72E-246	85.432	26	37.9	Q9ER34	Aconitate hydratase, mitochondrial	Aco2
24	Cytoplasmic	4.901448	1.44E+08	3.40E-31	36.171	5	16.2	Q62651	Delta(3,5)-Delta(2,4)-dienoyl-CoA isomerase, mitochondrial	Ech1
24	Cytoplasmic	4.799846	3.23E+08	7.32E-18	39.613	4	22.1	Q99NAS	Isocitrate dehydrogenase [NAD] subunit alpha, mitochondrial	Idh3a
24	Cytoplasmic	4.78996	2.39E+08	6.33E-39	59.756	9	8.7	P04762	Catalase	Cat
24	Cytoplasmic	4.748113	7.96E+07	4.75E-47	62.315	4	17.2	F1LDQ45	Epsin-2	Epn2
24	Cytoplasmic	4.738214	1.19E+09	0	30.803	15	67.5	Q62764	Y-box-binding protein 3	Ybx3
24	Cytoplasmic	4.731712	2.63E+08	1.97E-52	47.247	8	33.2	P29524	Plasminogen activator inhibitor 2 type A	Serpinb2
24	Cytoplasmic	4.672242	1.97E+08	2.01E-71	41.783	10	46	G3V9U2	3-ketoacyl-CoA thiolase, mitochondrial	Acaa2
24	Cytoplasmic	4.665485	3.93E+09	3.08E-106	23.212	32	33	M0R7B4	similar to Histone H1.2	LOC84828
24	Cytoplasmic	4.475875	7.02E+07	6.30E-18	15.957	2	34.7	Q8K3F3	Protein phosphatase 1 regulatory subunit 14B	Ppp1r14b
24	Cytoplasmic	4.46608	1.83E+08	2.87E-32	127.67	9	11.2	F1LM57	DNA-directed RNA polymerase	Polr1b
24	Cytoplasmic	4.449388	4.53E+07	1.43E-22	44.453	5	15.9	D3ZKD3	RNA demethylase ALKBH5	Alkbh5

Time p.i (hours)	Fraction	Fold change	Intensity	PEP	Mol. weight [kDa]	Count	Sequence coverage [%]	Protein IDs	Protein names	Gene names
24	Cytoplasmic	4.437345	3.13E+07	5.10E-13	29.299	6	15.8	Q5M916	Multiple myeloma tumor-associated protein 2 homolog	Mmtag2
24	Cytoplasmic	4.414816	3.20E+07	4.80E-63	62.733	2	5.1	Q4V8B4	Chromatin assembly factor 1, subunit B (P60	Chaf1b
24	Cytoplasmic	4.397731	6.60E+07	0	39.652	3	47.2	Q6URK4	Heterogeneous nuclear ribonucleoprotein A3	Hnrnpa3
24	Cytoplasmic	4.383658	3.79E+08	3.24E-130	50.9	22	49.8	Q9JKB7	Guanine deaminase	Gda
24	Cytoplasmic	4.334446	1.03E+08	6.96E-54	28.299	7	30.3	B0BNN3	Carbonic anhydrase 1	Ca1
24	Cytoplasmic	4.329192	5.95E+07	2.58E-27	32.264	3	10	Q68G41	Enoyl-CoA delta isomerase 1, mitochondrial	Eci1
24	Cytoplasmic	4.237468	4.04E+07	1.07E-08	62.592	2	6.1	D3Z9M1	methyltransferase like 16	Mettl16
24	Cytoplasmic	4.222616	2.35E+09	6.46E-280	102.54	60	47.3	P27881	Hexokinase-2	Hk2
24	Cytoplasmic	4.217986	1.47E+08	4.65E-96	57.807	4	14.4	Q02253	Methylmalonate-semialdehyde dehydrogenase [acylating], mitochondrial	Aldh6a1
24	Cytoplasmic	4.16008	2.67E+08	7.82E-44	48.769	10	32.3	B0BN64	Polymerase (RNA) I associated factor 1 (Predicted)	Polr1e
24	Cytoplasmic	4.117479	1.43E+09	2.61E-254	85.719	29	36.5	P47860	6-phosphofructokinase type C:6-phosphofructokinase	Pfkp
24	Cytoplasmic	4.071164	3.78E+07	1.89E-29	209.48	7	5	D3ZN13	programmed cell death 11	Pdccl11
24	Cytoplasmic	4.069673	4.32E+07	3.68E-41	30.056	3	17.3	Q5I034	Uncharacterized protein	
24	Cytoplasmic	4.05976	6.47E+07	4.39E-72	65.147	5	10.6	D3ZMZ9	guanine nucleotide binding protein-like 3 (nucleolar)-like	Gnl3l
24	Cytoplasmic	4.038283	9.58E+07	4.05E-40	39.04	4	21.5	Q02874	Core histone macro-H2A.1	H2afy
24	Cytoplasmic	4.031668	9.64E+07	1.29E-37	79.632	5	11.5	Q5XJ05	Protein SPA1 homolog	Soad1
24	Cytoplasmic	4.027724	6.56E+07	6.06E-20	61.794	3	16.4	D4AAZ8	Interferon regulatory factor 2 binding protein 1 (Predicted)	Irf2bp1
24	Cytoplasmic	4.021879	5.38E+08	2.35E-291	68.26	19	41.6	Q5XJ07	Lipoma-preferred partner homolog	Lpp
24	Cytoplasmic	4.020747	5.84E+08	2.09E-293	85.965	24	45	Q3B8Q1	Nucleolar RNA helicase 2	Ddx21
24	Cytoplasmic	3.983746	2.51E+08	1.39E-111	67.196	9	29.7	Q32PY7	Far upstream element-binding protein 1	Fubp1
24	Cytoplasmic	3.958201	1.62E+08	1.45E-61	34.951	9	29.4	P13B03	Electron transfer flavoprotein subunit alpha, mitochondrial	Etfal
24	Cytoplasmic	3.884853	1.21E+08	1.77E-34	58.968	6	23.8	G3V645	2-5'-oligoadenylate synthase-like protein 1	Oasl
24	Cytoplasmic	3.881083	2.31E+08	6.63E-13	36.132	4	21.5	Q64591	2,4-dienoyl-CoA reductase, mitochondrial	Decr1
24	Cytoplasmic	3.814464	4.75E+08	1.48E-84	47.655	9	26.6	B5DFB2	retinoblastoma binding protein 4	Rbbp4
24	Cytoplasmic	3.808944	1.26E+08	5.34E-61	64.949	4	11.7	Q5XJ01	La-related protein 7	Larp7

Time p.i (hours)	Fraction	Fold change	Intensity	PEP	Mol. weight [kDa]	Count	Sequence coverage [%]	Protein IDs	Protein names	Gene names
24	Cytoplasmic	3.769602	1.40E+08	7.15E-32	101.8	7	15.6	D3ZDT1	erythrocyte membrane protein band 4.1-like 2	Epb4112
24	Cytoplasmic	3.704115	1.68E+08	1.17E-74	57.54	7	26.2	Q5U2N1	negative elongation factor complex member A	Nelfa
24	Cytoplasmic	3.703704	1.03E+08	6.62E-63	27.687	6	30.6	Q68FU3	Electron transfer flavoprotein subunit beta	Etfb
24	Cytoplasmic	3.524229	3.93E+08	1.45E-77	81.8	21	30.1	Q6P0K8	Junction plakoglobin	Jup
24	Cytoplasmic	3.498094	8.18E+08	5.21E-145	194.19	47	30.8	O54889	DNA-directed RNA polymerase I subunit	Polr1a
24	Cytoplasmic	3.475722	1.28E+09	6.64E-175	41.963	17	32.7	D3ZRN3	actin, beta-like 2	Actb12
24	Cytoplasmic	3.332556	8.26E+08	8.19E-180	152.28	35	25.7	O35821	Myb-binding protein 1A	Mybbp1a
24	Cytoplasmic	3.170376	1.57E+09	0	60.07	29	48.3	Q9QZ86	Nucleolar protein 58	Nop58

Appendix C

Functional Annotation of differentially expressed proteins during *T. gondii* infection of IEC-6

Functional annotation of SILAC proteins modulated during *T. gondii* infection using the protein annotation through evolutionary relationship (PANTHER) Gene Ontology (GO) classification system (<http://www.pantherdb.org> Version 10) [Mi et al, 2013]. Results filtered by significant ($p<0.05$) enrichment of proteins.

Time p.i (hours)	GO biological process	Fold change	P-value
2	negative regulation of apoptotic signalling pathway	> 5	3.36E-03
2	regulation of intrinsic apoptotic signalling pathway	> 5	8.56E-03
24	isocitrate metabolic process	> 5	7.54E-03
24	2-oxoglutarate metabolic process	> 5	5.70E-04
24	tricarboxylic acid cycle	> 5	1.44E-05
24	citrate metabolic process	> 5	4.16E-05
24	tricarboxylic acid metabolic process	> 5	6.01E-06
24	aerobic respiration	> 5	1.00E-04
24	fatty acid beta-oxidation	> 5	8.16E-03
24	dicarboxylic acid metabolic process	> 5	4.84E-07
24	protein homotetramerization	> 5	1.03E-03
24	fatty acid catabolic process	> 5	6.89E-03
24	cellular respiration	> 5	3.80E-05
24	monocarboxylic acid catabolic process	> 5	2.83E-02
24	pyridine nucleotide metabolic process	> 5	1.20E-02
24	nicotinamide nucleotide metabolic process	> 5	1.20E-02
24	oxidoreduction coenzyme metabolic process	> 5	4.17E-03
24	energy derivation by oxidation of organic compounds	> 5	6.61E-06
24	generation of precursor metabolites and energy	> 5	1.71E-08
24	pyridine-containing compound metabolic process	> 5	2.21E-02
24	protein tetramerization	> 5	1.12E-02
24	coenzyme metabolic process	> 5	3.37E-05
24	negative regulation of apoptotic signalling pathway	> 5	1.46E-03
24	organic acid catabolic process	> 5	3.21E-02
24	carboxylic acid catabolic process	> 5	3.21E-02
24	cofactor metabolic process	> 5	8.61E-05
24	monocarboxylic acid metabolic process	> 5	2.11E-08
24	lipid catabolic process	> 5	1.69E-02
24	carboxylic acid metabolic process	> 5	2.57E-14

Time p.i (hours)	GO biological process	Fold change	P-value
24	oxoacid metabolic process	> 5	1.74E-15
24	organic acid metabolic process	4.92	4.89E-15
24	oxidation-reduction process	4.66	1.58E-14
24	fatty acid metabolic process	4.53	1.32E-02
24	ncRNA metabolic process	4.41	3.90E-03
24	response to hypoxia	4.39	1.86E-03
24	response to decreased oxygen levels	4.32	2.38E-03
24	response to oxygen levels	4.19	1.76E-03
24	single-organism catabolic process	3.71	1.60E-05
24	small molecule metabolic process	3.6	5.87E-14
24	response to nutrient levels	3.55	9.39E-04
24	response to extracellular stimulus	3.39	2.15E-03
24	RNA processing	3.3	1.82E-02
24	protein complex subunit organization	2.92	1.17E-05
24	organonitrogen compound metabolic process	2.82	1.96E-04
24	protein complex assembly	2.8	5.82E-03
24	protein complex biogenesis	2.8	5.82E-03
24	single-organism biosynthetic process	2.71	1.13E-02
24	negative regulation of cell death	2.63	3.09E-02
24	macromolecular complex assembly	2.51	1.10E-02
24	response to hormone	2.47	4.63E-02
24	single-organism metabolic process	2.37	5.28E-13
24	cellular component biogenesis	2.34	8.22E-05
24	catabolic process	2.3	2.46E-02
24	organic substance transport	2.2	3.53E-02
24	macromolecular complex subunit organization	2.19	3.66E-03
24	response to external stimulus	2.18	7.57E-03
24	response to stress	2.1	2.21E-05
24	nitrogen compound metabolic process	1.96	2.15E-05

Appendix D

Tight Junction Proteome

Comprehensive list of known TJ proteins constructed by integrating current functional annotations, protein-protein interactions and known signalling pathways [Aijaz et al, 2006; Anderson and Van Itallie, 2009; Balda and Matter 2008 and 2009; Chiba et al, 2008; Dorfel and Huber, 2012; Furuse and Tsukits, 2006; Gonzalez-Mariscal et al, 2008; Kohler and Zahraoui, 2005; Lui et al, 2003; Matter et al, 2005; Matter and Balda, 2003 and 2014; McNeil et al, 2006; Morimoto et al, 2005; Muller et al, 2005; Salama et al, 2006; Schneeberger and Lynch, 2004; Suzuki et al, 2006; Tang, 2006; Turksen and Troy, 2004; Ye et al, 2006; Zahraoui, 2005].

Protein annotation	Protein IDs	Protein names	Gene names	Protein Length (aa)
Transmembrane Proteins	Q86SU0	Immunoglobulin-like domain-containing receptor 1	ILDR1	546
	Q71H61	Immunoglobulin-like domain-containing receptor 2	ILDR2	639
	Q5DX21	Immunoglobulin superfamily member 11	IGSF11	431
	Q8NE79	Blood vessel epicardial substance	BVES	360
	P78310	Coxsackievirus and adenovirus receptor	CAR	365
	095832	Claudin-1	CLDN1	211
	P57739	Claudin-2	CLDN2	230
	015551	Claudin-3	CLDN3	220
	014493	Claudin-4	CLDN4	209
	000501	Claudin-5	CLDN5	218
	P56747	Claudin-6	CLDN6	220
	095471	Claudin-7	CLDN7	211
	P56748	Claudin-8	CLDN8	225
	095484	Claudin-9	CLDN9	217
	P78369	Claudin-10	CLDN10	228
	075508	Claudin-11	CLDN11	207
	P56749	Claudin-12	CLDN12	244
	Q9Z0S4	Claudin-13	Cldn13	211
	095500	Claudin-14	CLDN14	239
	P56746	Claudin-15	CLDN15	228
	Q9Y5I7	Claudin-16 (Paracellin-1)	CLDN16 PCLN1	305
	P56750	Claudin-17	CLDN17	224
	P56856	Claudin-18	CLDN18	261
	Q8N6F1	Claudin-19	CLDN19	224
	P56880	Claudin-20	CLDN20	219
	Q8N7P3	Claudin-22	CLDN22	220
	Q96B33	Claudin-23	CLDN23	292
	A6NM45	Putative claudin-24	CLDN24	220
	C9JDP6	Putative claudin-25	CLDN25	229

Protein annotation	Protein IDs	Protein names	Gene names	Protein Length (aa)
	Q9D563 B1AQL3 Q9H6B4 Q9BUF7 O95727 Q96AP7 Q9Y624 P57087 Q9BX67 Q9NSI5 Q86X29 Q96A59 Q16625 Q8N4S9	Transmembrane protein 114 (Claudin-26) Transmembrane protein 235 (Claudin-27) CXADR-like membrane protein Protein crumbs homolog 3 Cytotoxic and regulatory T-cell molecule Endothelial cell-selective adhesion molecule Junctional adhesion molecule A Junctional adhesion molecule B Junctional adhesion molecule C Immunoglobulin superfamily member 5 Lipolysis-stimulated lipoprotein receptor MARVEL domain-containing protein 3 Occludin MARVEL domain-containing protein 2 (Tricellulin)	Tmem114 Cldn26 Tmem235 Cldn27 CLMP ACAM ASAM CRB3 CRTAM ESAM JAM1 JAM2 JAM3 IGSF5 JAM4 LSR MARVELD3 OCLN MARVELD2 TRIC	222 211 373 120 393 390 299 298 310 407 649 401 522 558
Scaffolding and Adaptor Proteins	Q4VCS5 P07355 Q9P2M7 Q14247 P82279 Q9BUF7 P36383 Q12959 P15311 P12814 Q13813 P33176 Q15334	Angiomotin Annexin A2 Cingulin Src substrate cortactin Protein crumbs homolog 1 Protein crumbs homolog 3 Gap junction gamma-1 protein Disks large homolog 1 Ezrin Alpha-actinin-1 Spectrin alpha chain, non-erythrocytic 1 Kinesin-1 heavy chain Lethal(2) giant larvae protein homolog 1	AMOT ANXA2 ANX2 ANX2L4 CAL11H LPC2D CGN CTTN EMS1 CRB1 CRB3 GJC1 GJA7 DLG1 EZR VII2 ACTN1 SPTAN1 NEAS SPTA2 KIF5B KNS KNS1 LLGL1 DLG4 HUGL HUGL	1084 339 1197 550 1406 120 396 904 586 892 2472 963 1064

Protein annotation	Protein IDs	Protein names	Gene names	Protein Length (aa)
	Q96QZ7	Membrane-associated guanylate kinase, WW and PDZ domain-containing protein 1	MAGI1 AIP3 BAIAP1 BAP1 TNRC19	1491
	Q86UL8	Membrane-associated guanylate kinase, WW and PDZ domain-containing protein 2	MAGI2 ACVRINP1 AIP1	1455
	Q5TCQ9	Membrane-associated guanylate kinase, WW and PDZ domain-containing protein 3	MAGI3	1506
P35240	Merlin	Canalicular multispecific organic anion transporter 2	NF2 SCH	595
015438		Multiple PDZ domain protein	ABCC3 CMOAT2 MLP2 MRP3	1527
075970	Myosin-2	Breast cancer anti-estrogen resistance protein 1	MPDZ MUPP1	2070
Q9UKX2		MAGUK p55 subfamily member 5	MYH2 MYHSA2	1941
P56945		Proteinase-activated receptor 1	BCAR1 CAS CASS1 CRKAS	870
Q8N3R9		Partitioning defective 3 homolog	MPP5	675
P25116		Partitioning defective 6 homolog alpha	F2R CF2R PAR1 TR	425
Q8TEW0		Cingulin-like protein 1	PARD3 PAR3 PAR3A	1356
Q9NPB6		InaD-like protein	PARD6A PAR6A	346
Q0VF96		Tight junction-associated protein 1	CGNL1 JACOP KIAA1749	1302
Q8NI35		Peroxisomal membrane protein 2	INADL PATJ	1801
Q5JT00		Protein 4.1	TJAP1 PILT TJP4	557
Q9NR77		Scaffold attachment factor B1	PXMP2 PMP22	195
P11171		Protein scribble homolog	EPB41 E41P	864
Q15424		Spectrin beta chain, non-erythrocytic 1	SAFB HAP HET SAFB1	915
Q14160		Syntaxin-4	SCRIB CRIB1 LAP4 SCRIB1 VARTUL	1630
Q01082		Tubulin alpha-4A chain	SPTBN1 SPTB2	2364
Q12846		Vasodilator-stimulated phosphoprotein	STX4 STX4A	297
P68366		Tight junction protein ZO-1	TUBA4A TUBA1	448
P50552		Tight junction protein ZO-2	VASP	380
Q07157		Tight junction protein ZO-3	TJP1 ZO1	1748
Q9UDY2			TJP2 X104 ZO2	1190
O95049			TJP3 ZO3	919

Protein annotation	Protein IDs	Protein names	Gene names	Protein Length (aa)
	P68133 P60709 P35221	Actin, alpha skeletal muscle Actin, cytoplasmic 1 Catenin alpha-1	ACTA1 ACTA ACTB CTNNNA1	377 375 906
Signalling Proteins	Q4VCS5 P34932 P84077 O15085 Q8TEW0 Q03135 P60953 P29033 P24385 Q03113 Q92974 P49840 Q96J02 Q9D4H4 Q95835 Q9NRM7 Q9HAP6 O14910 Q9NUF9 Q15334 P26927 Q02779 P51153 P20336 P20337 P61006	Angiomotin Heat shock 70 kDa protein 4 ADP-ribosylation factor 1 Rho guanine nucleotide exchange factor 11 Partitioning defective 3 homolog Caveolin-1 Cell division control protein 42 homolog Gap junction beta-2 protein G1/S-specific cyclin-D1 Guanine nucleotide-binding protein subunit alpha-12 Rho guanine nucleotide exchange factor 2 Glycogen synthase kinase-3 alpha E3 ubiquitin-protein ligase Itchy homolog Angiomotin-like protein 1 Serine/threonine-protein kinase LATS1 Serine/threonine-protein kinase LATS2 Protein lin-7 homolog B Protein lin-7 homolog A Protein lin-7 homolog C Lethal(2) giant larvae protein homolog 1 Hepatocyte growth factor-like protein Mitogen-activated protein kinase kinase kinase 10 Ras-related protein Rab-13 Ras-related protein Rab-3A Ras-related protein Rab-3B Ras-related protein Rab-8A	AMOT HSPA4 APG2 ARF1 ARHGEF11 PARD3 PAR3 PAR3A CAV1 CAV CDC42 GJB2 CCND1 BCL1 PRAD1 GNA12 ARHGEF2 KIAA0651 LFP40 GSK3A ITCH Amot1 LAT51 WARTS LAT52 KPM LIN7B MALS2 VEL12 LIN7A MALS1 VEL11 LIN7C MALS3 VEL13 LLGL1 DLG4 HUGL HUGL1 MST1 D3F15S2 DNF15S2 HGFL MAP3K10 MLK2 MST RAB13 GIG4 RAB3A RAB3B RAB8A MEL RAB8	1084 840 181 1522 1356 178 191 226 295 381 986 483 903 968 1130 1088 207 233 197 1064 711 954 203 220 219 207

Protein annotation	Protein IDs	Protein names	Gene names	Protein Length (aa)
	P63000	Ras-related C3 botulinum toxin substrate 1	RAC1 TC25 MIG5	192
	P04049	RAF proto-oncogene serine/threonine-protein kinase	RAF1 RAF	648
	P11233	Ras-related protein Ral-A	RAL1 RAL	206
	Q9Y3L5	Ras-related protein Rap-2c	RAP2C	183
	P01111	GTPase Nras	NRAS HRAS1	189
	P01112	GTPase HRas	HRAS HRAS1	189
	P10301	Ras-related protein R-Ras	RRAS	218
	P62070	Ras-related protein R-Ras2	RRAS2 TC21	204
	014807	Ras-related protein M-Ras	MRAS RRAS3	208
	P01116	GTPase Kras	KRAS KRAS2 RASK2	189
	P61586	Transforming protein RhoA	RHOA ARH12 ARHA RHO12	193
	Q68EM7	Rho GTPase-activating protein 17	ARHgap17 RICH1 MSTP066	881
	060645	Exocyst complex component 3	MSTP110	
	Q96A65	Exocyst complex component 4	EXOC3 SEC6 SEC6L1	756
	Q9Y3L3	SH3 domain-binding protein 1	EXOC4 KIAA1699 SEC8 SEC8L1	974
	Q9HC7	E3 ubiquitin-protein ligase SMURF1	SH3BP1	701
	000161	Synaptosomal-associated protein 23	SMURF1 KIAA1625	757
	P60880	Synaptosomal-associated protein 25	SNAP23 SNAP	211
	P01137	Transforming growth factor beta-1	TGFB1 TGFB	206
	P61812	Transforming growth factor beta-2	TGFB2	390
	000292	Left-right determination factor 2	LEFTY2 EBFA1 LEFTY1	414
	Q13009	T-lymphoma invasion and metastasis-inducing protein 1	LEFTY2 EBFA1 LEFTY1	366
	P01375	Tumor necrosis factor	TGFB4	1591
	Q6XZF7	Dynamin-binding protein	TIAM1	233
	095249	Golgi SNAP receptor complex member 1	TNF TNFA TNFSF2	233
	014653	Golgi SNAP receptor complex member 2	DNMBP	1577
	P23763	Vesicle-associated membrane protein 1	GOSR1 GS28	250
			GOSR2 GS27	212
			VAMP1 SYB1	118

Protein annotation	Protein IDs	Protein names	Gene names	Protein Length (aa)
Kinases and Phosphatases	P63027	Vesicle-associated membrane protein 2	VAMP2 SYB2	116
	Q15836	Vesicle-associated membrane protein 3	VAMP3 SYB3	100
	075396	Vesicle-trafficking protein SEC22b	SEC22B SEC22L1	215
	Q9P0L0	Vesicle-associated membrane protein-associated protein A	VAPA VAP33	249
RAC-alpha serine/threonine-protein kinase	P31749	RAC-alpha serine/threonine-protein kinase	AKT1 PRK RAC	480
	P41743	Protein kinase C iota type	PRKCI DXS1179E	596
	Q05513	Protein kinase C zeta type	PRKCZ PKC2	592
	P51451	Tyrosine-protein kinase Blk	BLK	505
	P12931	Proto-oncogene tyrosine-protein kinase Src	SRC SRC1	536
	P07947	Tyrosine-protein kinase Yes	YES1 YES	543
	O14936	Peripheral plasma membrane protein CASK	CASK LIN2	926
	P11802	Cyclin-dependent kinase 4	CDK4	303
	P48729	Casein kinase I isoform alpha	CSNK1A1	337
	P49674	Casein kinase I isoform epsilon	CSNK1E	416
	P68400	Casein kinase II subunit alpha	CSNK2A1 CK2A1	391
	P67870	Casein kinase II subunit beta	CSNK2B CK2N G5A	215
	P27361	Mitogen-activated protein kinase 3	MAPK3 ERK1 PRK M3	379
	P09769	Tyrosine-protein kinase Fgr	FGR SRC2	529
	P06241	Tyrosine-protein kinase Fyn	FYN	537
	P08631	Tyrosine-protein kinase HCK	HCK	526
	Q13418	Integrin-linked protein kinase	ILK ILK1 ILK2	452
	P45983	Mitogen-activated protein kinase 8	MAPK8 JNK1 PRK M8 SAPK1 SAPK1C	427
Tyrosine-protein kinase	P06239	Tyrosine-protein kinase Lck	LCK	509
	P07948	Tyrosine-protein kinase Lyn	LYN JTK8	512
	Q02750	Dual specificity mitogen-activated protein kinase kinase kinase 1	MAP2K1 MEK1 PRK MK1	393
	Q13233	Mitogen-activated protein kinase kinase kinase 1	MAP3K1 MAPKKK1 MEKK MEK K1	1512
	Q7KZI7	Serine/threonine-protein kinase MARK2	MARK2 EMK1	788

Protein annotation	Protein IDs	Protein names	Gene names	Protein Length (aa)
	Q15746 P24723 Q13153 P42336	Myosin light chain kinase, smooth muscle Protein kinase C eta type Serine/threonine-protein kinase PAK 1 Phosphatidylinositol 4,5-bisphosphate 3-kinase catalytic subunit alpha isoform	MYLK MLCK MLCK1 MYLK1 PRKCH PRKCL PRKCL PAK1 PIK3CA	1914 683 545 1068
	P42338 P17252 P05771 P05129 Q05655 P41743 Q04759 P62136 P36873 P62140 P67775 P62714 P67775 P62714 P60484 Q15835 Q13464 O75116 P15692 P49765 P49767 Q96J92 Q9NYL2	Phosphatidylinositol 4,5-bisphosphate 3-kinase catalytic subunit beta isoform Protein kinase C alpha type Protein kinase C beta type Protein kinase C gamma type Protein kinase C delta type Protein kinase C iota type Protein kinase C theta type Serine/threonine-protein phosphatase PP1-alpha catalytic subunit Serine/threonine-protein phosphatase PP1-gamma catalytic subunit Serine/threonine-protein phosphatase PP1-beta catalytic subunit Serine/threonine-protein phosphatase 2A catalytic subunit alpha isoform Serine/threonine-protein phosphatase 2A catalytic subunit beta isoform Serine/threonine-protein phosphatase 2A catalytic subunit alpha isoform Serine/threonine-protein phosphatase 2A catalytic subunit beta isoform Phosphatidylinositol 3,4,5-trisphosphate 3-phosphatase and dual-specificity protein phosphatase PTEN Rhodopsin kinase	PIK3CB PIK3C1 PRKCA PRKCA PRKACA PRKCB PRKCB PRKCB1 PRKCG PRKCG PRKCD PRKCI PRKQC PRKCT PPP1CA PPP1A PPP1CC PPP1CB PPP2CA PPP2CB PPP2CA PPP2CB PTEN MMAC1 TEP1 GRK1 RHOK ROCK1 ROCK2 VEGFA VEGF VEGFB VRF VEGFC WNK4 PRKWNK4 ZAK MLTK HCCS4	1070 672 671 697 676 596 706 330 323 327 309 309 309 403 563 1354 1388 232 207 419 1243 800

Protein annotation	Protein IDs	Protein names	Gene names	Protein Length (aa)
Transcriptional and Postranscriptional Regulators	P05412 P49715 P33240 Q12996 Q05048 P19419 P01100 Q00613 Q9NR48 P01106 Q92797 Q9GZV5 P28347 P46937 P16989	Transcription factor AP-1 CCAAT/enhancer-binding protein alpha Cleavage stimulation factor subunit 2 Cleavage stimulation factor subunit 3 Cleavage stimulation factor subunit 1 ETS domain-containing protein Elk-1 Proto-oncogene c-Fos Heat shock factor protein 1 Histone-lysine N-methyltransferase ASH1L Myc proto-oncogene protein Symplekin WW domain-containing transcription regulator protein 1 Transcriptional enhancer factor TEF-1 Transcriptional coactivator YAP1 Y-box-binding protein 3	JUN CEBPA CEBP CSTF2 CSTF3 CSTF1 ELK1 FOS G0S7 HSF1 HSTF1 ASH1L KIAA1420 KMT2H MYC SYMPK SPK WWTR1 TAZ TEAD1 TCF13 TEF1 YAP1 YAP65 YBX3 CSDA DBPA	331 358 577 717 431 428 380 529 2969 439 1274 400 426 504 372

Appendix E

BLAST search results and GO annotation

Potential *T. gondii* interactions with occludin ECLs were identified by BLAST searching for homology between the rat occludin domain sequences and the *T. gondii* genome using NCBI-BLAST provided at www.toxodb.org (release number 24 14th April 2015) [Gajria et al, 2008]. The database was used to search for occludin homology first with *T. gondii* ME49 stain, followed by GT1 and lastly the VEG strain genomes. Protein function classification by GO annotation was provided by www.toxodb.org (release number 24 14th April 2015) [Gajria et al, 2008].

T. gondii proteins with homology to occludin domains are annotated in the table below. Gene IDs are only given for a single strain, searched in the order above, if homology was found for more than one strain. The annotated proteins discussed in chapters five and six are highlighted in red. TMD: number of transmembrane domains.

Occludin homology domain	Gene ID	Protein annotation	MW (Da)	Length (aa)	TMD
ECL1+ECL2	TGME49_119850	hypothetical protein, conserved	56662	538	0
ECL1+ECL2	TGME49_081590	hypothetical protein	13874	116	2
ECL1+ECL2	TGME49_116550	hypothetical protein	12988	113	2
ECL1+ECL2	TGME49_036540	RRM domain-containing protein	53440	513	0
ECL1+ECL2	TGME49_119890	hypothetical protein	25535	236	0
ECL1+ECL2	TGME49_025830	hypothetical protein	104168	989	0
ECL1+ECL2	TGME49_064610	heterogeneous nuclear ribonucleoprotein A3, putative	44975	430	0
ECL1+ECL2	TGME49_062620	Gbp1p protein, putative	31761	293	0
ECL1+ECL2	TGME49_036650	DEAD/DEAH box helicase, putative	59969	550	0
ECL1+ECL2	TGME49_012850	hypothetical protein	43503	414	0
ECL1+ECL2	TGME49_035930	KH domain-containing protein	64265	570	0
ECL1+ECL2	TGME49_064150	hypothetical protein	31441	307	0
ECL1+ECL2	TGME49_072010	nucleolar protein family A, putative	20932	210	0
ECL1+ECL2	TGME49_069690	hypothetical protein	94305	865	1
ECL1+ECL2	TGME49_013850	hypothetical protein	15644	147	1
ECL1+ECL2	TGME49_070170	hypothetical protein	21290	223	0
ECL1+ECL2	TGME49_091930	nucleolar phosphoprotein nucleolin, putative	73118	705	0
ECL1+ECL2	TGME49_025320	hypothetical protein, conserved	54459	504	0
ECL1+ECL2	TGME49_040560	microsomal glutathione S-transferase 3, putative	22204	205	3
ECL1+ECL2	TGME49_111430	fibrillarin, putative	31989	304	0
ECL1+ECL2	TGME49_066800	integral membrane protein, putative	32533	302	4
ECL1+ECL2	TGME49_004480	DnaJ domain-containing protein	66709	606	0
ECL1+ECL2	TGME49_032660	58 kDa phosphoprotein, putative	45143	425	0
ECL1+ECL2	TGME49_026250	ATP-dependent RNA helicase, putative	78594	734	0
ECL1+ECL2	TGME49_027340	hypothetical protein	15173	136	2
ECL1+ECL2	TGME49_090870	patched family domain-containing protein, conserved	130574	1178	12
ECL1+ECL2	TGME49_020390	hypothetical protein	27530	258	4
ECL1+ECL2	TGME49_109200	zinc finger (CCCH type) protein, putative	101662	1051	0
ECL1	TGME49_119850	hypothetical protein, conserved	56662	538	0
ECL1	TGME49_036540	RRM domain-containing protein	53440	513	0
ECL1	TGME49_119890	hypothetical protein	25535	236	0
ECL1	TGME49_081590	hypothetical protein	13874	116	2
ECL1	TGME49_116550	hypothetical protein	12988	113	2
ECL1	TGME49_025830	hypothetical protein	104168	989	0
ECL1	TGME49_064610	heterogeneous nuclear ribonucleoprotein A3, putative	44975	430	0
ECL1	TGME49_036650	DEAD/DEAH box helicase, putative	59969	550	0
ECL1	TGME49_062620	Gbp1p protein, putative	31761	293	0
ECL1	TGME49_012850	hypothetical protein	43503	414	0
ECL1	TGME49_035930	KH domain-containing protein	64265	570	0
ECL1	TGME49_072010	nucleolar protein family A, putative	20932	210	0
ECL1	TGME49_069690	hypothetical protein	94305	865	1
ECL1	TGME49_013850	hypothetical protein	15644	147	1
ECL1	TGME49_091930	nucleolar phosphoprotein nucleolin, putative	73118	705	0
ECL1	TGME49_111430	fibrillarin, putative	31989	304	0
ECL1	TGME49_004480	DnaJ domain-containing protein	66709	606	0
ECL1	TGME49_032660	58 kDa phosphoprotein, putative	45143	425	0
ECL1	TGME49_070170	hypothetical protein	21290	223	0
ECL1	TGME49_026250	ATP-dependent RNA helicase, putative	78594	734	0
ECL1	TGME49_064150	hypothetical protein	31441	307	0
ECL1	TGME49_030940	hypothetical protein	28883	284	0
ECL1	TGGT1_065230	conserved hypothetical protein	27259	247	0
ECL1	TGME49_105520	40S ribosomal protein S2, putative	29336	269	0
ECL1	TGME49_069650	hypothetical protein	51441	492	0
ECL1	TGME49_065430	hypothetical protein	10883	101	0
ECL1	TGME49_014150	mitochondrial import inner membrane translocase subunit, putative	19551	188	1
ECL1	TGME49_120600	glycine-rich protein 2, putative	23061	209	0

Occludin homology domain	Gene ID	Protein annotation	MW (Da)	Length (aa)	TMD
ECL1	TGME49_061680	hypothetical protein	155128	1464	0
ECL1	TGME49_089540	hypothetical protein, conserved	100518	937	0
ECL1	TGME49_112220	mitochondrial import inner membrane translocase subunit TIM17, putative	22613	213	0
ECL1	TGME49_078680	hypothetical protein	22776	215	0
ECL1	TGME49_064640	bromodomain domain-containing protein	140477	1354	0
ECL1	TGME49_038510	hypothetical protein, conserved	116256	1082	0
ECL1	TGVEG_047760	conserved hypothetical protein	63095	588	0
ECL1	TGME49_059640	nucleoporin, putative	302390	2894	0
ECL1	TGME49_062610	hypothetical protein	68234	637	7
ECL1	TGME49_094290	der1-like family domain-containing protein, conserved	32059	293	5
ECL1	TGME49_057360	hypothetical protein	155183	1457	0
ECL1	TGME49_121520	P23 co-chaperone, putative	24784	226	1
ECL1	TGME49_017540	splicing factor, putative	38105	351	0
ECL1	TGME49_075440	granule antigen protein GRA6	23309	224	2
ECL1	TGME49_003210	hypothetical protein	34602	334	0
ECL1	TGME49_113270	hypothetical protein	151891	1546	0
ECL1	TGME49_121500	CELF family protein, putative	50939	475	0
ECL1	TGME49_086730	signal recognition particle 19 kDa protein, putative	24016	222	0
ECL1	TGME49_082020	hypothetical protein	41558	394	1
ECL1	TGME49_058390	DnaJ protein, putative	44654	397	0
ECL1	TGME49_045710	MORN repeat protein, putative	31259	273	0
ECL1	TGME49_013030	hypothetical protein	35156	323	0
ECL1	TGME49_106380	U1 small nuclear ribonucleoprotein, putative	22084	215	0
ECL1	TGME49_003780	hypothetical protein	145088	1475	0
ECL1	TGME49_017880	KH domain-containing protein	41468	412	0
ECL1	TGME49_045500	dipeptidyl peptidase IV domain-containing protein	173470	1584	0
ECL1	TGME49_037520	hypothetical protein	114772	1147	0
ECL1	TGME49_032170	hypothetical protein	80969	745	1
ECL1	TGGT1_046955	hypothetical protein	41377	404	0
ECL1	TGME49_053080	replication protein A2, putative	28748	278	0
ECL1	TGME49_118160	major sperm protein domain-containing protein	25976	239	1
ECL1	TGME49_109200	zinc finger (CCCH type) protein, putative	101662	1051	0
ECL1	TGME49_097430	hypothetical protein, conserved	25337	248	0
ECL1	TGME49_016080	hypothetical protein, conserved	79433	709	0
ECL1	TGME49_014750	hypothetical protein	119986	1108	0
ECL1	TGME49_056030	hypothetical protein	29223	256	0
ECL1	TGME49_027870	hypothetical protein	11224	103	0
ECL1	TGME49_100200	histone H2A	15920	155	0
ECL1	TGME49_111400	hypothetical protein, conserved	158711	1520	0
ECL1	TGME49_073630	DnaJ domain-containing protein	16113	141	0
ECL1	TGGT1_087090	hypothetical protein	34811	332	0
ECL1	TGME49_045660	hypothetical protein, conserved	69146	667	0
ECL1	TGME49_073760	heat shock protein 70, putative	72881	674	0
ECL1	TGME49_110560	hypothetical protein	208093	1898	14
ECL1	TGME49_057350	eukaryotic translation initiation factor, putative	89777	820	0
ECL1	TGME49_000280	WD-repeat protein, putative	90213	834	0
ECL1	TGME49_047550	heat shock protein 60	60915	575	0
ECL1	TGME49_040560	microsomal glutathione S-transferase 3, putative	22204	205	3
ECL1	TGME49_106560	hypothetical protein	67326	698	0
ECL1	TGME49_034920	hypothetical protein	119455	1112	0
ECL1	TGME49_077980	dynein light chain, putative	11494	103	0
ECL1	TGME49_105790	hypothetical protein	206111	1918	0
ECL1	TGME49_105780	exoribonuclease, putative	138631	1239	0
ECL1	TGME49_036120	hypothetical protein, conserved	32073	298	1
ECL1	TGGT1_065550	conserved hypothetical protein	114940	1057	0
ECL1	TGME49_095620	zinc finger (CCCH type) protein, putative	128507	1237	0

Occludin homology domain	Gene ID	Protein annotation	MW (Da)	Length (aa)	TMD
ECL1	TGME49_093640	hypothetical protein	22001	190	0
ECL1	TGME49_091330	hypothetical protein	25513	228	0
ECL1	TGME49_068570	zinc finger (CCCH type) protein, putative	44240	422	0
ECL1	TGME49_000370	protein farnesyltransferase beta subunit, putative	69876	638	0
ECL1	TGME49_033480	SRS29C (= SRS2, P35)	39120	372	0
ECL1	TGVEG_081500	conserved hypothetical protein	39605	377	0
ECL1	TGME49_120050	ribosomal protein L5, putative	35342	310	0
ECL1	TGGT1_060630	conserved hypothetical protein	93141	927	0
ECL1	TGME49_057720	phospholipid-transporting P-type ATPase, putative	247041	2225	9
ECL1	TGME49_120010	hypothetical protein	98244	964	0
ECL1	TGVEG_001300	hypothetical protein	11868	101	2
ECL1	TGGT1_089980	UVb-resistance protein uvr8, putative	62124	578	0
ECL1	TGME49_091140	CCR4-Not complex component, Not1 domain-containing protein, conserved	265871	2562	0
ECL1	TGME49_003030	hypothetical protein	37346	342	7
ECL1	TGME49_047420	hypothetical protein	37365	347	3
ECL1	TGME49_009450	TLD domain-containing protein	85277	817	0
ECL1	TGVEG_035400	plant ubiquilin, putative	118954	1158	0
ECL1	TGME49_039130	Tyrosine kinase-like (TKL) protein	180152	1658	0
ECL1	TGME49_119590	hypothetical protein	236539	2180	0
ECL1	TGGT1_053690	DEAD/DEAH box helicase, putative	61270	564	0
ECL1	TGME49_014530	DnaJ domain-containing protein	77968	714	0
ECL1	TGME49_094990	hypothetical protein	20012	209	0
ECL1	TGME49_098600	leucine zipper-like transcriptional regulator	91036	855	0
ECL1	TGME49_020860	DEAD/DEAH box helicase, putative	65159	602	0
ECL1	TGME49_002780	Rhopty kinase family protein ROP25	120370	1122	2
ECL1	TGME49_020080	hypothetical protein	28124	271	1
ECL1	TGME49_106660	RNA pseudouridine synthase domain containing protein	676333	6535	0
ECL1	TGVEG_066630	hypothetical protein	13419	117	0
ECL1	TGME49_055910	hypothetical protein, conserved	24955	231	0
ECL1	TGGT1_013970	conserved hypothetical protein	46590	447	0
ECL1	TGGT1_112930	conserved hypothetical protein	68675	723	0
ECL1	TGME49_060520	hypothetical protein	48430	472	0
ECL1	TGME49_021550	CMGC kinase, MAPK family, MEK kinase-related (incomplete catalytic triad)	65458	599	0
ECL1	TGME49_007430	ATP-dependent RNA helicase DDX family protein, putative	82793	768	0
ECL1	TGME49_040340	hypothetical protein	134545	1276	0
ECL1	TGME49_065250	alpha-1 type II collagen, putative	160181	1564	0
ECL1	TGME49_026620	hypothetical protein	171138	1636	0
ECL1	TGME49_043310	hypothetical protein	132520	1266	0
ECL1	TGME49_083880	RNA binding motif-containing protein	87772	802	0
ECL1	TGME49_005680	transmembrane domain-containing protein	79066	805	6
ECL1	TGME49_115520	microneme protein, putative	36590	348	1
ECL1	TGME49_027660	DNA methyltransferase 2, putative	90211	834	0
ECL1	TGME49_009220	hypothetical protein	75638	671	0
ECL1	TGME49_116680	RNA pseudouridylate synthase domain-containing protein	289808	2780	0
ECL1	TGME49_026320	hypothetical protein	72508	698	0
ECL2	TGME49_015720	hypothetical protein	22634	201	2
ECL2	TGGT1_027950	conserved hypothetical protein	64228	610	0
ECL2	TGGT1_028070	conserved hypothetical protein	85264	799	0
ECL2	TGME49_017960	hypothetical protein	88351	830	0
ECL2	TGME49_087630	hypothetical protein	103529	975	0
ECL2	TGME49_020280	SCP-like domain-containing protein	47796	434	0
ECL2	TGME49_055900	hypothetical protein, conserved	27781	248	6
ECL2	TGME49_065430	hypothetical protein	10883	101	0
ECL2	TGVEG_088510	hypothetical protein	14236	122	1
ECL2	TGME49_053110	kinesin motor domain-containing protein	70584	645	0
ECL2	TGME49_030430	hypothetical protein	26382	236	0

Occludin homology domain	Gene ID	Protein annotation	MW (Da)	Length (aa)	TMD
ECL2	TGME49_062660	hypothetical protein	75308	701	7
ECL2	TGME49_060630	Dnaj domain-containing protein	76803	675	3
ECL2	TGME49_024780	SRS domain-containing protein	23720	218	0
ECL2	TGME49_011040	Sec61beta family protein	10104	99	1
ECL2	TGME49_066600	serine proteinase inhibitor, putative	12769	121	0
C-terminus	TGME49_013290	hypothetical protein	35483	320	0
C-terminus	TGME49_059900	hypothetical protein, conserved	81632	720	1
C-terminus	TGME49_112980	hypothetical protein, conserved	19688	162	0
C-terminus	TGME49_121390	hypothetical protein, conserved	42787	388	0
C-terminus	TGME49_009840	hypothetical protein	37722	307	0
C-terminus	TGGT1_036010	DHHC domain-containing protein, putative	96056	873	5
C-terminus	TGME49_003770	hypothetical protein	31965	291	0
C-terminus	TGME49_111750	hypothetical protein	28084	250	0
C-terminus	TGME49_058850	hypothetical protein	32750	276	0
C-terminus	TGME49_004100	Wee kinase	261583	2445	0
C-terminus	TGME49_074160	hypothetical protein	58727	525	0
C-terminus	TGME49_105860	CAM kinase, CDPK family TgCDPK1_2 (TGTPK4)	60431	537	0
C-terminus	TGME49_109400	chromosome segregation protein, putative	216856	1967	0
C-terminus	TGGT1_057060	NBP2B protein, putative	27327	251	0
C-terminus	TGME49_067310	myosin heavy chain, putative	51766	443	0
C-terminus	TGME49_016480	NMD3 protein	79320	721	0
C-terminus	TGME49_036090	hypothetical protein	18602	159	0
C-terminus	TGME49_114230	general transcription factor IIIC, putative	78275	695	0
C-terminus	TGME49_033430	hypothetical protein	101604	935	0
C-terminus	TGME49_052440	GPI-anchor transamidase, putative	66484	604	0
C-terminus	TGME49_021500	dual specificity protein phosphatase, catalytic domain-containing protein	109090	982	0
C-terminus	TGME49_053160	hypothetical protein	47298	433	0
C-terminus	TGME49_046140	hypothetical protein	111732	1033	0
C-terminus	TGME49_073970	corA-like Mg2+ transporter domain-containing protein	59769	537	2
C-terminus	TGME49_005050	hypothetical protein	133820	1207	0
C-terminus	TGME49_047000	TPR domain-containing protein	96859	888	1
C-terminus	TGME49_042860	plectin, putative	61535	544	0
C-terminus	TGME49_042750	hypothetical protein	445183	3900	0
C-terminus	TGME49_050720	intraflagellar transport protein component IFT74/72, putative	69502	606	0
C-terminus	TGME49_088270	hypothetical protein	45389	421	0
C-terminus	TGME49_044470	viral A-type inclusion protein repeat family	290408	2595	0
C-terminus	TGME49_037870	hypothetical protein, conserved	59175	538	0
C-terminus	TGME49_116630	hypothetical protein	98122	861	0
C-terminus	TGME49_075330	hypothetical protein	49391	456	0
C-terminus	TGME49_049520	hypothetical protein	21440	189	0
C-terminus	TGME49_042790	trichohyalin, putative	254916	2238	1
C-terminus	TGME49_084170	zinc finger DHHC domain-containing protein	96632	880	3
C-terminus	TGME49_050330	hypothetical protein	30475	263	0
C-terminus	TGME49_012880	hypothetical protein	560139	4817	0
C-terminus	TGME49_043930	hypothetical protein	101349	943	0
C-terminus	TGME49_091000	PHD-finger domain-containing protein	57115	527	0
C-terminus	TGME49_056060	nucleosome assembly protein, putative	89466	812	0
C-terminus	TGME49_053380	hypothetical protein	165275	1670	0
C-terminus	TGME49_097300	hypothetical protein	11997	107	0
C-terminus	TGME49_112070	hypothetical protein	43777	379	0
C-terminus	TGME49_087520	hypothetical protein	19609	167	0
C-terminus	TGME49_002250	hypothetical protein	98751	930	2
C-terminus	TGME49_003900	hypothetical protein, conserved	112395	951	0
C-terminus	TGME49_094790	hypothetical protein	37700	351	0
C-terminus	TGGT1_107350	conserved hypothetical protein	62632	547	0
C-terminus	TGGT1_056130	conserved hypothetical protein	42369	370	0

Occludin homology domain	Gene ID	Protein annotation	MW (Da)	Length (aa)	TMD
C-terminus	TGME49_055700	hypothetical protein	389376	3552	0
C-terminus	TGME49_090620	hypothetical protein	291935	2617	0
Whole	TGME49_081590	hypothetical protein	13874	116	2
Whole	TGME49_116550	hypothetical protein	12988	113	2
Whole	TGME49_119850	hypothetical protein, conserved	56662	538	0
Whole	TGME49_036540	RRM domain-containing protein	53440	513	0
Whole	TGME49_119890	hypothetical protein	25535	236	0
Whole	TGME49_013290	hypothetical protein	35483	320	0
Whole	TGME49_025830	hypothetical protein	104168	989	0
Whole	TGME49_064610	heterogeneous nuclear ribonucleoprotein A3, putative	44975	430	0
Whole	TGME49_062620	Gbp1p protein, putative	31761	293	0
Whole	TGME49_036650	DEAD/DEAH box helicase, putative	59969	550	0
Whole	TGME49_012850	hypothetical protein	43503	414	0
Whole	TGME49_112980	hypothetical protein, conserved	19688	162	0
Whole	TGME49_035930	KH domain-containing protein	64265	570	0
Whole	TGME49_059900	hypothetical protein, conserved	81632	720	1
Whole	TGME49_121390	hypothetical protein, conserved	42787	388	0
Whole	TGME49_009840	hypothetical protein	37722	307	0
Whole	TGME49_064150	hypothetical protein	31441	307	0
Whole	TGGT1_068110	conserved hypothetical protein	15149	120	0
Whole	TGME49_069690	hypothetical protein	94305	865	1
Whole	TGME49_072010	nucleolar protein family A, putative	20932	210	0
Whole	TGGT1_002130	conserved hypothetical protein	47404	433	0
Whole	TGME49_003770	hypothetical protein	31965	291	0
Whole	TGME49_111750	hypothetical protein	28084	250	0
Whole	TGME49_013850	hypothetical protein	15644	147	1
Whole	TGGT1_020450	conserved hypothetical protein	32034	255	0
Whole	TGGT1_094450	conserved hypothetical protein	106483	932	0
Whole	TGME49_004100	Wee kinase	261583	2445	0
Whole	TGME49_074160	hypothetical protein	58727	525	0
Whole	TGME49_105860	CAM kinase, CDPK family TgCDPK1_2 (TGTPK4)	60431	537	0
Whole	TGGT1_077210	conserved hypothetical protein	390621	3561	0
Whole	TGGT1_036010	DHHC domain-containing protein, putative	96056	873	5
Whole	TGME49_109400	chromosome segregation protein, putative	216856	1967	0
Whole	TGGT1_057060	NBP2B protein, putative	27327	251	0
Whole	TGME49_005050	hypothetical protein	133820	1207	0
Whole	TGGT1_026910	conserved hypothetical protein	111220	1030	0
Whole	TGME49_067310	myosin heavy chain, putative	51766	443	0
Whole	TGME49_070170	hypothetical protein	21290	223	0
Whole	TGME49_036090	hypothetical protein	18602	159	0
Whole	TGME49_058850	hypothetical protein	32750	276	0
Whole	TGGT1_020470	conserved hypothetical protein	543156	5074	1
Whole	TGME49_091930	nucleolar phosphoprotein nucleolin, putative	73118	705	0
Whole	TGME49_062950	enterophilin-2L, putative	79898	717	0
Whole	TGME49_052440	GPI-anchor transamidase, putative	66484	604	0
Whole	TGME49_033430	hypothetical protein	101604	935	0
Whole	TGGT1_024770	conserved hypothetical protein	120268	1124	0
Whole	TGME49_025320	hypothetical protein, conserved	54459	504	0
Whole	TGGT1_047160	conserved hypothetical protein	445037	3900	0
Whole	TGME49_021500	dual specificity protein phosphatase, catalytic domain-containing protein	109090	982	0

Appendix F

Publication

Weight CM, et al., Elucidating pathways of *Toxoplasma gondii* invasion in the gastrointestinal tract: Involvement of the tight junction protein occludin, *Microbes and Infection* (2015)



ELSEVIER



Institut Pasteur

Microbes and Infection xx (2015) 1e 12



www.elsevier.com/locate/micinf

Original article

Elucidating pathways of *Toxoplasma gondii* invasion in the gastrointestinal tract: Involvement of the tight junction protein occludin

Caroline M. Weight^{a,c,1,2}, Emily J. Jones^{a,c,2}, Nikki Horn^a, Nikolaus Wellner^b, Simon R. Carding^{a,c,*}

^a Gut Health and Food Safety Institute Strategic Programme, Norwich Research Park, Norwich, NR4 7UA, UK

^b Analytical Sciences Unit, Institute of Food Research, Norwich Research Park, Norwich, NR4 7UA, UK

^c Norwich Medical School, University of East Anglia, Norwich Research Park, Norwich, NR4 7UA, UK

Received 17 April 2015; accepted 2 July 2015

Available online ***

Abstract

Toxoplasma gondii is an obligate intracellular parasite infecting one third of the world's population. The small intestine is the parasite's primary route of infection, although the pathway of epithelium transmigration remains unclear. Using an *in vitro* invasion assay and live imaging we showed that *T. gondii* (RH) tachyzoites infect and transmigrate between adjacent intestinal epithelial cells in polarized monolayers without altering barrier integrity, despite eliciting the production of specific inflammatory mediators and chemokines. During invasion, *T. gondii* co-localized with occludin. Reducing the levels of endogenous cellular occludin with specific small interfering RNAs significantly reduced the ability of *T. gondii* to penetrate between and infect epithelial cells. Furthermore, an *in vitro* invasion and binding assays using recombinant occludin fragments established the capacity of the parasite to bind occludin and in particular to the extracellular loops of the protein. These findings provide evidence for occludin playing a role in the invasion of *T. gondii* in small intestinal epithelial cells.

© 2015 Institut Pasteur. Published by Elsevier Masson SAS. All rights reserved.

Keywords: *Toxoplasma gondii*; Occludin; Invasion; Intestinal epithelial cells

1. Introduction

The ability of *Toxoplasma gondii* to infect almost any warm blooded animal and virtually any nucleated cell makes it the most prevalent parasitic infection worldwide. It is estimated that up to one third the world's human population is infected, although prevalence varies between countries [1,2]. In the United States, it is estimated that approximately 22% of the population 12 years and older have been infected with *T.*

gondii whereas in certain South American countries, the frequency of seropositive individuals is as high as 75% [3]. With the exception of the immunocompromised and pregnant women, *T. gondii* causes a relatively asymptomatic infection of typical fever-like symptoms. The majority of infections occur following the consumption of contaminated, undercooked meat, unwashed vegetables and contaminated water supplies [4,5]. The gastrointestinal tract is therefore a major route of *T. gondii* infection in most cases [6,7]. Tachyzoites are the life form of *T. gondii* that disseminate out of the gut and migrate through the body and infect the brain and muscles, where they convert to bradyzoites that form dormant, long lived and non-immunogenic cysts [8]. How the parasite transmigrates intestinal epithelial cells is unclear, although there is evidence that the paracellular pathway is important for parasite dissemination [9].

* Corresponding author: Institute of Food Research, Norwich Research Park, Norwich, NR4 7UA, UK. Tel.: +44 (0) 1603 251410.

E-mail address: Simon.Carding@Ifr.ac.uk (SR. Carding).

¹ Present address: Immunology Section, Leukocyte Migration Group, Department of Experimental Medicine, BMC D14, Lund University, Lund, Sweden.

² Authors contributed equally.

<http://dx.doi.org/10.1016/j.micinf.2015.07.001>

1206-4579 © 2015 Institut Pasteur. Published by Elsevier Masson SAS. All rights reserved.

Please cite this article in press as: Weight CM, et al., Elucidating pathways of *Toxoplasma gondii* invasion in the gastrointestinal tract: Involvement of the tight junction protein occludin, *Microbes and Infection* (2015), <http://dx.doi.org/10.1016/j.micinf.2015.07.001>

The small intestinal epithelial barrier consists of a single layer of intestinal epithelial cells (IECs) that separate the luminal contents from the underlying mucosa. These cells express apico-lateral junctional proteins, the most apical of which is the tight junction (TJ). TJs provide a barrier for the regulated passage of ions, uncharged molecules and macromolecules. They consist of a complex of over 100 proteins, the interactions of which determine barrier function. Prominent TJ proteins include the claudin family members that control permeability, junctional adhesion molecules that govern cell polarity and migration, and the MARVEL proteins such as occludin, which regulates permeability to macromolecules, while a variety of other integral membrane proteins, peripheral membrane proteins and signaling proteins such as Zonula occludens-1 (ZO-1) make up the remaining TJ complex [10–12]. TJs are dynamic in nature and often consist of mobile pools within the membrane and cytoplasm that are involved in recycling and turnover of the protein. In the case of occludin this mobility is associated with changes in phosphorylation status [13,14].

TJs are targeted by pathogens as a mechanism of host invasion. For example, the enteric pathogens *Vibrio cholera* and *Clostridium perfringens* secrete proteases and enterotoxins, respectively, that degrade occludin and claudins [15]. A paracellular route of entry between cells via intercellular adhesion molecule 1 (ICAM-1) by *T. gondii* has been reported [9] and we have previously shown that *T. gondii* bradyzoites and cysts affect the cellular distribution of occludin in barrier epithelial cells both *in vitro* and *in vivo* [16,17].

Using epithelial cells derived from within the crypts of Lieberkühn of the murine small intestinal epithelium, we investigated the pathways by which *T. gondii* invades (defined as infection into cells and transmigration between cells via the paracellular pathway) the intestinal epithelium.

2. Materials and methods

2.1. Cells

The rodent small IEC lines m-IC_{c12} and IEC-6 were maintained as previously described [18,19]. To reduce occludin expression, m-IC_{c12} cells were cultured either on 13 mm coverslips (for H&E staining), in 6 well plates (for immunoblotting), or on transwell cell culture inserts (for transmigration assays). In each case 0.38 µg of occludin-specific siRNA (a mixture of three 19–25 nucleotides, Santa Cruz) in transfection media (OptiMEM, Invitrogen) was added to the cell cultures for 6 h at 37 °C, washed and then incubated for a further 24 h in normal growth media. As a control, m-IC_{c12} cells were incubated with scrambled (non-silencing, scRNA) siRNAs (Santa Cruz). Occludin knockdown was assessed by immunoblotting and immunocytochemistry. Bead arrays (30 Plex Bead Mixture, BD Biosciences) were used to quantify cytokines and chemokines in cell supernatants, according to the manufacturers' instructions and analyzed using a Cytomics FC500 MPL (Beckman Coulter).

2.2. Parasites

The type 1 RH strain of *T. gondii* tachyzoites stably expressing YFP [20] were maintained by continuous passage in confluent monolayers of Hs27 Human Fetal Foreskin Fibroblasts (European Collection of Cell Cultures) in DMEM supplemented with 2 mmol/L L-Glutamine and 10% FBS at 37°C in 5% CO₂. Pelleted parasites were collected after 90% HFF lysis by centrifugation at 1000 g for 15 min.

2.3. Transmigration and infection assays

m-IC_{c12} cells were plated onto the apical compartment of polyethylene terephthalate (PET) cell culture transwell inserts (8 µm pore size, BD Biosciences) within a 24 well plate. TEER was measured using an Epithelial Tissue Volt Ohmmeter 2 (World Precision Instruments). By day 13, inserts contained confluent, polarized monolayers of cells. Barrier permeability was assessed by periodic TEER measurements and flux of FITC-conjugated dextran (3–5 kDa; Sigma-Aldrich) across the transwell membrane; 1 mg/ml FITC-dextran was added to the apical compartment and media from the basal compartment was analyzed for FITC content using a FLUOstar OPTIMA microplate reader (BMG Labtech). FITC-dextran quantification was determined from a standard curve generated using standards of known concentration. Transmigrating parasites were identified from the basal compartment by centrifugation and analyzing by flow cytometry using a Cytomics FC500 MPL. Data was analyzed post-collection using FlowJo version 7.6 (TreeStar).

2.4. Immunocytochemistry

m-IC_{c12} cells were fixed in either 2% formaldehyde (to visualize the parasites) or acetone (to visualize the TJ proteins), permeabilized with 0.2% Triton X-100 and incubated with blocking buffer (0.2% Triton X-100, 3% BSA, 3% goat serum, 3% fish skin gelatin in PBS) prior to incubation with primary antibodies including occludin, claudin-2 (Invitrogen), ZO-1 (Santa Cruz) and β-catenin (BD Biosciences). Controls consisted of either no primary antibody or isotype matched antibodies of irrelevant specificity. A 1:1 mixture of Rhodamine-peanut and -wheat germ agglutinin (Vector Labs) was used to visualize the apical membrane. For transwell cultures, the PET membrane was extracted from the insert and placed cell side up onto a glass microscope slide with DePeX (BDH) and covered with a glass coverslip. To visualize intracellular parasites, m-IC_{c12} cells grown on 13 mm diameter glass coverslips (BDH), fixed (2% formaldehyde), permeabilized and H&E counterstained before mounting and viewing using an upright or inverted LSM510 META on a Zeiss AxioVert 200M microscope. Images were analyzed on LSM software or AxioVision image viewer. Z stacks were composed of 1 µm interval sections with the 40× objective unless stated otherwise. To visualize occludin by Z stack, cells were marked for the apical and basal membrane using surface carbohydrates and β-catenin respectively. This provided a

Please cite this article in press as: Weight CM, et al., Elucidating pathways of *Toxoplasma gondii* invasion in the gastrointestinal tract: Involvement of the tight junction protein occludin, *Microbes and Infection* (2015), <http://dx.doi.org/10.1016/j.micinf.2015.07.001>

distinction between cell domains where tight junction proteins are expressed. Throughout experiments, polarized cells were of similar depth and therefore their plane of imaging was consistent as possible. In addition, these markers provided a boundary between the membrane and cytoplasm of each cell. Image quantification was carried out using the Integrated Density tool from Image J1.47V.

2.5. Electron microscopy

IECs were plated onto collagen gel-coated Thermanox coverslips in 35 mm dishes (Ibidi) and cultured for 8 days prior to incubation with RH-YFP *T. gondii* tachyzoites for 2 h. Media was removed and cells rinsed in PBS before fixing with 3% glutaraldehyde (Agar Scientific) in 0.1 M cacodylate buffer (pH 7.2) for 2 h. Further details of sample preparation can be found in the supplementary information. Samples were visualized using a Zeiss Supra 55 VP FEG SEM, operating at 3 kV (Zeiss).

2.6. Two-photon-microscope live imaging

IEC-6 were plated onto 35 mm µ-dishes (Ibidi) coated with Matrigel® (Corning) and cultured for four days. Cells were labeled by staining with CellTracker™ Red CMPTX (Invitrogen) prior to apical addition of RH-YFP *T. gondii* tachyzoites immediately before imaging. Images were acquired using a LaVision BioTec TriM Scope II 2-photon microscope (Bielefeld) based on a Nikon Eclipse Ti optical inverted microscope with a Nikon 40x water immersion (Apo LWD λS NA 1.15) objective (Nikon UK Ltd) and a temperature control system (Life Imaging Services). Multi photon excitation was provided by a Coherent Chameleon Sapphire laser (Coherent Inc.) at 1060 nm to simultaneously excite CellTracker™ Red and RH-YFP *T. gondii*. Typical image volumes were 100 × 100 × 27 µm and Z-stacks were separated by 1 µm. Time resolved data were acquired by continuous measuring of Z-stacks for up to 30 min. The frame rate was 51.2 s with these parameters. Images were analysed with the Fiji/ImageJ package.

2.7. Immunoblotting

mIC_{c12} cells were lysed in ice-cold lysis buffer (1% Triton X-100, 100 mM NaCl, 25 mM Tris-HCl, pH 7.4, 1 mM sodium orthovanadate, 5 mM EDTA, 2 mM EGTA, 50 µM phenylmethylsulfonyl fluoride (PMSF), 25 mM sodium fluoride, 10× protease inhibitor cocktail and 15× phosphatase inhibitor cocktail (Sigma-Aldrich)) by repeatedly passing through a 19 gage needle before centrifuging at 16,100 g for 10 min at 4 °C. Protein quantification was determined using the DC Protein Assay Kit (BioRad Labs). To provide additional verification of equal loading across lanes, densitometry analysis was performed on coomassie-stained gels by scanning and imaging gels using Quantity One software (version 4.6.1). For immunoblotting, samples were transferred onto Hybond C+ nitrocellulose

membranes (Amersham Biosciences), blocked in 5% BSA in TTBS (150 mM NaCl, 20 mM Tris Base, 0.1% Tween-20, pH 7.4) and incubated in 1% BSA in TTBS buffer with primary antibodies for 24 h at 4 °C and secondary HRP conjugates (Santa Cruz) for 1 h at 25 °C. Membranes were imaged using the enhanced SuperSignal West Pico Chemiluminescent substrate (Pierce Chemical Company) and visualized with a Fluor-S-Multi Imager (Bio-Rad) and Quantity One software (version 4.5.2).

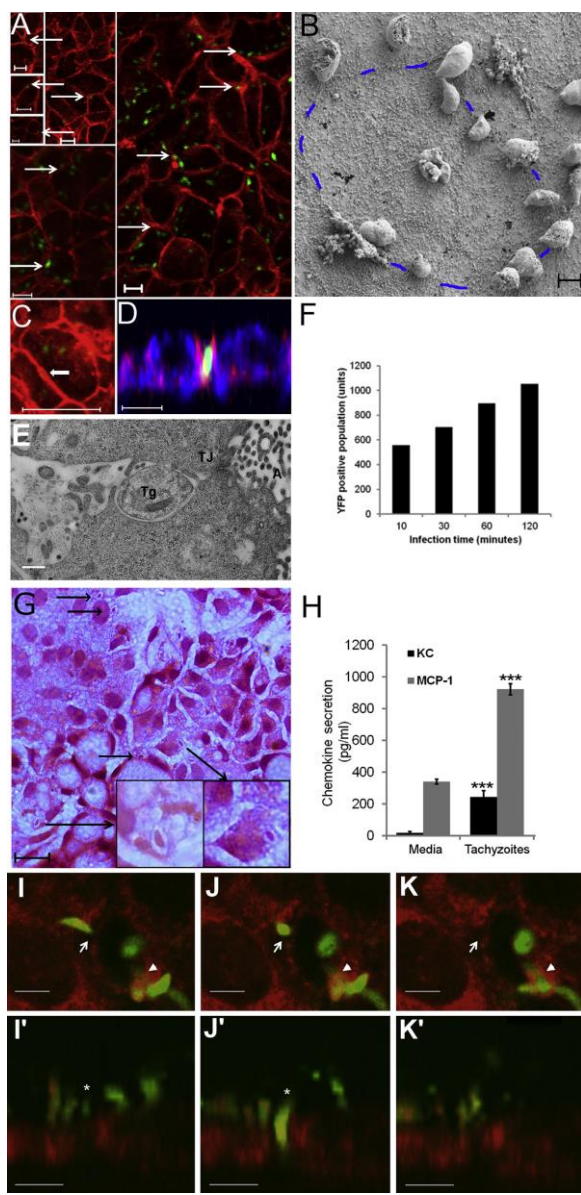
2.8. Recombinant occludin peptides

DNA regions coding for extracellular loop (ECL) 1 (residues 85 to 138) (184bp) ECL2 (residues 191 to 241) (167bp), ECL1+ECL2 (residues 85 to 241) (485bp) and C-terminus (residues 261 to 521) (800bp) murine occludin fragments were PCR amplified from pBABE-FLAG + Occ plasmid DNA (Britta Engelhardt, University of Bern, Switzerland) [21] using the following primer pairs: ECL1-F, ATGCCATATGAACTTGCTTGGGACAG-3' and ECL1-R, 5'- AGCAGCCGGATCCTAGCCTTTGGCTGCTTGGGT-3' (full length ECL1); ECL2-F, 5'-ATGCCATATGATAATGGGAGTGAACCCC-3' and ECL2-R, 5'-ATGGATCCTACTGGGGATCAAACACAC-3' (full length ECL2); ECL1-F, 5'-ATGCCATATGGCTGTGAAACCCGAAG-3' and ECL2-R, 5'-ATGGATCCTAAAGTTCCCGTCTG-3' (full length C-terminus). PCR products were cloned into the NdeI and BamHI sites of the expression vector pET15b (Novagen) and sequence-verified prior to transforming *Escherichia coli* Rosetta2 (DE3) pLysS. *E. coli* expressing His-tagged-protein products were purified using the Ni-NTA purification system (Qiagen) under denaturing conditions according to the manufacturer's instructions. Eluted proteins were immediately re-natured through the removal of urea by sequential dialysis. The purity of the recombinant occludin peptides was determined by SDS-PAGE.

3. Occludin-parasite binding assays

IEC-6 cells were plated onto 13 mm diameter glass coverslips (BDH) and cultured for 4 days prior to apical addition of either RH-YFP *T. gondii* tachyzoites (control) or RH-YFP *T. gondii* tachyzoites pre-incubated with 2 µM recombinant occludin peptides for 15 min, for 2 h. To visualize intracellular parasites, IEC-6 cells were permeabilized and H&E counterstained before mounting and imaging of parasitophorous vacuoles using an inverted Zeiss AxioVert 200M microscope. Images were analyzed on AxioVision image viewer with 6–12 fields of view recorded for each slide.

For peptide-parasite binding assays His-tagged occludin peptides or a His-tagged mCherry protein (20 µM in 6 M urea in buffer I (PBS with 1 mM CaCl and 0.05% Tween-20)) were immobilised onto Schott Nexterion H slides (Jena, Germany) of a 16-well superstructure in a humidified chamber for 2 h at 20 °C. Wells were washed in decreasing concentrations of urea



Please cite this article in press as: Weight CM, et al., Elucidating pathways of *Toxoplasma gondii* invasion in the gastrointestinal tract: Involvement of the tight junction protein occludin, *Microbes and Infection* (2015), <http://dx.doi.org/10.1016/j.micinf.2015.07.001>

(4–0 M) in buffer I then blocking solution for 1 h (25 mM ethanolamine in 100 mM sodium borate buffer). The wells were then washed in buffer I and incubated with YFP *T. gondii* tachyzoites (10^6 per well) for 2 h at 20 °C. Slides were fixed with 2% formaldehyde prior to mounting and bound parasites were visualized by UV microscopy (Zeiss AxioVert 200M microscope and AxioVision image viewer). Parasites were counted using fluorescent pixel counts at 63× magnification (Adobe Photoshop CS6) with 6–12 fields of view recorded for each well.

3.1. Statistical analysis

All data was assessed for normal distribution using the Kolmogorov–Smirnov test and for homogeneity of variance by the Bartlett's test. For parametric data, an independent *t* test, or a one-way ANOVA was carried out. For non-parametric data the Mann–Whitney U test and the Kruskal–Wallis test was used. Post-Hoc analyzes were carried out with Tukey's Multiple Comparison Test or Dunn's and Dunnett's Multiple Comparison tests. Data was analyzed using Prism GraphPad software. *P* values of less than 0.05 were considered significant. **P* < 0.05, ***P* < 0.01, ****P* < 0.001, *****P* < 0.0001. Any data points that were two or more standard deviations away from the mean were considered outliers and disregarded from analyzes. Error bars represent (±SEM) unless stated otherwise.

4. Results

4.1. Experimental approach

We used a cell culture model of the mammalian intestinal epithelium to investigate how *T. gondii* interacts with and can breach the intestinal barrier. Virulent type 1 strain RH, *T. gondii* tachyzoites-YFP [20] were used in conjunction with the small intestine-derived epithelial cell lines m-IC_{c12} [18] and IEC-6 [19] to assess barrier function, visualize and characterize parasite interactions with TJ complexes and to quantify parasite transmigration. Natural infection of *T. gondii* normally occurs via sporozoites or bradyzoites that invade the intestine and differentiate into tachyzoites. However, tachyzoites also contribute to the pathogenesis of acute

toxoplasmosis [22,23] and are infective via the oral route [24,25,16]. m-IC_{c12} cells resemble those found along the lower crypt–villous axis with cytoplasmic accumulation of sucrose isomaltase, expression of the polymeric Ig receptor and cystic fibrosis transmembrane conductance regulator Cl⁻ channel, and the ability to produce Paneth cells [18]. IEC-6 cells possess characteristics of normal crypt epithelial cells and differentiate in culture, developing cell surface alkaline-phosphatase (ALP) enzyme activity [19,26].

4.2. *T. gondii* parasites cluster around cellular junctions

T. gondii tachyzoites dispersed over the apical surface of a confluent polarized monolayer of m-IC_{c12}, frequently settled around epithelial cellular junctions as seen by both immunofluorescence (Fig. 1A, C and D) and electron microscopy (Fig. 1B and E). The apical surface of cells is covered by microvilli and cell edges appear raised on SEM, which is highlighted in Fig. 1B. Using TEM, parasites were observed below the apical tight junction complex (TJ, Fig. 1E) and between cells (large structures above and below the parasite). This distribution of parasites suggests the paracellular pathway may be a route of infection and/or transmigration, as proposed previously [9]. Parasites were also seen in association with the cell apical membrane, indicating multiple points of cell contact and possible docking receptors.

Using m-IC_{c12} grown on transwell inserts the number of YFP-expressing parasites transmigrating from the apical to basal compartment increased over time and up to 2 h after incubation (Fig. 1F). Intracellular parasites were contained within a parasitophorous vacuole appearing as a white halo surrounding the parasite (Fig. 1G). Parasite egression from infected cells was not considered an important factor within this time frame [27].

To establish whether IECs responded to *T. gondii* in this model system, cytokine and chemokine secretion was analyzed. Among those tested, significant increases in both keratinocyte chemoattractant (KC, the murine homolog of IL-8) and monocyte chemoattractant protein-1 (MCP-1) were detected in epithelial cell-conditioned media in the presence of *T. gondii* (Fig. 1H). No changes in interferon-γ, interleukin

Fig. 1. *T. gondii* localizes to epithelial cellular junctions before paracellular transmigration and/or infection. (A) Polarized m-IC_{c12} cultured on cell inserts were exposed to YFP-*T. gondii* for 2 h and stained for β-catenin (red). Arrows represent cells with parasites clustered around the lateral cell edge. Images are representative of those obtained from more than ten experiments with replicates. Scale bar = 10 μm. Further evidence for lateral localization of parasites was provided by scanning electron microscopy; visualized parasites clustered around cell edges as highlighted in blue (B). Scale bar = 2 μm. Parasites were seen penetrating the epithelial cells via the paracellular pathway (white arrow) as indicated by staining with occludin (red, C), β-catenin and surface carbohydrates (red and blue respectively, D), and, by transmission electron microscopy (E). TJ, tight junction; Tg, *T. gondii*; A, apical surface. Scale bar = 20 μm for (C and D) and 500 nm for (E). Experiments were carried out once with biological replicates for SEM and TEM. (F) Parasite transmigration across polarized monolayers was quantified by sampling the basal compartment for YFP-parasites after their addition to the apical compartment, using flow cytometry. (G) Intracellular parasites are contained within a parasitophorous vacuole appearing as a white halo surrounding the parasite (arrow) following H&E staining. Scale bar = 20 μm. (H) Supernatant from IECs, cultured in six well dishes and exposed to 1.5×10^6 parasites for 24 h, were assayed for the presence of cytokines using a bead array. Data represents three independent experiments with biological replicates. ****P* < 0.0001. (I–K) 2-Photon-microscope live imaging of IEC-6 monolayers (red) exposed to *T. gondii* (green) (See Video S1). Sequential frames from Video S1 show a transmigrating parasite targeting the epithelial cellular junction (white arrows). Following initial localization to the cellular junction (I), the parasite re-orientates (J) and enters the paracellular junction (K). A static intracellular parasite is clearly visible (White arrowheads). Corresponding YZ images show the parasite (marked *) localizes above the epithelial cellular junction (I'), re-orientates and moves between cells in the paracellular junction (J') and transmigrates through the epithelium (K'). The paracellular junction region is visible as a non-stained space between cells (red). Images are representative of those obtained from two experiments with replicates. Scale bar = 5 μm.

Please cite this article in press as: Weight CM, et al., Elucidating pathways of *Toxoplasma gondii* invasion in the gastrointestinal tract: Involvement of the tight junction protein occludin, *Microbes and Infection* (2015), <http://dx.doi.org/10.1016/j.micinf.2015.07.001>

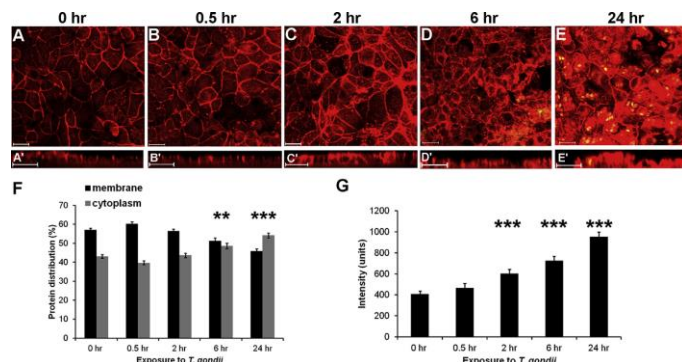


Fig. 2. *T. gondii* alters the distribution of occludin. (A–E) m-IC_{c12} cells grown on inserts were exposed to either media alone (A) or with parasites for 0.5 h (B), 2 h (C), 6 h (D) or 24 h (E), prior to staining with anti-occludin antibodies (red). A'–E' represents XZ images of corresponding XY optical slide images. Scale bar = 20 μm. Images are representative of those collected from ten experiments with biological replicates. (F) Image quantification was used to assess occludin distribution across membrane and cytoplasmic cellular compartments as well as total cellular levels of occludin (G) prior and post exposure to parasites. The graphs represent image quantification of between 30 and 90 cells across 3 to 10 independent experiments using Image J. ** = P < 0.002 and P < 0.0001 comparing with no exposure to parasites.

(IL)-6, IL-10, IL-12, macrophage inflammatory protein (MIP)-1 α , MIP-1 β or tumor necrosis factor- α were detected (data not shown).

Collectively these observations reveal the ability of *T. gondii* to invade cultured IECs via infection and transmigration, with a preference for cellular boundaries as a site of epithelial cell interaction and adherence. In addition, the epithelial cells responded to the parasites via the production of specific inflammatory mediators.

4.3. *T. gondii* target cellular junctions and transmigrate through the epithelium via the paracellular pathway

The route of parasite infection and transmigration was further investigated using 2-photon microscope-based live imaging. The still images taken from the video (Video S1) and shown in Fig. 1I–K illustrate the migration of YFP-*T. gondii* parasites across (I–K) and then through (I'–K') the epithelial cell monolayer. Labeling of the monolayer with Cell-TracerTM Red emphasized the epithelial cell junctions (X plane; I–K) and paracellular space (Z plane; I'–K'), visible as non-stained regions between adjacent epithelial cells. The video highlights the rapid re-orientation and entry of the parasite into the paracellular space (Fig. 1J and J' and Video S1) in a process taking less than 52 s. The parasite then appears to transmigrate through the monolayer, leaving the paracellular space empty (Fig. 1K and K' and Video S1). Paracellular egression of a parasite through the basal monolayer was also observed within minutes post-infection (data not shown).

Supplementary video related to this article can be found at <http://dx.doi.org/10.1016/j.micinf.2015.07.001>.

4.4. *T. gondii* induces changes in the distribution of the tight junction protein occludin

Staining m-IC_{c12} cell monolayers with anti-occludin antibodies prior to and after exposure to *T. gondii* revealed that occludin localization changed over time in the presence of *T. gondii* (Fig. 2). Over the time course, there was a decrease in occludin associated with the TJ complexes with staining concentrated intracellularly (Fig. 2A–E and A'–E'). This was verified by image quantification (Fig. 2F and G). In detail, after 30 min, occludin appeared more concentrated at junctions compared with non-infected m-IC_{c12} cells (Fig. 2B). After 2 h, the changes in occludin redistribution were more apparent, becoming apically enhanced within the cytoplasm (Fig. 2C'). Following 6 h of infection, the presence of occludin at the tight junction complex was fractured compared to the control, and was found increasingly in the cytoplasm (Fig. 2D and D'). After 24 h this phenomenon was even more pronounced (Fig. 2E and E'). We have also observed a similar pattern of occludin redistribution in m-IC_{c12} cells in response to *T. gondii* (RH tachyzoite-derived) bradyzoites [17].

In summary, the immunofluorescence images demonstrate the ability of *T. gondii* to affect changes in the distribution and partitioning of occludin between the cytoplasm, cell membrane and TJ specific domains of m-IC_{c12} epithelial cells.

4.5. *T. gondii* transmigrates between epithelial cells without affecting other junction-associated proteins or barrier function

To determine if other junctional proteins were also affected by *T. gondii*, m-IC_{c12} cells were analyzed for the expression of

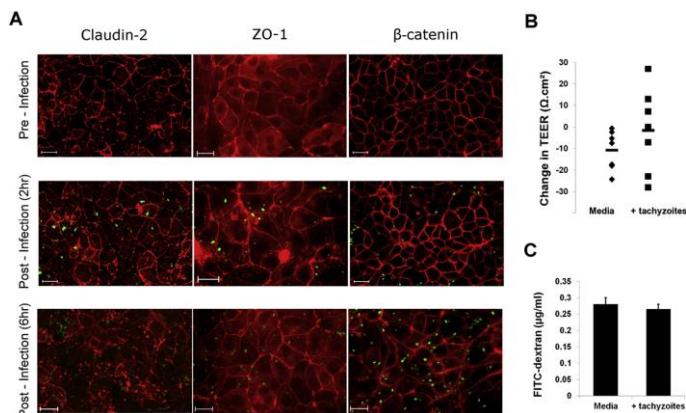


Fig. 3. *T. gondii* does not globally affect junctional proteins or epithelial barrier function. (A) m-IC_{c12} cells were stained for claudin-2, ZO-1 or β-catenin, pre- and post-infection (2 h or 6 h) with live parasites. Scale bar = 20 μm. Results are representative of 3 or more independent experiments with replicates. (B) Changes in barrier function were assessed by measuring TEER in response to parasites after 2 h exposure. The data shown represents results from seven separate determinations with biological replicates. P = 0.2. (C) Epithelial permeability was assessed by measuring transmigration of FITC-dextran across epithelial cells cultured in transwells prior and after 2 h exposure to parasites. The data shown represents results from three separate determinations with biological replicates. P = 0.4.

claudin-2, ZO-1 and β-catenin. Claudin 2 is a transmembrane protein of the tight junction complex primarily involved in the regulation of permeability. ZO-1 is a scaffold protein that connects with occludin, and β-catenin is an adherens junction protein that was chosen to compare whether multiple paracellular junctions were affected by *T. gondii* in our system. In comparison to the parasite-induced redistribution of occludin, the distribution of other junctional proteins was not obviously altered upon exposure to *T. gondii* after 2 h (Fig. 3A). Staining at the junctions was still apparent and unaffected by the presence of the parasite. After 6 h exposure, tight junction protein expression appeared more punctate although adherens junctions were unchanged. However, co-localization of these other proteins with *T. gondii* was not readily observed. Therefore these differences in expression may be attributed to indirect effects following changes in occludin distribution because, for example, ZO-1 interacts with occludin [28].

To determine if transmigrating parasites affected epithelial barrier integrity, transepithelial electrical resistance (TEER) and permeability were measured. After 2 h of exposure to parasites there were no significant differences in TEER (Fig. 3B) or permeability to 3–5 kDa FITC-dextran between non-infected (media) and infected m-IC_{c12} monolayers (Fig. 3C). Similar findings of unaltered TEER and permeability were also seen at earlier (0.5 h) and later (6 h) intervals of parasite exposure (data not shown). These findings show that *T. gondii* tachyzoites do not adversely affect the integrity of the intestinal epithelial barrier, in agreement with previous studies using kidney- and trophoblast-derived cell lines [9].

Immunofluorescence analysis of parasite-epithelial cell co-cultures also showed that tachyzoites co-localized with

occludin which appeared to concentrate at the points of parasite entry into, or between cells (Fig. 4A–E). Antibody complexes did not bind to the parasite alone (Fig. 4F). After infection, occludin was localized at or in close proximity to parasites inside infected cells (Fig. 4C–E and G–I).

4.6. *T. gondii* infection and transmigration through epithelial cells is reduced in cells expressing lower levels of occludin

To determine if occludin was required for *T. gondii* infection and/or transmigration, m-IC_{c12} cells were treated for 48 h with occludin-specific small interfering RNA (siRNA) prior to incubating with parasites. Occludin knockdown was confirmed by immunoblotting with levels of reduction equating to ~35%, which persisted for up to 6 days post treatment (Fig. 5A and data not shown). Treatment with occludin-specific siRNA had no effect on barrier function as determined via TEER measurements and permeability to 3–5 kDa dextran (Fig. 5B–C). Immunofluorescent staining of siRNA-treated cells confirmed reduced levels of occludin in cells treated with occludin-specific siRNA (Fig. 5H) and showed that occludin-specific siRNA had no discernable off-target effects as evidenced by expression of other TJ proteins including claudin-2, ZO-1 and β-catenin that was unaffected by the siRNA treatment (Fig. 5I–K).

To determine whether or not expression levels of occludin were important for the attachment, invasion and transmigration of *T. gondii*, m-IC_{c12} cells treated with siRNAs against occludin were incubated with parasites. As the parasitophorous vacuole in infected cells is impermeable to H&E it

Please cite this article in press as: Weight CM, et al., Elucidating pathways of *Toxoplasma gondii* invasion in the gastrointestinal tract: Involvement of the tight junction protein occludin, *Microbes and Infection* (2015), <http://dx.doi.org/10.1016/j.micinf.2015.07.001>

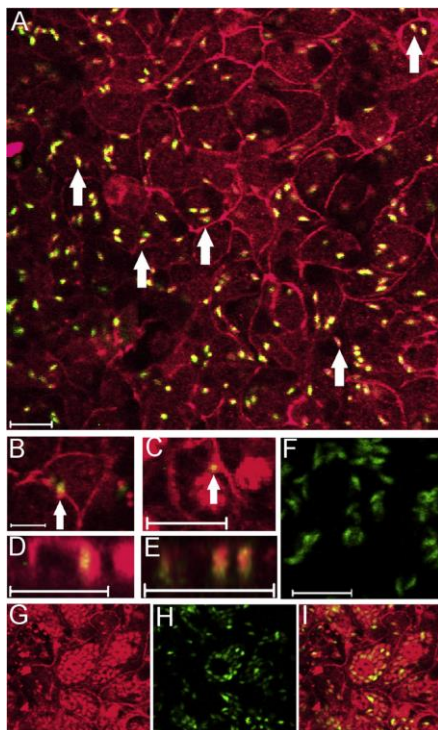


Fig. 4. *T. gondii* co-localizes with occludin during infection and transmigration. (A) m-IC_{c12} cells were exposed to *T. gondii* (green) for 2 h and stained for occludin (red) with co-localization (arrows) appearing yellow. Magnified images of individual cells show a transmigrating parasite (B) and an internalized parasite (C). (D) and (E) highlight occludin-parasite co-localization in the XZ plane. Anti-occludin antibodies do not stain the parasites in isolation (F). By 24 h post-infection occludin is redistributed intracellularly (G) with multiple parasites residing within infected cells (H). (I) shows the merged (G) and (H) images. Scale bar = 20 μm. Images are representative of those from three to ten independent experiments with biological replicates.

is possible to quantify the numbers of extracellular (adhered, Fig. 5D) and intracellular parasites (Fig. 5E) using H&E stained preparations of IECs. In cells with reduced levels of occludin there was a modest but significant decrease in the number of adherent parasites (Fig. 5D), which correlated with a significant decrease in the proportion of cells infected by *T. gondii* compared to cells treated with non-silencing siRNAs (Fig. 5E). In addition, significantly fewer transmigrating parasites were detected in occludin siRNA-treated cells compared to non-silencing siRNA-treated cells (Fig. 5F) despite the number of apical parasites present in each sample being equivalent (Fig. 5G).

Following exposure to *T. gondii*, residual occludin in occludin siRNA-treated cells was redistributed in a similar way to that seen in non-treated or non-silencing siRNA-treated cells (Fig. 5H), suggesting that *T. gondii* was still able to interact with the residual occludin. By contrast, there were no changes in the distribution of other junctional proteins following infection of occludin-reduced cells (Fig. 5I–K).

4.7. *T. gondii* binds the extracellular loops of occludin

To determine *T. gondii* tachyzoite interactions with occludin, an *in vitro* infection assay was developed to assess changes in cellular attachment. As the extracellular loops (ECLs) of occludin bind to each other on adjacent cells [29,30] we speculated that this part of the molecule is most likely to be accessible to interact with *T. gondii* in the paracellular space. Prior to infection of IEC-6, *T. gondii* tachyzoites were pre-incubated with occludin peptides (ECL2, amino acid residues 191 to 241; ECL1 + ECL2, residues 85 to 241 and, as a control, C-terminus residues 261 to 521, (Fig. 6A–B)). Extracellular, attached parasites were identified by the absence of an intracellular parasitophorous vacuole. Pre-incubation of *T. gondii* pre-incubation with the ECL1 + ECL2 and to a lesser extent the C-terminus peptide, significantly reduced attachment to the epithelial cells (Fig. 7A), suggesting *T. gondii* tachyzoites physically interact with the ECL1 + 2 and C-terminus peptides, which blocks parasite attachment to IEC-6.

To determine if occludin and *T. gondii* tachyzoites can physically interact, a solid phase *in vitro* binding assay was developed. YFP-parasites were incubated in individual wells of a modified microscope chamber slide to which occludin peptides (ECL1, amino acid residues 85 to 138; ECL2, amino acid residues 191 to 241; ECL1 + ECL2, residues 85 to 241 and, as a control, C-terminus residues 261 to 521, (Fig. 6A–B)) were immobilized. The images in Fig. 7B show the aggregation and clustering of large numbers of parasites in wells containing the ECL1 + ECL2 occludin peptide. This contrasted with the low density of parasites randomly scattered across wells containing the C-terminus peptide, or in control wells containing an irrelevant protein (mCherry) or, peptide-binding media alone. Image quantification of bound parasites showed that the highest levels of bound parasites were in wells coated with the ECL1 + ECL2 and ECL1 peptides, suggesting that *T. gondii* tachyzoites can bind the extracellular loops of occludin and in particular, to ECL1 (Fig. 7C).

5. Discussion

Here, we provide evidence of the ability of *T. gondii* tachyzoites to access the paracellular pathway as a means of invading and transmigrating polarized intestinal epithelial cell monolayers. We have also presented evidence indicating a physical interaction can occur, at least *in vitro*, between *T. gondii* and intestinal epithelial TJ complexes via occludin. Ingested parasites (sporozoites in oocysts and bradyzoites in tissue cysts) invade the intestine and differentiate into

Please cite this article in press as: Weight CM, et al., Elucidating pathways of *Toxoplasma gondii* invasion in the gastrointestinal tract: Involvement of the tight junction protein occludin, *Microbes and Infection* (2015), <http://dx.doi.org/10.1016/j.micinf.2015.07.001>

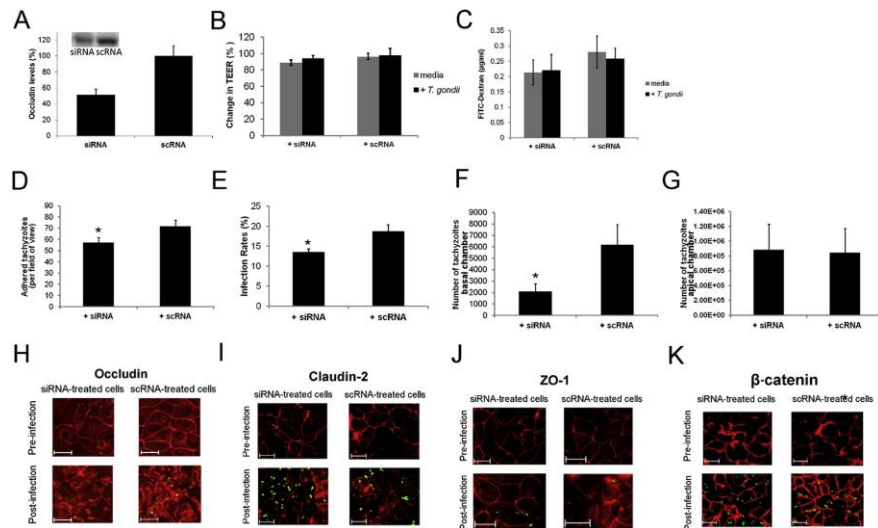


Fig. 5. Reduction of occludin expression impacts on parasite infection and transmigration. m-IC_{c12} were cultured on plastic to 80% confluence before adding occludin small interfering (siRNA) or non-silencing siRNA (scRNA). (A) Reduction of occludin was determined by immunoblotting 48 h post-transfection. Immunoblots were analyzed by densitometry with the values graphically shown, representing the levels of occludin in siRNA cell lysates relative to non-silenced siRNA-treated cells. Data is a representative from one of three independent experiments. Barrier function of siRNA-treated cells was assessed by measuring TEER (B, $P = 0.5673$) and permeability to FITC-dextran at 2 h post-parasite infection (C, $P = 0.83$). A value of 100% represents no change in TEER. The data shown represents results from three or more independent experiments with replicates. (D and E) m-IC_{c12} cells on coverslips were H&E stained to visualize and count parasites. Parasites that did not appear to have a white halo, indicative of intracellular parasitophorous vacuoles containing parasites, were assumed to be attached but not intracellular (D). Data represents results from four independent experiments with biological replicates. * $P = 0.0129$. (E) Infectivity of siRNA-treated cells was determined by counting the number of H&E-stained cells infected with parasites. Between 48 and 73 fields of view were recorded for each treatment with the data shown representing the percentage of cells infected compared to non-treated cells from four independent experiments with replicates. * $P = 0.0191$. (F) The ability of parasites to transmigrate occludin-reduced cells was determined in transwell cultures using flow cytometry to visualize and quantify parasites appearing in the basal compartment 2 h post-infection. The data shown represents results from three independent experiments with biological replicates. * $P = 0.0157$. (G) To establish that there were no discrepancies in the initial number of parasites incubated with the cells, parasites were collected and counted from the apical chamber of cells grown on transwell inserts. Data represents results from three independent experiments with biological replicates. $P = 0.9705$. (H–K) Cells grown on inserts for 11 days were treated with either occludin-specific siRNA or non-specific siRNA. (H) Cells were visualized for the presence of occludin 48 h post-transfection. Cells were also visualized for changes in occludin distribution following exposure to *T. gondii* for 2 h. Images are representative of 4 independent experiments. (I–K) Other junctional proteins were not affected by the reduction of occludin. Images represent data from three or more independent experiments. Scale bar = 20 μ m.

tachyzoites, followed by the spread of the organisms hemogenously and via lymphatics [8]. Our studies on the mechanism of epithelial cell transmigration by *T. gondii* tachyzoites are, we believe, relevant to the role this stage plays in host infection and dissemination across boundary epithelial cells. Occludin may therefore be a modulator of parasite transmigration via the paracellular pathway.

Many enteric pathogens have evolved mechanisms for targeting TJ-associated proteins for invasion. Alterations in the distribution or integrity of occludin are associated with infection of IECs by pathogens that cause gastroenteritis including *Salmonella typhimurium* [31] and enteropathogenic *E. coli* [32]. Whether or not other infectious life stages of *T. gondii* and the slow cyst-forming bradyzoite stage that is

mostly associated with natural infections [33], also target the paracellular pathway, remains to be determined. Of relevance, we have shown that bradyzoites derived from the YFP-expressing RH tachyzoites used in this study also induce alterations in occludin distribution in m-IC_{c12} epithelial cells [17]. However, in contrast to tachyzoite invasion, bradyzoites caused an increase in epithelial permeability. As bradyzoites contain different surface antigens to tachyzoites it is probable that there are multiple antigens and proteins the parasites use to infect different cells [34].

The redistribution of occludin in IECs exposed to *T. gondii* was seen across the epithelial cell monolayer despite only a proportion of infected cells. This dichotomy could result from direct and transient contact with parasites [35]. Alternatively,

Please cite this article in press as: Weight CM, et al., Elucidating pathways of *Toxoplasma gondii* invasion in the gastrointestinal tract: Involvement of the tight junction protein occludin, *Microbes and Infection* (2015), <http://dx.doi.org/10.1016/j.micinf.2015.07.001>

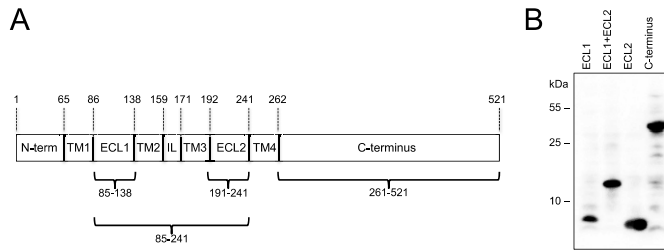


Fig. 6. Recombinant murine occludin peptides. (A) Occludin peptides corresponding to amino acids 191–241 (full length ECL2), 85–241 (full length ECL1+ECL2) and 261–521 (full length C-terminus) were generated as described in the Materials and Methods section. Amino acid number and distribution across the N terminus, transmembrane domains (TM), extracellular loops (ECL), intracellular loop (IL) and C-terminus were adapted from www.zonapse.net/occludin. (B) Peptide purity was assessed by immunoblotting using commercial anti-occludin antibodies.

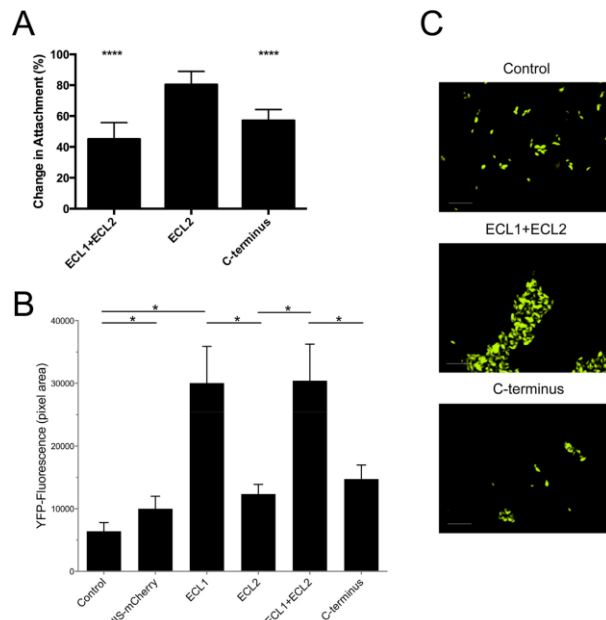


Fig. 7. *T. gondii* binds the extracellular loops of occludin. (A) The apical surface of IEC-6 was exposed for 2 h with either *T. gondii* (control) or *T. gondii* pre-incubated with 2 μM recombinant occludin peptides and were subsequently stained with H&E to visualize and count parasites. Parasites that did not have a white halo, indicative of intracellular parasitophorous vacuoles containing parasites, were assumed to be attached but not intracellular. Between 6 and 12 fields of view were recorded for each treatment with the data shown representing the normalized change in parasite attachment when parasites were pre-incubated with recombinant occludin peptides compared to non-treated parasites (control). Data shown is from three independent experiments with replicates. *** = $P < 0.001$, **** = $P < 0.0001$. (B and C) In a solid-phase parasite-occludin binding assay YFP-parasites were incubated with HIS-tagged ECL1+ECL2, ECL1, ECL2, or C-terminus fragments of murine occludin immobilized to individual wells of a chamber slide with bound parasites visualized by UV microscopy. Wells containing a HIS-tagged mCherry recombinant protein and/or binding buffer alone (Control) were used as controls. (B) Binding of parasites to occludin peptides was quantified by fluorescent pixel counts using 6–12 fields of view per well (* = $P < 0.05$, ** = $P < 0.01$). Data represents three independent experiments with replicates. (C) The fluorescent images shown are representative of those obtained from three experiments with replicates. Scale bar = 20 μm.

Please cite this article in press as: Weight CM, et al., Elucidating pathways of *Toxoplasma gondii* invasion in the gastrointestinal tract: Involvement of the tight junction protein occludin, *Microbes and Infection* (2015), <http://dx.doi.org/10.1016/j.micinf.2015.07.001>

infected cells secrete cytokines and chemokines in response to pathogen exposure that may act upon neighboring cells and TJ complexes in a paracrine fashion [36–38].

The reduction of cellular occludin following siRNA treatment decreased transmigration by ~65%, but only decreased invasion by ~20%. Occludin may therefore be of more importance for the transmigration of *T. gondii* rather than invasion of IECs. Alternatively, changes in paracellular macromolecular flux, which is in part regulated by occludin, could also affect transmigration rates [12,29]. Without inhibitory occludin antibodies recognizing the extracellular domains, it was not possible to perform competition or neutralizing assays as a complimentary approach to quantify parasite transmigration between or infection into IECs. The decrease in attachment and infection following the partial reduction of occludin expression indicates that occludin may also be required for *T. gondii* to enter epithelial cells.

The identity of parasite-derived occludin binding partners was not established here. Preliminary data from immunoprecipitation and mass spectrometry analyses reveals parasite microneme and dense granule proteins to be associated with occludin (data not shown). Given that *T. gondii* is capable of invading most cell types, it is perhaps surprising that only a few cell surface receptors and *T. gondii* ligands have so far been identified. Amongst these, *T. gondii* can attach via GPI-anchored membrane proteins (e.g. SAG1) to host glucosamine receptors [39], and to galectin-like molecules on the cell surface [40], which assist in the formation of the microneme MIC1-MIC6 protein complex that is secreted during infection [41]. MIC2 binds to ICAM-1 on the surface of IECs and this interaction is considered important for parasite transmigration [9]. Sulfated glycosaminoglycans (GAGs), heparin sulfated proteoglycans and sialic acid residues on host cells have also been shown to mediate binding and invasion of *T. gondii* [42–44]. These molecules represent possible adherence receptors on IECs that the parasite can manipulate before migrating to the lateral junctions.

After 24 h of infection, IECs contained multiple parasites that remain co-localized with occludin. Peptides of ECL1 and ECL2 can increase the rate of occludin turnover and as *T. gondii* binds the extracellular loops of occludin, it is possible that endocytosis of occludin may occur following interactions with the parasite [45,46]. This could explain why after 24 h of infection the concentration of cellular occludin was increased compared to non-infected cells. Increased rates of recycling are also thought to be a common mechanism in pathogen invasion [47]. Alternatively, there may be increased synthesis of occludin, which was not addressed in this study. The results of our occludin binding assay suggest that *T. gondii* may associate with ECL1. This loop contains a high percentage of tyrosine and glycine residues that are thought to provide flexibility to the molecule, which also possesses self-associating properties [30].

In summary, we have provided evidence of *T. gondii* tachyzoites targeting the paracellular pathway as a means of transmigrating epithelial cell monolayers in a process that appears to involve interactions with occludin. These findings

have implications for understanding how *T. gondii* invades its host and further highlights the susceptibility of the intestinal epithelial barrier to pathogens that target the most apical junctional complexes.

Conflict of interest

The authors declare no conflicts of interest.

Acknowledgments

The work was supported by an Institute Strategic Programme Grant IFR/08/1 and PhD studentships from the BBSRC (CMW; BB/D526488/1) and UEA (EJJ). The authors are grateful to Dr. Kathryn Cross and Dr. Mary Parker for assistance with EM at the Analytical Sciences Unit, Dr. Duncan Gaskin for assistance in the development the occludin-parasite binding assay, at the Institute of Food Research, UK, and Dr. Britta Engelhardt, University of Bern, Switzerland for providing the pBABA-FLAG + Occ plasmid.

References

- [1] Weiss LM, Dubey JP. Toxoplasmosis: a history of clinical observations. *Int J Parasitol* 2009;39:895–901.
- [2] Sukhana Y. Toxoplasmosis: beyond animals to humans. *Trends Parasitol* 2006;22:137–42.
- [3] Montoya JG, Liesenfeld O. *Toxoplasmosis* Lancet 2004;363:1965–76.
- [4] Jones JL, Dubey JP. Waterborne toxoplasmosis – recent developments. *Exp Parasitol* 2010;124:10–25.
- [5] Jones JL, Dubey JP. Foodborne toxoplasmosis. *Clin Infect Dis* 2012;55:845–51.
- [6] Coombes JL, Charszar BA, Han SJ, Halkias J, Chan SW, Koshy AA, et al. Motile invaded neutrophils in the small intestine of *Toxoplasma gondii*-infected mice reveal a potential mechanism for parasite spread. *Proc Natl Acad Sci U S A* 2013;110:E1913–22.
- [7] Gregg B, Taylor BC, John B, Tait-Wojno ED, Girgis NM, Miller N, et al. Replication and distribution of *Toxoplasma gondii* in the small intestine after oral infection with tissue cysts. *Infect Immun* 2013;81:1635–43.
- [8] Dubey JP. Bradyzoite-induced murine toxoplasmosis: stage conversion, pathogenesis, and tissue cyst formation in mice fed bradyzoites of different strains of *Toxoplasma gondii*. *J Eukaryot Microbiol* 1997;44:592–602.
- [9] Barragan A, Brossier F, Sibley LD. Transepithelial migration of *Toxoplasma gondii* involves an interaction of intercellular adhesion molecule 1 (ICAM-1) with the parasite adhesin MIC2. *Cell Microbiol* 2005;7:561–8.
- [10] Krug SM, Gunzel D, Conrad MP, Lee IF, Amasheh S, Fromm M, et al. Charge-selective claudin channels. *Ann N Y Acad Sci* 2012;1257:20–8.
- [11] Chiba H, Osawai M, Murata M, Kojima T, Sawada N. Transmembrane proteins of tight junctions. *Biochim Biophys Acta* 2008;1778:588–600.
- [12] Al-Sadi R, Khatib K, Guo S, Ye D, Youssef M, Ma T. Occludin regulates macromolecule flux across the intestinal epithelial tight junction barrier. *Am J Physiol Gastrointest Liver Physiol* 2011;300:G1054–64.
- [13] Wong V. Phosphorylation of occludin correlates with occludin localization and function at the tight junction. *Am J Physiol* 1997;273:C1859–67.
- [14] Raleigh DR, Boe DM, Yu D, Weber CR, Marchiando AM, Bradford EM, et al. Occludin S408 phosphorylation regulates tight junction protein interactions and barrier function. *J Cell Biol* 2011;193:565–82.
- [15] Bonazzi M, Cossart P. Impenetrable barriers or entry portals? The role of cell-cell adhesion during infection. *J Cell Biol* 2011;195:349–58.
- [16] Dalton JE, Cruickshank SM, Egan CE, Mears R, Newton DJ, Andrew EM, et al. Intraepithelial gamma delta+ lymphocytes maintain

- the integrity of intestinal epithelial tight junctions in response to infection. *Gastroenterology* 2006;131:818–29.
- [17] Weight CM, Carding SR. The protozoan pathogen *Toxoplasma gondii* targets the paracellular pathway to invade the intestinal epithelium. *Ann N Y Acad Sci* 2012;1258:135–42.
- [18] Bens M, Bogdanova A, Cluzeaud F, Miquerol L, Kerneis S, Krahenbuhl JP, et al. Transimmortalized mouse intestinal cells (m-ICel2) that maintain a crypt phenotype. *Am J Physiol* 1996;270:C1666–74.
- [19] Quaroni A, Wands J, Trelstad RL, Issebacher KJ. Epithelioid cell cultures from rat small intestine. Characterization by morphologic and immunologic criteria. *J Cell Biol* 1979;80:248–65.
- [20] Gubbels MJ, Li C, Striepen B. High-throughput growth assay for *Toxoplasma gondii* using yellow fluorescent protein. *Antimicrob Agents Chemother* 2003;47:309–16.
- [21] Bamforth SD, Kniess U, Wolburg H, Engelhardt B, Risau W. A dominant mutant of occludin disrupts tight junction structure and function. *J Cell Sci* 1999;112(Pt 12):1879–88.
- [22] Djurkovic-Djukovic O, Djokic V, Vujanic M, Zivkovic T, Bobic B, Nikolic A, et al. Kinetics of parasite burdens in blood and tissues during murine toxoplasmosis. *Exp Parasitol* 2012;131:372–6.
- [23] Hill RD, Su C. High tissue burden of *Toxoplasma gondii* is the hallmark of acute virulence in mice. *Vet Parasitol* 2012;187:36–43.
- [24] Dubey JP. Re-examination of resistance of *Toxoplasma gondii* tachyzoites and bradyzoites to pepsin and trypsin digestion. *Parasitology* 1998;116(Pt 1):43–50.
- [25] Bonametti AM, Passos JN, Koga da Silva EM, Macedo ZS. Probable transmission of acute toxoplasmosis through breast feeding. *J Trop Pediatr* 1997;43:116.
- [26] Wood SR, Zhao Q, Smith LH, Daniels CK. Altered morphology in cultured rat intestinal epithelial IEC-6 cells is associated with alkaline phosphatase expression. *Tissue Cell* 2003;35:47–58.
- [27] Morisaki JH, Heuser JE, Sibley LD. Invasion of *Toxoplasma gondii* occurs by active penetration of the host cell. *J Cell Sci* 1995;108(Pt 6):2457–64.
- [28] Fanning AS, Jameson BJ, Jesaitis LA, Anderson JM. The tight junction protein ZO-1 establishes a link between the transmembrane protein occludin and the actin cytoskeleton. *J Biol Chem* 1998;273:29745–53.
- [29] Blasig IE, Winkler L, Lassowski B, Mueller SL, Zuleger N, Krause E, et al. On the self-association potential of transmembrane tight junction proteins. *Cell Mol Life Sci* 2006;63:505–14.
- [30] Nusrat A, Brown GT, Tom J, Drake A, Bui TT, Quan C, et al. Multiple protein interactions involving proposed extracellular loop domains of the tight junction protein occludin. *Mol Biol Cell* 2005;16:1725–34.
- [31] Boyle EC, Brown NF, Finlay BB. *Salmonella enterica* serovar *Typhimurium* effectors SopB, SopE, SopE2 and SipA disrupt tight junction structure and function. *Cell Microbiol* 2006;8:1946–57.
- [32] Muza-Moons MM, Schneeberger EE, Hecht GA. Enteropathogenic *Escherichia coli* infection leads to appearance of aberrant tight junctions strands in the lateral membrane of intestinal epithelial cells. *Cell Microbiol* 2004;6:783–93.
- [33] Black MW, Boothroyd JC. Lytic cycle of *Toxoplasma gondii*. *Microbiol Mol Biol Rev* 2000;64:607–23.
- [34] Speer CA, Dubey JP. Ultrastructural differentiation of *Toxoplasma gondii* schizonts (types B to E) and gamonts in the intestines of cats fed bradyzoites. *Int J Parasitol* 2005;35:193–206.
- [35] Lavine MD, Arizabalaga G. Induction of mitotic S-phase of host and neighboring cells by *Toxoplasma gondii* enhances parasite invasion. *Mol Biochem Parasitol* 2009;164:95–9.
- [36] Denney CF, Eckmann L, Reed SL. Chemokine secretion of human cells in response to *Toxoplasma gondii* infection. *Infect Immun* 1999;67:1547–52.
- [37] Dolowschiak T, Chassin C, Ben Makdem S, Fuchs TM, Weiss S, Vandewalle A, et al. Potentiation of epithelial innate host responses by intercellular communication. *PLoS Pathog* 2010;6:e1001194.
- [38] Kasper CA, Sorg I, Schmitz C, Tschan T, Wischnewski H, Kim ML, et al. Cell-cell propagation of NF- κ B transcription factor and MAP kinase activation amplifies innate immunity against bacterial infection. *Immunity* 2010;33:804–16.
- [39] Mineo JR, McLeod R, Mack D, Smith J, Khan IA, Ely KH, et al. Antibodies to *Toxoplasma gondii* major surface protein (SAG-1, P30) inhibit infection of host cells and are produced in murine intestine after peroral infection. *J Immunol* 1993;150:3951–64.
- [40] Debiere-Grockiego F, Niehus S, Coddeville B, Elass E, Poirier F, Weingart R, et al. Binding of *Toxoplasma gondii* glycosylphosphatidylinositols to galectin-3 is required for their recognition by macrophages. *J Biol Chem* 2010;285:32744–50.
- [41] Saouros S, Edwards-Jones B, Reiss M, Sawmynden K, Cota E, Simpson P, et al. A novel galectin-like domain from *Toxoplasma gondii* micronemal protein I assists the folding, assembly, and transport of a cell adhesion complex. *J Biol Chem* 2005;280:38583–91.
- [42] Carruthers VB, Hakansson S, Giddings OK, Sibley LD. *Toxoplasma gondii* uses sulfated proteoglycans for substrate and host cell attachment. *Infect Immun* 2000;68:4005–11.
- [43] Jacquet A, Coulon L, De Neve J, Daminet V, Haumont M, Garcia L, et al. The surface antigen SAG3 mediates the attachment of *Toxoplasma gondii* to cell-surface proteoglycans. *Mol Biochem Parasitol* 2001;116:35–44.
- [44] Monteiro VG, Soares CP, de Souza W. Host cell surface sialic acid residues are involved on the process of penetration of *Toxoplasma gondii* into mammalian cells. *FEMS Microbiol Lett* 1998;164:323–7.
- [45] Wong V, Gumbiner BM. A synthetic peptide corresponding to the extracellular domain of occludin perturbs the tight junction permeability barrier. *J Cell Biol* 1997;136:399–409.
- [46] Lacaz-Vieira F, Jaeger MM, Farshori P, Kachar B. Small synthetic peptides homologous to segments of the first external loop of occludin impair tight junction resealing. *J Membr Biol* 1999;168:289–97.
- [47] Veiga E, Gutman JA, Bonazzi M, Bourot E, Toledo-Aranha A, Lin AE, et al. Invasive and adherent bacterial pathogens co-opt host clathrin for infection. *Cell Host Microbe* 2007;2:340–51.

Please cite this article in press as: Weight CM, et al., Elucidating pathways of *Toxoplasma gondii* invasion in the gastrointestinal tract: Involvement of the tight junction protein occludin, *Microbes and Infection* (2015), <http://dx.doi.org/10.1016/j.micinf.2015.07.001>

Bibliography

1. Aijaz, S., M.S. Balda, and K. Matter, *Tight junctions: molecular architecture and function.* Int Rev Cytol, 2006. **248**: p. 261-98.
2. Aijaz, S., et al., *Binding of GEF-H1 to the tight junction-associated adaptor cingulin results in inhibition of Rho signaling and G1/S phase transition.* Dev Cell., 2005. **8**(5): p. 777-86.
3. Al-Sadi, R., et al., *Occludin regulates macromolecule flux across the intestinal epithelial tight junction barrier.* Am J Physiol Gastrointest Liver Physiol., 2011. **300**(6): p. G1054-64. doi: 10.1152/ajpgi.00055.2011. Epub 2011 Mar 17.
4. Alexander, J.S., et al., *Activated T-lymphocytes express occludin, a component of tight junctions.* Inflammation., 1998. **22**(6): p. 573-82.
5. Allison, J.P. and W.L. Havran, *The immunobiology of T cells with invariant gamma delta antigen receptors.* Annu Rev Immunol, 1991. **9**: p. 679-705.
6. Amanchy, R., D.E. Kalume, and A. Pandey, *Stable isotope labeling with amino acids in cell culture (SILAC) for studying dynamics of protein abundance and posttranslational modifications.* Sci STKE, 2005. **2005**(267): p. pl2.
7. Amasheh, M., et al., *TNFalpha-induced and berberine-antagonized tight junction barrier impairment via tyrosine kinase, Akt and NFkappaB signaling.* J Cell Sci, 2010. **123**(Pt 23): p. 4145-55.
8. Amasheh, S., et al., *Claudin-2 expression induces cation-selective channels in tight junctions of epithelial cells.* J Cell Sci., 2002. **115**(Pt 24): p. 4969-76.
9. Ametani, A., et al., *Consecutive events of growth, differentiation and death of the small intestinal epithelial cell line, IEC-6.* In Vitro Cell Dev Biol Anim, 1996. **32**(3): p. 127-30.
10. Amieva, M.R., et al., *Disruption of the epithelial apical-junctional complex by Helicobacter pylori CagA.* Science, 2003. **300**(5624): p. 1430-4.
11. Anderson, J.M. and C.M. Van Itallie, *Tight junctions and the molecular basis for regulation of paracellular permeability.* Am J Physiol., 1995. **269**(4 Pt 1): p. G467-75.
12. Anderson, J.M. and C.M. Van Itallie, *Tight junctions.* Curr Biol., 2008. **18**(20): p. R941-3. doi: 10.1016/j.cub.2008.07.083.
13. Anderson, J.M. and C.M. Van Itallie, *Physiology and function of the tight junction.* Cold Spring Harb Perspect Biol., 2009. **1**(2): p. a002584. doi: 10.1101/cshperspect.a002584.
14. Anderson, J.M., C.M. Van Itallie, and A.S. Fanning, *Setting up a selective barrier at the apical junction complex.* Curr Opin Cell Biol., 2004. **16**(2): p. 140-5.
15. Ando-Akatsuka, Y., et al., *Interspecies diversity of the occludin sequence: cDNA cloning of human, mouse, dog, and rat-kangaroo homologues.* J Cell Biol., 1996. **133**(1): p. 43-7.

16. Andreeva, A.Y., et al., *Protein kinase C regulates the phosphorylation and cellular localization of occludin*. J Biol Chem, 2001. **276**(42): p. 38480-6.
17. Andreeva, I.E., et al., *Studies on interaction of phosphorylase kinase from rabbit skeletal muscle with glycogen in the presence of ATP and ADP*. Biochim Biophys Acta, 2001. **1549**(2): p. 188-96.
18. Andreeva, O.I., et al., [Interaction of HIV-1 reverse transcriptase and bacteriophage T7 RNA polymerase with NTP phosphonate analogs and inorganic pyrophosphate]. Mol Biol (Mosk), 2001. **35**(5): p. 844-56.
19. Andrew, E.M. and S.R. Carding, *Murine gammadelta T cells in infections: beneficial or deleterious?* Microbes Infect., 2005. **7**(3): p. 529-36. Epub 2005 Feb 3.
20. Angelow, S., E.E. Schneeberger, and A.S. Yu, *Claudin-8 expression in renal epithelial cells augments the paracellular barrier by replacing endogenous claudin-2*. J Membr Biol., 2007. **215**(2-3): p. 147-59. Epub 2007 May 22.
21. Antonetti, D.A., et al., *Vascular permeability in experimental diabetes is associated with reduced endothelial occludin content: vascular endothelial growth factor decreases occludin in retinal endothelial cells*. Penn State Retina Research Group. Diabetes, 1998. **47**(12): p. 1953-9.
22. Aono, S. and Y. Hirai, *Phosphorylation of claudin-4 is required for tight junction formation in a human keratinocyte cell line*. Exp Cell Res, 2008. **314**(18): p. 3326-39.
23. Appleford, P.J. and J.E. Smith, *Strain and stage specific variation in Toxoplasma gondii antigens*. Int J Parasitol., 2000. **30**(11): p. 1187-91.
24. Arnott, I.D., K. Kingstone, and S. Ghosh, *Abnormal intestinal permeability predicts relapse in inactive Crohn disease*. Scand J Gastroenterol., 2000. **35**(11): p. 1163-9.
25. Baert, F.J., et al., *Tumor necrosis factor alpha antibody (infliximab) therapy profoundly down-regulates the inflammation in Crohn's ileocolitis*. Gastroenterology., 1999. **116**(1): p. 22-8.
26. Bahia-Oliveira, L.M., et al., *Highly endemic, waterborne toxoplasmosis in north Rio de Janeiro state, Brazil*. Emerg Infect Dis., 2003. **9**(1): p. 55-62.
27. Bal, M.S., et al., *The hinge region of the scaffolding protein of cell contacts, zonula occludens protein 1, regulates interacting with various signaling proteins*. J Cell Biochem., 2012. **113**(3): p. 934-45.
28. Balda, M.S., et al., *Multiple domains of occludin are involved in the regulation of paracellular permeability*. J Cell Biochem, 2000. **78**(1): p. 85-96.
29. Balda, M.S., M.D. Garrett, and K. Matter, *The ZO-1-associated Y-box factor ZONAB regulates epithelial cell proliferation and cell density*. J Cell Biol., 2003. **160**(3): p. 423-32.
30. Balda, M.S., et al., *Assembly and sealing of tight junctions: possible participation of G-proteins, phospholipase C, protein kinase C and calmodulin*. J Membr Biol., 1991. **122**(3): p. 193-202.

31. Balda, M.S. and K. Matter, *Transmembrane proteins of tight junctions*. Semin Cell Dev Biol., 2000. **11**(4): p. 281-9.
32. Balda, M.S. and K. Matter, *Epithelial cell adhesion and the regulation of gene expression*. Trends Cell Biol., 2003. **13**(6): p. 310-8.
33. Balda, M.S. and K. Matter, *Tight junctions at a glance*. J Cell Sci., 2008. **121**(Pt 22): p. 3677-82. doi: 10.1242/jcs.023887.
34. Balda, M.S. and K. Matter, *Tight junctions and the regulation of gene expression*. Biochim Biophys Acta., 2009. **1788**(4): p. 761-7. doi: 10.1016/j.bbamem.2008.11.024. Epub 2008 Dec 11.
35. Balda, M.S. and K. Matter, *Tight junctions in health and disease*. Semin Cell Dev Biol, 2014. **36**: p. 147-8.
36. Balda, M.S., et al., *Functional dissociation of paracellular permeability and transepithelial electrical resistance and disruption of the apical-basolateral intramembrane diffusion barrier by expression of a mutant tight junction membrane protein*. J Cell Biol., 1996. **134**(4): p. 1031-49.
37. Balish, E. and T. Warner, *Enterococcus faecalis induces inflammatory bowel disease in interleukin-10 knockout mice*. Am J Pathol., 2002. **160**(6): p. 2253-7.
38. Banan, A., et al., *theta Isoform of protein kinase C alters barrier function in intestinal epithelium through modulation of distinct claudin isoforms: a novel mechanism for regulation of permeability*. J Pharmacol Exp Ther, 2005. **313**(3): p. 962-82.
39. Banchereau, J., et al., *Immunobiology of dendritic cells*. Annu Rev Immunol, 2000. **18**: p. 767-811.
40. Barker, N., et al., *Identification of stem cells in small intestine and colon by marker gene Lgr5*. Nature., 2007. **449**(7165): p. 1003-7. Epub 2007 Oct 14.
41. Barragan, A., F. Brossier, and L.D. Sibley, *Transepithelial migration of Toxoplasma gondii involves an interaction of intercellular adhesion molecule 1 (ICAM-1) with the parasite adhesin MIC2*. Cell Microbiol., 2005. **7**(4): p. 561-8.
42. Barragan, A. and L.D. Sibley, *Transepithelial migration of Toxoplasma gondii is linked to parasite motility and virulence*. J Exp Med., 2002. **195**(12): p. 1625-33.
43. Barragan, A. and L.D. Sibley, *Migration of Toxoplasma gondii across biological barriers*. Trends Microbiol., 2003. **11**(9): p. 426-30.
44. Barton, E.S., et al., *Junction adhesion molecule is a receptor for reovirus*. Cell, 2001. **104**(3): p. 441-51.
45. Bassi, A., et al., *Cost of illness of inflammatory bowel disease in the UK: a single centre retrospective study*. Gut., 2004. **53**(10): p. 1471-8.
46. Bastian, S.E., et al., *Transport of IGF-I across epithelial cell monolayers*. J Endocrinol, 1999. **162**(3): p. 361-9.
47. Bazzoni, G., et al., *Interaction of junctional adhesion molecule with the tight junction components ZO-1, cingulin, and occludin*. J Biol Chem., 2000. **275**(27): p. 20520-6.
48. Beatch, M., et al., *The tight junction protein ZO-2 contains three PDZ*

- (PSD-95/Discs-Large/ZO-1) domains and an alternatively spliced region.* J Biol Chem., 1996. **271**(42): p. 25723-6.
49. Behnke, M.S., et al., *Virulence differences in Toxoplasma mediated by amplification of a family of polymorphic pseudokinases.* Proc Natl Acad Sci U S A., 2011. **108**(23): p. 9631-6. doi: 10.1073/pnas.1015338108. Epub 2011 May 17.
50. Bellmann, C., et al., *Highly conserved cysteines are involved in the oligomerization of occludin-redox dependency of the second extracellular loop.* Antioxid Redox Signal, 2014. **20**(6): p. 855-67.
51. Bens, M., et al., *Transimmortalized mouse intestinal cells (m-ICc12) that maintain a crypt phenotype.* Am J Physiol., 1996. **270**(6 Pt 1): p. C1666-74.
52. Berglund, J.J., et al., *Regulation of human jejunal transmucosal resistance and MLC phosphorylation by Na(+) -glucose cotransport.* Am J Physiol Gastrointest Liver Physiol., 2001. **281**(6): p. G1487-93.
53. Beuneu, H., et al., *Visualizing the functional diversification of CD8+ T cell responses in lymph nodes.* Immunity, 2010. **33**(3): p. 412-23.
54. Bevins, C.L. and N.H. Salzman, *Paneth cells, antimicrobial peptides and maintenance of intestinal homeostasis.* Nat Rev Microbiol., 2011. **9**(5): p. 356-68. doi: 10.1038/nrmicro2546. Epub 2011 Mar 22.
55. Birkenfeld, J., et al., *Cellular functions of GEF-H1, a microtubule-regulated Rho-GEF: is altered GEF-H1 activity a crucial determinant of disease pathogenesis?* Trends Cell Biol, 2008. **18**(5): p. 210-9.
56. Black, M.W. and J.C. Boothroyd, *Lytic cycle of Toxoplasma gondii.* Microbiol Mol Biol Rev, 2000. **64**(3): p. 607-23.
57. Blader, I.J., I.D. Manger, and J.C. Boothroyd, *Microarray analysis reveals previously unknown changes in Toxoplasma gondii-infected human cells.* J Biol Chem, 2001. **276**(26): p. 24223-31.
58. Blader, I.J. and J.P. Saeij, *Communication between Toxoplasma gondii and its host: impact on parasite growth, development, immune evasion, and virulence.* Apmis., 2009. **117**(5-6): p. 458-76. doi: 10.1111/j.1600-0463.2009.02453.x.
59. Blair, S.A., et al., *Epithelial myosin light chain kinase expression and activity are upregulated in inflammatory bowel disease.* Lab Invest., 2006. **86**(2): p. 191-201.
60. Blasig, I.E., et al., *On the self-association potential of transmembrane tight junction proteins.* Cell Mol Life Sci, 2006. **63**(4): p. 505-14.
61. Blom, N., et al., *Prediction of post-translational glycosylation and phosphorylation of proteins from the amino acid sequence.* Proteomics, 2004. **4**(6): p. 1633-49.
62. Bontell, I.L., et al., *Whole genome sequencing of a natural recombinant Toxoplasma gondii strain reveals chromosome sorting and local allelic variants.* Genome Biol., 2009. **10**(5): p. R53. doi: 10.1186/gb-2009-10-5-r53. Epub 2009 May 20.
63. Boothroyd, J.C. and M.E. Grigg, *Population biology of Toxoplasma gondii and its relevance to human infection: do different strains cause different disease?* Curr Opin Microbiol., 2002. **5**(4): p. 438-42.

64. Boothroyd, J.C., et al., *The surface of Toxoplasma: more and less*. Int J Parasitol, 1998. **28**(1): p. 3-9.
65. Bouzid, M., D. Steverding, and K.M. Tyler, *Detection and surveillance of waterborne protozoan parasites*. Curr Opin Biotechnol, 2008. **19**(3): p. 302-6. doi: 10.1016/j.copbio.2008.05.002. Epub 2008 Jun 2.
66. Boyle, J.P., et al., *Just one cross appears capable of dramatically altering the population biology of a eukaryotic pathogen like Toxoplasma gondii*. Proc Natl Acad Sci U S A, 2006. **103**(27): p. 10514-9. Epub 2006 Jun 26.
67. Bradley, P.J. and L.D. Sibley, *Rhoptries: an arsenal of secreted virulence factors*. Curr Opin Microbiol, 2007. **10**(6): p. 582-7.
68. Bradley, P.J., et al., *Proteomic analysis of rhoptry organelles reveals many novel constituents for host-parasite interactions in Toxoplasma gondii*. J Biol Chem, 2005. **280**(40): p. 34245-58.
69. Brandtzaeg, P., et al., *Terminology: nomenclature of mucosa-associated lymphoid tissue*. Mucosal Immunol, 2008. **1**(1): p. 31-7. doi: 10.1038/mi.2007.9.
70. Broer, S., *Amino acid transport across mammalian intestinal and renal epithelia*. Physiol Rev, 2008. **88**(1): p. 249-86. doi: 10.1152/physrev.00018.2006.
71. Brunet, J., et al., *Toxoplasma gondii exploits UHRF1 and induces host cell cycle arrest at G2 to enable its proliferation*. Cell Microbiol, 2008. **10**(4): p. 908-20.
72. Buchanan, J., et al., *Managing the long term care of inflammatory bowel disease patients: The cost to European health care providers*. J Crohns Colitis, 2011. **5**(4): p. 301-16. doi: 10.1016/j.crohns.2011.02.005. Epub 2011 Mar 10.
73. Burg, J.L., et al., *Molecular analysis of the gene encoding the major surface antigen of Toxoplasma gondii*. J Immunol, 1988. **141**(10): p. 3584-91.
74. Buschmann, M.M., et al., *Occludin OCEL-domain interactions are required for maintenance and regulation of the tight junction barrier to macromolecular flux*. Mol Biol Cell, 2013. **24**(19): p. 3056-68. doi: 10.1091/mbc.E12-09-0688. Epub 2013 Aug 7.
75. Buxton, D., *Protozoan infections (Toxoplasma gondii, Neospora caninum and Sarcocystis spp.) in sheep and goats: recent advances*. Vet Res, 1998. **29**(3-4): p. 289-310.
76. Camacho Leal Mdel, P., et al., *p130Cas/BCAR1 scaffold protein in tissue homeostasis and pathogenesis*. Gene, 2015. **562**(1): p. 1-7.
77. Capaldo, C.T. and I.G. Macara, *Depletion of E-cadherin disrupts establishment but not maintenance of cell junctions in Madin-Darby canine kidney epithelial cells*. Mol Biol Cell, 2007. **18**(1): p. 189-200. Epub 2006 Nov 8.
78. Capaldo, C.T. and A. Nusrat, *Cytokine regulation of tight junctions*. Biochim Biophys Acta, 2009. **1788**(4): p. 864-71. doi: 10.1016/j.bbamem.2008.08.027. Epub 2008 Oct 8.
79. Cario, E., G. Gerken, and D.K. Podolsky, *Toll-like receptor 2 controls mucosal inflammation by regulating epithelial barrier function*.

- Gastroenterology, 2007. **132**(4): p. 1359-74.
80. Carroll, K.M., et al., *Differentiation of rat small intestinal epithelial cells by extracellular matrix*. Am J Physiol, 1988. **254**(3 Pt 1): p. G355-60.
81. Carruthers, V. and J.C. Boothroyd, *Pulling together: an integrated model of Toxoplasma cell invasion*. Curr Opin Microbiol., 2007. **10**(1): p. 83-9. Epub 2006 Jul 11.
82. Carruthers, V.B., *Host cell invasion by the opportunistic pathogen Toxoplasma gondii*. Acta Trop., 2002. **81**(2): p. 111-22.
83. Carruthers, V.B. and F.M. Tomley, *Microneme proteins in apicomplexans*. Subcell Biochem, 2008. **47**: p. 33-45.
84. Caserta, J.A., et al., *Development and application of a mouse intestinal loop model to study the in vivo action of Clostridium perfringens enterotoxin*. Infect Immun, 2011. **79**(8): p. 3020-7.
85. Cepek, K.L., D.L. Rimm, and M.B. Brenner, *Expression of a candidate cadherin in T lymphocytes*. Proc Natl Acad Sci U S A, 1996. **93**(13): p. 6567-71.
86. Cerede, O., et al., *Synergistic role of micronemal proteins in Toxoplasma gondii virulence*. J Exp Med., 2005. **201**(3): p. 453-63. Epub 2005 Jan 31.
87. Cereijido, M., R.G. Contreras, and L. Gonzalez-Mariscal, *Development and alteration of polarity*. Annu Rev Physiol, 1989. **51**: p. 785-95.
88. Cereijido, M., et al., *Tight junction and polarity interaction in the transporting epithelial phenotype*. Biochim Biophys Acta., 2008. **1778**(3): p. 770-93. Epub 2007 Sep 15.
89. Cereijido, M., et al., *Polarized monolayers formed by epithelial cells on a permeable and translucent support*. J Cell Biol, 1978. **77**(3): p. 853-80.
90. Cesbron-Delauw, M.F., et al., *Similarities between the primary structures of two distinct major surface proteins of Toxoplasma gondii*. J Biol Chem., 1994. **269**(23): p. 16217-22.
91. Chandramohanadas, R., et al., *Apicomplexan parasites co-opt host calpains to facilitate their escape from infected cells*. Science, 2009. **324**(5928): p. 794-7.
92. Chang, H., C. Zhang, and Y. Cao, *Expression and distribution of symplekin regulates the assembly and function of the epithelial tight junction*. Histochem Cell Biol, 2012. **137**(3): p. 319-27.
93. Chen, D., et al., *The loss of alphaSNAP downregulates the expression of occludin in the intestinal epithelial cell of acute pancreatitis model*. Pancreatology, 2014. **14**(5): p. 347-55.
94. Chen, H., D.M. Choudhury, and S.W. Craig, *Coincidence of actin filaments and talin is required to activate vinculin*. J Biol Chem., 2006. **281**(52): p. 40389-98. Epub 2006 Oct 29.
95. Chen, Z., O.S. Harb, and D.S. Roos, *In silico identification of specialized secretory-organelle proteins in apicomplexan parasites and in vivo validation in Toxoplasma gondii*. PLoS One., 2008. **3**(10): p. e3611. doi: 10.1371/journal.pone.0003611. Epub 2008 Oct 31.

96. Cheroutre, H., F. Lambolez, and D. Mucida, *The light and dark sides of intestinal intraepithelial lymphocytes*. Nat Rev Immunol., 2011. **11**(7): p. 445-56. doi: 10.1038/nri3007.
97. Chiba, H., et al., *Transmembrane proteins of tight junctions*. Biochim Biophys Acta, 2008. **1778**(3): p. 588-600.
98. Chtanova, T., et al., *Real-time interactive two-photon photoconversion of recirculating lymphocytes for discontinuous cell tracking in live adult mice*. J Biophotonics, 2014. **7**(6): p. 425-33.
99. Citi, S., et al., *Cingulin, a new peripheral component of tight junctions*. Nature., 1988. **333**(6170): p. 272-6.
100. Citi, S., et al., *Cingulin: characterization and localization*. J Cell Sci., 1989. **93**(Pt 1): p. 107-22.
101. Claude, P., *Morphological factors influencing transepithelial permeability: a model for the resistance of the zonula occludens*. J Membr Biol., 1978. **39**(2-3): p. 219-32.
102. Claude, P. and D.A. Goodenough, *Fracture faces of zonulae occludentes from "tight" and "leaky" epithelia*. J Cell Biol., 1973. **58**(2): p. 390-400.
103. Clayburgh, D.R., et al., *Coordinated epithelial NHE3 inhibition and barrier dysfunction are required for TNF-mediated diarrhea in vivo*. J Clin Invest., 2006. **116**(10): p. 2682-94.
104. Cohen, A.M., et al., *Characterisation of global protein expression by two-dimensional electrophoresis and mass spectrometry: proteomics of Toxoplasma gondii*. Int J Parasitol, 2002. **32**(1): p. 39-51.
105. Cohen, C.J., et al., *The coxsackievirus and adenovirus receptor is a transmembrane component of the tight junction*. Proc Natl Acad Sci U S A., 2001. **98**(26): p. 15191-6. Epub 2001 Dec 4.
106. Cook, A.J., et al., *Sources of toxoplasma infection in pregnant women: European multicentre case-control study. European Research Network on Congenital Toxoplasmosis*. Bmj., 2000. **321**(7254): p. 142-7.
107. Coombes, J.L., et al., *Motile invaded neutrophils in the small intestine of Toxoplasma gondii-infected mice reveal a potential mechanism for parasite spread*. Proc Natl Acad Sci U S A, 2013. **110**(21): p. E1913-22.
108. Coppens, I., et al., *Toxoplasma gondii sequesters lysosomes from mammalian hosts in the vacuolar space*. Cell, 2006. **125**(2): p. 261-74.
109. Cordenonsi, M., et al., *Xenopus laevis occludin. Identification of in vitro phosphorylation sites by protein kinase CK2 and association with cingulin*. Eur J Biochem, 1999. **264**(2): p. 374-84.
110. Cording, J., et al., *In tight junctions, claudins regulate the interactions between occludin, tricellulin and marvelD3, which, inversely, modulate claudin oligomerization*. J Cell Sci., 2013. **126**(Pt 2): p. 554-64. doi: 10.1242/jcs.114306. Epub 2012 Nov 30.
111. Courret, N., et al., *CD11c- and CD11b-expressing mouse leukocytes transport single Toxoplasma gondii tachyzoites to the brain*. Blood., 2006. **107**(1): p. 309-16. Epub 2005 Jul 28.

112. Cox, J. and M. Mann, *MaxQuant enables high peptide identification rates, individualized p.p.b.-range mass accuracies and proteome-wide protein quantification*. Nat Biotechnol., 2008. **26**(12): p. 1367-72. doi: 10.1038/nbt.1511. Epub 2008 Nov 30.
113. Coyne, C.B. and J.M. Bergelson, *CAR: a virus receptor within the tight junction*. Adv Drug Deliv Rev., 2005. **57**(6): p. 869-82.
114. Cummings, J.R., S. Keshav, and S.P. Travis, *Medical management of Crohn's disease*. Bmj., 2008. **336**(7652): p. 1062-6. doi: 10.1136/bmj.39547.603218.AE.
115. Cummins, P.M., *Occludin: one protein, many forms*. Mol Cell Biol, 2012. **32**(2): p. 242-50.
116. Cunningham, K.E. and J.R. Turner, *Myosin light chain kinase: pulling the strings of epithelial tight junction function*. Ann N Y Acad Sci, 2012. **1258**: p. 34-42.
117. D'Inca, R., et al., *Intestinal permeability test as a predictor of clinical course in Crohn's disease*. Am J Gastroenterol., 1999. **94**(10): p. 2956-60.
118. da Silva, C.V., et al., *ARF6, PI3-kinase and host cell actin cytoskeleton in Toxoplasma gondii cell invasion*. Biochem Biophys Res Commun, 2009. **378**(3): p. 656-61.
119. da Silva, R.A., et al., *[Infestation by triatomines in rural settlement and resettlement areas the Region of Pontal do Paranapanema, State of Sao Paulo]*. Rev Soc Bras Med Trop., 2007. **40**(5): p. 527-32.
120. da Silva, R.C. and H. Langoni, *Toxoplasma gondii: host-parasite interaction and behavior manipulation*. Parasitol Res., 2009. **105**(4): p. 893-8. doi: 10.1007/s00436-009-1526-6. Epub 2009 Jun 23.
121. Dalton, J.E., et al., *Intraepithelial gammadelta⁺ lymphocytes maintain the integrity of intestinal epithelial tight junctions in response to infection*. Gastroenterology., 2006. **131**(3): p. 818-29.
122. Danial, N.N., *BAD: undertaker by night, candyman by day*. Oncogene, 2008. **27 Suppl 1**: p. S53-70.
123. Darsigny, M., et al., *Loss of hepatocyte-nuclear-factor-4alpha affects colonic ion transport and causes chronic inflammation resembling inflammatory bowel disease in mice*. PLoS One, 2009. **4**(10): p. e7609.
124. Datta, S.R., et al., *Akt phosphorylation of BAD couples survival signals to the cell-intrinsic death machinery*. Cell, 1997. **91**(2): p. 231-41.
125. de Munro, R.M., et al., *Spontaneous cystogenesis of Toxoplasma gondii in feline epithelial cells in vitro*. Folia Parasitol (Praha), 2014. **61**(2): p. 113-9.
126. Defilippi, P., P. Di Stefano, and S. Cabodi, *p130Cas: a versatile scaffold in signaling networks*. Trends Cell Biol, 2006. **16**(5): p. 257-63.
127. Delom, F. and E. Chevet, *Phosphoprotein analysis: from proteins to proteomes*. Proteome Sci, 2006. **4**: p. 15.
128. Delorme-Walker, V., et al., *Toxofilin upregulates the host cortical*

- actin cytoskeleton dynamics, facilitating Toxoplasma invasion.* J Cell Sci, 2012. **125**(Pt 18): p. 4333-42.
129. Denker, B.M., et al., *Involvement of a heterotrimeric G protein alpha subunit in tight junction biogenesis.* J Biol Chem., 1996. **271**(42): p. 25750-3.
130. Derouin, F. and H. Pelloux, *Prevention of toxoplasmosis in transplant patients.* Clin Microbiol Infect., 2008. **14**(12): p. 1089-101. doi: 10.1111/j.1469-0691.2008.02091.x.
131. Derouin, F., P. Thulliez, and S. Romand, *Schizophrenia and serological methods for diagnosis of toxoplasmosis.* Clin Infect Dis., 2002. **34**(1): p. 127-9.
132. Di Pierro, M., et al., *Zonula occludens toxin structure-function analysis. Identification of the fragment biologically active on tight junctions and of the zonulin receptor binding domain.* J Biol Chem, 2001. **276**(22): p. 19160-5.
133. Diamond, J.M., *Channels in epithelial cell membranes and junctions.* Fed Proc., 1978. **37**(12): p. 2639-43.
134. Dimier, I.H. and D.T. Bout, *Rat intestinal epithelial cell line IEC-6 is activated by recombinant interferon-gamma to inhibit replication of the coccidian Toxoplasma gondii.* Eur J Immunol, 1993. **23**(4): p. 981-3.
135. Ding, L., et al., *Inflammation and disruption of the mucosal architecture in claudin-7-deficient mice.* Gastroenterology, 2012. **142**(2): p. 305-15.
136. Dobrosotskaya, I., R.K. Guy, and G.L. James, *MAGI-1, a membrane-associated guanylate kinase with a unique arrangement of protein-protein interaction domains.* J Biol Chem., 1997. **272**(50): p. 31589-97.
137. Dobrowolski, J.M., V.B. Carruthers, and L.D. Sibley, *Participation of myosin in gliding motility and host cell invasion by Toxoplasma gondii.* Mol Microbiol., 1997. **26**(1): p. 163-73.
138. Dorfel, M.J. and O. Huber, *A phosphorylation hotspot within the occludin C-terminal domain.* Ann N Y Acad Sci, 2012.
139. Dorfel, M.J. and O. Huber, *Modulation of tight junction structure and function by kinases and phosphatases targeting occludin.* J Biomed Biotechnol, 2012: p. 23.
140. Dorfel, M.J., et al., *CK2-dependent phosphorylation of occludin regulates the interaction with ZO-proteins and tight junction integrity.* Cell Commun Signal, 2013. **11**(1): p. 40.
141. Dorfel, M.J., J.K. Westphal, and O. Huber, *Differential phosphorylation of occludin and tricellulin by CK2 and CK1.* Ann N Y Acad Sci, 2009. **1165**: p. 69-73.
142. Dragsten, P.R., R. Blumenthal, and J.S. Handler, *Membrane asymmetry in epithelia: is the tight junction a barrier to diffusion in the plasma membrane?* Nature., 1981. **294**(5843): p. 718-22.
143. Drenckhahn, D. and R. Dermietzel, *Organization of the actin filament cytoskeleton in the intestinal brush border: a quantitative and qualitative immunoelectron microscope study.* J Cell Biol., 1988. **107**(3): p. 1037-48.

144. Dubey, J.P., *Bradyzoite-induced murine toxoplasmosis: stage conversion, pathogenesis, and tissue cyst formation in mice fed bradyzoites of different strains of Toxoplasma gondii*. J Eukaryot Microbiol., 1997. **44**(6): p. 592-602.
145. Dubey, J.P., *Advances in the life cycle of Toxoplasma gondii*. Int J Parasitol., 1998. **28**(7): p. 1019-24.
146. Dubey, J.P., *Re-examination of resistance of Toxoplasma gondii tachyzoites and bradyzoites to pepsin and trypsin digestion*. Parasitology., 1998. **116**(Pt 1): p. 43-50.
147. Dubey, J.P., *Toxoplasmosis in pigs--the last 20 years*. Vet Parasitol., 2009. **164**(2-4): p. 89-103. doi: 10.1016/j.vetpar.2009.05.018. Epub 2009 May 23.
148. Dubey, J.P., D.S. Lindsay, and C.A. Speer, *Structures of Toxoplasma gondii tachyzoites, bradyzoites, and sporozoites and biology and development of tissue cysts*. Clin Microbiol Rev., 1998. **11**(2): p. 267-99.
149. Dubey, J.P., et al., *Oocyst-induced murine toxoplasmosis: life cycle, pathogenicity, and stage conversion in mice fed Toxoplasma gondii oocysts*. J Parasitol., 1997. **83**(5): p. 870-82.
150. Dubremetz, J.F., *Rhoptries are major players in Toxoplasma gondii invasion and host cell interaction*. Cell Microbiol., 2007. **9**(4): p. 841-8.
151. Duckworth, C.A. and A.J. Watson, *Analysis of epithelial cell shedding and gaps in the intestinal epithelium*. Methods Mol Biol, 2011. **763**: p. 105-14.
152. Dupont, C.D., D.A. Christian, and C.A. Hunter, *Immune response and immunopathology during toxoplasmosis*. Semin Immunopathol., 2012. **34**(6): p. 793-813. doi: 10.1007/s00281-012-0339-3. Epub 2012 Sep 7.
153. Dupont, C.D., et al., *Parasite fate and involvement of infected cells in the induction of CD4+ and CD8+ T cell responses to Toxoplasma gondii*. PLoS Pathog., 2014. **10**(4): p. e1004047. doi: 10.1371/journal.ppat.1004047. eCollection 2014 Apr.
154. Duronio, V., *The life of a cell: apoptosis regulation by the PI3K/PKB pathway*. Biochem J, 2008. **415**(3): p. 333-44.
155. Dvorak, J.A. and M.S. Crane, *Vertebrate cell cycle modulates infection by protozoan parasites*. Science, 1981. **214**(4524): p. 1034-6.
156. Dzierszinski, F., et al., *Targeted disruption of the glycosylphosphatidylinositol-anchored surface antigen SAG3 gene in Toxoplasma gondii decreases host cell adhesion and drastically reduces virulence in mice*. Mol Microbiol., 2000. **37**(3): p. 574-82.
157. Dzierszinski, F., et al., *Dynamics of Toxoplasma gondii differentiation*. Eukaryot Cell., 2004. **3**(4): p. 992-1003.
158. Ebnet, K., et al., *Junctional adhesion molecule interacts with the PDZ domain-containing proteins AF-6 and ZO-1*. J Biol Chem., 2000. **275**(36): p. 27979-88.
159. Ebnet, K., et al., *Junctional adhesion molecules (JAMs): more molecules with dual functions?* J Cell Sci., 2004. **117**(Pt 1): p. 19-29.

160. Edelblum, K.L., et al., *Dynamic migration of gammadelta intraepithelial lymphocytes requires occludin*. Proc Natl Acad Sci U S A., 2012. **109**(18): p. 7097-102. doi: 10.1073/pnas.1112519109. Epub 2012 Apr 17.
161. Egan, C.E., S.B. Cohen, and E.Y. Denkers, *Insights into inflammatory bowel disease using Toxoplasma gondii as an infectious trigger*. Immunol Cell Biol, 2012. **90**(7): p. 668-75.
162. Egarter, S., et al., *The toxoplasma Acto-MyoA motor complex is important but not essential for gliding motility and host cell invasion*. PLoS One., 2014. **9**(3): p. e91819. doi: 10.1371/journal.pone.0091819. eCollection 2014.
163. Elias, M.C., et al., *Chromosome localization changes in the Trypanosoma cruzi nucleus*. Eukaryot Cell., 2002. **1**(6): p. 944-53.
164. Elphick, D.A. and Y.R. Mahida, *Paneth cells: their role in innate immunity and inflammatory disease*. Gut., 2005. **54**(12): p. 1802-9.
165. Etournay, R., et al., *Shroom2, a myosin-VIIa- and actin-binding protein, directly interacts with ZO-1 at tight junctions*. J Cell Sci., 2007. **120**(Pt 16): p. 2838-50. Epub 2007 Jul 31.
166. Ewaschuk, J.B., et al., *The role of antibiotic and probiotic therapies in current and future management of inflammatory bowel disease*. Curr Gastroenterol Rep., 2006. **8**(6): p. 486-98.
167. Fanning, A.S. and J.M. Anderson, *Protein-protein interactions: PDZ domain networks*. Curr Biol., 1996. **6**(11): p. 1385-8.
168. Fanning, A.S. and J.M. Anderson, *Zonula occludens-1 and -2 are cytosolic scaffolds that regulate the assembly of cellular junctions*. Ann N Y Acad Sci, 2009.
169. Fanning, A.S., et al., *The tight junction protein ZO-1 establishes a link between the transmembrane protein occludin and the actin cytoskeleton*. J Biol Chem., 1998. **273**(45): p. 29745-53.
170. Fanning, A.S., L.L. Mitic, and J.M. Anderson, *Transmembrane proteins in the tight junction barrier*. J Am Soc Nephrol., 1999. **10**(6): p. 1337-45.
171. Farkas, A.E., C.T. Capaldo, and A. Nusrat, *Regulation of epithelial proliferation by tight junction proteins*. Ann N Y Acad Sci, 2012.
172. Farquhar, M.G. and G.E. Palade, *Junctional complexes in various epithelia*. J Cell Biol, 1963. **17**: p. 375-412.
173. Farshori, P. and B. Kachar, *Redistribution and phosphorylation of occludin during opening and resealing of tight junctions in cultured epithelial cells*. J Membr Biol, 1999. **170**(2): p. 147-56.
174. Fasano, A., et al., *Zonula occludens toxin modulates tight junctions through protein kinase C-dependent actin reorganization, in vitro*. J Clin Invest., 1995. **96**(2): p. 710-20.
175. Faust, N., et al., *Insertion of enhanced green fluorescent protein into the lysozyme gene creates mice with green fluorescent granulocytes and macrophages*. Blood, 2000. **96**(2): p. 719-26.
176. Feldman, G.J., J.M. Mullin, and M.P. Ryan, *Occludin: structure, function and regulation*. Adv Drug Deliv Rev., 2005. **57**(6): p. 883-917.
177. Fentress, S.J., et al., *The arginine-rich N-terminal domain of ROP18*

- is necessary for vacuole targeting and virulence of *Toxoplasma gondii*.* Cell Microbiol., 2012. **14**(12): p. 1921-33. doi: 10.1111/cmi.12022. Epub 2012 Sep 20.
178. Ferraris, R.P. and J. Diamond, *Regulation of intestinal sugar transport.* Physiol Rev., 1997. **77**(1): p. 257-302.
 179. Ferreira, I.M., et al., *Toxoplasma gondii: genotyping of strains from Brazilian AIDS patients with cerebral toxoplasmosis by multilocus PCR-RFLP markers.* Exp Parasitol., 2008. **118**(2): p. 221-7. Epub 2007 Aug 19.
 180. Fihn, B.M., A. Sjoqvist, and M. Jodal, *Permeability of the rat small intestinal epithelium along the villus-crypt axis: effects of glucose transport.* Gastroenterology., 2000. **119**(4): p. 1029-36.
 181. Fink, L., et al., *Laser-microdissection for cell type- and compartment-specific analyses on genomic and proteomic level.* Exp Toxicol Pathol, 2006. **57 Suppl 2**: p. 25-9.
 182. Flegr, J., et al., *Increased risk of traffic accidents in subjects with latent toxoplasmosis: a retrospective case-control study.* BMC Infect Dis, 2002. **2**: p. 11.
 183. Fletcher, S.J., et al., *Analysis of occludin trafficking, demonstrating continuous endocytosis, degradation, recycling and biosynthetic secretory trafficking.* PLoS One., 2014. **9**(11): p. e111176. doi: 10.1371/journal.pone.0111176. eCollection 2014.
 184. Fletcher, S.J. and J.Z. Rappoport, *Tight junction regulation through vesicle trafficking: bringing cells together.* Biochem Soc Trans., 2014. **42**(1): p. 195-200. doi: 10.1042/BST20130162.
 185. Frenal, K. and D. Soldati-Favre, *Role of the parasite and host cytoskeleton in apicomplexa parasitism.* Cell Host Microbe, 2009. **5**(6): p. 602-11.
 186. Fujimoto, K., *Freeze-fracture replica electron microscopy combined with SDS digestion for cytochemical labeling of integral membrane proteins. Application to the immunogold labeling of intercellular junctional complexes.* J Cell Sci., 1995. **108**(Pt 11): p. 3443-9.
 187. Fujita, H., et al., *Differential expression and subcellular localization of claudin-7, -8, -12, -13, and -15 along the mouse intestine.* J Histochem Cytochem., 2006. **54**(8): p. 933-44. Epub 2006 May 1.
 188. Fujita, K., et al., *Clostridium perfringens enterotoxin binds to the second extracellular loop of claudin-3, a tight junction integral membrane protein.* FEBS Lett, 2000. **476**(3): p. 258-61.
 189. Furtado, J.M., et al., *Toxoplasma gondii tachyzoites cross retinal endothelium assisted by intercellular adhesion molecule-1 in vitro.* Immunol Cell Biol. 2012. **90**(9): p912-915.
 190. Furtado, G.C., Y. Cao, and K.A. Joiner, *Laminin on *Toxoplasma gondii* mediates parasite binding to the beta 1 integrin receptor alpha 6 beta 1 on human foreskin fibroblasts and Chinese hamster ovary cells.* Infect Immun., 1992. **60**(11): p. 4925-31.
 191. Furuse, M., *Knockout animals and natural mutations as experimental and diagnostic tool for studying tight junction functions in vivo.* Biochim Biophys Acta, 2009. **1788**(4): p. 813-9.
 192. Furuse, M., *Molecular basis of the core structure of tight junctions.*

- Cold Spring Harb Perspect Biol., 2010. **2**(1): p. a002907. doi: 10.1101/cshperspect.a002907.
193. Furuse, M., et al., *Overexpression of occludin, a tight junction-associated integral membrane protein, induces the formation of intracellular multilamellar bodies bearing tight junction-like structures*. J Cell Sci, 1996. **109** (Pt 2): p. 429-35.
 194. Furuse, M., et al., *Claudin-1 and -2: novel integral membrane proteins localizing at tight junctions with no sequence similarity to occludin*. J Cell Biol., 1998. **141**(7): p. 1539-50.
 195. Furuse, M., et al., *Conversion of zonulae occludentes from tight to leaky strand type by introducing claudin-2 into Madin-Darby canine kidney I cells*. J Cell Biol, 2001. **153**(2): p. 263-72.
 196. Furuse, M., et al., *Occludin: a novel integral membrane protein localizing at tight junctions*. J Cell Biol., 1993. **123**(6 Pt 2): p. 1777-88.
 197. Furuse, M., et al., *Direct association of occludin with ZO-1 and its possible involvement in the localization of occludin at tight junctions*. J Cell Biol., 1994. **127**(6 Pt 1): p. 1617-26.
 198. Furuse, M., et al., *A single gene product, claudin-1 or -2, reconstitutes tight junction strands and recruits occludin in fibroblasts*. J Cell Biol, 1998. **143**(2): p. 391-401.
 199. Furuse, M. and S. Tsukita, *Claudins in occluding junctions of humans and flies*. Trends Cell Biol., 2006. **16**(4): p. 181-8. Epub 2006 Mar 14.
 200. Gajria, B., et al., *ToxoDB: an integrated Toxoplasma gondii database resource*. Nucleic Acids Res., 2008. **36**(Database issue): p. D553-6. Epub 2007 Nov 14.
 201. Garcia, J.L., *Vaccination concepts against Toxoplasma gondii*. Expert Rev Vaccines., 2009. **8**(2): p. 215-25. doi: 10.1586/14760584.8.2.215.
 202. Garrod, K.R., et al., *Dissecting T cell contraction in vivo using a genetically encoded reporter of apoptosis*. Cell Rep, 2012. **2**(5): p. 1438-47.
 203. Gasteiger, J., *Chemoinformatics: a new field with a long tradition*. Anal Bioanal Chem, 2006. **384**(1): p. 57-64.
 204. Ghassemifar, M.R., et al., *Occludin TM4(-): an isoform of the tight junction protein present in primates lacking the fourth transmembrane domain*. J Cell Sci., 2002. **115**(Pt 15): p. 3171-80.
 205. Gilbert, L.A., et al., *Toxoplasma gondii targets a protein phosphatase 2C to the nuclei of infected host cells*. Eukaryot Cell, 2007. **6**(1): p. 73-83.
 206. Gillin, F.D., D.S. Reiner, and J.M. McCaffery, *Cell biology of the primitive eukaryote Giardia lamblia*. Annu Rev Microbiol, 1996. **50**: p. 679-705.
 207. Glotfelty, L.G., et al., *Microtubules are required for efficient epithelial tight junction homeostasis and restoration*. Am J Physiol Cell Physiol., 2014. **307**(3): p. C245-54. doi: 10.1152/ajpcell.00336.2013. Epub 2014 Jun 11.
 208. Gonzalez, V., et al., *Host cell entry by apicomplexa parasites requires*

- actin polymerization in the host cell.* Cell Host Microbe, 2009. **5**(3): p. 259-72.
- 209. Gonzalez-Mariscal, L., et al., *Tight junction proteins.* Prog Biophys Mol Biol, 2003. **81**(1): p. 1-44.
 - 210. Gonzalez-Mariscal, L., R. Tapia, and D. Chamorro, *Crosstalk of tight junction components with signaling pathways.* Biochim Biophys Acta, 2008. **1778**(3): p. 729-56.
 - 211. Goodenough, D.A. and D.L. Paul, *Beyond the gap: functions of unpaired connexon channels.* Nat Rev Mol Cell Biol., 2003. **4**(4): p. 285-94.
 - 212. Goodenough, D.A. and J.P. Revel, *A fine structural analysis of intercellular junctions in the mouse liver.* J Cell Biol., 1970. **45**(2): p. 272-90.
 - 213. Goplen, M., et al., *Entamoeba histolytica contains an occludin-like protein that can alter colonic epithelial barrier function.* PLoS One, 2013. **8**(9): p. e73339. doi: 10.1371/journal.pone.0073339. eCollection 2013.
 - 214. Graham, W.V., et al., *No static at all.* Ann N Y Acad Sci, 2009.
 - 215. Gregg, B., et al., *Replication and distribution of Toxoplasma gondii in the small intestine after oral infection with tissue cysts.* Infect Immun, 2013. **81**(5): p. 1635-43.
 - 216. Grigg, M.E., et al., *Unusual abundance of atypical strains associated with human ocular toxoplasmosis.* J Infect Dis., 2001. **184**(5): p. 633-9. Epub 2001 Jul 24.
 - 217. Grimwood, J., J.R. Mineo, and L.H. Kasper, *Attachment of Toxoplasma gondii to host cells is host cell cycle dependent.* Infect Immun, 1996. **64**(10): p. 4099-104.
 - 218. Grimwood, J. and J.E. Smith, *Toxoplasma gondii: the role of a 30-kDa surface protein in host cell invasion.* Exp Parasitol., 1992. **74**(1): p. 106-11.
 - 219. Grimwood, J. and J.E. Smith, *Toxoplasma gondii: the role of parasite surface and secreted proteins in host cell invasion.* Int J Parasitol, 1996. **26**(2): p. 169-73.
 - 220. Gu, J.M., et al., *A novel splice variant of occludin deleted in exon 9 and its role in cell apoptosis and invasion.* Febs J., 2008. **275**(12): p. 3145-56. doi: 10.1111/j.1742-4658.2008.06467.x. Epub 2008 May 16.
 - 221. Gubbels, M.J., C. Li, and B. Striepen, *High-throughput growth assay for Toxoplasma gondii using yellow fluorescent protein.* Antimicrob Agents Chemother., 2003. **47**(1): p. 309-16.
 - 222. Guillemot, L., et al., *The cytoplasmic plaque of tight junctions: a scaffolding and signalling center.* Biochim Biophys Acta., 2008. **1778**(3): p. 601-13. doi: 10.1016/j.bbamem.2007.09.032. Epub 2007 Oct 9.
 - 223. Gumbiner, B., *Structure, biochemistry, and assembly of epithelial tight junctions.* Am J Physiol., 1987. **253**(6 Pt 1): p. C749-58.
 - 224. Gumbiner, B.M., *Breaking through the tight junction barrier.* J Cell Biol., 1993. **123**(6 Pt 2): p. 1631-3.
 - 225. Gumbiner, B.M., *Regulation of cadherin-mediated adhesion in*

- morphogenesis*. Nat Rev Mol Cell Biol., 2005. **6**(8): p. 622-34.
226. Guo, X., et al., *Regulation of adherens junctions and epithelial paracellular permeability: a novel function for polyamines*. Am J Physiol Cell Physiol, 2003. **285**(5): p. C1174-87.
 227. Guy-Grand, D., et al., *Two gut intraepithelial CD8+ lymphocyte populations with different T cell receptors: a role for the gut epithelium in T cell differentiation*. J Exp Med., 1991. **173**(2): p. 471-81.
 228. Hakansson, S., et al., *Time-lapse video microscopy of gliding motility in Toxoplasma gondii reveals a novel, biphasic mechanism of cell locomotion*. Mol Biol Cell, 1999. **10**(11): p. 3539-47.
 229. Hakimi, M.A. and A. Bougdour, *Toxoplasma's ways of manipulating the host transcriptome via secreted effectors*. Curr Opin Microbiol, 2015. **26**: p. 24-31.
 230. Hamazaki, Y., et al., *Multi-PDZ domain protein 1 (MUPP1) is concentrated at tight junctions through its possible interaction with claudin-1 and junctional adhesion molecule*. J Biol Chem., 2002. **277**(1): p. 455-61. Epub 2001 Oct 31.
 231. Hanajima-Ozawa, M., et al., *Enteropathogenic Escherichia coli, Shigella flexneri, and Listeria monocytogenes recruit a junctional protein, zonula occludens-1, to actin tails and pedestals*. Infect Immun, 2007. **75**(2): p. 565-73.
 232. Harhaj, N.S. and D.A. Antonetti, *Regulation of tight junctions and loss of barrier function in pathophysiology*. Int J Biochem Cell Biol., 2004. **36**(7): p. 1206-37.
 232. Harhaj, N.S., et al., *VEGF activation of protein kinase C stimulates occludin phosphorylation and contributes to endothelial permeability*. Invest Ophthalmol Vis Sci, 2006. **47**(11): p. 5106-15.
 234. Harsha, H.C., H. Molina, and A. Pandey, *Quantitative proteomics using stable isotope labeling with amino acids in cell culture*. Nat Protoc, 2008. **3**(3): p. 505-16.
 235. Hartsock, A. and W.J. Nelson, *Adherens and tight junctions: structure, function and connections to the actin cytoskeleton*. Biochim Biophys Acta., 2008. **1778**(3): p. 660-9. Epub 2007 Jul 27.
 236. Hayashi, R., et al., *Comparison of drug transporter gene expression and functionality in Caco-2 cells from 10 different laboratories*. Eur J Pharm Sci, 2008. **35**(5): p. 383-96.
 237. Heimesaat, M.M., et al., *Gram-negative bacteria aggravate murine small intestinal Th1-type immunopathology following oral infection with Toxoplasma gondii*. J Immunol., 2006. **177**(12): p. 8785-95.
 238. Heller, F., et al., *Interleukin-13 is the key effector Th2 cytokine in ulcerative colitis that affects epithelial tight junctions, apoptosis, and cell restitution*. Gastroenterology., 2005. **129**(2): p. 550-64.
 239. Hermiston, M.L. and J.I. Gordon, *Inflammatory bowel disease and adenomas in mice expressing a dominant negative N-cadherin*. Science., 1995. **270**(5239): p. 1203-7.
 240. Hidalgo, I.J., T.J. Raub, and R.T. Borchardt, *Characterization of the human colon carcinoma cell line (Caco-2) as a model system for intestinal epithelial permeability*. Gastroenterology, 1989. **96**(3): p.

736-49.

241. Hildebrand, J.D., *Shroom regulates epithelial cell shape via the apical positioning of an actomyosin network*. *J Cell Sci.*, 2005. **118**(Pt 22): p. 5191-203. Epub 2005 Oct 25.
242. Hill, D. and J.P. Dubey, *Toxoplasma gondii: transmission, diagnosis and prevention*. *Clin Microbiol Infect.*, 2002. **8**(10): p. 634-40.
243. Hinze-Selch, D., et al., *A controlled prospective study of toxoplasma gondii infection in individuals with schizophrenia: beyond seroprevalence*. *Schizophr Bull.*, 2007. **33**(3): p. 782-8. Epub 2007 Mar 26.
244. Hirabayashi, S., et al., *JAM4, a junctional cell adhesion molecule interacting with a tight junction protein, MAGI-1*. *Mol Cell Biol.*, 2003. **23**(12): p. 4267-82.
245. Hitziger, N., et al., *Dissemination of Toxoplasma gondii to immunoprivileged organs and role of Toll/interleukin-1 receptor signalling for host resistance assessed by in vivo bioluminescence imaging*. *Cell Microbiol.*, 2005. **7**(6): p. 837-48.
246. Hjerrild, M. and S. Gammeltoft, *Phosphoproteomics toolbox: computational biology, protein chemistry and mass spectrometry*. *FEBS Lett*, 2006. **580**(20): p. 4764-70.
247. Hoff, E.F. and V.B. Carruthers, *Is Toxoplasma egress the first step in invasion?* *Trends Parasitol.*, 2002. **18**(6): p. 251-5.
248. Hollander, D., et al., *Increased intestinal permeability in patients with Crohn's disease and their relatives. A possible etiologic factor*. *Ann Intern Med.*, 1986. **105**(6): p. 883-5.
249. Hooper, L.V., D.R. Littman, and A.J. Macpherson, *Interactions between the microbiota and the immune system*. *Science.*, 2012. **336**(6086): p. 1268-73. doi: 10.1126/science.1223490. Epub 2012 Jun 6.
250. Hooper, L.V. and A.J. Macpherson, *Immune adaptations that maintain homeostasis with the intestinal microbiota*. *Nat Rev Immunol.*, 2010. **10**(3): p. 159-69. doi: 10.1038/nri2710.
251. Howe, D.K., et al., *Determination of genotypes of Toxoplasma gondii strains isolated from patients with toxoplasmosis*. *J Clin Microbiol.*, 1997. **35**(6): p. 1411-4.
252. Howe, D.K. and L.D. Sibley, *Toxoplasma gondii comprises three clonal lineages: correlation of parasite genotype with human disease*. *J Infect Dis.*, 1995. **172**(6): p. 1561-6.
253. Howe, D.K., B.C. Summers, and L.D. Sibley, *Acute virulence in mice is associated with markers on chromosome VIII in Toxoplasma gondii*. *Infect Immun.*, 1996. **64**(12): p. 5193-8.
254. Hu, K., et al., *Cytoskeletal components of an invasion machine--the apical complex of Toxoplasma gondii*. *PLoS Pathog*, 2006. **2**(2): p. e13.
255. Humbert, P., S. Russell, and H. Richardson, *Dlg, Scribble and Lgl in cell polarity, cell proliferation and cancer*. *Bioessays.*, 2003. **25**(6): p. 542-53.
256. Hunter, C.A. and L.D. Sibley, *Modulation of innate immunity by Toxoplasma gondii virulence effectors*. *Nat Rev Microbiol.*, 2012.

- 10**(11): p. 766-78. doi: 10.1038/nrmicro2858.
257. Ikenouchi, J., et al., *Tricellulin constitutes a novel barrier at tricellular contacts of epithelial cells*. J Cell Biol., 2005. **171**(6): p. 939-45.
258. Ikenouchi, J., et al., *Loss of occludin affects tricellular localization of tricellulin*. Mol Biol Cell., 2008. **19**(11): p. 4687-93. doi: 10.1091/mbc.E08-05-0530. Epub 2008 Sep 3.
259. Ikenouchi, J., et al., *Requirement of ZO-1 for the formation of belt-like adherens junctions during epithelial cell polarization*. J Cell Biol., 2007. **176**(6): p. 779-86.
260. Inagaki-Ohara, K., et al., *Intraepithelial lymphocytes express junctional molecules in murine small intestine*. Biochem Biophys Res Commun., 2005. **331**(4): p. 977-83.
261. Innes, E.A., *A brief history and overview of Toxoplasma gondii*. Zoonoses Public Health., 2010. **57**(1): p. 1-7. doi: 10.1111/j.1863-2378.2009.01276.x. Epub 2009 Sep 10.
262. Innes, E.A., et al., *Developing vaccines to control protozoan parasites in ruminants: dead or alive?* Vet Parasitol., 2011. **180**(1-2): p. 155-63. doi: 10.1016/j.vetpar.2011.05.036. Epub 2011 May 27.
263. Isaac-Renton, J., et al., *Detection of Toxoplasma gondii oocysts in drinking water*. Appl Environ Microbiol., 1998. **64**(6): p. 2278-80.
264. Ismail, A.S., et al., *Gammadelta intraepithelial lymphocytes are essential mediators of host-microbial homeostasis at the intestinal mucosal surface*. Proc Natl Acad Sci U S A., 2011. **108**(21): p. 8743-8. doi: 10.1073/pnas.1019574108. Epub 2011 May 9.
265. Itoh, M., *ARHGEF11, a regulator of junction-associated actomyosin in epithelial cells*. Tissue Barriers, 2013. **1**(2): p. e24221.
266. Itoh, M., et al., *Direct binding of three tight junction-associated MAGUKs, ZO-1, ZO-2, and ZO-3, with the COOH termini of claudins*. J Cell Biol., 1999. **147**(6): p. 1351-63.
267. Itoh, M., et al., *Involvement of ZO-1 in cadherin-based cell adhesion through its direct binding to alpha catenin and actin filaments*. J Cell Biol., 1997. **138**(1): p. 181-92.
268. Itoh, M., et al., *Rho GTP exchange factor ARHGEF11 regulates the integrity of epithelial junctions by connecting ZO-1 and RhoA- myosin II signaling*. Proc Natl Acad Sci U S A, 2012. **109**(25): p. 9905-10.
269. Ivanov, A.I., *Actin motors that drive formation and disassembly of epithelial apical junctions*. Front Biosci, 2008. **13**: p. 6662-81.
270. Ivanov, A.I., A. Nusrat, and C.A. Parkos, *Endocytosis of epithelial apical junctional proteins by a clathrin-mediated pathway into a unique storage compartment*. Mol Biol Cell, 2004. **15**(1): p. 176-88.
271. Ivanov, A.I., A. Nusrat, and C.A. Parkos, *Endocytosis of the apical junctional complex: mechanisms and possible roles in regulation of epithelial barriers*. Bioessays., 2005. **27**(4): p. 356-65.
272. Ivanov, A.I., C.A. Parkos, and A. Nusrat, *Cytoskeletal regulation of epithelial barrier function during inflammation*. Am J Pathol., 2010. **177**(2): p. 512-24. doi: 10.2353/ajpath.2010.100168. Epub 2010 Jun 25.

273. Jan, G., et al., *A Toxoplasma type 2C serine-threonine phosphatase is involved in parasite growth in the mammalian host cell*. Microbes Infect, 2009. **11**(12): p. 935-45.
274. Jeng, Y.J., C.S. Watson, and M.L. Thomas, *Identification of vitamin D-stimulated alkaline phosphatase in IEC-6 cells, a rat small intestine crypt cell line*. Exp Cell Res, 1994. **212**(2): p. 338-43.
275. Jepson, M.A., et al., *Rapid disruption of epithelial barrier function by Salmonella typhimurium is associated with structural modification of intercellular junctions*. Infect Immun, 1995. **63**(1): p. 356-9.
276. Jesaitis, L.A. and D.A. Goodenough, *Molecular characterization and tissue distribution of ZO-2, a tight junction protein homologous to ZO-1 and the Drosophila discs-large tumor suppressor protein*. J Cell Biol, 1994. **124**(6): p. 949-61.
277. Jia, B., et al., *Genome-wide comparative analysis revealed significant transcriptome changes in mice after Toxoplasma gondii infection*. Parasit Vectors, 2013. **6**: p. 161.
278. Joberty, G., et al., *The cell-polarity protein Par6 links Par3 and atypical protein kinase C to Cdc42*. Nat Cell Biol, 2000. **2**(8): p. 531-9.
279. Johansson, M.E. and G.C. Hansson, *Is the intestinal goblet cell a major immune cell?* Cell Host Microbe., 2014. **15**(3): p. 251-2. doi: 10.1016/j.chom.2014.02.014.
280. Jones, J.L. and J.P. Dubey, *Foodborne toxoplasmosis*. Clin Infect Dis., 2012. **55**(6): p. 845-51. doi: 10.1093/cid/cis508. Epub 2012 May 22.
281. Jones, J.L., et al., *Toxoplasma gondii infection in the United States: seroprevalence and risk factors*. Am J Epidemiol., 2001. **154**(4): p. 357-65.
282. Jones, J.L., et al., *Congenital toxoplasmosis: a review*. Obstet Gynecol Surv., 2001. **56**(5): p. 296-305.
283. Juge, N., *Microbial adhesins to gastrointestinal mucus*. Trends Microbiol., 2012. **20**(1): p. 30-9. doi: 10.1016/j.tim.2011.10.001. Epub 2011 Nov 14.
284. Kale, G., et al., *Tyrosine phosphorylation of occludin attenuates its interactions with ZO-1, ZO-2, and ZO-3*. Biochem Biophys Res Commun, 2003. **302**(2): p. 324-9.
285. Karam, S.M., *Lineage commitment and maturation of epithelial cells in the gut*. Front Biosci, 1999: p. D286-98.
286. Kasper, L.H., J.H. Crabb, and E.R. Pfefferkorn, *Purification of a major membrane protein of Toxoplasma gondii by immunoabsorption with a monoclonal antibody*. J Immunol., 1983. **130**(5): p. 2407-12.
287. Kasper, L.H. and J.R. Mineo, *Attachment and invasion of host cells by Toxoplasma gondii*. Parasitol Today., 1994. **10**(5): p. 184-8.
288. Katsume, T., et al., *Cortactin associates with the cell-cell junction protein ZO-1 in both Drosophila and mouse*. J Biol Chem., 1998. **273**(45): p. 29672-7.
289. Katz, K.D., et al., *Intestinal permeability in patients with Crohn's disease and their healthy relatives*. Gastroenterology., 1989. **97**(4):

- p. 927-31.
290. Kaufmann, S.H., *gamma/delta and other unconventional T lymphocytes: what do they see and what do they do?* Proc Natl Acad Sci U S A, 1996. **93**(6): p. 2272-9.
291. Khan, A., et al., *Phenotypic and gene expression changes among clonal type I strains of Toxoplasma gondii*. Eukaryot Cell., 2009. **8**(12): p. 1828-36. doi: 10.1128/EC.00150-09. Epub 2009 Oct 2.
292. Khan, A., et al., *Common inheritance of chromosome Ia associated with clonal expansion of Toxoplasma gondii*. Genome Res., 2006. **16**(9): p. 1119-25. Epub 2006 Aug 10.
293. Khan, A., et al., *Genetic analyses of atypical Toxoplasma gondii strains reveal a fourth clonal lineage in North America*. Int J Parasitol., 2011. **41**(6): p. 645-55. doi: 10.1016/j.ijpara.2011.01.005. Epub 2011 Feb 12.
294. Kiela, P.R. and F.K. Ghishan, *Ion transport in the intestine*. Curr Opin Gastroenterol., 2009. **25**(2): p. 87-91. doi: 10.1097/MOG.0b013e3283260900.
295. Kieschnick, H., et al., *Toxoplasma gondii attachment to host cells is regulated by a calmodulin-like domain protein kinase*. J Biol Chem, 2001. **276**(15): p. 12369-77.
296. Kiesslich, R., et al., *Identification of epithelial gaps in human small and large intestine by confocal endomicroscopy*. Gastroenterology., 2007. **133**(6): p. 1769-78. Epub 2007 Sep 16.
297. Kim, E., et al., *Clustering of Shaker-type K⁺ channels by interaction with a family of membrane-associated guanylate kinases*. Nature., 1995. **378**(6552): p. 85-8.
298. Kim, K., *Role of proteases in host cell invasion by Toxoplasma gondii and other Apicomplexa*. Acta Trop, 2004. **91**(1): p. 69-81.
299. Kim, K. and L.M. Weiss, *Toxoplasma gondii: the model apicomplexan*. Int J Parasitol., 2004. **34**(3): p. 423-32.
300. Kim, K. and L.M. Weiss, *Toxoplasma: the next 100years*. Microbes Infect., 2008. **10**(9): p. 978-84. doi: 10.1016/j.micinf.2008.07.015. Epub 2008 Jul 10.
301. Kim, L. and E.Y. Denkers, *Toxoplasma gondii triggers Gi-dependent PI 3-kinase signaling required for inhibition of host cell apoptosis*. J Cell Sci, 2006. **119**(Pt 10): p. 2119-26.
302. Kim, Y.S. and S.B. Ho, *Intestinal goblet cells and mucins in health and disease: recent insights and progress*. Curr Gastroenterol Rep., 2010. **12**(5): p. 319-30. doi: 10.1007/s11894-010-0131-2.
303. Kimura, H., et al., *Bacterial lipopolysaccharide reduced intestinal barrier function and altered localization of 7H6 antigen in IEC-6 rat intestinal crypt cells*. J Cell Physiol, 1997. **171**(3): p. 284-90.
304. Kimura, Y., et al., *Expression of occludin, tight-junction-associated protein, in human digestive tract*. Am J Pathol, 1997. **151**(1): p. 45-54.
305. Kinoshita, E., et al., *Recognition of phosphate monoester dianion by an alkoxide-bridged dinuclear zinc(II) complex*. Dalton Trans, 2004(8): p. 1189-93.
306. Kleinman, H.K. and G.R. Martin, *Matrigel: basement membrane*

- matrix with biological activity.* Semin Cancer Biol, 2005. **15**(5): p. 378-86.
307. Klok, A. M., et al., Soluble ICAM-1 serum levels in patients with intermediate uveitis. Br J Ophthalmol, 1999. **83**: p. 847-851.
308. Klose, J., *From 2-D electrophoresis to proteomics.* Electrophoresis, 2009. **30 Suppl 1**: p. S142-9.
309. Knoop, K.A., M.J. Miller, and R.D. Newberry, *Transepithelial antigen delivery in the small intestine: different paths, different outcomes.* Curr Opin Gastroenterol, 2013. **29**(2): p. 112-8. doi: 10.1097/MOG.0b013e32835cf1cd.
310. Kohler, H., et al., *Salmonella enterica serovar Typhimurium regulates intercellular junction proteins and facilitates transepithelial neutrophil and bacterial passage.* Am J Physiol Gastrointest Liver Physiol, 2007. **293**(1): p. G178-87.
311. Kohler, K. and A. Zahraoui, *Tight junction: a co-ordinator of cell signalling and membrane trafficking.* Biol Cell, 2005. **97**(8): p. 659-65.
312. Kojima, T., et al., *Tight junction proteins and signal transduction pathways in hepatocytes.* Histol Histopathol, 2009. **24**(11): p. 1463-72.
313. Kortbeek, L.M., et al., *Congenital toxoplasmosis and DALYs in the Netherlands.* Mem Inst Oswaldo Cruz, 2009. **104**(2): p. 370-3.
314. Koshy, A.A., et al., *Toxoplasma co-opts host cells it does not invade.* PLoS Pathog, 2012. **8**(7): p. e1002825.
315. Kowalik, S., W. Clauss, and H. Zahner, *Toxoplasma gondii: changes of transepithelial ion transport in infected HT29/B6 cell monolayers.* Parasitol Res, 2004. **92**(2): p. 152-8.
316. Krishna, R., et al., *A large-scale proteogenomics study of apicomplexan pathogens-Toxoplasma gondii and Neospora caninum.* Proteomics, 2015. **15**(15): p. 2618-28.
317. Krug, S.M., et al., *Tricellulin forms a barrier to macromolecules in tricellular tight junctions without affecting ion permeability.* Mol Biol Cell, 2009. **20**(16): p. 3713-24. doi: 10.1091/mcb.E09-01-0080. Epub 2009 Jun 17.
318. Krug, S.M., J.D. Schulzke, and M. Fromm, *Tight junction, selective permeability, and related diseases.* Semin Cell Dev Biol, 2014. **36**: p. 166-76.
319. Kruger, M., et al., *SILAC mouse for quantitative proteomics uncovers kindlin-3 as an essential factor for red blood cell function.* Cell, 2008. **134**(2): p. 353-64.
320. Kuriyama, M., et al., *Identification of AF-6 and canoe as putative targets for Ras.* J Biol Chem, 1996. **271**(2): p. 607-10.
321. Lacaz-Vieira, F., et al., *Small synthetic peptides homologous to segments of the first external loop of occludin impair tight junction resealing.* J Membr Biol, 1999. **168**(3): p. 289-97.
322. Laliberte, J. and V.B. Carruthers, *Host cell manipulation by the human pathogen Toxoplasma gondii.* Cell Mol Life Sci, 2008. **65**(12): p. 1900-15.
323. Lamont, J.T., *Mucus: the front line of intestinal mucosal defense.* Ann

- N Y Acad Sci, 1992. **664**: p. 190-201.
324. Laukoetter, M.G., et al., *JAM-A regulates permeability and inflammation in the intestine in vivo*. J Exp Med., 2007. **204**(13): p. 3067-76. Epub 2007 Nov 26.
 325. Lavine, M.D. and G. Arrizabalaga, *Induction of mitotic S-phase of host and neighboring cells by Toxoplasma gondii enhances parasite invasion*. Mol Biochem Parasitol, 2009. **164**(1): p. 95-9.
 326. Lawrence, D.W., K.M. Comerford, and S.P. Colgan, *Role of VASP in reestablishment of epithelial tight junction assembly after Ca²⁺ switch*. Am J Physiol Cell Physiol., 2002. **282**(6): p. C1235-45.
 327. Lax, A.J. and W. Thomas, *How bacteria could cause cancer: one step at a time*. Trends Microbiol, 2002. **10**(6): p. 293-9.
 328. Lehman, T.A., et al., *p53 mutations in human immortalized epithelial cell lines*. Carcinogenesis, 1993. **14**(5): p. 833-9.
 329. Lei, Y., M. Davey, and J.T. Ellis, *Attachment and invasion of Toxoplasma gondii and Neospora caninum to epithelial and fibroblast cell lines in vitro*. Parasitology., 2005. **131**(Pt 5): p. 583-90.
 330. Lekutis, C., D.J. Ferguson, and J.C. Boothroyd, *Toxoplasma gondii: identification of a developmentally regulated family of genes related to SAG2*. Exp Parasitol., 2000. **96**(2): p. 89-96.
 331. Lekutis, C., et al., *Surface antigens of Toxoplasma gondii: variations on a theme*. Int J Parasitol., 2001. **31**(12): p. 1285-92.
 332. Lemieux, E., et al., *Constitutively active MEK1 is sufficient to induce epithelial-to-mesenchymal transition in intestinal epithelial cells and to promote tumor invasion and metastasis*. Int J Cancer, 2009. **125**(7): p. 1575-86.
 333. Lenaerts, K., et al., *Comparative proteomic analysis of cell lines and scrapings of the human intestinal epithelium*. BMC Genomics, 2007. **8**: p. 91.
 334. Li, W.Y., C.L. Huey, and A.S. Yu, *Expression of claudin-7 and -8 along the mouse nephron*. Am J Physiol Renal Physiol., 2004. **286**(6): p. F1063-71. Epub 2004 Jan 13.
 335. Li, Y., et al., *Structure of the conserved cytoplasmic C-terminal domain of occludin: identification of the ZO-1 binding surface*. J Mol Biol., 2005. **352**(1): p. 151-64.
 336. Liang, G.H. and C.R. Weber, *Molecular aspects of tight junction barrier function*. Curr Opin Pharmacol, 2014. **19**: p. 84-9.
 337. Lim, D.C., et al., *Toxoplasma and Plasmodium protein kinases: roles in invasion and host cell remodelling*. Int J Parasitol, 2012. **42**(1): p. 21-32.
 338. Lin, N., et al., *Information assessment on predicting protein-protein interactions*. BMC Bioinformatics, 2004. **5**: p. 154.
 339. Lindquist, R.L., et al., *Visualizing dendritic cell networks in vivo*. Nat Immunol, 2004. **5**(12): p. 1243-50.
 340. Lindsay, D.S. and J.P. Dubey, *Toxoplasma gondii: the changing paradigm of congenital toxoplasmosis*. Parasitology., 2011. **138**(14): p. 1829-31. doi: 10.1017/S0031182011001478. Epub 2011 Sep 9.

341. Little, S.E., *Future challenges for parasitology: vector control and one health in the Americas*. Vet Parasitol., 2013. **195**(3-4): p. 249-55. doi: 10.1016/j.vetpar.2013.04.006. Epub 2013 Apr 6.
342. Liu, Y., et al., *Human junction adhesion molecule regulates tight junction resealing in epithelia*. J Cell Sci., 2000. **113**(Pt 13): p. 2363-
343. Lorenzi, H., et al., *Local admixture of amplified and diversified secreted pathogenesis determinants shapes mosaic Toxoplasma gondii genomes*. Nature Comms., 2015. **7**: p1-12
344. Lu, R., et al., *PKCiota interacts with Rab14 and modulates epithelial barrier function through regulation of claudin-2 levels*. Mol Biol Cell, 2015. **26**(8): p. 1523-31.
345. Lu, R., L. Stewart, and J.M. Wilson, *Scaffolding protein GOPC regulates tight junction structure*. Cell Tissue Res., 2015. **360**(2): p. 321-32. doi: 10.1007/s00441-014-2088-1. Epub 2015 Jan 24.
346. Luces, C. and K. Bodger, *Economic burden of inflammatory bowel disease: a UK perspective*. Expert Rev Pharmacoecon Outcomes Res., 2006. **6**(4): p. 471-82. doi: 10.1586/14737167.6.4.471.
347. Lyons, R.E., R. McLeod, and C.W. Roberts, *Toxoplasma gondii tachyzoite-bradyzoite interconversion*. Trends Parasitol., 2002. **18**(5): p. 198-201.
348. Ma, J.S., et al., *Selective and strain-specific NFAT4 activation by the Toxoplasma gondii polymorphic dense granule protein GRA6*. J Exp Med, 2014. **211**(10): p. 2013-32.
349. Machado, F.C., et al., *Recruitment of galectin-3 during cell invasion and intracellular trafficking of Trypanosoma cruzi extracellular amastigotes*. Glycobiology., 2014. **24**(2): p. 179-84. doi: 10.1093/glycob/cwt097. Epub 2013 Nov 12.
350. Machado, F.S., et al., *Pathogenesis of Chagas disease: time to move on*. Front Biosci, 2012. **4**: p. 1743-58.
351. Machen, T.E., D. Erlij, and F.B. Wooding, *Permeable junctional complexes. The movement of lanthanum across rabbit gallbladder and intestine*. J Cell Biol., 1972. **54**(2): p. 302-12.
352. Maciel, A.A., et al., *Role of retinol in protecting epithelial cell damage induced by Clostridium difficile toxin A*. Toxicon, 2007. **50**(8): p. 1027-40.
353. Madara, J.L., *Intestinal absorptive cell tight junctions are linked to cytoskeleton*. Am J Physiol., 1987. **253**(1 Pt 1): p. C171-5.
354. Mandell, K.J., et al., *Junctional adhesion molecule 1 regulates epithelial cell morphology through effects on beta1 integrins and Rap1 activity*. J Biol Chem., 2005. **280**(12): p. 11665-74. Epub 2005 Jan 27.
355. Mandell, K.J., I.C. McCall, and C.A. Parkos, *Involvement of the junctional adhesion molecule-1 (JAM1) homodimer interface in regulation of epithelial barrier function*. J Biol Chem., 2004. **279**(16): p. 16254-62. Epub 2004 Jan 28.
356. Mandell, K.J. and C.A. Parkos, *The JAM family of proteins*. Adv Drug Deliv Rev., 2005. **57**(6): p. 857-67.
357. Manger, I.D., A.B. Hehl, and J.C. Boothroyd, *The surface of Toxoplasma tachyzoites is dominated by a family of*

- glycosylphosphatidylinositol-anchored antigens related to SAG1.* Infect Immun., 1998. **66**(5): p. 2237-44.
358. Mankertz, J., et al., *Gene expression of the tight junction protein occludin includes differential splicing and alternative promoter usage.* Biochem Biophys Res Commun., 2002. **298**(5): p. 657-66.
359. Mann, M., *Functional and quantitative proteomics using SILAC.* Nat Rev Mol Cell Biol, 2006. **7**(12): p. 952-8.
360. Marchiando, A.M., W.V. Graham, and J.R. Turner, *Epithelial barriers in homeostasis and disease.* Annu Rev Pathol, 2010. **5**: p. 119-44.
361. Marchiando, A.M., et al., *The epithelial barrier is maintained by in vivo tight junction expansion during pathologic intestinal epithelial shedding.* Gastroenterology., 2011. **140**(4): p. 1208-1218.e1-2. doi: 10.1053/j.gastro.2011.01.004. Epub 2011 Jan 13.
362. Marchiando, A.M., et al., *Caveolin-1-dependent occludin endocytosis is required for TNF-induced tight junction regulation in vivo.* J Cell Biol, 2010. **189**(1): p. 111-26.
363. Marcial, M.A., S.L. Carlson, and J.L. Madara, *Partitioning of paracellular conductance along the ileal crypt-villus axis: a hypothesis based on structural analysis with detailed consideration of tight junction structure-function relationships.* J Membr Biol., 1984. **80**(1): p. 59-70.
364. Martin-Padura, I., et al., *Junctional adhesion molecule, a novel member of the immunoglobulin superfamily that distributes at intercellular junctions and modulates monocyte transmigration.* J Cell Biol, 1998. **142**(1): p. 117-27.
365. Martincic, K., et al., *Increase in the 64-kDa subunit of the polyadenylation/cleavage stimulatory factor during the G0 to S phase transition.* Proc Natl Acad Sci U S A, 1998. **95**(19): p. 11095-100.
366. Martinez-Estrada, O.M., et al., *Association of junctional adhesion molecule with calcium/calmodulin-dependent serine protein kinase (CASK/LIN-2) in human epithelial caco-2 cells.* J Biol Chem, 2001. **276**(12): p. 9291-6.
367. Matsumoto, H., et al., *Biosynthesis of alkaline phosphatase during differentiation of the human colon cancer cell line Caco-2.* Gastroenterology, 1990. **98**(5 Pt 1): p. 1199-207.
368. Matter, K., et al., *Mammalian tight junctions in the regulation of epithelial differentiation and proliferation.* Curr Opin Cell Biol., 2005. **17**(5): p. 453-8.
369. Matter, K. and M.S. Balda, *Signalling to and from tight junctions.* Nat Rev Mol Cell Biol., 2003. **4**(3): p. 225-36.
370. Matter, K. and M.S. Balda, *Functional analysis of tight junctions.* Methods., 2003. **30**(3): p. 228-34.
371. Matter, K. and M.S. Balda, *SnapShot: Epithelial tight junctions.* Cell, 2014. **157**(4): p. 992-992.e1.
372. Mayer, L., *Mucosal immunity.* Pediatrics., 2003. **111**(6 Pt 3): p. 1595-600.
373. McCaffrey, G., et al., *Occludin oligomeric assembly at tight junctions of the blood-brain barrier is disrupted by peripheral inflammatory*

- hyperalgesia.* J Neurochem, 2008. **106**(6): p. 2395-409.
374. McCarthy, K.M., et al., *Occludin is a functional component of the tight junction.* J Cell Sci., 1996. **109**(Pt 9): p. 2287-98.
375. McClatchy, D.B., et al., *15N metabolic labeling of mammalian tissue with slow protein turnover.* J Proteome Res, 2007. **6**(5): p. 2005-10.
376. McClatchy, D.B., et al., *Quantification of the synaptosomal proteome of the rat cerebellum during post-natal development.* Genome Res, 2007. **17**(9): p. 1378-88.
377. McCole, D.F., *Phosphatase regulation of intercellular junctions.* Tissue Barriers, 2013. **1**(5): p. e26713.
378. McGhee, J.R. and K. Fujihashi, *Inside the mucosal immune system.* PLoS Biol., 2012. **10**(9): p. e1001397. doi: 10.1371/journal.pbio.1001397. Epub 2012 Sep 25.
379. Meddings, J., *What role does intestinal permeability have in IBD pathogenesis?* Inflamm Bowel Dis, 2008: p. 20719.
380. Medina, R., et al., *Occludin localization at the tight junction requires the second extracellular loop.* J Membr Biol, 2000. **178**(3): p. 235-47.
381. Mehta, S., et al., *Defects in the adherens junction complex (E-cadherin/ beta-catenin) in inflammatory bowel disease.* Cell Tissue Res., 2015. **360**(3): p. 749-60. doi: 10.1007/s00441-014-1994-6. Epub 2014 Sep 20.
382. Mercier, C., et al., *Targeted disruption of the GRA2 locus in Toxoplasma gondii decreases acute virulence in mice.* Infect Immun., 1998. **66**(9): p. 4176-82.
383. Mi, H., et al., *Large-scale gene function analysis with the PANTHER classification system.* Nat Protoc, 2013. **8**(8): p. 1551-66.
384. Millet, Y.A., et al., *Insights into Vibrio cholerae intestinal colonization from monitoring fluorescently labeled bacteria.* PLoS Pathog, 2014. **10**(10): p. e1004405.
385. Mineo, J.R. and L.H. Kasper, *Attachment of Toxoplasma gondii to host cells involves major surface protein, SAG-1 (P30).* Exp Parasitol., 1994. **79**(1): p. 11-20.
386. Mineo, J.R., et al., *Antibodies to Toxoplasma gondii major surface protein (SAG-1, P30) inhibit infection of host cells and are produced in murine intestine after peroral infection.* J Immunol., 1993. **150**(9): p. 3951-64.
387. Mineta, K., et al., *Predicted expansion of the claudin multigene family.* FEBS Lett., 2011. **585**(4): p. 606-12. doi: 10.1016/j.febslet.2011.01.028. Epub 2011 Jan 26.
388. Mittal, V. and R.L. Ichhpujani, *Toxoplasmosis - An update.* Trop Parasitol., 2011. **1**(1): p. 9-14. doi: 10.4103/2229-5070.72109.
389. Mixter, P.F., et al., *Mouse T lymphocytes that express a gamma delta T-cell antigen receptor contribute to resistance to Salmonella infection in vivo.* Infect Immun., 1994. **62**(10): p. 4618-21.
390. Molestina, R.E., N. El-Guendy, and A.P. Sinai, *Infection with Toxoplasma gondii results in dysregulation of the host cell cycle.* Cell Microbiol, 2008. **10**(5): p. 1153-65.
391. Molodecky, N.A., et al., *Increasing incidence and prevalence of the*

- inflammatory bowel diseases with time, based on systematic review.* Gastroenterology., 2012. **142**(1): p. 46-54.e42; quiz e30. doi: 10.1053/j.gastro.2011.10.001. Epub 2011 Oct 14.
- 392. Monteiro, A.C. and C.A. Parkos, *Intracellular mediators of JAM-A-dependent epithelial barrier function.* Ann N Y Acad Sci, 2012.
 - 393. Monteiro, A.C., et al., *JAM-A associates with ZO-2, afadin, and PDZ-GEF1 to activate Rap2c and regulate epithelial barrier function.* Mol Biol Cell, 2013. **24**(18): p. 2849-60.
 - 394. Montoya, J.G. and O. Liesenfeld, *Toxoplasmosis.* Lancet., 2004. **363**(9425): p. 1965-76.
 - 395. Montoya, J.G. and J.S. Remington, *Toxoplasmic chorioretinitis in the setting of acute acquired toxoplasmosis.* Clin Infect Dis., 1996. **23**(2): p. 277-82.
 - 396. Montrose, M.H., *The future of GI and liver research: editorial perspectives: I. Visions of epithelial research.* Am J Physiol Gastrointest Liver Physiol., 2003. **284**(4): p. G547-50.
 - 397. Mooseker, M.S., *Organization, chemistry, and assembly of the cytoskeletal apparatus of the intestinal brush border.* Annu Rev Cell Biol, 1985. **1**: p. 209-41.
 - 398. Morimoto, S., et al., *Rab13 mediates the continuous endocytic recycling of occludin to the cell surface.* J Biol Chem, 2005. **280**(3): p. 2220-8.
 - 399. Morisaki, J.H., J.E. Heuser, and L.D. Sibley, *Invasion of Toxoplasma gondii occurs by active penetration of the host cell.* J Cell Sci., 1995. **108**(Pt 6): p. 2457-64.
 - 400. Mowat, A.M., *Anatomical basis of tolerance and immunity to intestinal antigens.* Nat Rev Immunol., 2003. **3**(4): p. 331-41.
 - 401. Mowat, A.M. and W.W. Agace, *Regional specialization within the intestinal immune system.* Nat Rev Immunol., 2014. **14**(10): p. 667-85. doi: 10.1038/nri3738. Epub 2014 Sep 19.
 - 402. Mowat, C., et al., *Guidelines for the management of inflammatory bowel disease in adults.* Gut., 2011. **60**(5): p. 571-607. doi: 10.1136/gut.2010.224154.
 - 403. Muller, S.L., et al., *The tight junction protein occludin and the adherens junction protein alpha-catenin share a common interaction mechanism with ZO-1.* J Biol Chem, 2005. **280**(5): p. 3747-56.
 - 404. Muresan, Z., D.L. Paul, and D.A. Goodenough, *Occludin 1B, a variant of the tight junction protein occludin.* Mol Biol Cell., 2000. **11**(2): p. 627-34.
 - 405. Muza-Moons, M.M., E.E. Schneeberger, and G.A. Hecht, *Enteropathogenic Escherichia coli infection leads to appearance of aberrant tight junction strands in the lateral membrane of intestinal epithelial cells.* Cell Microbiol, 2004. **6**(8): p. 783-93.
 - 406. Naftalin, R.J. and S. Tripathi, *Passive water flows driven across the isolated rabbit ileum by osmotic, hydrostatic and electrical gradients.* J Physiol, 1985. **360**: p. 27-50.
 - 407. Nagel, S.D. and J.C. Boothroyd, *The major surface antigen, P30, of Toxoplasma gondii is anchored by a glycolipid.* J Biol Chem., 1989.

- 264**(10): p. 5569-74.
408. Nagineni, C. N., Detrick, B., and Hooks, J. J., *Toxoplasma gondii infection induces gene expression and secretion of interleukin 1 (IL-1), IL-6, granulocyte-macrophage colony stimulating factor, and intercellular adhesion molecule 1 by human retinal pigment epithelial cells.*, 2000. **68**(1): p407-10.
409. Nash, T.E., *Surface antigenic variation in Giardia lamblia*. Mol Microbiol., 2002. **45**(3): p. 585-90.
410. Nelson, M.M., et al., *Modulation of the host cell proteome by the intracellular apicomplexan parasite Toxoplasma gondii*. Infect Immun, 2008. **76**(2): p. 828-44.
411. Nicoletti, C., M. Regoli, and E. Bertelli, *Dendritic cells in the gut: to sample and to exclude?* Mucosal Immunol., 2009. **2**(5): p. 462. doi: 10.1038/mi.2009.92.
412. Niess, J.H., et al., *CX3CR1-mediated dendritic cell access to the intestinal lumen and bacterial clearance*. Science., 2005. **307**(5707): p. 254-8.
413. Niess, J.H. and H.C. Reinecker, *Dendritic cells in the recognition of intestinal microbiota*. Cell Microbiol., 2006. **8**(4): p. 558-64.
414. Niessen, C.M., *Tight junctions/adherens junctions: basic structure and function*. J Invest Dermatol., 2007. **127**(11): p. 2525-32.
415. Nunbhakdi-Craig, V., et al., *Protein phosphatase 2A associates with and regulates atypical PKC and the epithelial tight junction complex*. J Cell Biol, 2002. **158**(5): p. 967-78.
416. Nusrat, A., et al., *Multiple protein interactions involving proposed extracellular loop domains of the tight junction protein occludin*. Mol Biol Cell, 2005. **16**(4): p. 1725-34.
417. Nusrat, A., et al., *The coiled-coil domain of occludin can act to organize structural and functional elements of the epithelial tight junction*. J Biol Chem, 2000. **275**(38): p. 29816-22.
418. Nusrat, A., J.R. Turner, and J.L. Madara, *Molecular physiology and pathophysiology of tight junctions. IV. Regulation of tight junctions by extracellular stimuli: nutrients, cytokines, and immune cells*. Am J Physiol Gastrointest Liver Physiol., 2000. **279**(5): p. G851-7.
419. Nusrat, A., et al., *Clostridium difficile toxins disrupt epithelial barrier function by altering membrane microdomain localization of tight junction proteins*. Infect Immun, 2001. **69**(3): p. 1329-36.
420. O'Farrell, P.H., *High resolution two-dimensional electrophoresis of proteins*. J Biol Chem, 1975. **250**(10): p. 4007-21.
421. O'Hara, A.M. and F. Shanahan, *The gut flora as a forgotten organ*. EMBO Rep., 2006. **7**(7): p. 688-93.
422. Odenwald, M.A. and J.R. Turner, *Intestinal permeability defects: is it time to treat?* Clin Gastroenterol Hepatol., 2013. **11**(9): p. 1075-83. doi: 10.1016/j.cgh.2013.07.001. Epub 2013 Jul 12.
423. Ohnishi, H., et al., *JACOP, a novel plaque protein localizing at the apical junctional complex with sequence similarity to cingulin*. J Biol Chem., 2004. **279**(44): p. 46014-22. Epub 2004 Jul 30.
424. Ong, S.E., et al., *Stable isotope labeling by amino acids in cell culture, SILAC, as a simple and accurate approach to expression proteomics*.

- Mol Cell Proteomics, 2002. **1**(5): p. 376-86.
425. Orzekowsky-Schroeder, R., et al., *In vivo spectral imaging of different cell types in the small intestine by two-photon excited autofluorescence*. J Biomed Opt, 2011. **16**(11): p. 116025.
426. Osanai, M., et al., *Epigenetic silencing of occludin promotes tumorigenic and metastatic properties of cancer cells via modulations of unique sets of apoptosis-associated genes*. Cancer Res, 2006. **66**(18): p. 9125-33.
427. Peixoto, L., et al., *Integrative genomic approaches highlight a family of parasite-specific kinases that regulate host responses*. Cell Host Microbe, 2010. **8**(2): p. 208-18.
428. Pelaseyed, T., et al., *The mucus and mucins of the goblet cells and enterocytes provide the first defense line of the gastrointestinal tract and interact with the immune system*. Immunol Rev., 2014. **260**(1): p. 8-20. doi: 10.1111/imr.12182.
429. Peralta-Ramirez, J., et al., *EspF Interacts with nucleation-promoting factors to recruit junctional proteins into pedestals for pedestal maturation and disruption of paracellular permeability*. Infect Immun, 2008. **76**(9): p. 3854-68.
430. Perez-Moreno, M. and E. Fuchs, *Catenins: keeping cells from getting their signals crossed*. Dev Cell., 2006. **11**(5): p. 601-12.
431. Peterson, L.W. and D. Artis, *Intestinal epithelial cells: regulators of barrier function and immune homeostasis*. Nat Rev Immunol., 2014. **14**(3): p. 141-53. doi: 10.1038/nri3608.
432. Pfaff, A. W., et al., *Toxoplasma gondii regulates ICAM-1 mediated monocyte adhesion to trophoblasts*. 2005. **83**(5): p483-9.
433. Philpott, D.J., et al., *Infection of T84 cells with enteropathogenic Escherichia coli alters barrier and transport functions*. Am J Physiol, 1996. **270**(4 Pt 1): p. G634-45.
434. Pizarro, T.T., et al., *Mouse models for the study of Crohn's disease*. Trends Mol Med, 2003. **9**(5): p. 218-22.
435. Plattner, F., et al., *Toxoplasma profilin is essential for host cell invasion and TLR11-dependent induction of an interleukin-12 response*. Cell Host Microbe., 2008. **3**(2): p. 77-87. doi: 10.1016/j.chom.2008.01.001.
436. Porter, S.B. and M.A. Sande, *Toxoplasmosis of the central nervous system in the acquired immunodeficiency syndrome*. N Engl J Med., 1992. **327**(23): p. 1643-8.
437. Possenti, A., et al., *Global proteomic analysis of the oocyst/sporozoite of Toxoplasma gondii reveals commitment to a host-independent lifestyle*. BMC Genomics, 2013. **14**: p. 183.
438. Potten, C.S. and M. Loeffler, *Stem cells: attributes, cycles, spirals, pitfalls and uncertainties. Lessons for and from the crypt*. Development, 1990. **110**(4): p. 1001-20.
439. Poupel, O., et al., *Toxofilin, a novel actin-binding protein from Toxoplasma gondii, sequesters actin monomers and caps actin filaments*. Mol Biol Cell, 2000. **11**(1): p. 355-68.
440. Prasad, S., et al., *Inflammatory processes have differential effects on claudins 2, 3 and 4 in colonic epithelial cells*. Lab Invest., 2005.

- 85**(9): p. 1139-62.
441. Prince, J.B., et al., *Cloning, expression, and cDNA sequence of surface antigen P22 from Toxoplasma gondii*. Mol Biochem Parasitol., 1990. **43**(1): p. 97-106.
442. Quan, J.H., et al., *Involvement of PI 3 kinase/Akt-dependent Bad phosphorylation in Toxoplasma gondii-mediated inhibition of host cell apoptosis*. Exp Parasitol, 2013. **133**(4): p. 462-71.
443. Quaroni, A., et al., *Epithelioid cell cultures from rat small intestine. Characterization by morphologic and immunologic criteria*. J Cell Biol., 1979. **80**(2): p. 248-65.
444. Quilliam, L.A., et al., *M-Ras/R-Ras3, a transforming ras protein regulated by Sos1, GFR1, and p120 Ras GTPase-activating protein, interacts with the putative Ras effector AF6*. J Biol Chem, 1999. **274**(34): p. 23850-7.
445. Rahner, C., L.L. Mitic, and J.M. Anderson, *Heterogeneity in expression and subcellular localization of claudins 2, 3, 4, and 5 in the rat liver, pancreas, and gut*. Gastroenterology., 2001. **120**(2): p. 411-22.
446. Rajasekaran, A.K., et al., *Catenins and zonula occludens-1 form a complex during early stages in the assembly of tight junctions*. J Cell Biol., 1996. **132**(3): p. 451-63.
447. Raleigh, D.R., et al., *Occludin S408 phosphorylation regulates tight junction protein interactions and barrier function*. J Cell Biol., 2011. **193**(3): p. 565-82. doi: 10.1083/jcb.201010065.
448. Raleigh, D.R., et al., *Tight junction-associated MARVEL proteins marveld3, tricellulin, and occludin have distinct but overlapping functions*. Mol Biol Cell., 2010. **21**(7): p. 1200-13. doi: 10.1091/mbc.E09-08-0734. Epub 2010 Feb 17.
449. Reese, M.L. and J.C. Boothroyd, *A conserved non-canonical motif in the pseudoactive site of the ROP5 pseudokinase domain mediates its effect on Toxoplasma virulence*. J Biol Chem., 2011. **286**(33): p. 29366-75. doi: 10.1074/jbc.M111.253435. Epub 2011 Jun 27.
450. Rescigno, M., et al., *Dendritic cells express tight junction proteins and penetrate gut epithelial monolayers to sample bacteria*. Nat Immunol., 2001. **2**(4): p. 361-7.
451. Reuss, L., Y. Segal, and G. Altenberg, *Regulation of ion transport across gallbladder epithelium*. Annu Rev Physiol, 1991. **53**: p. 361-73.
452. Reyes, C.C., et al., *Anillin regulates cell-cell junction integrity by organizing junctional accumulation of Rho-GTP and actomyosin*. Curr Biol., 2014. **24**(11): p. 1263-70. doi: 10.1016/j.cub.2014.04.021. Epub 2014 May 15.
453. Rigbolt, K.T. and B. Blagoev, *Quantitative phosphoproteomics to characterize signaling networks*. Semin Cell Dev Biol, 2012. **23**(8): p. 863-71.
454. Rimoldi, M., et al., *Intestinal epithelial cells control dendritic cell function*. Ann N Y Acad Sci, 2004: p. 66-74.
455. Robben, P.M., et al., *Production of IL-12 by macrophages infected with Toxoplasma gondii depends on the parasite genotype*. J

- Immunol., 2004. **172**(6): p. 3686-94.
456. Robert, R., et al., *Specific binding of neoglycoproteins to Toxoplasma gondii tachyzoites*. Infect Immun., 1991. **59**(12): p. 4670-3.
457. Rothen-Rutishauser, B., et al., *Formation of multilayers in the caco-2 cell culture model: a confocal laser scanning microscopy study*. Pharm Res, 2000. **17**(4): p. 460-5.
458. Runkle, E.A., et al., *Occludin localizes to centrosomes and modifies mitotic entry*. J Biol Chem, 2011. **286**(35): p. 30847-58.
459. Saeij, J.P., G. Arrizabalaga, and J.C. Boothroyd, *A cluster of four surface antigen genes specifically expressed in bradyzoites, SAG2CDXY, plays an important role in Toxoplasma gondii persistence*. Infect Immun., 2008. **76**(6): p. 2402-10. doi: 10.1128/IAI.01494-07. Epub 2008 Mar 17.
460. Saeij, J.P., J.P. Boyle, and J.C. Boothroyd, *Differences among the three major strains of Toxoplasma gondii and their specific interactions with the infected host*. Trends Parasitol., 2005. **21**(10): p. 476-81.
461. Saeij, J.P., et al., *Polymorphic secreted kinases are key virulence factors in toxoplasmosis*. Science., 2006. **314**(5806): p. 1780-3.
462. Saeij, J.P., et al., *Bioluminescence imaging of Toxoplasma gondii infection in living mice reveals dramatic differences between strains*. Infect Immun., 2005. **73**(2): p. 695-702.
463. Saeij, J.P., et al., *Toxoplasma co-opts host gene expression by injection of a polymorphic kinase homologue*. Nature., 2007. **445**(7125): p. 324-7. Epub 2006 Dec 20.
464. Sahu, A., et al., *Host response profile of human brain proteome in toxoplasma encephalitis co-infected with HIV*. Clin Proteomics, 2014. **11**(1): p. 39.
465. Saitoh, Y., et al., *Tight junctions. Structural insight into tight junction disassembly by Clostridium perfringens enterotoxin*. Science., 2015. **347**(6223): p. 775-8. doi: 10.1126/science.1261833.
466. Saitou, M., et al., *Mammalian occludin in epithelial cells: its expression and subcellular distribution*. Eur J Cell Biol., 1997. **73**(3): p. 222-31.
467. Saitou, M., et al., *Occludin-deficient embryonic stem cells can differentiate into polarized epithelial cells bearing tight junctions*. J Cell Biol., 1998. **141**(2): p. 397-408.
468. Saitou, M., et al., *Complex phenotype of mice lacking occludin, a component of tight junction strands*. Mol Biol Cell., 2000. **11**(12): p. 4131-42.
469. Sakakibara, A., et al., *Possible involvement of phosphorylation of occludin in tight junction formation*. J Cell Biol., 1997. **137**(6): p. 1393-401.
470. Salama, N.N., N.D. Eddington, and A. Fasano, *Tight junction modulation and its relationship to drug delivery*. Adv Drug Deliv Rev, 2006. **58**(1): p. 15-28.
471. Salzman, N.H., M.A. Underwood, and C.L. Bevins, *Paneth cells, defensins, and the commensal microbiota: a hypothesis on intimate*

- interplay at the intestinal mucosa.* Semin Immunol., 2007. **19**(2): p. 70-83. Epub 2007 May 7.
472. Samarin, S.N., et al., *Rho/Rho-associated kinase-II signaling mediates disassembly of epithelial apical junctions.* Mol Biol Cell, 2007. **18**(9): p. 3429-39.
473. Sanchez-Pulido, L., et al., *MARVEL: a conserved domain involved in membrane apposition events.* Trends Biochem Sci., 2002. **27**(12): p. 599-601.
474. Sancho, E., E. Batlle, and H. Clevers, *Live and let die in the intestinal epithelium.* Curr Opin Cell Biol., 2003. **15**(6): p. 763-70.
475. Sandle, G.I., *Pathogenesis of diarrhea in ulcerative colitis: new views on an old problem.* J Clin Gastroenterol., 2005. **39**(4 Suppl 2): p. S49-52.
476. Savage, D.C., *Microbial ecology of the gastrointestinal tract.* Annu Rev Microbiol, 1977. **31**: p. 107-33.
477. Scharl, M., et al., *AMP-activated protein kinase mediates the interferon-gamma-induced decrease in intestinal epithelial barrier function.* J Biol Chem., 2009. **284**(41): p. 27952-63. doi: 10.1074/jbc.M109.046292. Epub 2009 Aug 4.
478. Scheid, M.P. and J.R. Woodgett, *PKB/AKT: functional insights from genetic models.* Nat Rev Mol Cell Biol, 2001. **2**(10): p. 760-8.
479. Schmidt, E., S.M. Kelly, and C.F. van der Walle, *Tight junction modulation and biochemical characterisation of the zonula occludens toxin C-and N-termini.* FEBS Lett, 2007. **581**(16): p. 2974-80.
480. Schneeberger, E.E. and R.D. Lynch, *Structure, function, and regulation of cellular tight junctions.* Am J Physiol., 1992. **262**(6 Pt 1): p. L647-61.
481. Schneeberger, E.E. and R.D. Lynch, *The tight junction: a multifunctional complex.* Am J Physiol Cell Physiol., 2004. **286**(6): p. C1213-28.
482. Schulz, O., et al., *Intestinal CD103+, but not CX3CR1+, antigen sampling cells migrate in lymph and serve classical dendritic cell functions.* J Exp Med., 2009. **206**(13): p. 3101-14. doi: 10.1084/jem.20091925. Epub 2009 Dec 14.
483. Schulzke, J.D., et al., *Epithelial transport and barrier function in occludin-deficient mice.* Biochim Biophys Acta., 2005. **1669**(1): p. 34-42.
484. Schulzke, J.D., et al., *Perspectives on tight junction research.* Ann N Y Acad Sci, 2012.
485. Scott, K.G., et al., *Intestinal infection with Giardia spp. reduces epithelial barrier function in a myosin light chain kinase-dependent fashion.* Gastroenterology., 2002. **123**(4): p. 1179-90.
486. Seth, A., et al., *Protein phosphatases 2A and 1 interact with occludin and negatively regulate the assembly of tight junctions in the CACO-2 cell monolayer.* J Biol Chem, 2007. **282**(15): p. 11487-98.
487. Sharma, P. and C.E. Chitnis, *Key molecular events during host cell invasion by Apicomplexan pathogens.* Curr Opin Microbiol, 2013. **16**(4): p. 432-7.

488. Shastri, A.J., et al., *GRA25 is a novel virulence factor of Toxoplasma gondii and influences the host immune response*. Infect Immun, 2014. **82**(6): p. 2595-605.
489. Shen, L., *Tight junctions on the move: molecular mechanisms for epithelial barrier regulation*. Ann N Y Acad Sci, 2012.
490. Shen, L., et al., *Myosin light chain phosphorylation regulates barrier function by remodeling tight junction structure*. J Cell Sci, 2006. **119**(Pt 10): p. 2095-106.
491. Shen, L., L. Su, and J.R. Turner, *Mechanisms and functional implications of intestinal barrier defects*. Dig Dis., 2009. **27**(4): p. 443-9. doi: 10.1159/000233282. Epub 2009 Nov 4.
492. Shen, L. and J.R. Turner, *Actin depolymerization disrupts tight junctions via caveolae-mediated endocytosis*. Mol Biol Cell., 2005. **16**(9): p. 3919-36. Epub 2005 Jun 15.
493. Shen, L., et al., *Tight junction pore and leak pathways: a dynamic duo*. Annu Rev Physiol, 2011. **73**: p. 283-309.
494. Shen, L., C.R. Weber, and J.R. Turner, *The tight junction protein complex undergoes rapid and continuous molecular remodeling at steady state*. J Cell Biol., 2008. **181**(4): p. 683-95. doi: 10.1083/jcb.200711165. Epub 2008 May 12.
495. Shin, K., S. Straight, and B. Margolis, *PATJ regulates tight junction formation and polarity in mammalian epithelial cells*. J Cell Biol., 2005. **168**(5): p. 705-11.
496. Sibley, L.D. and J.W. Ajioka, *Population structure of Toxoplasma gondii: clonal expansion driven by infrequent recombination and selective sweeps*. Annu Rev Microbiol, 2008. **62**: p. 329-51.
497. Sibley, L.D., et al., *Genetic diversity of Toxoplasma gondii in animals and humans*. Philos Trans R Soc Lond B Biol Sci., 2009. **364**(1530): p. 2749-61. doi: 10.1098/rstb.2009.0087.
498. Sibley, L.D., et al., *Regulated secretion of multi-lamellar vesicles leads to formation of a tubulo-vesicular network in host-cell vacuoles occupied by Toxoplasma gondii*. J Cell Sci, 1995. **108** (Pt 4): p. 1669-77.
499. Siliciano, J.D. and D.A. Goodenough, *Localization of the tight junction protein, ZO-1, is modulated by extracellular calcium and cell-cell contact in Madin-Darby canine kidney epithelial cells*. J Cell Biol., 1988. **107**(6 Pt 1): p. 2389-99.
500. Simon, D.B., et al., *Paracellin-1, a renal tight junction protein required for paracellular Mg²⁺ resorption*. Science., 1999. **285**(5424): p. 103-6.
501. Simonovic, I., et al., *Enteropathogenic Escherichia coli dephosphorylates and dissociates occludin from intestinal epithelial tight junctions*. Cell Microbiol, 2000. **2**(4): p. 305-15.
502. Siu, E.R., et al., *An occludin-focal adhesion kinase protein complex at the blood-testis barrier: a study using the cadmium model*. Endocrinology, 2009. **150**(7): p. 3336-44.
503. Sjo, A., K.E. Magnusson, and K.H. Peterson, *Protein kinase C activation has distinct effects on the localization, phosphorylation and detergent solubility of the claudin protein family in tight and*

- leaky epithelial cells.* J Membr Biol, 2010. **236**(2): p. 181-9.
504. Smales, C., et al., *Occludin phosphorylation: identification of an occludin kinase in brain and cell extracts as CK2.* FEBS Lett, 2003. **545**(2-3): p. 161-6.
505. Smith, J.E., *A ubiquitous intracellular parasite: the cellular biology of Toxoplasma gondii.* Int J Parasitol., 1995. **25**(11): p. 1301-9.
506. Soldati, D., J.F. Dubremetz, and M. Lebrun, *Microneme proteins: structural and functional requirements to promote adhesion and invasion by the apicomplexan parasite Toxoplasma gondii.* Int J Parasitol, 2001. **31**(12): p. 1293-302.
507. Soler, A.P., et al., *Increased tight junctional permeability is associated with the development of colon cancer.* Carcinogenesis, 1999. **20**(8): p. 1425-31.
508. Sonoda, N., et al., *Clostridium perfringens enterotoxin fragment removes specific claudins from tight junction strands: Evidence for direct involvement of claudins in tight junction barrier.* J Cell Biol., 1999. **147**(1): p. 195-204.
509. Speer, C.A., S. Clark, and J.P. Dubey, *Ultrastructure of the oocysts, sporocysts, and sporozoites of Toxoplasma gondii.* J Parasitol, 1998. **84**(3): p. 505-12.
510. Speer, C.A., et al., *Time lapse video microscopy and ultrastructure of penetrating sporozoites, types 1 and 2 parasitophorous vacuoles, and the transformation of sporozoites to tachyzoites of the VEG strain of Toxoplasma gondii.* J Parasitol, 1997. **83**(4): p. 565-74.
511. Spitz, J., et al., *Enteropathogenic Escherichia coli adherence to intestinal epithelial monolayers diminishes barrier function.* Am J Physiol, 1995. **268**(2 Pt 1): p. G374-9.
512. Stagg, A.J., et al., *The dendritic cell: its role in intestinal inflammation and relationship with gut bacteria.* Gut., 2003. **52**(10): p. 1522-9.
513. Steed, E., M.S. Balda, and K. Matter, *Dynamics and functions of tight junctions.* Trends Cell Biol., 2010. **20**(3): p. 142-9. doi: 10.1016/j.tcb.2009.12.002. Epub 2010 Jan 12.
514. Steed, E., et al., *Identification of MarvelD3 as a tight junction-associated transmembrane protein of the occludin family.* BMC Cell Biol, 2009. **10**(95): p. 1471-2121.
515. Steinberg, T.H., et al., *Global quantitative phosphoprotein analysis using Multiplexed Proteomics technology.* Proteomics, 2003. **3**(7): p. 1128-44.
516. Stevenson, B.R., et al., *Identification of ZO-1: a high molecular weight polypeptide associated with the tight junction (zonula occludens) in a variety of epithelia.* J Cell Biol., 1986. **103**(3): p. 755-66.
517. Stone, K.P., A.J. Kastin, and W. Pan, *NFkB is an unexpected major mediator of interleukin-15 signaling in cerebral endothelia.* Cell Physiol Biochem, 2011. **28**(1): p. 115-24.
518. Su, C., et al., *Recent expansion of Toxoplasma through enhanced oral transmission.* Science., 2003. **299**(5605): p. 414-6.
519. Su, C., et al., *Globally diverse Toxoplasma gondii isolates comprise*

- six major clades originating from a small number of distinct ancestral lineages.* Proc Natl Acad Sci U S A., 2012. **109**(15): p. 5844-9. doi: 10.1073/pnas.1203190109. Epub 2012 Mar 19.
520. Sumagin, R., et al., *Transmigrated neutrophils in the intestinal lumen engage ICAM-1 to regulate the epithelial barrier and neutrophil recruitment.* Mucosal Immunol, 2014. **7**(4): p. 905-15.
521. Sumagin, R. and Parkos, C. A., *Epithelial adhesion molecules and the regulation of intestinal homeostasis during neutrophil Transepithelial migration.* Tissue Barriers, 2015. **3**: p. 1-2.
522. Suzuki, H., et al., *Crystal structure of a claudin provides insight into the architecture of tight junctions.* Science., 2014. **344**(6181): p. 304-7. doi: 10.1126/science.1248571.
523. Suzuki, H., et al., *Model for the architecture of claudin-based paracellular ion channels through tight junctions.* J Mol Biol., 2015. **427**(2): p. 291-7. doi: 10.1016/j.jmb.2014.10.020. Epub 2014 Nov 4.
524. Suzuki, T., *Regulation of intestinal epithelial permeability by tight junctions.* Cell Mol Life Sci., 2013. **70**(4): p. 631-59. doi: 10.1007/s00018-012-1070-x. Epub 2012 Jul 11.
525. Suzuki, T., et al., *PKC eta regulates occludin phosphorylation and epithelial tight junction integrity.* Proc Natl Acad Sci U S A, 2009. **106**(1): p. 61-6.
526. Suzuki, T., et al., *Apical localization of sodium-dependent glucose transporter SGLT1 is maintained by cholesterol and microtubules.* Acta Histochem Cytochem, 2006. **39**(6): p. 155-61.
527. Suzuki, Y., F.K. Conley, and J.S. Remington, *Differences in virulence and development of encephalitis during chronic infection vary with the strain of Toxoplasma gondii.* J Infect Dis., 1989. **159**(4): p. 790-4.
528. Takagaki, Y., et al., *The human 64-kDa polyadenylation factor contains a ribonucleoprotein-type RNA binding domain and unusual auxiliary motifs.* Proc Natl Acad Sci U S A, 1992. **89**(4): p. 1403-7.
529. Takahashi, A., et al., *Role of C-terminal regions of the C-terminal fragment of Clostridium perfringens enterotoxin in its interaction with claudin-4.* J Control Release, 2005. **108**(1): p. 56-62.
530. Tamura, A., et al., *Loss of claudin-15, but not claudin-2, causes Na⁺ deficiency and glucose malabsorption in mouse small intestine.* Gastroenterology., 2011. **140**(3): p. 913-23. doi: 10.1053/j.gastro.2010.08.006. Epub 2010 Aug 18.
531. Tamura, A. and S. Tsukita, *Paracellular barrier and channel functions of TJ claudins in organizing biological systems: advances in the field of barriology revealed in knockout mice.* Semin Cell Dev Biol, 2014. **36**: p. 177-85.
532. Tanaka, S., et al., *Transcriptome analysis of mouse brain infected with Toxoplasma gondii.* Infect Immun, 2013. **81**(10): p. 3609-19.
533. Tang, V.W., *Proteomic and bioinformatic analysis of epithelial tight junction reveals an unexpected cluster of synaptic molecules.* Biol Direct, 2006. **1**: p. 37.
534. Tang, V.W. and D.A. Goodenough, *Paracellular ion channel at the*

- tight junction.* Biophys J, 2003. **84**(3): p. 1660-73.
535. Tardieu, I. and R. Menard, *Migration of Apicomplexa across biological barriers: the Toxoplasma and Plasmodium rides.* Traffic, 2008. **9**(5): p. 627-35.
536. Tash, B.R., et al., *The occludin and ZO-1 complex, defined by small angle X-ray scattering and NMR, has implications for modulating tight junction permeability.* Proc Natl Acad Sci U S A, 2012. **109**(27): p. 10855-60.
537. Tavelin, S., et al., *A new principle for tight junction modulation based on occludin peptides.* Mol Pharmacol, 2003. **64**(6): p. 1530-40.
538. Taylor, S., et al., *A secreted serine-threonine kinase determines virulence in the eukaryotic pathogen Toxoplasma gondii.* Science., 2006. **314**(5806): p. 1776-80.
539. Templeton, T.J., *Whole-genome natural histories of apicomplexan surface proteins.* Trends Parasitol, 2007. **23**(5): p. 205-12.
540. Tenter, A.M., A.R. Heckereth, and L.M. Weiss, *Toxoplasma gondii: from animals to humans.* Int J Parasitol., 2000. **30**(12-13): p. 1217-58.
541. Terry, S., et al., *Rho signaling and tight junction functions.* Physiology (Bethesda), 2010. **25**(1): p. 16-26.
542. Tilley, M., et al., *Toxoplasma gondii sporozoites form a transient parasitophorous vacuole that is impermeable and contains only a subset of dense-granule proteins.* Infect Immun., 1997. **65**(11): p. 4598-605.
543. Tobioka, H., et al., *Polarized distribution of carcinoembryonic antigen is associated with a tight junction molecule in human colorectal adenocarcinoma.* J Pathol, 2002. **198**(2): p. 207-12.
544. Tomavo, S., *The major surface proteins of Toxoplasma gondii: structures and functions.* Curr Top Microbiol Immunol, 1996. **219**: p. 45-54.
545. Tomavo, S., R.T. Schwarz, and J.F. Dubremetz, *Evidence for glycosyl-phosphatidylinositol anchoring of Toxoplasma gondii major surface antigens.* Mol Cell Biol., 1989. **9**(10): p. 4576-80.
546. Tremblay, E., et al., *Gene expression profiles of normal proliferating and differentiating human intestinal epithelial cells: a comparison with the Caco-2 cell model.* J Cell Biochem, 2006. **99**(4): p. 1175-86.
547. Tsukamoto, T. and S.K. Nigam, *Role of tyrosine phosphorylation in the reassembly of occludin and other tight junction proteins.* Am J Physiol, 1999. **276**(5 Pt 2): p. F737-50.
548. Tsukita, S., M. Furuse, and M. Itoh, *Molecular dissection of tight junctions.* Cell Struct Funct., 1996. **21**(5): p. 381-5.
549. Tsukita, S., M. Furuse, and M. Itoh, *Multifunctional strands in tight junctions.* Nat Rev Mol Cell Biol, 2001. **2**(4): p. 285-93.
550. Turksen, K. and T.C. Troy, *Barriers built on claudins.* J Cell Sci, 2004. **117**(Pt 12): p. 2435-47.
551. Turner, H.L. and J.R. Turner, *Good fences make good neighbors: Gastrointestinal mucosal structure.* Gut Microbes., 2010. **1**(1): p. 22-29.

552. Turner, J.R., *Show me the pathway! Regulation of paracellular permeability by Na(+) -glucose cotransport*. Adv Drug Deliv Rev., 2000. **41**(3): p. 265-81.
553. Turner, J.R., *Intestinal mucosal barrier function in health and disease*. Nat Rev Immunol., 2009. **9**(11): p. 799-809. doi: 10.1038/nri2653.
554. Turner, J.R., et al., *The role of molecular remodeling in differential regulation of tight junction permeability*. Semin Cell Dev Biol, 2014. **36**: p. 204-12.
555. Turner, J.R. and J.L. Madara, *Physiological regulation of intestinal epithelial tight junctions as a consequence of Na(+) -coupled nutrient transport*. Gastroenterology., 1995. **109**(4): p. 1391-6.
556. Turner, J.R., et al., *Physiological regulation of epithelial tight junctions is associated with myosin light-chain phosphorylation*. Am J Physiol., 1997. **273**(4 Pt 1): p. C1378-85.
557. Ukabam, S.O., J.R. Clamp, and B.T. Cooper, *Abnormal small intestinal permeability to sugars in patients with Crohn's disease of the terminal ileum and colon*. Digestion., 1983. **27**(2): p. 70-4.
558. Unno, A., et al., *Visualization of Toxoplasma gondii stage conversion by expression of stage-specific dual fluorescent proteins*. Parasitology., 2009. **136**(6): p. 579-88. doi: 10.1017/S0031182009005836. Epub 2009 Apr 16.
559. Vaillant, V., et al., *Foodborne infections in France*. Foodborne Pathog Dis., 2005. **2**(3): p. 221-32.
560. van der Flier, L.G. and H. Clevers, *Stem cells, self-renewal, and differentiation in the intestinal epithelium*. Annu Rev Physiol, 2009. **71**: p. 241-60.
561. van der Valk, M.E., et al., *Healthcare costs of inflammatory bowel disease have shifted from hospitalisation and surgery towards anti-TNFalpha therapy: results from the COIN study*. Gut., 2014. **63**(1): p. 72-9. doi: 10.1136/gutjnl-2012-303376. Epub 2012 Nov 7.
562. Van Itallie, C., C. Rahner, and J.M. Anderson, *Regulated expression of claudin-4 decreases paracellular conductance through a selective decrease in sodium permeability*. J Clin Invest., 2001. **107**(10): p. 1319-27.
563. Van Itallie, C.M. and J.M. Anderson, *Occludin confers adhesiveness when expressed in fibroblasts*. J Cell Sci, 1997. **110** (Pt 9): p. 1113-21.
564. Van Itallie, C.M. and J.M. Anderson, *Claudins and epithelial paracellular transport*. Annu Rev Physiol, 2006. **68**: p. 403-29.
565. Van Itallie, C.M. and J.M. Anderson, *Architecture of tight junctions and principles of molecular composition*. Semin Cell Dev Biol, 2014. **36**: p. 157-65.
566. Van Itallie, C.M., et al., *The N and C termini of ZO-1 are surrounded by distinct proteins and functional protein networks*. J Biol Chem, 2013. **288**(19): p. 13775-88.
567. Van Itallie, C.M., et al., *Structure of the claudin-binding domain of Clostridium perfringens enterotoxin*. J Biol Chem., 2008. **283**(1): p. 268-74. Epub 2007 Oct 31.

568. Van Itallie, C.M., et al., *ZO-1 stabilizes the tight junction solute barrier through coupling to the perijunctional cytoskeleton*. Mol Biol Cell., 2009. **20**(17): p. 3930-40. doi: 10.1091/mbc.E09-04-0320. Epub 2009 Jul 15.
569. Van Itallie, C.M., et al., *Occludin is required for cytokine-induced regulation of tight junction barriers*. J Cell Sci., 2010. **123**(Pt 16): p. 2844-52. doi: 10.1242/jcs.065581. Epub 2010 Jul 27.
570. Van Itallie, C.M., et al., *Claudin-2-dependent changes in noncharged solute flux are mediated by the extracellular domains and require attachment to the PDZ-scaffold*. Ann N Y Acad Sci, 2009.
571. Van Itallie, C.M., et al., *Biotin ligase tagging identifies proteins proximal to E-cadherin, including lipoma preferred partner, a regulator of epithelial cell-cell and cell-substrate adhesion*. J Cell Sci., 2014. **127**(Pt 4): p. 885-95. doi: 10.1242/jcs.140475. Epub 2013 Dec 11.
572. van Meer, G. and K. Simons, *The function of tight junctions in maintaining differences in lipid composition between the apical and the basolateral cell surface domains of MDCK cells*. Embo J., 1986. **5**(7): p. 1455-64.
573. Vetrano, S., et al., *Unique role of junctional adhesion molecule-a in maintaining mucosal homeostasis in inflammatory bowel disease*. Gastroenterology., 2008. **135**(1): p. 173-84. doi: 10.1053/j.gastro.2008.04.002. Epub 2008 Apr 11.
574. Villard, O., et al., *Comparison of four commercially available avidity tests for Toxoplasma gondii-specific IgG antibodies*. Clin Vaccine Immunol., 2013. **20**(2): p. 197-204. doi: 10.1128/CVI.00356-12. Epub 2012 Dec 12.
575. Vogelmann, R. and W.J. Nelson, *Fractionation of the epithelial apical junctional complex: reassessment of protein distributions in different substructures*. Mol Biol Cell., 2005. **16**(2): p. 701-16. Epub 2004 Nov 17.
576. Volpe, D.A., *Variability in Caco-2 and MDCK cell-based intestinal permeability assays*. J Pharm Sci, 2008. **97**(2): p. 712-25.
577. Vyas, A., et al., *Behavioral changes induced by Toxoplasma infection of rodents are highly specific to aversion of cat odors*. Proc Natl Acad Sci U S A., 2007. **104**(15): p. 6442-7. Epub 2007 Apr 2.
578. Wada, M., et al., *Loss of claudins 2 and 15 from mice causes defects in paracellular Na⁺ flow and nutrient transport in gut and leads to death from malnutrition*. Gastroenterology., 2013. **144**(2): p. 369-80. doi: 10.1053/j.gastro.2012.10.035. Epub 2012 Oct 23.
579. Walter, J.K., et al., *The oligomerization of the coiled coil-domain of occludin is redox sensitive*. Ann N Y Acad Sci, 2009. **1165**: p. 19-27.
580. Wan, H., et al., *Quantitative structural and biochemical analyses of tight junction dynamics following exposure of epithelial cells to house dust mite allergen Der p 1*. Clin Exp Allergy, 2000. **30**(5): p. 685-98.
581. Wang, F., et al., *Interferon-gamma and tumor necrosis factor-alpha synergize to induce intestinal epithelial barrier dysfunction by up-regulating myosin light chain kinase expression*. Am J Pathol., 2005.

- 166**(2): p. 409-19.
582. Wang, F., et al., *RACK1 regulates VEGF/Flt1-mediated cell migration via activation of a PI3K/Akt pathway*. J Biol Chem, 2011. **286**(11): p. 9097-106.
583. Wang, Y. and H. Yin, *Research progress on surface antigen 1 (SAG1) of Toxoplasma gondii*. Parasit Vectors, 2014. **7**(180): p. 1756-3305.
584. Wang, Z., et al., *The second loop of occludin is required for suppression of Raf1-induced tumor growth*. Oncogene., 2005. **24**(27): p. 4412-20.
585. Wasmuth, J.D., et al., *Integrated bioinformatic and targeted deletion analyses of the SRS gene superfamily identify SRS29C as a negative regulator of Toxoplasma virulence*. MBio, 2012. **3**(6).
586. Wastling, J.M., et al., *Proteomes and transcriptomes of the Apicomplexa--where's the message?* Int J Parasitol, 2009. **39**(2): p. 135-43.
587. Watson, A.J., *Claudins and barrier dysfunction in intestinal inflammation: cause or consequence?* Gut., 2015. **64**(10): p. 1501-2. doi: 10.1136/gutjnl-2014-309110. Epub 2015 Feb 18.
588. Watson, A.J., et al., *Epithelial barrier function in vivo is sustained despite gaps in epithelial layers*. Gastroenterology, 2005. **129**(3): p. 902-12.
589. Watson, C.J., et al., *Interferon-gamma selectively increases epithelial permeability to large molecules by activating different populations of paracellular pores*. J Cell Sci., 2005. **118**(Pt 22): p. 5221-30. Epub 2005 Oct 25.
590. Weber, C.R., *Dynamic properties of the tight junction barrier*. Ann N Y Acad Sci, 2012.
591. Weber, C.R., et al., *Epithelial myosin light chain kinase activation induces mucosal interleukin-13 expression to alter tight junction ion selectivity*. J Biol Chem., 2010. **285**(16): p. 12037-46. doi: 10.1074/jbc.M109.064808. Epub 2010 Feb 22.
592. Weight, C. M, *The interactions of Toxoplasma gondii with epithelial tight junctions*. PhD Thesis, University of East Anglia, 2011.
593. Weight, C.M. and S.R. Carding, *The protozoan pathogen Toxoplasma gondii targets the paracellular pathway to invade the intestinal epithelium*. Ann N Y Acad Sci, 2012.
594. Weight, C.M., et al., *Elucidating pathways of Toxoplasma gondii invasion in the gastrointestinal tract: Involvement of the tight junction protein occludin*. Microbes Infect, 2015.
595. Weiss, L.M. and J.P. Dubey, *Toxoplasmosis: A history of clinical observations*. Int J Parasitol., 2009. **39**(8): p. 895-901. doi: 10.1016/j.ijpara.2009.02.004. Epub 2009 Feb 13.
596. Weiss, L.M., et al., *Toxoplasma gondii proteomics*. Expert Rev Proteomics., 2009. **6**(3): p. 303-13. doi: 10.1586/epr.09.16.
597. Werk, R., *How does Toxoplasma gondii enter host cells?* Rev Infect Dis., 1985. **7**(4): p. 449-57.
598. Willott, E., et al., *The tight junction protein ZO-1 is homologous to the Drosophila discs-large tumor suppressor protein of septate junctions*. Proc Natl Acad Sci U S A., 1993. **90**(16): p. 7834-8.

599. Winkler, L., et al., *Molecular determinants of the interaction between Clostridium perfringens enterotoxin fragments and claudin-3*. J Biol Chem., 2009. **284**(28): p. 18863-72. doi: 10.1074/jbc.M109.008623. Epub 2009 May 8.
600. Wittchen, E.S., J. Haskins, and B.R. Stevenson, *Protein interactions at the tight junction. Actin has multiple binding partners, and ZO-1 forms independent complexes with ZO-2 and ZO-3*. J Biol Chem., 1999. **274**(49): p. 35179-85.
601. Wolpert, S., M.L. Wong, and B.L. Bass, *Matrix alters the proliferative response of enterocytes to growth factors*. Am J Surg, 1996. **171**(1): p. 109-12.
602. Wong, V., *Phosphorylation of occludin correlates with occludin localization and function at the tight junction*. Am J Physiol, 1997. **273**(6 Pt 1): p. C1859-67.
603. Wong, V. and B.M. Gumbiner, *A synthetic peptide corresponding to the extracellular domain of occludin perturbs the tight junction permeability barrier*. J Cell Biol., 1997. **136**(2): p. 399-409.
604. Wood, S.R., et al., *Altered morphology in cultured rat intestinal epithelial IEC-6 cells is associated with alkaline phosphatase expression*. Tissue Cell, 2003. **35**(1): p. 47-58.
605. Wroblewski, L.E., et al., *Helicobacter pylori dysregulation of gastric epithelial tight junctions by urease-mediated myosin II activation*. Gastroenterology., 2009. **136**(1): p. 236-46. doi: 10.1053/j.gastro.2008.10.011. Epub 2008 Oct 9.
606. Wu, C.C., et al., *Metabolic labeling of mammalian organisms with stable isotopes for quantitative proteomic analysis*. Anal Chem, 2004. **76**(17): p. 4951-9.
607. Wuchty, S., *Computational prediction of host-parasite protein interactions between P. falciparum and H. sapiens*. PLoS One, 2011. **6**(11): p. e26960.
608. Wyatt, J., et al., *Intestinal permeability and the prediction of relapse in Crohn's disease*. Lancet, 1993. **341**(8858): p. 1437-9.
609. Xia, D., et al., *The proteome of Toxoplasma gondii: integration with the genome provides novel insights into gene expression and annotation*. Genome Biol, 2008. **9**(7): p. R116.
610. Xia, G., et al., *Heparin-binding EGF-like growth factor preserves crypt cell proliferation and decreases bacterial translocation after intestinal ischemia/reperfusion injury*. J Pediatr Surg, 2002. **37**(7): p. 1081-7; discussion 1081-7.
611. Xing, H., et al., *HSF1 modulation of Hsp70 mRNA polyadenylation via interaction with symplekin*. J Biol Chem, 2004. **279**(11): p. 10551-5.
612. Xu, B.J., et al., *Direct analysis of laser capture microdissected cells by MALDI mass spectrometry*. J Am Soc Mass Spectrom, 2002. **13**(11): p. 1292-7.
613. Yamada, S., et al., *Deconstructing the cadherin-catenin-actin complex*. Cell, 2005. **123**(5): p. 889-901.
614. Yamamoto, M., et al., *A single polymorphic amino acid on Toxoplasma gondii kinase ROP16 determines the direct and strain-specific activation of Stat3*. J Exp Med, 2009. **206**(12): p. 2747-60.

615. Yamamoto, T., et al., *The Ras target AF-6 interacts with ZO-1 and serves as a peripheral component of tight junctions in epithelial cells*. J Cell Biol, 1997. **139**(3): p. 785-95.
616. Yang, L., et al., *ICAM-1 regulates neutrophil adhesion and transcellular migration of TNF-alpha-activated vascular endothelium under flow*. Blood, 2005. **106**: p584-592.
617. Yano, T., et al., *The association of microtubules with tight junctions is promoted by cingulin phosphorylation by AMPK*. J Cell Biol, 2013. **203**(4): p. 605-14. doi: 10.1083/jcb.201304194.
618. Yap, A.S., J.M. Mullin, and B.R. Stevenson, *Molecular analyses of tight junction physiology: insights and paradoxes*. J Membr Biol, 1998. **163**(3): p. 159-67.
619. Yasen, M., et al., *The up-regulation of Y-box binding proteins (DNA binding protein A and Y-box binding protein-1) as prognostic markers of hepatocellular carcinoma*. Clin Cancer Res, 2005. **11**(20): p. 7354-61.
620. Ye, D., I. Ma, and T.Y. Ma, *Molecular mechanism of tumor necrosis factor-alpha modulation of intestinal epithelial tight junction barrier*. Am J Physiol Gastrointest Liver Physiol, 2006. **290**(3): p. G496-504.
621. Yokoyama, S., et al., *alpha-catenin-independent recruitment of ZO-1 to nectin-based cell-cell adhesion sites through afadin*. Mol Biol Cell, 2001. **12**(6): p. 1595-609.
622. Yolken, R.H., et al., *Antibodies to Toxoplasma gondii in individuals with first-episode schizophrenia*. Clin Infect Dis, 2001. **32**(5): p. 842-4. Epub 2001 Feb 28.
623. Yoshida, N., K.M. Tyler, and M.S. Llewellyn, *Invasion mechanisms among emerging food-borne protozoan parasites*. Trends Parasitol, 2011. **27**(10): p. 459-66. doi: 10.1016/j.pt.2011.06.006. Epub 2011 Aug 15.
624. Yurist-Doutsch, S., et al., *Gastrointestinal microbiota-mediated control of enteric pathogens*. Annu Rev Genet, 2014. **48**: p. 361-82.
625. Zahraoui, A., *Properties of Rab13 interaction with protein kinase A*. Methods Enzymol, 2005. **403**: p. 723-32.
626. Zeissig, S., et al., *Changes in expression and distribution of claudin 2, 5 and 8 lead to discontinuous tight junctions and barrier dysfunction in active Crohn's disease*. Gut, 2007. **56**(1): p. 61-72. Epub 2006 Jul 5.
627. Zemljic-Harpf, A.E., et al., *Vinculin directly binds zonula occludens-1 and is essential for stabilizing connexin-43-containing gap junctions in cardiac myocytes*. J Cell Sci, 2014. **127**(Pt 5): p. 1104-16. doi: 10.1242/jcs.143743. Epub 2014 Jan 10.
628. Zhang, Q., et al., *Enteropathogenic Escherichia coli changes distribution of occludin and ZO-1 in tight junction membrane microdomains in vivo*. Microb Pathog, 2010. **48**(1): p. 28-34.
629. Zhang, Y.G., et al., *Salmonella infection upregulates the leaky protein claudin-2 in intestinal epithelial cells*. PLoS One, 2013. **8**(3): p. e58606. doi: 10.1371/journal.pone.0058606. Epub 2013 Mar 11.
630. Zhou, D.H., et al., *Modulation of mouse macrophage proteome*

- induced by Toxoplasma gondii tachyzoites in vivo.* Parasitol Res, 2011. **109**(6): p. 1637-46.
- 631. Zhou, D.H., et al., *Changes in the proteomic profiles of mouse brain after infection with cyst-forming Toxoplasma gondii.* Parasit Vectors, 2013. **6**: p. 96.
 - 632. Zhou, D.H., et al., *Comparative proteomic analysis of different Toxoplasma gondii genotypes by two-dimensional fluorescence difference gel electrophoresis combined with mass spectrometry.* Electrophoresis, 2014. **35**(4): p. 533-45.
 - 633. Zhou, H., et al., *Differential proteomic profiles from distinct Toxoplasma gondii strains revealed by 2D-difference gel electrophoresis.* Exp Parasitol, 2013. **133**(4): p. 376-82.
 - 634. Zhou, K., et al., *Actin-related protein2/3 complex regulates tight junctions and terminal differentiation to promote epidermal barrier formation.* Proc Natl Acad Sci U S A., 2013. **110**(40): p. E3820-9. doi: 10.1073/pnas.1308419110. Epub 2013 Sep 16.
 - 635. Zihni, C., M.S. Balda, and K. Matter, *Signalling at tight junctions during epithelial differentiation and microbial pathogenesis.* J Cell Sci, 2014. **127**(Pt 16): p. 3401-13.